SKB

TECHNICAL REPORT 89-15

Comparison between radar data and geophysical, geological, and hydrological borehole parameters by multivariate analysis of data

Serje Carlsten, Lennart Lindqvist, Olle Olsson

Swedish Geological Company, Uppsala

March 1989

SVENSK KÄRNBRÄNSLEHANTERING AB
SWEDISH NUCLEAR FUEL AND WASTE MANAGEMENT CO

BOX 5864 S-102 48 STOCKHOLM
TEL 08-665 28 00 TELEX 13108-SKB

COMPARISON BETWEEN RADAR DATA AND GEOPHYSICAL, GEOLOGICAL, AND HYDROLOGICAL BOREHOLE PARAMETERS BY MULTIVARIATE ANALYSIS OF DATA

Seje Carlsten, Lennart Lindqvist, Olle Olsson
Swedish Geological Company, Uppsala

March 1989

SVERIGES GEOLOGISKA AB
Division Ingenjörsgeologi
Uppdragsgivare: SKB
Uppdragsnummer: 87-138

REPORT
ID-no: IRAP 88 283
Date : 1989-03-11

COMPARISON BETWEEN RADAR DATA AND GEOPHYSICAL, GEOLOGICAL, AND HYDROLOGICAL BOREHOLE PARAMETERS BY MULTIVARIATE ANALYSIS OF DATA.

SEJE CARLSTEN
LENNART LINDQVIST
OLLE OLSSON

ABSTRACT

The borehole radar technique has been developed to its present status by a group at the Swedish Geological Company (SGAB), funded by the International Stripa Project and SKB. Several radar measurements have been performed at different sites. Included in this report are data from the sites Klipperås, Finnsjön, Saltsjötunnel, Stripa and Ävrö.

The object of the present work is to study the correlation between radar reflectors and geophysical, geological and hydraulical parameters from the boreholes. An additional objective is to show what information can be gained by the borehole radar with respect to waterflow and geological structures in crystalline rock. The tool for making the data modelling is Multivariate Data Analysis (SIMCA). For the data modelling there are two algorithms available in the SIMCA software. One for Principal Component analysis and one for Partial Least Squares regression analysis (PLS and PLS2). The PLS method gives the best results for the purpose of correlation between radar intensity and other variables.

The result from the Principal Component, PLS, and PLS2 analysis shows that the strongest correlations results in a division between highly fractured rock and low fractured rock at all sites. Also, PLS and PLS2 analysis show that there is a good correlation between high radar intensity and highly fractured rock in the boreholes at all sites. The correlation between radar intensity and hydraulic conductivity is more ambiguous. Two of the investigated sites, Stripa and Finnsjön, exhibit good correlation between radar intensity and hydraulic conductivity, while the correlation at Ävrö is lower and at Saltsjötunnel it is poor. Hydraulic conductivity was not included in the analysis of the Klipperås data. The best correlation in the data from Klipperås was obtained between radar intensity and fractured lithological contacts. The degree of correlation between radar intensity and lithological contacts at the other four sites was lower than for Klipperås.

Keywords: Radar, SIMCA, Multivariate Data Analysis, Fracture zones, Hydraulic conductivity.

TABLE OF CONTENTS

		Page
	ABSTRACT	i
	SUMMARY	iv
1	INTRODUCTION	1
1.1	BACKGROUND	1
1.2	DESCRIPTION OF THE RAMAC BOREHOLE RADAR SYSTEM	2
1.2.1	The RAMAC system	2
1.2.2	Configuration of single hole measurements	3
1.2.3	Processing and interpretation of single hole radar reflection data	6
2	MULTIVARIATE DATA ANALYSIS	8
2.1	PRINCIPAL COMPONENT ANALYSIS	9
2.2	PLS AND PLS2 MODELLING	12
2.3	DATA ANALYTICAL STRATEGY	16
3	AVAILABLE RAW DATA AND PREPARATION OF DATA FILES	17
3.1	GENERAL	17
3.2	DESCRIPTION OF VARIABLES USED	18
3.3	RADAR MEASUREMENTS	25
3.4	CREATING 1-METER SECTIONS	26
3.5	DESCRIPTION OF PRESENTED RESULTS	28
4	KLIPPERÅS STUDY SITE	37
4.1	GEOLOGICAL OVERVIEW OF KLIPPERÅS	37
4.2	PRINCIPAL COMPONENT ANALYSIS OF THE DATA FROM KLIPPERÅS	41
4.3	PLS-ANALYSIS OF THE DATA FROM KLIPPERÅS	43
4.4	PLS2-ANALYSIS OF THE DATA FROM KLIPPERÅS	49
4.5	COMPARISON WITH PREVIOUS INTERPRETATION OF RADAR DATA FROM KLIPPERÅS	51
5	FINNSJÖN STUDY SITE	52
5.1	GEOLOGICAL OVERVIEW OF FINNSJÖN	52
5.2	PRINCIPAL COMPONENT ANALYSIS OF THE DATA FROM FINNSJÖN	56
5.3	PLS-ANALYSIS OF THE DATA FROM FINNSJÖN	58
5.4	PLS2-ANALYSIS OF THE DATA FROM FINNSJÖN	60
5.5	COMPARISON WITH PREVIOUS INTERPRETATION OF RADAR DATA FROM FINNSJÖN	62
6	SALTSJÖTUNNEL SITE	63
6.1	GEOLOGICAL OVERVIEW OF SALTSJÖTUNNEL	63
6.2	PRINCIPAL COMPONENT ANALYSIS OF THE DATA FROM SALTSJÖTUNNEL	67
6.3	PLS-ANALYSIS OF THE DATA FROM SALTSJÖTUNNEL	69
6.4	PLS2-ANALYSIS OF THE DATA FROM SALTSJÖTUNNEL	71
6.5	COMPARISON WITH PREVIOUS INTERPRETATION OF RADAR DATA FROM SALTSJÖTUNNEL	73

7	STRIPA SITE	75
7.1	GEOLOGICAL OVERVIEW OF STRIPA	75
7.2	PRINCIPAL COMPONENT ANALYSIS OF THE DATA FROM STRIPA	80
7.3	PLS-ANALYSIS OF THE DATA FROM STRIPA	82
7.4	PLS2- ANALYSIS OF THE DATA FROM STRIPA	84
7.5	COMPARISON WITH PREVIOUS INTERPRETATION OF RADAR DATA FROM STRIPA	86
8	ÄVRÖ STUDY SITE	87
8.1	GEOLOGICAL OVERVIEW OF ÄVRÖ	87
8.2	PRINCIPAL COMPONENT ANALYSIS OF THE DATA FROM ÄVRÖ	92
8.3	PLS-ANALYSIS OF THE DATA FROM ÄVRÖ	94
8.4	PLS2-ANALYSIS OF THE DATA FROM ÄVRÖ	96
8.5	COMPARISON WITH PREVIOUS INTERPRETATION OF RADAR DATA FROM ÄVRÖ	98
9	PHYSICAL PROPERTIES OF CORE SAMPLES FROM THE BOREHOLES KFI09, KFI11, KKL02, and F2	99
10	DISCUSSION	109
10.1	EXPERIENCES FROM USE OF THE SIMCA METHOD	109
10.2	COMPARISON OF SIMCA RESULTS FROM THE SITES	119
10.3	SUMMARY CONCLUSIONS	122
	ACKNOWLEDGEMENTS	124
	REFERENCES	125
	APPENDICES	

Appendix A : Boreholes included in the SIMCA investigation.

Appendix B: Status of the variables from the investigated sites.

Appendix C: Variable plots from Principal Component analysis, PLS and PLS2 analysis of data from the investigated sites.

Appendix D: Measurements on core samples from the boreholes KFI09, KFI11, KKL02 and F2.

SUMMARY

The borehole radar technique has been developed to its present status by a group at the Swedish Geological Company (SGAB), funded by the International Stripa Project and SKB. Radar measurements have been performed at different sites inside and outside Sweden. The present work comprise analysis of data from five separate sites in Sweden, namely Klipperås, Finnsjön, Saltsjötunnel, Stripa and Ävrö. Radar measurements have been made in three different configurations; singlehole, crosshole and Vertical Radar Profiling. In the current work only singlehole reflection data has been analyzed.

The objective of the present work is to study the correlation between radar reflections and geophysical, geological and hydraulic parameters from the boreholes. A special effort is put on studying the correlation with hydraulically conductive features.

The tool for making the data modelling is Multivariate Data Analysis (SIMCA). The program used, available at SGAB, can handle up to 200 variables (logs) and 6 000 samples (measurement points). For the data modelling there are two algorithms available in the SIMCA software, one for Principal Component analysis (PC) and one for Partial Least Squares regression analysis (PLS and PLS2). Radar intensity was the selected variable in the PLS-analysis and radar intensity together with hydraulic conductivity were the selected variables in the PLS2-analysis.

In the Principal Component analysis the first component from all sites give a description of variables connected to low fractured rock on one side of the component and variables connected to highly fractured rock on the other side. High radar intensity generally occurs in principal components with lower degree of correlation.

The PLS-analysis shows a high degree of correlation between highly fractured rock and high radar intensity at all sites. At Klipperås the high fracturing is associated with lithological contacts. At the other four sites lithological contacts do not show up in the first and strongest component. However, at Stripa lithological contact occurs in the second component.

The PLS2 analysis shows a good correlation between radar intensity and hydraulic conductivity at Stripa and Finnsjön. At Ävrö the correlation between radar intensity and hydraulic conductivity is somewhat

lower and at Saltsjötunnel site the correlation is poor. However, the correlation between hydraulic conductivity and other variables representing fractured rock at Ävrö and Saltsjötunnel sites in general is less, while radar intensity on the other hand shows good correlation to those variables. Hydraulic conductivity was not included in the Klipperås data due to too large section length of the hydraulic conductivity measurement. The PLS2 analysis from Klipperås regarding radar angles did not show any significant correlations.

The SIMCA method has been a useful instrument in the work of establishing correlation between radar intensity and other geophysical, geological and hydrological borehole parameters. The best result regarding radar intensity was received with the PLS method. The combined result shows that borehole radar detects fractured sections and both sealed and fractured lithological contacts. The correlation between radar intensity and hydraulic conductivity is somewhat ambiguous. Some of the radar detected sections exhibit high hydraulic conductivity and some of them do not.

The great advantage of the radar method compared to other borehole methods is that it gives geometric information about structures at considerable distances from the boreholes. The SIMCA analysis compares radar results to other data related to properties in the borehole. This gives an idea of what causes radar reflexes since the reflexes originate from outside the borehole.

1 INTRODUCTION

1.1 BACKGROUND

The borehole radar technique has been developed to its present status by a group at the Swedish Geological Company (SGAB), funded by the International Stripa Project and SKB. Radar measurements have been performed at several study sites. Amongst them are Klipperås, Finnsjön, Saltsjötunnel, Stripa, and Ävrö. Radar measurements have also been performed outside Sweden, i.e. Grimsel (Switzerland), URL (Canada), Japan etc. One or more of the following configurations have been used for the measurements: singlehole, crosshole and Vertical Radar Profiling (VRP). Every survey has generated new experiences about the radar technique. Which has led to continuous improvements of the radar equipment and the data evaluation methods. However, a comprehensive evaluation of the gained experiences has not been made previously.

The objective of this report is to study the correlation between borehole radar results and geophysical, geological and hydraulical parameters from the boreholes. An additional objective is to show what information can be gained by borehole radar with respect to waterflow and geological structures in crystalline rock. The tool for making the data modelling is Multivariate Data Analysis (SIMCA).

Borehole data from five study sites is included in this report: Klipperås, Finnsjön, Saltsjötunnel, Stripa and Ävrö.

1.2 DESCRIPTION OF THE RAMAC BOREHOLE RADAR SYSTEM

1.2.1 The RAMAC system

RAMAC is a short pulse borehole radar system. The system was originally developed by the Swedish Geological Co. (SGAB) as a part of the International Stripa Project. A continued development to make the system adapted for field work on a production basis has later been funded by SKB.

The radar system (RAMAC) consists of five different parts;

- a microcomputer with two 5 inch floppy disc units for control of measurements, data storage, data presentation and signal analysis.
- a control unit for timing control, storage and stacking of single radar measurements.
- a borehole transmitter for generation of short radar pulses.
- a borehole receiver for detection and digitization of radar pulses.
- a motordriven cable winch with an optical borehole cable for transmission of trigger signals to the borehole probes and data from the receiver to the control unit.

The RAMAC system works in principle in the following manner: A short current pulse is fed to the transmitter antenna, which generates a radar pulse that propagates through the rock. The pulse is made as short as possible to obtain high resolution. The pulse is received by the same type of antenna, amplified, and registered as a function of time. The receiver may be located in the same borehole as the transmitter or in any other borehole. From the full wave record of the signal the distance (travel time) to a reflector, the strength of the reflection, and the attenuation and delay of the direct wave between transmitter and receiver may be deduced.

The recording of the signal is similar to that of a sampling oscilloscope, i.e. for each pulse from the transmitter only one sample of the received electric signal is taken at a specific time. When the next pulse is generated a new sample is taken which is displaced slightly in time. Thus, after a number of samples a replica of the entire signal is recorded. The sampling frequency and the length and position of

the sampled time interval can be set by the operator.

Optical fibers are used for transmission of the trigger signals from the computer to the borehole probes and for transmission of data from the receiver to the control unit. The optical fibers have no electrical conductivity and will not support waves propagating along the borehole. Another advantage of optical fibers is that they do not pick up electrical noise and as the signal is digitized down-hole there is no deterioration of the signal along the cable. The quality of the results will thus be independent of cable length.

There is no direct connection between the transmitter and the receiver. Both probes are instead connected directly to the control unit and the transmitter and the receiver can be put into the same as well as into separate holes. In other words, the radar may be used for both singlehole and crosshole measurements. The system also provides absolute timing of the transmitted pulses and calibrated gain in the receiver, which makes it possible to measure the travel time and the amplitude of the radar pulses in a crosshole measurement and hence provide data for a tomographic analysis. The absolute time depends on length of the optical fibers and is hence a quantity which has to be obtained through calibration for a given set of optical fibers. The block diagram of the control unit, transmitter and receiver is shown in Fig. 1.1 and the technical specifications of the system are given in Table 1.1.

1.2.2 Configuration of singlehole measurements

In singlehole measurements the transmitter and receiver are located in the same borehole. The transmitter and receiver are kept at a fixed separation by glassfiber rods. The transmitter-receiver array is moved along the borehole and measurements are made at fixed intervals. The measurement at each position takes about 30 seconds including the movement to the next measuring position. The separation of measurement points is normally 0.5 or 1 m.

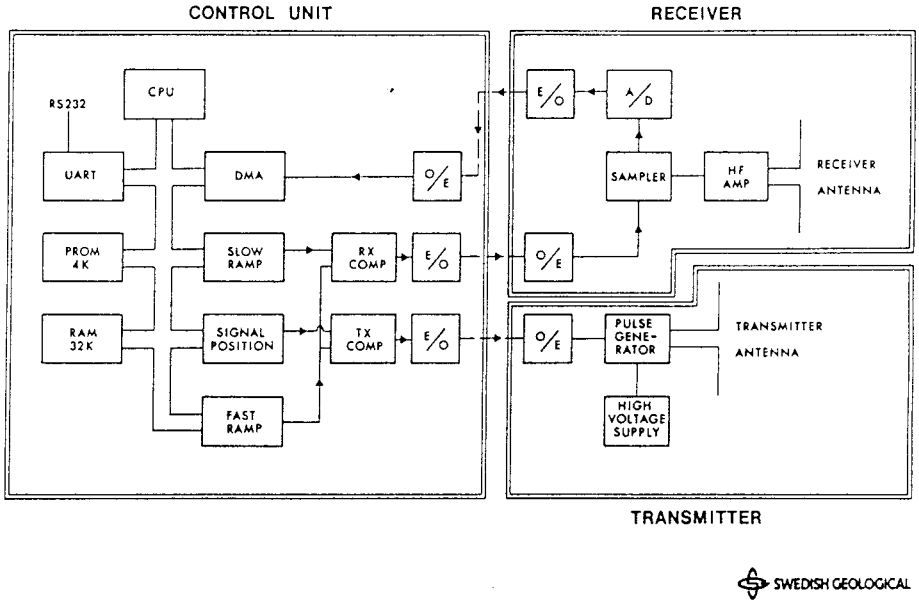

Fig. 1.1 Block diagram of the RAMAC borehole radar system.

Table 1.1 Technical specifications of the borehole radar system.

General	
Frequency range	20-80 MHz
Total dynamic range	150 dB
Sampling time accuracy	1 ns
Maximum optical fiber length	1000 m
Maximum operating pressure	100 Bar
Outer diameter of transmitter/receiver	48 mm
Minimum borehole diameter	56 mm
Transmitter	
Peak power	500 W
Operating time	10 h
Length	4.8 m
Weight	16 kg
Receiver	
Bandwidth	10-200 MHz
A/D converter	16 bit
Least significant bit at antenna terminals	1 μV
Data transmission rate	1.2 MB
Operating time	10 h
Length	5.4 m
Weight	18 kg
Control unit	
Microprocessor	RCA 1806
Clock frequency	5 MHz
Pulse repetition frequency	43.1 kHz
Sampling frequency	30-1000 MHz
No of samples	256-4096
No of stacks	1-32767
Time window	0-11 μs

1.2.3 Processing and interpretation of singlehole radar reflection data

Interpretation procedure

The principle of a singlehole reflection measurement is depicted in Fig. 1.2. The transmitter and receiver are lowered or pushed into the same hole while the distance between them is kept constant. The result is displayed in the form of a diagram where the position of the probes is shown along one axis and the propagation distance along the other axis. The amplitude of the received signal is shown in a grey scale where black corresponds to large positive signals, white to large negative signals and grey to small signals.

The distance to a reflecting object is determined by measuring the difference in arrival time between the direct and the reflected pulse. The basic assumption is that the speed of propagation is the same everywhere. The two basic patterns are point reflectors and plane reflectors as shown in Fig. 1.2.

From the radar reflection measurements it is possible to determine the angle of intersection between the hole and a fracture plane and also the point of intersection. This is done with the aid of a theoretically computed nomogram (Olsson, Falk, Forslund, Lundmark, and Sandberg, 1987a). The information contained in the radar images is cylindrically symmetric as dipole antennas have been used due the small borehole diameter. Consequently one can not obtain the complete orientation of a fracture plane from measurements in a single borehole. The orientation can however be determined by combining results from two or more boreholes. In this multiple borehole analysis the possible orientations of a fracture plane are displayed as a curve in a Wulff diagram. There is one curve for each borehole measured and the intersection of the curves define the orientation of the zone.

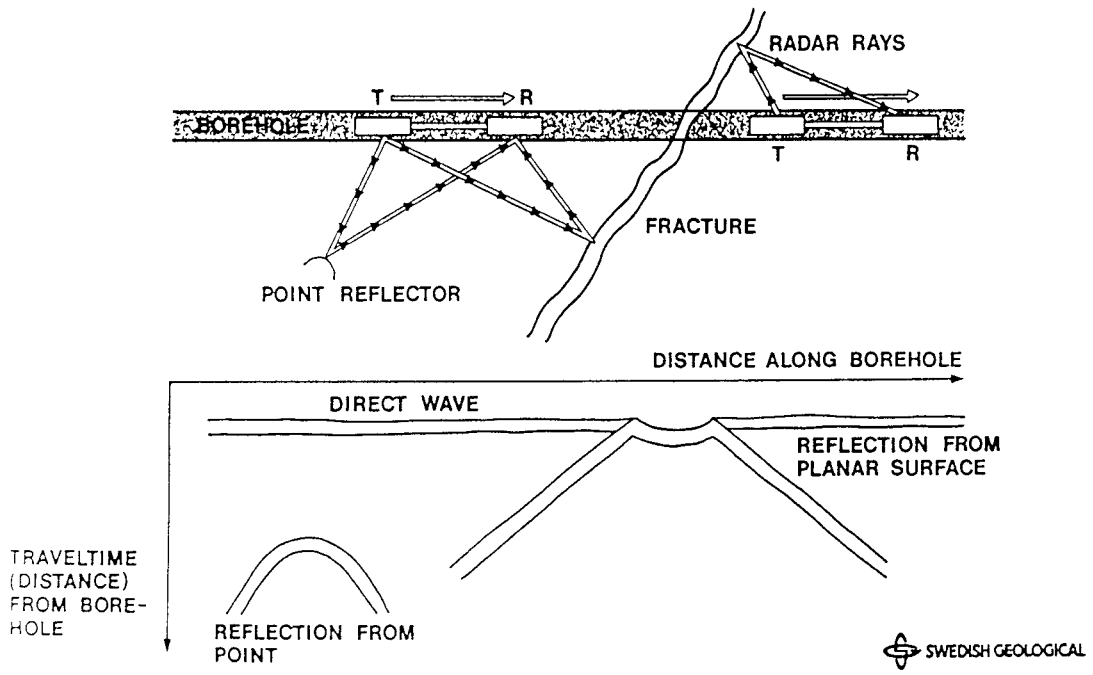

Fig. 1.2 The principle of the borehole reflection radar and the characteristic patterns generated by plane and point reflectors.

Data processing

In many cases reflections from fracture zones and other inhomogeneities in the rock mass are not readily observed in the original radar data. In order to enhance reflections the radar data are digitally filtered.

A suitable filter for this purpose is the moving average filter. The filter is constructed so that the average is formed of a number of traces adjacent to the trace to be filtered and the average is subtracted from the centre trace. This is done for all traces along the borehole. With this type of filter, features on the radar signals which are similar for several adjacent traces will be removed. This includes the direct pulse as well as structures nearly parallel to the borehole. The width of the filter, i.e. the number of traces included in the average, is chosen close to one wavelength.

2 MULTIVARIATE DATA ANALYSIS

The starting point in all multivariate data analysis is a data matrix measured for N objects and K variables. In our case an object corresponds to a borehole section, and a variable represents a measured parameter (e.g. fracture frequency, hydraulic conductivity or resistivity). The objective of multivariate data analysis is to evaluate certain characteristics of the data set or to create a model of the features in a certain system. Usually the system is complex and several different parameters interact. In addition there may be a random component added to some variables as well as measurement errors which vary in character for different variables and objects. In a data matrix there may also be objects that systematically or randomly differ from the main trends in the system. These are called outliers. Special attention must be paid to the outliers, which if included in the data set will influence the data evaluation too much.

In most problems analyzed, there exist a relation between the variables measured. This effect should of course be used to build the models of the data set.

From theory and from our knowledge and experience we can recognize a correlation of several variables as a certain feature or relationship between variables. If some objects in the data matrix reveal this correlation we can be convinced that these objects has this special feature. If just one variable at the time is examinated, it is normally difficult or impossible to indicate the special features of the objects, see e.g. Wold et al (1983, 1987) and Wold (1985). To evaluate the information contained in a data matrix it is important to understand and to have knowledge of the system that is to be evaluated, knowledge of the software used, as well as a data analytical strategy to apply on the data. Multivariate modelling has been used extensively in several research fields, e.g. for mineral prospecting (Lindqvist and Lundholm, 1985), geochemical and geophysical exploration (Esbensen et al, 1987 and Lindqvist et al, 1987), and in predicting permeability and porosity from petrophysical logs (Esbensen and Martens, 1987).

The SIMCA software has been used in this study to evaluate and to model the relationships existing in the data matrix. Since the variables are correlated to a certain extent, the multivariate approach to data analysis will give more information than using single variable evaluation of the data matrix. For the data modelling there are two algorithms available

in the SIMCA software. One for Principal Component analysis (PC) and one for Partial Least Squares regression analysis (PLS). These two algorithms are used for different purposes as described below.

2.1 PRINCIPAL COMPONENT ANALYSIS.

In general, the goals for the multivariate data analysis using the Principal Component analysis method are the simplification of a data table, creating models, noise reduction, outlier detection, variable and object selection, correlation evaluation, classification, and prediction.

Figure 2.1 shows an example where some objects indicated with black dots have been measured for three different variables. Depending on different characters of the objects, they will of course be located in different places in the three dimensional space, according to the value of these variables.

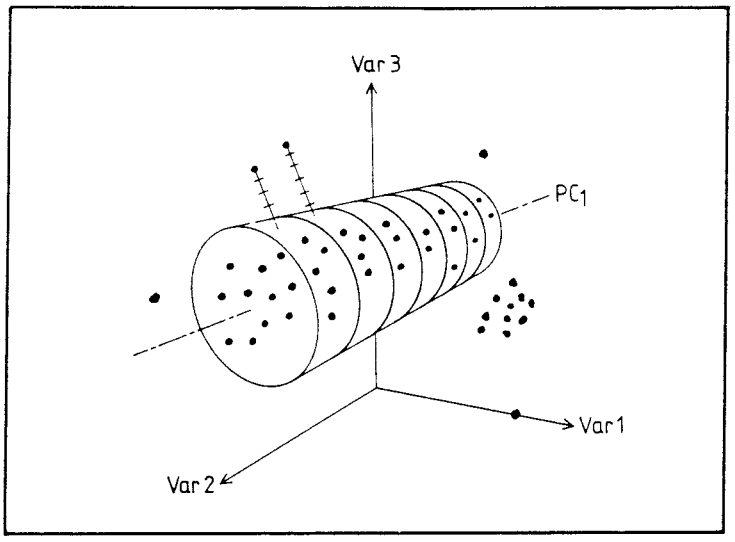

Fig. 2.1 Calculating the first principal component (PC1) from three variables. Outliers are datapoints outside the confidence volume.

The idea of the Principal Component analysis is to find a direction in the data space that will indicate typical features. These features are indicated by large variation in one direction or another. It is then a geometrical problem to find these directions in the data space. In most cases this direction will not coincide with any single variable. In Figure 2.1, the first principal component is indicated with PC1.

The second variable shows a high correlation with the first component (PC1), the main direction along the elongated volume surrounding the objects. Since the second variable is closely correlated with the first component, it is interpreted as an important variable for the data structure expressed by the first component.

The location of each object along this feature, the first principal component (PC1), is expressed as a numerical value, usually ranging between ±3 since it is expressed in terms of the standard deviation of the objects along the axis. This value is called the object score.

The next step in a Principal Component analysis is to find the second most important direction in the data space (PC2). This direction will be

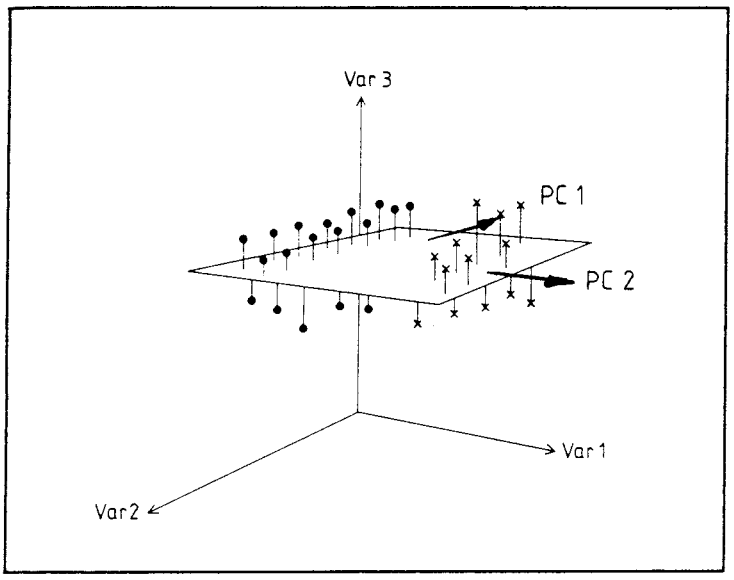

Fig. 2.2 A feature plane defined by the first two principal components. The object residuals to the plane are also indicated.

perpendicular to the first component and it will indicate the second most important feature. These two first principal components, PC1 and PC2, can bee seen as two vectors spanning up a feature plane as in Figure 2.2. On this plane all the objects can be projected.

The residual of each object to the plane surface can be explained as the object deviation from the two most important features. This residual could be interpreted in this example as a random noise component since it has a small and random variation. The residual variance, the noise, can then be excluded by using a two component model for the objects.

Using more variables than three will not be any problem for the SIMCA software. In fact, the program available at SGAB can handle up to 200 variables and 6000 samples with no problem. The program can also calculate as many principal components as the number of variables.

Having accepted that data will just be transformed to a new coordinate system in a geometrical manner, outlined by the data itself, the understanding of the transformation from the original variables to the principal components will not be difficult. By projecting the original variables along the components or the component planes, the data features are easily understood and expressed in the original variables.

It is important to notice that in the data analysis, the first component will show the most obvious information in the data matrix. Components that come up later indicate successively less important features in the data matrix but they may be important for the solution of the specific problem under study or the data analytical strategy. It is the person who has the knowledge of the problem that must decide the importance of each component.

If the components that are extracted are to indicate a main feature in the data, they must not be influenced by a few outlying samples. In this case, if outliers exist as in Figure 2.1, these must be excluded before running the Principal Component analysis. Otherwise the components can point in directions that are strongly influenced by single objects and they will not represent a dominating feature in the data matrix, but rather the feature of an outlying object.

By running the data through the Principal Component analysis several times, single variable outliers as well as multivariable outliers can be extracted from the data modelling. Having extracted all outliers, the resulting models will be robust and will not change significantly if some samples are excluded or included. This is a strong feature of the multivariate modelling approach.

To a model defined by one or several principal components a confidence volume is calculated. In one dimension the confidence volume is a cylinder-like neighborhood as in Figure 2.1, in two dimensions the confidence volume is a box and so on. The confidence volume is expressed in standard deviations giving approximately 95 percent of the objects inside of two standard deviations.

2.2 PLS AND PLS2 MODELLING.

In many data analytical problems some objects have been measured or analyzed for two different kinds of variables. The important objective may be to evaluate or model the relation between these two groups of variables.

Examples of such problems are measurements of a patients health and drugs used, chemical analysis of food and taste of the food, geophysical logging of the bedrock and corresponding hydraulic conductivity, geophysical logging of the bedrock and the relation to borehole radar intensity.

The difference between the two blocks are how the measurements are made or that they represent different features covering the same problem. In the PLS analysis the variables are divided into an X-block with the independent variables and the Y-block with the corresponding dependent variables.

The PLS method can be used to evaluate the relation between different variables and objects which is similar to the Principal Component analysis method. The advantage of using the PLS method instead of the Principal Component method is that the data structure for the Y-block is emphasized and the relation between the two blocks is obtained.

The PLS-analysis modelling procedure can be explained as a method to find the relation between two sets of variables measured on the same object. PLS-analysis

will extract the systematic variation from the X-variables that are most relevant for prediction of the variation of the Y-variables. In this manner the information in the Y-variables will be enhanced and brought forward.

The method can be compared with a stepwise linear regression technique between the X- and Y-variables, generalized as in Figure 2.3. Using the X-variables a relation model is obtained that will fit the Y-variables as well as possible.

In more detail, the connection between the two variable blocks is a least square linear regression technique between the object scores from the two different blocks of variables, X and Y. The location of each object along the component, p, in the X-block will be termed t and the corresponding location of the object along the component, q, in the Y-block will be termed u, as in Figure 2.4. The calculation of p and q is an iterative algorithm giving the information in the Y-block the possibility to adjust the p component in the X-block through the regression technique.

After extraction of the first component, the residual variation of both the X- and Y-variables will be used to model a second and a less important component in a similar manner as for the Principal Component analysis, and so forth for more components until a relevant model is obtained.

The SIMCA program contains two different types of the PLS algorithm, one called PLS used for models with just one Y- variable and one called PLS2 used for models with several Y-variables. There are no other differences in the algorithms.

Once a relational model between the two sets of variables is obtained the correlation between the variables and the objects are interpreted in the same manner as for the Principal Component analysis method. The resulting model can be used for two main objectives. The first objective is to evaluate the similarity between the two blocks and to obtain the relational model and to evaluate how much of the variation in the Y-block can be predicted by using the X-variables. The second objective will be to use the X-variables and the model to predict unknown Y-variables.

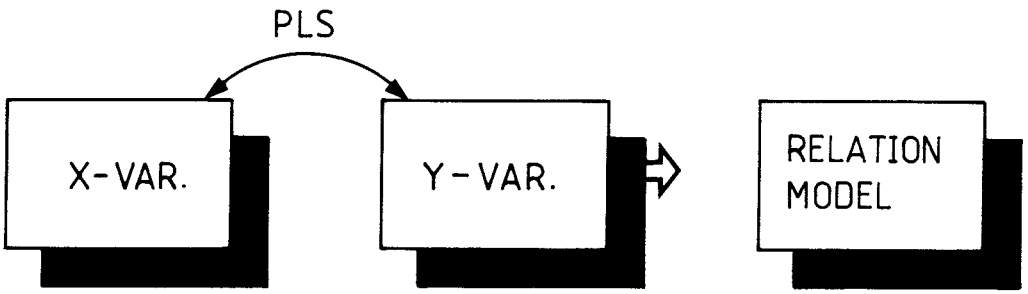

Fig. 2.3 Generalized description of PLS.

In PLS modelling as well as for ordinary Principal Component analysis classification, the distance of each object to the model is calculated which can be compared with the size of the confidence volume. Hence, outliers with a large distance to the model can be pinpointed and should be evaluated carefully. This feature of the SIMCA classification is an advantage, since new objects coming from other investigations can be compared with the model. If the objects are inside the confidence volume the objects are similar to the objects that have been used to create the model and the resulting interpretation of the new objects are comparable.

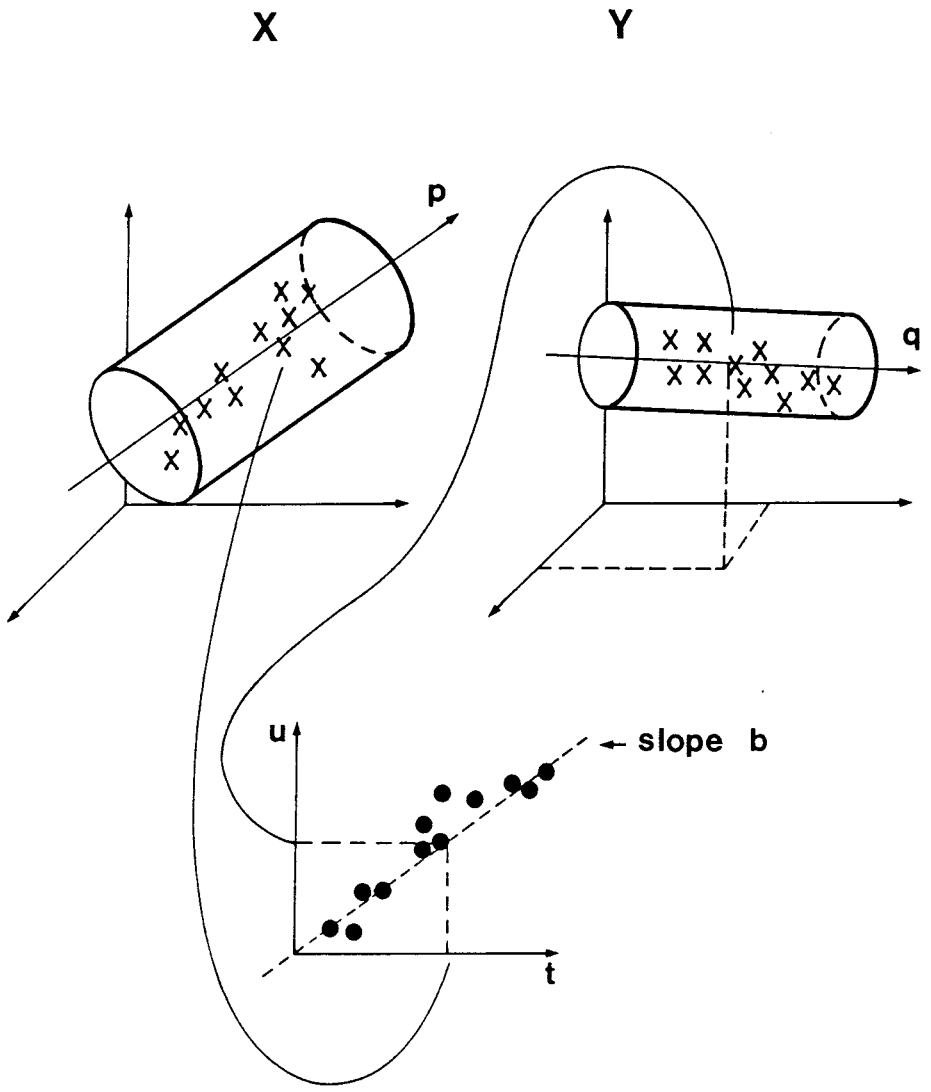

Fig. 2.4 The PLS method applied on 3 X and 3 Y variables. The regression technique applied on the principal component scores are used to connect the two variable spaces.

2.3 DATA ANALYTICAL STRATEGY.

In the data analysis it is important to define a data analytical strategy. The most important issue is to define what shall be achieved by the data analytical procedure. The selection of objects, variables and type of treatment must be defined depending on the type of problem. The data analytical strategy must then be specially designed for every situation.

Our objectives are to create a model from different variables measured in the borehole, in order to establish the correlation between radar intensity and other variables. The data analytical strategy was decided to be:

- present and evaluate the correlation structure between objects and variables by using the Principal Component, PLS and PLS2 method,
- delete outlying objects by evaluating the principal component score plots for the objects,
- delete variables that are not relevant for the problem,
- interpret the principal components to understand the features they represent,
- obtain acceptable models for each site.

3 AVAILABLE RAW DATA AND PREPARATION OF DATA FILES.

3.1 GENERAL.

The boreholes which have been used in the SIMCA analysis are listed in Appendix A. It should be noted that data from parts of the boreholes of Finnsjön have not been used since they have not been core mapped with the computerized core mapping system along their entire length, which is necessary for use with SIMCA.

The data types used in this report can be divided into the following main groups, namely: geophysical data, geological data, radar data, and hydraulic conductivity data. The geophysical data comprise variables 1-11 in the data type list below, the geological data comprise variables 12-49, radar data variables 58-64 and finally hydraulic conductivity variable 65.

All geophysical data, except for Stripa, is stored at and has been collected from the SKB database in Stockholm. The geophysical data from Stripa is stored at the Prime computer at SGAB, Luleå.

The geological data is stored at the SKB database, except for the Stripa data, which is kept at SGAB in form of floppy discs. However, all geological data used in this report has been read from floppy discs kept at SGAB since software was available for creation of fracture mineral frequency logs, rock type logs and rock border logs from the geological data.

The radar data used in the report has been collected from the reports on radar investigations listed in the references. Files containing depth of intersection and intensity of radar structures has manually been created from the reports and from reprocessed radar plots.

The hydraulic conductivity data has been collected from the SKB database in Stockholm, except for Stripa and parts of Finnsjön. The hydraulic conductivity data from the boreholes in Stripa was stored at SGAB in Uppsala. The hydraulic measurement in Stripa had been performed by the British Geological Survey. The hydraulic conductivity data concerning the boreholes in Finnsjön was partly collected from Andersson et al. (1988) and the input file was created manually.

The data types represent varying degrees of spatial resolution along the boreholes. In order to make data

comparable and hence also suitable for SIMCA analysis they have to be given a common resolution. In this project all data has been averaged or interpolated to represent 1 m sections in the boreholes.

3.2 DESCRIPTION OF VARIABLES USED.

The following list of variables is the basic model which has been used for all sites included in this study, with some exceptions. The variables used for the different sites are listed in Appendix B.

The geophysical borehole log methods used in this study can be divided into three categories, logs sensitive to lithology (gamma, single point resistance and susceptibility), logs sensitive to fracturing (single point resistance, normal resistivity, lateral resistivity, sonic and self potential) and logs sensitive to hydraulic properties (temperature gradient, temperature, salinity of borehole fluid, and resistivity of borehole fluid).

1 **Gamma log (GA)**, measures the natural gamma radiation of the rock. Generally, high radiation values correspond to acid rock (granite and pegmatite), and low values to basic rock. Also, infiltration of radon-charged water can cause very high gamma radiation levels in boreholes.

2 **Geohm log (GE)**, or single point resistance, measures the contact resistance between the probe and the borehole wall. The log is sensitive to changes in the resistivity of the rock in the wall normally caused by conducting minerals or fractures. The log gives high resolution of small fractures.

3 **Lateral resistivity log (LR)**, indicates the presence of fracture zones and conducting minerals by low values. Rock with few fractures is indicated by high lateral resistivity.

4 **Normal resistivity log (NR)**, indicates the presence of fracture zones and conducting minerals by low values. Unfractured rock is indicated by high normal resistivity.

Table 3.1 Basic model of variables used in the SIMCA analysis.

---

1. GA = Gamma log
2. GE = Geohm log or single point resistance
3. LR = Lateral resistivity log
4. NR = Normal resistivity log
5. SO = Sonic log
6. SP = Self potential
7. SU = Susceptibility log
8. QT = Temperature
9. QG = Vertical temperature gradient
10. QR = Borehole fluid resistivity
11. QS = Salinity
12. F0 = Fracture zone freq.0-15 deg.
13. S0 = Single fracture freq. 0-15 deg.
14. F1 = Fracture zone freq.16-30 deg.
15. S1 = Single fracture freq.16-30 deg.
16. F3 = Fracture zone freq.31-45 deg.
17. S3 = Single fracture freq.31-45 deg.
18. F4 = Fracture zone freq.46-60 deg.
19. S4 = Single fracture freq.46-60 deg.
20. F6 = Fracture zone freq.61-75 deg.
21. S6 = Single fracture freq.61-75 deg.
22. F7 = Fracture zone freq.76-90 deg.
23. S7 = Single fracture freq.76-90 deg.
24. F9 = Fracture zone freq.0-90 deg.
25. S9 = Single fracture freq.0-90 deg.
26. C9 = Fracture freq. in crushed zone 0-90 deg.
27. FS = Total fracture freq.0-90 deg.
28. Ca = Calcite
29. Fe = Fe-oxide
30. Hm = Hematite
31. Py = Pyrite
32. Ep = Epidote
33. Cl = Chlorite
34. xx = Rocktype
35. xx = "
36. xx = "
37. xx = "
38. xx = "
39. xx = "
40. xx = "
41. xx = "
42. xx = "
43. xx = "
44. xx = "
45. xx = "
46. xx = "
47. xx = "
48. xx = "
49. rb = Lithological contact
50. ZZ = Vertical depth

Table 3.1 Continued

51. De = Density of core
52. Po = Porosity of core
53. Su = Susceptibility of core
54. Qv = Q-value of core
55. Re = Remanence of core
56. Rs = Resistivity of core
57. Ip = IP of core
58. RI = Radar intensity
59. A1 = Radar angle 0-10 deg.
60. A2 = Radar angle 11-20 deg.
61. A3 = Radar angle 21-30 deg.
62. A4 = Radar angle 31-45 deg.
63. A6 = Radar angle 46-60 deg.
64. A9 = Radar angle 61-90 deg.
65. HC = Hydraulic conductivity

---

5 **Sonic log (SO)**, records the time required for a compressional sound wave to travel between the transmitter and the receiver. The log is sensitive to fractures. The travel path for the elastic waves is near to the borehole wall and the tool is mainly sensitive to features close to the borehole wall. High sonic travel times indicate highly fractured rock. However, travel time of the recorded sound wave might oscillate strongly between low and high values when passing through fractured sections due to cycle skipping, i.e. individual values picked out might give misleading information about the character of the rock.

6 **Self potential (SP)**, gives information about conducting minerals, ion concentration variations, and groundwater flow in or out of the borehole. The occurrence of conductive minerals can cause large SP anomalies, while the other factors generally cause smaller anomalies.

7 **Susceptibility log (SU)**, measures the induced magnetization. The susceptibility of a rock is dependent on the type and amount of magnetic minerals present in the rock, i.e. mainly magnetite or pyrrhotite.

8 **Temperature log (QT)**, shows the temperature of the borehole liquid. Water flow along the borehole can result in a water temperature different from the temperature of the surrounding rock. Waterflow in the

borehole can be represented by abrupt changes of the temperature curve. Changes to both high and low temperature might occur. The evaluation of the temperature log in the multivariate data analysis has to be treated carefully, since both high and low values might indicate waterflow.

9 **Vertical temperature gradient (QG)**, exhibits the change of the temperature in degrees/kilometre. High magnitude of the temperature gradient indicates waterflow. However, water inflow may be associated with both large positive and negative temperature gradients which makes this variable less suitable for multivariate data analysis.

10 **Borehole fluid resistivity (QR)**, is measured by a five electrode system placed inside a plastic tube. It is used together with the temperature log to determine the salinity of the borehole fluid. High resistivity indicates low salinity.

11 **Salinity (QS)**, is a result from simultaneous measurement of temperature and borehole fluid resistivity. The salinity log can indicate waterflow between intersecting zones and the open borehole. The waterflow can be indicated by either low or high salinity. The evaluation of the log has to be treated carefully since both high or low values can indicate waterflow and it is therefore difficult to use the log in multivariate data analysis.

12-27 **Different features of fractures**. The fracture frequency from the core mapping used in this study, has been divided into four main groups. The different groups of angles to core axis (12-23) have not been used, and are hence not included in this description.

24 **Fracture zone frequency, 0-90 degrees (F9)**, contains all coated fractures in sections with more than 10 coated fractures per meter in the core. All coated fractures are included without consideration to the angle to core axis.

25 **Single fracture frequency, 0-90 degrees (S9)**, contains all coated fractures in sections with less than 10 coated fractures per meter. All coated fractures are included without consideration to the angle to core axis.

26 **Fracture frequency in crushed zones, 0-90 degrees (C9)**, contains all coated fractures in sections with more than 50 coated fractures per meter. All coated fractures are included without consideration to the angle to core axis.

27 **Total fracture frequency, 0-90 degrees (FS)**, contains the total sum of all coated fractures without consideration to the angle to core axis.

The six variables containing frequency of fracture minerals are derived from the core mapping. The same set of minerals have been used for all investigated sites. A more detailed discussion concerning the use of fracture minerals in this study can be found later in the report.

28 **Calcite (Ca)**, a common and widespread fracture mineral.

29 **Fe-oxide (Fe)**, a fracture mineral which is thought to occur at sections with waterflow, hence indicating waterflow.

30 **Hematite (Hm)**, a fracture mineral which has a lower degree of oxidization than the Fe-oxide minerals.

31 **Pyrite (Py)**, the most common and widespread of the sulfide minerals. Occurs often together with many different minerals.

32 **Epidote (Ep)**, is an alteration product of ferromagnesian minerals and is a common and widespread fracture mineral.

33 **Chlorite (Cl)**, is an alteration product of ferromagnesian minerals and is a common and widespread fracture mineral.

34-48 **Rock type**. The rocktype variables are derived from the original core mapping and they differ slightly between the investigated sites. Empty variables are denoted dummies and are used as reserves. Rock types used at each site are defined in Tables 4.1, 5.1, 6.1, 7.1 and 8.1.

49 **Lithological contact (rb)**. This variable marks the occurrence of different rock types or degree of tectonization adjacent in the core. Borehole radar is thought to be sensitive for changes in rock type.

50 **Vertical depth (ZZ)**, is not activated in this study, since borehole radar is not considered to be dependent of depth.

51-57 **Geophysical measurements on core samples**, are not activated in this study because they comprise only a few measurements in every cored borehole.

58 **Radar intensity (RI)**. This is one of the most important variables in this study. It describes the interpreted intensity of the radar reflections in a scale where 0= no radar intensity (used as background values), 1= low intensity, 2= medium intensity, and 3= high intensity. The classification of radar intensity is qualitative.

59-64 **Radar angles to borehole axis (A1-A9)**. The angles of radar reflections to borehole axis have not been used in this study, because it is considered to be without interest for correlation of radar reflections to other borehole investigations.

65 **Hydraulic conductivity (HC)**. This variable is considered to be an important feature to investigate regarding the correlation to borehole radar reflections. The hydraulic conductivity is not used at sites where the measurements only comprised 10- or 20 m-sections.

There has been a desire to investigate if fracture minerals act as indicators of waterflow in the boreholes and can be correlated to radar intensity. Also, there has been a desire to investigate if the SIMCA analysis method shows any correlation between the presence of clay minerals in the boreholes and radar intensity. During preparation of the datafiles a number of difficulties were encountered due to that different data collection procedures had been used at the various sites.

It was found that clay minerals had been mapped in the core log almost exclusively as "LM", i.e. light (bright) mineral. However, this group includes many

unidentified minerals besides clay minerals. Often the mapping crew has made a special comment that a particular fracture contained clay minerals. In some boreholes the abbreviation "LM" is not present at all and only a comment in the core log indicates that clay minerals are present on a particular fracture surface. Only one borehole at the Finnsjön study site has been mapped with the use of a special code for clay minerals (CM). The SIMCA software works with certain positions in the core log files and there is a need to use predefined two-lettered mineral codes. An adjustment of the core logs to include clay mineral information and to fit the SIMCA software would include an extensive preparation, including remapping of the cores, which was considered impossible to include within the framework of this study.

The presence of Fe-oxide in the fractures is considered as being a possible indicator of waterflow through the fractures (Tullborg, 1986; Andersson and Lindqvist, 1988). The mapping of Fe-oxide in the core logs from the different sites is much more consistently done than for the clay minerals. At the Klipperås study site Fe-oxide and hematite were not separated in the boreholes KKL01, KKL02, KKL03, KKL04, KKL05 and KKL07. However, in the core mapping of the remaining boreholes, Fe-oxide and hematite were identified specifically. This resulted in a special PLS-analysis for the boreholes where Fe-oxide and hematite were identified as separate items. For the boreholes at the Finnsjön study site Fe-oxide is mapped together with hematite. In the boreholes at the Saltsjötunnel site Fe-oxide has been mapped as a specific mineral. At Stripa only hematite was encountered in the core logs, but it was removed during the process of deleting outliers in the data set used for the SIMCA analysis. Fe-oxide has been mapped as a specific fracture mineral at the Ävrö study site. Hence, it was possible to use Fe-oxide and hematite in the SIMCA analysis only for some of the sites.

Calcite, chlorite, pyrite and epidote have been mapped in the same way in all boreholes at all sites without exceptions. They are included at all sites to the extent they occur in the core logs. The exception is Stripa where only epidote is included.

The resolution of the hydraulic single hole tests differ between the sites. The hydraulic conductivity was not included in the analyses of the Klipperås data, as it was measured with 20 meter section length. Creation of 1-meter sections from the 20-meter sections would imply that the same value would be given to all 1-meter sections within the 20-meter

section. This would cause a smoothening and loss of resolution of the hydraulic conductivity data which would have made it impossible to use them in the SIMCA analysis.

The hydraulic single hole tests at Finnsjön were performed with 2-meter section length from which 1-meter sections were created by giving the same value to the two one meter sections. The hydraulic single hole tests at the Saltsjötunnel site were performed with 10-meter section length and partly with 2-meter section length. 1-meter sections were created by giving the same value to the two 1-meter sections. In Stripa the hydraulic single hole tests were performed more irregularly. There was a variation of used section length between 2 meter and 13 meter. The wide sections often overlap each other with a couple of meters. Measurements with small section length were performed afterwards at selected intervals in the boreholes where high hydraulic conductivity had been measured in the large section length measurement. In order to obtain a smoother distribution and avoid the large steps between the small and large section length measurement, 1-meter sections were created by interpolation between the different measurements. The hydraulic conductivity measurement at Ävrö in borehole KAV01 between 22-438 m were performed with 2-meter section length while 10-meter section length was used between 20-720 m. In the SIMCA analysis only data from the parts of the boreholes with the 2-meter measurement was used. 1-meter sections were created from the 2-meter sections by giving the same value to the two one meter sections. In the SIMCA analysis borehole KAV03 was not included since all hydraulic measurement were performed with 10-meter section length.

3.3 RADAR MEASUREMENTS.

In order to maintain a qualitatively similar and comparable status of the different radar measured boreholes used in this investigation, most of them have been reprocessed and partly reevaluated.

The radar measurements in the boreholes are normally performed in 1 meter steps. Since there is some uncertainty in the interpreted intersection of the radar reflection with the borehole, each intersection point has been given an interval 5 meters wide with the interpreted intersection in the middle of the interval. Some of the 1-meter sections within the 5-

meter interval occur as outliers in the object plots and have been excluded in the analysis.

The intensity of each radar reflection has been given a value from 1 to 3, where 1 indicates low intensity, 2 moderate intensity, and 3 high intensity. It should be noted that the intensity of the radar reflections in singlehole radar measurements is affected not only by the reflecting media, but also to a high degree by the relative orientation of the reflecting media to the borehole. This means that planar structures with a large angle to the borehole axis, e.g. 80-90 degrees, occur as weak reflections even if they might have properties very favorable for detection by borehole radar. With a more favorable orientation to the borehole the intensity would have been stronger.

The intersection angle of the radar reflections are of interest only in the geometrical description of the geological and tectonical model of an actual investigation site. The radar angles are not relevant parameters in a correlation between radar intensity and other borehole data. However, the radar angles were used in a special SIMCA analysis of the Klipperås data in order to evaluate the influence of borehole direction in relation to the orientation of the major structural features.

3.4 CREATING 1-METER SECTIONS.

To be able to statistically correlate and integrate different kinds of variables in the borehole the original variables must be transformed to an equal measurement density or section length. In our case the section length is selected to 1 meter. Since data is measured and collected with several different methods each having a different data density resolution and penetration depth in the surrounding rock, different methods are used for representation of the variables in one meter sections. Five different methods are used:

-**Averaging** the measured values if there are several measured values within each 1-meter section. Usually this method is convenient when the measuring method used has a small depth of investigation giving a highly varying value within the 1-meter section. This method is used for e.g. the gamma log which has one data value every 10 centimeters.

-**Linear interpolation** between surrounding samples. This method is used for variables that have a large investigation depth and the separation between measurement points is higher than 1 meter. This method is used e.g. for the borehole fluid salinity which has a 5 meter point separation as well as for the temperature which has a point separation slightly larger than 1 meter due to the depth correction for the stretching of the logging cable. The method was also used for the hydraulic data from Stripa.

-**Binary coding** is used to indicate the presence or absence of a specific variable. E.g. each rock type is set to one single variable and coded by using "1" if the section contains the rock type and "0" if the rock type is not present.

-**Set the section value** to the value from a single point measurement within the section, even though that the measurement represents a value from a single fracture, fissure or similar. This type is used e.g. for the parameters from the core logging.

-**Set a missing value code** to the section if the above methods can not be used to assign a value to the section, or the parameter has not been measured.

This way of transforming the original data to a similar section length is necessary but it will introduce a smoothing effect and a partially fictive correlation. Since SIMCA is used as a tool to separate the information in each single value into two parts, existing correlation and random noise variations, the smoothing effect is partially handled by the SIMCA method.

There are also other effects that must be considered i.e. the tension of the logging cable that increases with the depth and is different for different methods. The fact that some methods are related to the ground level and other to the top of the casing for the borehole must also be treated.

For some sections, e.g. the rock type coding, the interface between different rock types is often located within a 1-meter section. In this case the dominating rock type will be assigned to the section. In some cases a very thin dike, completely within a 1-meter section, may disappear. This kind of smoothing may cause that other variables will not correlate as they should. These sections may appear in the object plots as outliers.

The depth of the midpoint of the first section used is set to 1.5 meter for all boreholes and all

variables. The geophysical logging variables are used as the variable controlling the modelled depth interval of each borehole. For the other variables a missing value code is used to fill up the entire borehole lengths. The borehole intervals used in this report are presented in appendix A.

Averaging within the section is used for the following variables: gamma (GA), geohm or single point resistance (GE), sonic (SO), self potential (SP), susceptibility (SU), lateral resistivity (LR), and normal resistivity (NR) (cf. Table 3.1).

Linear interpolation is used for the following variables: temperature of borehole liquid (QT), temperature gradient (QG), resistivity of borehole fluid (QR), and salinity of borehole fluid (QS), and hydraulic conductivity (HC) from Stripa.

Set the section value from a measurement within the section. For the geophysical variables where the measurements are located at the border between two sections, the value is assigned to both neighboring sections. This method is used for the following variables: single fracture frequency (S9), fracture zone frequency (F9), fracture frequency in crushed zones (C9), total fracture frequency (FS), calcite (Ca), Fe-oxide (Fe), hematite (Hm), pyrite (Py), epidote (Ep), chlorite (Cl), radar intensity (RI) and hydraulic conductivity (HC).

Binary coding is used for the rock types and lithological contacts (rb).

3.5 DESCRIPTION OF PRESENTED RESULTS.

To exemplify how to read and interpret the information from the SIMCA-plots, a variable plot from Principal Component analysis of data from Klipperås will be presented in detail.

The variables shown in the variable plots consist of different geophysical logs, geological features, hydraulic conductivity and radar intensity. The definitions of all variables are presented in chapter 3.2. Figure 3.1 is an example of two logs which are closely associated to each other, namely fracture frequency and normal resistivity. The highest value of the fracture frequency log can be found at 50 m

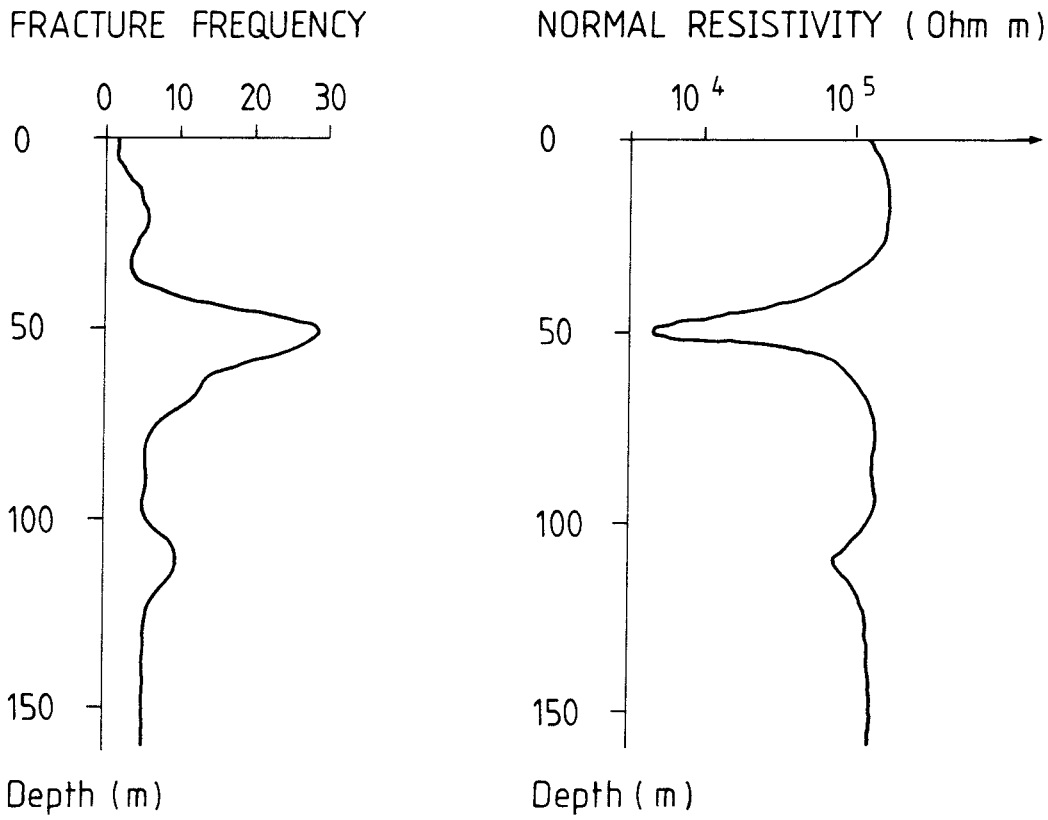

Fig. 3.1 An example of fracture frequency log and normal resistivity log in a fictive borehole.

depth in the borehole and the lowest value of the normal resistivity log is found at the same depth. We note that low values of fracture frequency correspond to high values of normal resistivity and vice versa. This implies that there is a strong negative correlation between the two logs. In the SIMCA variable plot the two logs fracture frequency and normal resistivity are represented by the abbreviations FS and NR, respectively. Figures 3.2 and 3.3 are examples of a variable plot. In a Principal Component analysis the two logs, or variables as they are called in the analysis, would be plotted on each side of the component center. The point where the variable is plotted always represents high values of the log or the presence of a binary coded variable, as is in the case of minerals, rock types etc. On a fictive line starting in the variable point and passing through the center point there is a mirror point representing low values of the log. The mirror point is situated at the same distance from the center point as the variable point. In Figure 3.3 there is an example of a mirror point to the variable fracture frequency (FS). The mirror point always represents low values of the log method or the absence of the variable, if it is represented as a binary coded variable. The mirror points are not shown in the plots. The mean value of the log is found at the center point.

From the example we can learn that the plotted variable point FS represents high fracture frequency and the plotted variable point NR high resistivity. The mirror point to NR, which represents low values of normal resistivity, is situated close to the point FS. The mirror point to FS, which represents low values of fracture frequency, is situated close to the point NR. Thus, it can be said that the variables exhibit a negative correlation to each other.

Figures 3.2 and 3.3 are examples of variable plots from Klipperås. A variable plot always consists of two principal components plotted together. Principal Component 1 (PC1) is always along the horizontal axis, while Principal Component 2 (PC2) and the following components, always are along the vertical axis. To read the content of Principal Component 1, all variable points have to be projected to the horizontal line passing through the center point, (Fig. 3.2). In our case the description of Principal Component 1 looks like this:

Negative side		Positive side
NR GE LR GA gr	++	SU SO SP RI do S9 rb ge F9 FS

Legend

++	Center point
GA	Gamma log
GE	Geohm log or single point resistance
LR	Lateral resistivity log
NR	Normal resistivity log
SO	Sonic log
SP	Self potential
SU	Susceptibility log
F9	Fracture zone frequency
S9	Single fracture frequency
FS	Fracture frequency
gr	Granite
do	Dolerite
ge	Greenstone
rb	Lithological contact
RI	Radar intensity

Note that variables with the longest distance from the center point in the plots are placed as far to the left or to the right as possible in the tables.

In the evaluation of the principal components it is important to understand that variables situated close to the center point are of less importance, if any importance at all, in the description of the specific principal component. These variables do not take part of the definition of the principal component and they can be left out of the description. In our case Principal Component 1 should look like this after deleting variables close to the component center:

Negative side		Positive side
NR GE LR GA gr	++	ge F9 FS

It should be noted that the terms "negative" and "positive" side is used in order to define on which side of the component center the variables occur. The terms do not have any other significance. One could use other suitable term instead, for example "left" or "right", "red" or "blue", "east" or "west" etc. However, the relative position of the variables is of interest.

It is of interest to know how much of the data (objects) that are included in the description of the different principal components. The value of

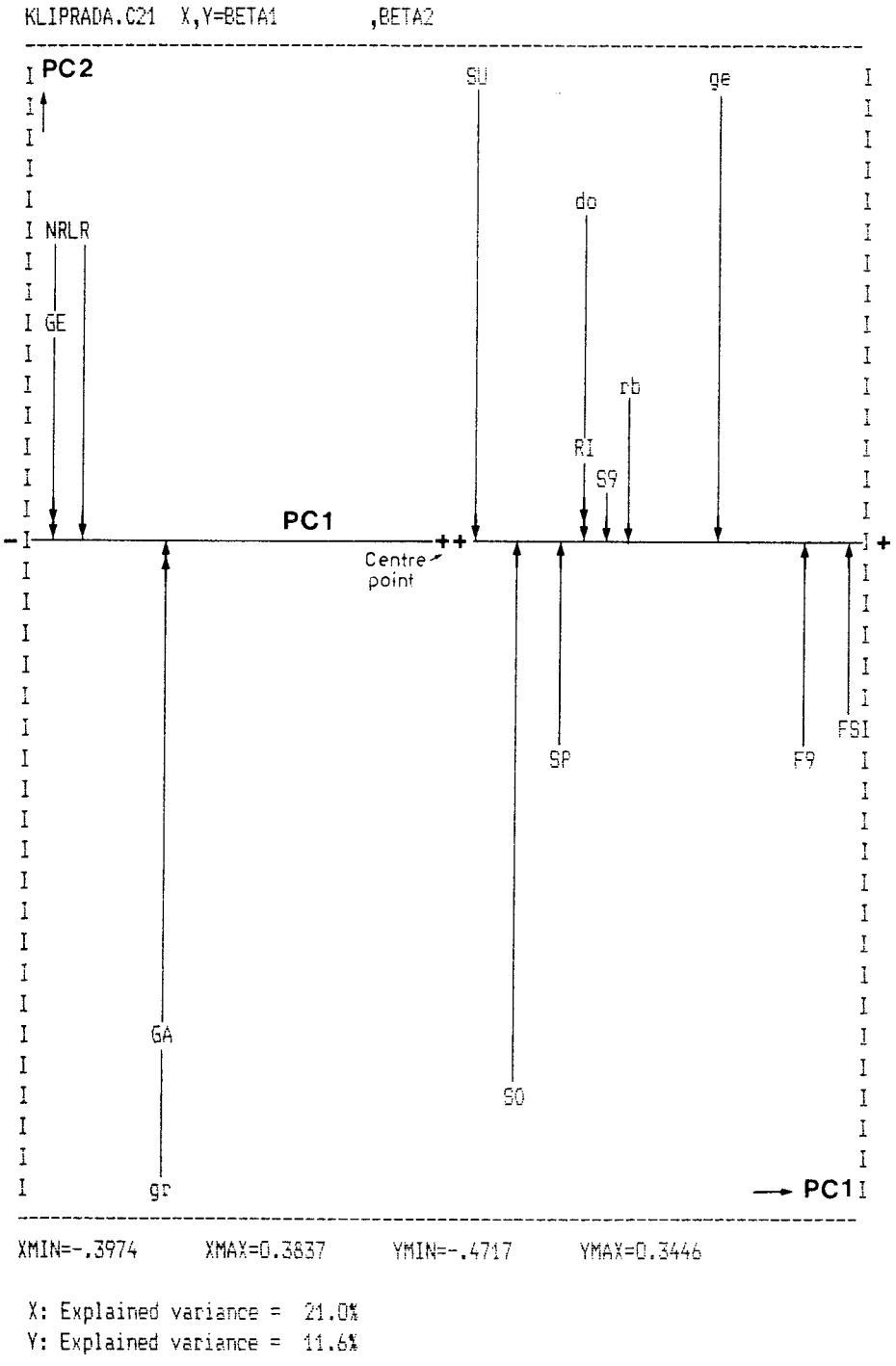

Fig. 3.2 Variable plot of Principal Component 1 and 2 from the Principal Component analysis of data from Klipperås. Solid lines with arrow indicate projection of variables.

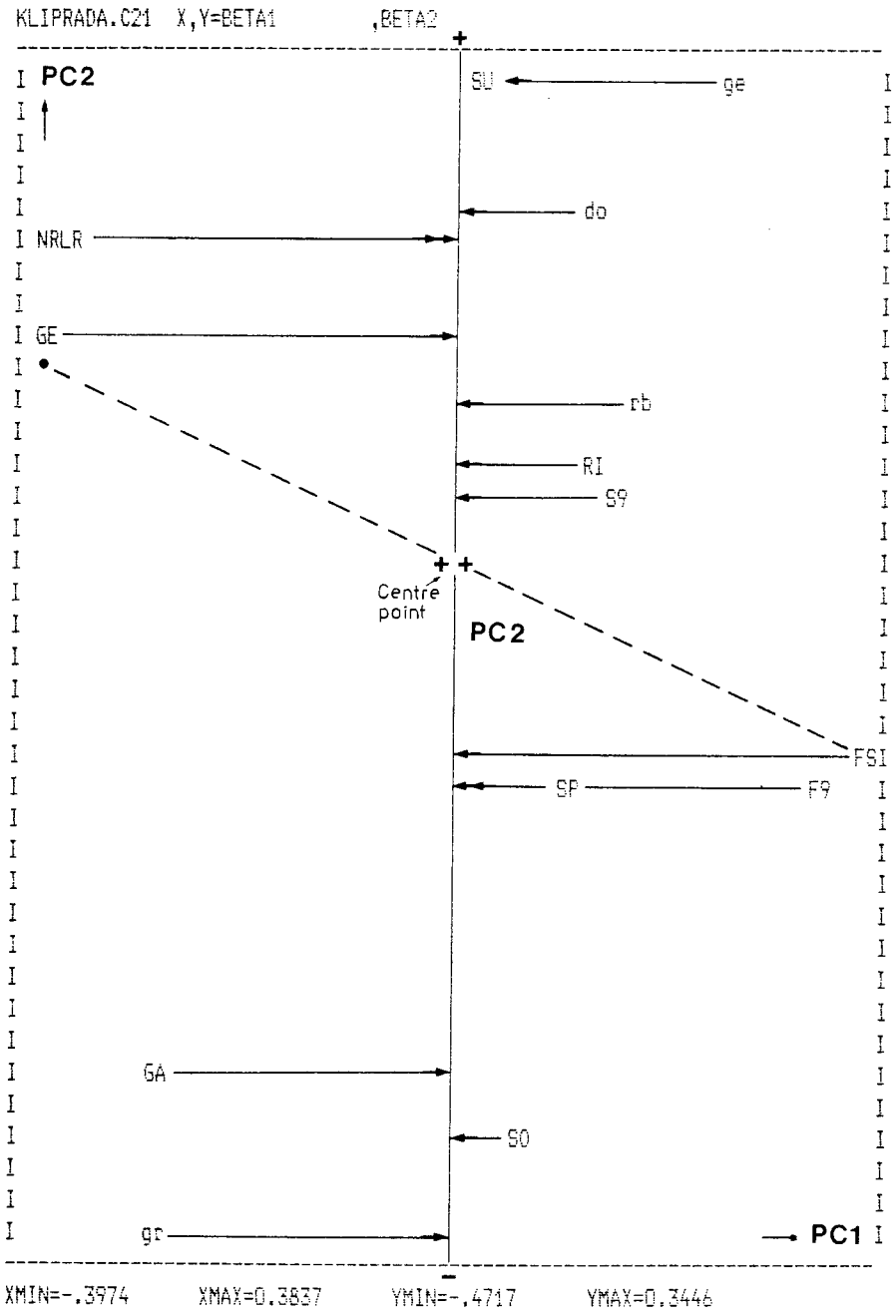

Fig.3.3 Variable plot of Principal Component 1 and 2 from the Principal Component analysis of data from Klipperås. Solid lines with arrow indicate projection of variables. Broken line indicates the fictive distance between the variable point FS and its mirror point. Filled circle indicates mirror point.

explained variance indicates this. In our case the value of explained variance for Principal Component 1 is 21.0 %. A theoretical value of 100 % is of course the highest. Principal Component 1 is the most important of the components and the degree of importance decreases with increasing component number.

If we continue with Principal Component 2 in Figure 3.3, we have to project the variables on the vertical y-axis which is passing through the center point. If we exclude the variables close to the component center, the description of Principal Component 2 is:

Negative side		Positive side
gr SO GA	++	LR NR do ge SU

At this stage we have defined the principal components, and now we can start to evaluate them. If we begin to look at Principal Component 1 on the negative side we find the variables normal (NR) and lateral resistivity (LR), single point resistance (GE), and gamma (GA), all of them representing high values. Also, we have the binary coded variable granite (gr) showing that granite is present on this side of the principal component. Furthermore, the variables fracture zones (F9) and fracture frequency (FS) which are situated with high values on the opposite side, the positive side, have mirror points representing low values on this side. The variables on the negative side together with the mirror points describe low fractured granite. If we look at the positive side of Principal Component 1 we can see the variables fracture frequency (FS) and frequency of fracture zones (F9), both representing high values. Also, the binary coded variable greenstone (ge) occurs showing the presence of greenstone on this side. The mirror points to the variables situated on the opposite side provides us with more information. For example, the mirror points to normal (NR) and lateral (LR) resistivity represents low values, thereby indicating fractured rock. The variables on the positive side together with the mirror points representing low values describe fractured greenstone. Let us continue with evaluation of Principal Component 2. Firstly, the explained variance shows that the Principal Component 2 is described by 11.6 % of the data, which is nearly half the amount of data in Principal Component 1. On the negative side there are the variables granite (gr) and gamma (GA) together with sonic (SO). The mirror points to lateral (LR) and normal (NR) resistivity indicates fractured rock at this side. Thus, the

negative side of Component 2 describes fractured granite. On the positive side the presence of the variables lateral (LR) and normal (NR) resistivity together with dolerite (do) and greenstone (ge) describes low fractured rock. The variable susceptibility (SU) indicates that the rock is magnetic, probably the dolerite. The mirror points to the variables on the opposite side is of less interest in this case. It can be said that the positive side of Principal Component 2 describes low fractured dolerite and greenstone.

Some guidelines for interpretation can be made after this detailed presentation of Principal Components.

* The variables have to be projected on the line representing the actual principal component to be read easily.

* It is of importance to use variables situated at long distance from the centerpoint.

* It is of importance to use the mirror points to the variables, since they provide us with important information about negative correlations.

* The value of the explained variance is useful when deciding how many principal components in the actual analysis which can be used.

* It is always the first principal component that includes largest amount of data. Increasing principal component number will give decreasing value of explained variance, i.e. decreasing content of data.

In this report three variations of SIMCA-analysis have been used.

* PC (Principal Component analysis).
* PLS (Partial Least Squares regression analysis).
* PLS2 (Partial Least Squares regression analysis).

A detailed presentation of the three variations is given in chapters 2.1 and 2.2. The Principal Component analysis allows all included variables to work independently. Thus, the Principal Component analysis gives a general description of the examinated material. In the PLS-analysis the variable radar intensity (RI) is put into the Y-block (Fig. 2.3) as a dependent variable, and the remaining active variables are put into the independent X-block. By doing this a relation between radar intensity (RI) and all active variables is obtained. The PLS2-analysis differ from PLS-analysis only by

allowing input of more than one dependent variable into the Y-block. In our case radar intensity (RI) and hydraulic conductivity (HC) are put together into the Y-block, and the remaining active variables are put into the independent X-block. By doing this the relation between all active variables to both radar intensity and hydraulic conductivity is obtained. One exception from this is the data analysis from Klipperås where radar angle and radar intensity are tested together in the Y-block.

4 KLIPPERÅS STUDY SITE.

4.1 GEOLOGICAL OVERVIEW.

A geological and tectonic description of the Klipperås study site is presented by Olkiewicz and Stejskal (1986). The overall distribution of rock types in the boreholes within the study site according to the core mapping (Egerth, 1986) is summarized in Table 4.1, together with abbreviations used in the SIMCA analysis.

The dominating rock type is granite, which is normally grey to red and coarse to medium grained. A few thin dykes of aplite and pegmatite also occur within the granite. Several porphyry dykes of acidic to intermediate composition occur within the area. According to the geological model the strike of the porphyry dykes is WNW-ESE and the dip is 75-90 degrees towards south, i.e. more or less vertical. Different types of porphyry dykes occur having different petrophysical properties. Greenstone is most frequently observed at the margins of the porphyry dykes with strike and dip directions parallel to the porphyry dykes. Dolerite dykes have a strike of NNE-SSW and the dip is 65-90 degrees to the east, while other mafic dykes have a strike of N-S and the dip is 80-90 degrees to the west, i.e. more or less vertical.

Deformed rock intervals consisting of tectonized, brecciated, and mylonitized rock occur rather frequently in the boreholes. Alteration occurs within the deformed intervals or in discrete zones in the undeformed granite. According to Sehlstedt and Stenberg (1986) several types of alteration have been observed; chloritization, red colouring of the rock mass and along fractures, hematite stained fracture surfaces and fractures coated with e.g. hydrate iron-oxides.

The location of the fracture zones and mafic dykes together with the borehole locations and their direction is shown in Figure 4.1.

Singlehole radar measurements with a center frequency of 22 MHz were performed in ten out of fourteen boreholes. Radar measurements with a center frequency of 60 MHz were also performed in six of the boreholes. Vertical Radar Profiling (VRP) were performed in six of the ten measured boreholes. A total of 7 857 m of singlehole radar reflection measurements and 834 m of VRP measurements were made at the study site.

All important fracture zones previously derived from core mapping and logging data were discovered during the analysis of the radar measurements. From the large scale pattern of the radar maps it is deduced that most radar reflecting structures are oriented in E-W and have a vertical or subvertical dip. Greenstone constitute the largest portion of these structures and can be considered as extensive structures and do not constitute isolated fragments in the rock mass. Dolerite dikes are oriented in a northerly direction.

A majority of the interpreted radar reflecting structures intersecting the boreholes are coupled together with low resistivity. All greenstones and mafic dikes (dolerite and basalt) which are characterized by low resistivity give rise to radar reflections. Most of the porphyries do not have a contrast in resistivity to the surrounding granite and they gave, as a consequence, only weak or no radar reflections at all. Wider fracture zones and other units with a very low resistivity give a strong loss in radar pulse energy. One example from a 22 MHz radar measurement from part of the borehole KKL14 is presented in Figure 4.2.

The borehole radar measurements gave a valuable contribution to the evaluation of the geological, geophysical and hydrogeological conditions at the Klipperås study site. The borehole radar results confirmed the tectonical model and also additional complementary information for construction of the three-dimensional model of the site.

Table 4.1 Rock type distribution in the boreholes at the Klipperås study site.

Rock type	Percentage	Abbreviation used in SIMCA
Granite	85.0	gr
Greenstone	7.0	ge
Porphyry dike	5.5	pp qp
Mafic dike (dolerite and amphibolite)	1.5	do am
Aplite and pegmatite	1.0	ap pe
	100.0	

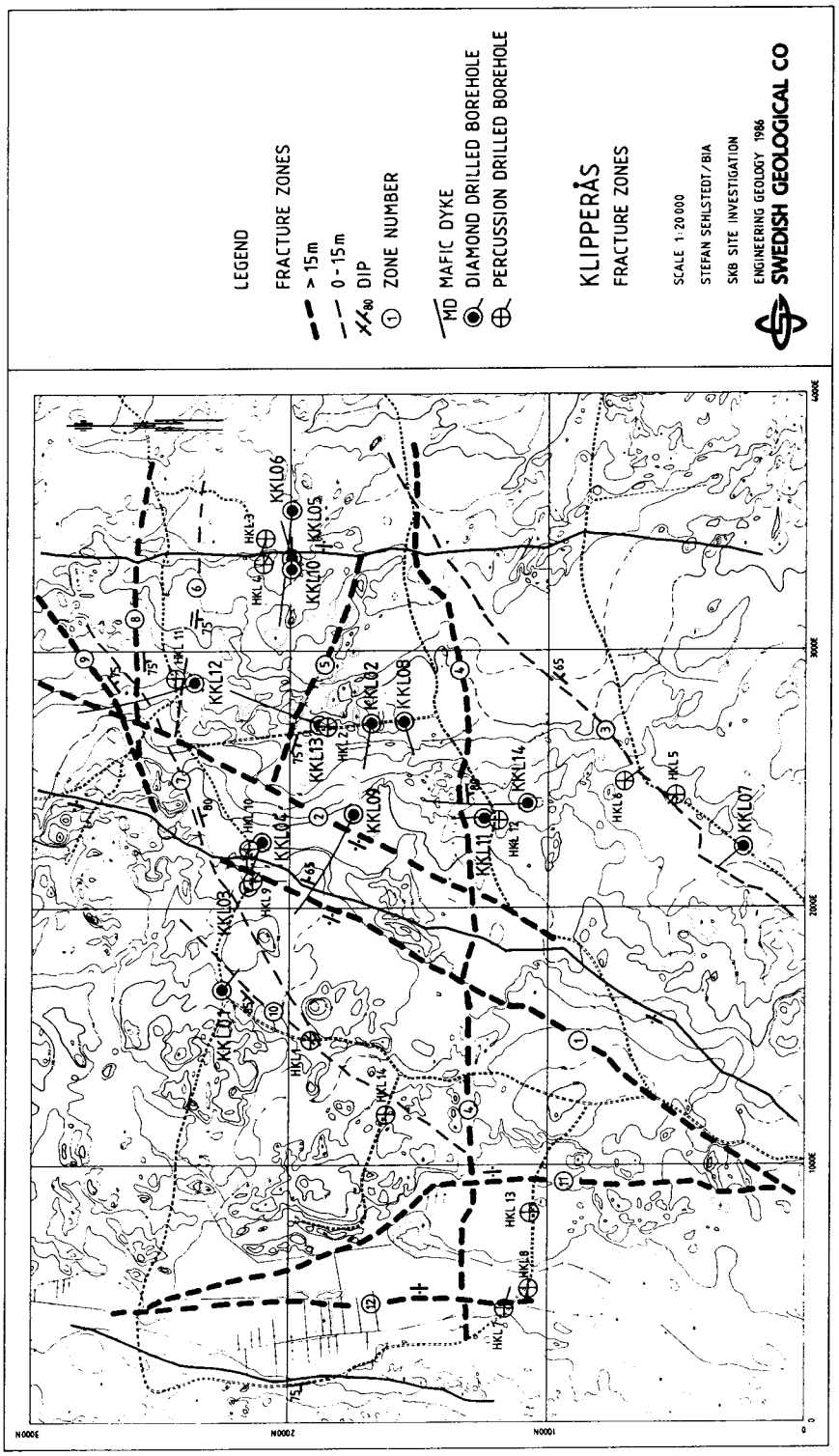

Fig. 4.1 Borehole location, fracture zones, and mafic dykes within the Klipperås study site.

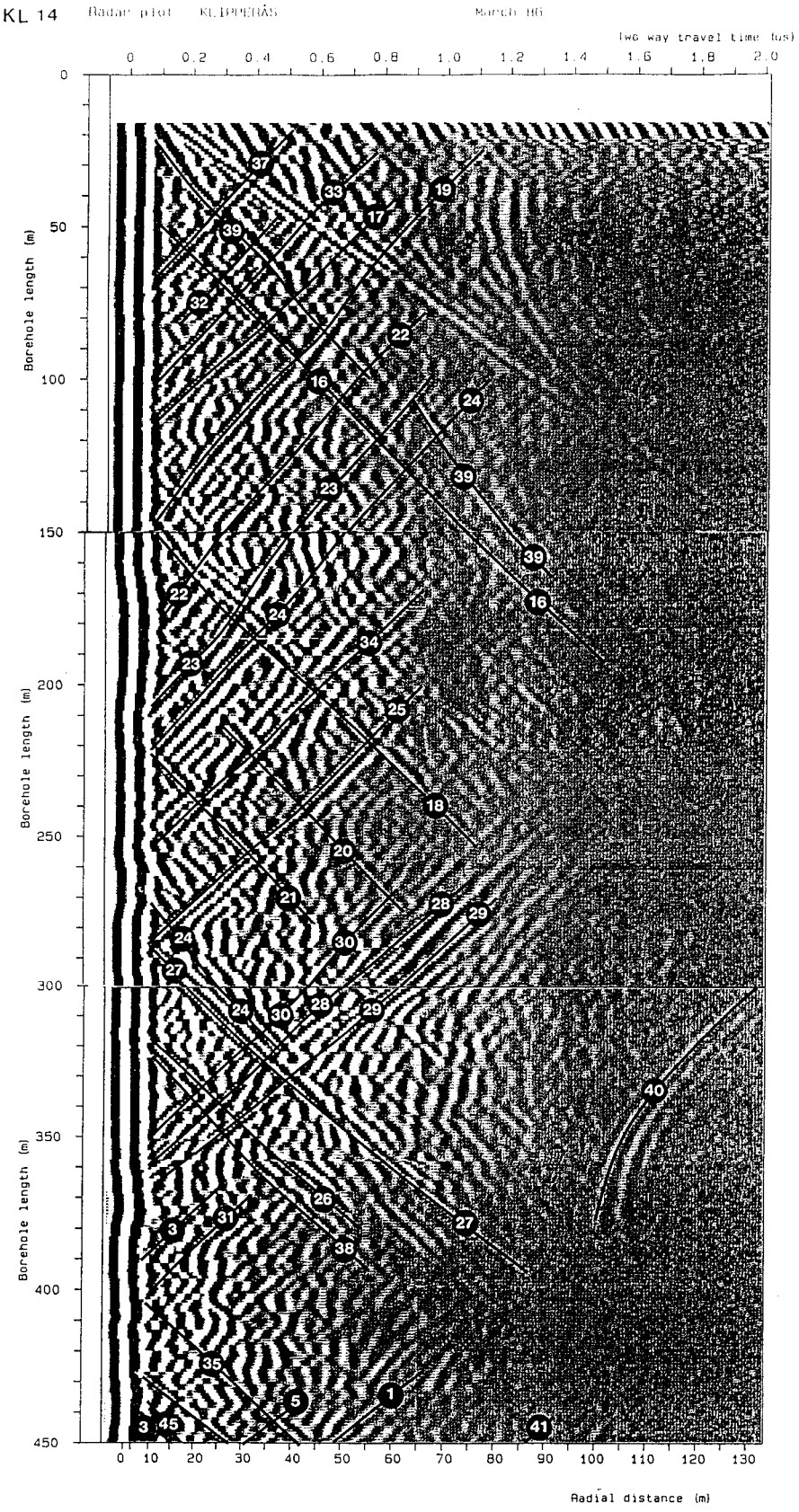

Fig. 4.2 Radar map for the borehole KKL14 between 0-450 m (22 MHz).

4.2 PRINCIPAL COMPONENT ANALYSIS OF THE DATA FROM KLIPPERÅS.

The Principal Component analysis of data from Klipperås shows that variables representing fracture frequency and different features of fracturing together with normal and lateral resistivity have an important role in the components. The components and the variables are presented in Table 4.2. The first components show a distinct division between low fractured and highly fractured rock. In this division lateral and normal resistivity have an important role in the description. The rock type at the low fractured side is granite and the rock type at the highly fractured side is greenstone. The high fracture frequency is represented by fracture zones, and indicated by the mirror points to lateral and normal resistivity which represents low values. The next component shows a division between highly fractured granite on one side and low fractured greenstone and dolerite on the opposite side. Here again the mirror points to lateral and normal resistivity correspond to low values on the fractured side.

Radar intensity occurs in components with lower degree of correlation. This means that variables representing highly fractured rock and low fractured rock, respectively, exhibit stronger correlations to each other than to the radar intensity. High radar intensity occurs firstly together with lithological contacts in general, thereafter with high fracture frequency and fracture zones. This confirms the conclusions made in the original interpretation of radar data from Klipperås (Carlsten et al., 1987) which was that lithological contacts constitute prominent radar reflectors.

Concluding the Principal Component analysis it can be stated that the strongest correlations give a division between low fractured and highly fractured rock. High radar intensity occurs at lithological contacts and sections with high fracture frequency.

Table 4.2 Components from the Principal Component analysis of data from the boreholes at the Klipperås study site.

Comp.	Explained variance	Negative		Positive
1	21.0	NR GE LR GA gr	++	ge F9 FS
2	11.6	gr SO GA	++	LR NR do ge SU
3	6.7	ge rb SP	++	do SU
4	6.5	SP do	++	FS F9
5	6.0	S9	++	SP F9
6	5.7	RI rb	++	SP
7	5.7	ge SO	++	do S9 SP
8	5.4	RI FS F9	++	rb SO SU
9	5.9	do rb	++	RI SU
10	5.9	SO	++	SU rb GA

Activated variables
++ = Center point
GA = Gamma log
GE = Geohm log or single point resistance
LR = Lateral resistivity log
NR = Normal resistivity log
SO = Sonic log
SP = Self potential
SU = Susceptibility log
F9 = Fracture zone freq.0-90 deg.
S9 = Single fracture freq.0-90 deg.
FS = Total fracture freq.0-90 deg.
gr = Granite
ge = Greenstone
do = Dolerite
rb = Lithological contact
RI = Radar intensity
HC = Hydraulic conductivity

4.3 PLS-ANALYSIS OF THE DATA FROM KLIPPERÅS.

PLS-analysis were performed on three different sets of data from the boreholes in Klipperås. The first analysis contains in essence the same set of variables as used at the other investigated sites. The second and the third PLS-analysis were made with emphasis put on correlation between radar intensity and fracture minerals thought indicate waterflow. This division of PLS-analyses was made in order to test the hypothesis that the presence of Fe-oxide as a fracture mineral could be used as an indication of waterflow through fractures (Tullborg, 1986; Andersson and Lindqvist, 1988). During the core mapping of the six boreholes KKL01-KKL05 and KKL07 in Klipperås, Fe-oxide and hematite were not separated. Hence it was only possible to use the data from the boreholes KKL06 and KKL08-KKL14 in the special PLS-analysis. Two different studies were made with the fracture mineral data. One analysis was made with the fracture mineral variables in addition to the variables used in the original PLS-analysis, and the other was made with the fracture mineral variables and the variables that are expected to indicate water flow, i.e. temperature gradient (QG), temperature (QT), salinity (QS) and resistivity of borehole fluid (QR).

In the first standard PLS-analysis, presented in Table 4.3, the values of explained variance indicate that only the first three components can be used for the description. Variables which are important for the description of the components are mainly different features of fracturing together with lateral and normal resistivity. The variable lithological contact also has a prominent part in the description of the components. In the same manner as in the Principal Component analysis, the PLS-analysis shows that the strongest correlations result in a division between low fractured and highly fractured rock. The first component shows that high radar intensity occurs in sections with high fracture frequency in form of fracture zones. The sections contains lithological contacts at greenstone and dolerite. Thus, the lithological contacts are highly fractured. The mirror points to lateral and normal resistivity indicate low resistivity values. In the next component it can be seen that high radar intensity also occurs at sections containing low fractured lithological contacts at dolerite. At these sections the normal resistivity is high. Furthermore, the third component shows that high radar intensity also occurs at sections with more general features,

such as fractured granite. These sections are not associated with lithological contacts. The mirror points to normal and lateral resistivity representing low values support the interpretation of fracturing.

Hydraulic conductivity was not included in the SIMCA-analysis from Klipperås for reasons mentioned in chapter 3.2.

To sum up, it can be stated that the PLS-analysis shows that a good correlation exists between radar intensity, lithological contacts, resistivity, and fracture frequency. High radar intensity occurs firstly at highly fractured lithological contacts, but also at low fractured contacts and at more generally fractured granite sections.

The second PLS-analysis, presented in Table 4.4, includes the same active variables as in the original PLS-analysis, plus those mentioned below. This analysis comprises data from fewer boreholes, i.e. KKL06 and KKL08-KKL14, and fracture mineral variables have been brought into the analysis, as well as variables connected to the waterflow.

In the second PLS-analysis the values of explained variance show that only the first two components can be used. Also, in this analysis different features of fracturing together with lateral and normal resistivity have importance. The first component shows that the strongest correlation results in a division between low fractured and highly fractured rock, as was the case in the previous analysis. By introducing variables representing fracture minerals into the analysis, a couple of smaller changes occurs compared to the previous PLS-analysis. The fracture minerals chlorite and calcite have stronger correlation with fracture frequency and fracture zones than was the case for greenstone, dolerite, and lithological contact. This can be explained by that chlorite and calcite are very common fracture minerals, and an increasing fracture frequency results in an increasing presence of those minerals. In the PLS-analysis this means that the three variables greenstone, dolerite, and lithological contact are pushed down and replaced by the fracture minerals which exhibit higher degree of correlation. Radar intensity in this analysis, as well as in the previous PLS-analysis, firstly shows strong correlation with fracture frequency represented by fracture zones. The mirror points to lateral and normal resistivity also indicate high fracturing. The presence of granite on the low fractured side indicates that the host rock for the fractured sections are other rock types than granite. Secondly, high radar intensity occurs in sections

with lithological contacts at dolerite. These sections are low fractured.

To sum up the second PLS-analysis, it can be said that this analysis, as well as the previous analyses, shows a distinct division between low fractured and highly fractured rock. Good correlation exists between radar intensity, fracture frequency, fracture minerals, and resistivity. Somewhat lower correlation exists between radar intensity and low fractured lithological contacts.

A comparison of the results from the first and second PLS-analysis shows that the introduction of the fracture mineral variables have caused a change in emphasis of what variables correlate most strongly with radar intensity. Excluding the fracture mineral variables radar intensity correlates most strongly with lithological contacts. But with the fracture mineral variables included the strongest correlation is to events which can be classified as fracture zones, while lithological contact appears in the second component.

The third PLS-analysis, presented in Table 4.5, includes only variables that might indicate waterflow, i.e. temperature gradient (QG), temperature of borehole fluid (QT), salinity of borehole fluid (QS) and resistivity of borehole fluid (QG), besides the fracture minerals. The data is from the boreholes KKL06 and KKL08-KKL14. The values of explained variance show that only the first two components can be included in a description of the data.

The third PLS-analysis gives a negative correlation between radar intensity and temperature gradient in the first component. The temperature gradient (QG) is a complex variable which is associated with large anomalies at locations where there is water flow either into or out of a borehole. The temperature gradient anomaly at such locations may be either positive or negative due to a number of factors, e.g. relative temperature difference between borehole fluid and formation fluid and water flow direction in the borehole. This character of temperature gradient anomalies may make the correlation with other variables quite spurious and difficult to interpret. In this case component 1 shows a negative correlation between radar intensity and temperature gradient and a positive correlation to the fracture minerals calcite and chlorite. This may be interpreted as a strong correlation between radar intensity and hydraulically conductive fracture zones.

Table 4.3 Components from PLS-analysis of data from all boreholes at the Klipperås study site. All variables except fracture minerals.

Comp.	Explained variance X	Y	Negative		Positive
1	26.8	9.8	NR GE LR gr GA	++	do rb ge F9 FS RI
2	8.8	6.7	SP ge FS S9 SO F9	++	NR SU do rb RI
3	12.9	5.6	SU ge do NR LR GE	++	SO GA gr RI
4	7.1	5.5	SO do	++	S9 NR RI
5	7.5	5.5	rb ge	++	RI
6	5.4	5.5	SU S9	++	NR rb SO RI
7	5.7	5.4	SP ge	++	S9 RI
8	5.1	5.5	SO LR	++	SP RI

Activated variables
++ = Center point
GA = Gamma log
GE = Geohm log or single point resistance
LR = Lateral resistivity log
NR = Normal resistivity log
SO = Sonic log
SP = Self potential
SU = Susceptibility log
F9 = Fracture zone freq.0-90 deg.
S9 = Single fracture freq.0-90 deg.
FS = Total fracture freq.0-90 deg.
gr = Granite
ge = Greenstone
do = Dolerite
rb = Lithological contact
RI = Radar intensity
HC = Hydraulic conductivity

Table 4.4 Components from PLS-analysis of data from the boreholes KKL06 and KKL08-KKL14 at the Klipperås study site, including all variables and fracture minerals.

Comp.	Explained variance X	Y	Negative	Positive
1	82.4	79.7	NR GE LR gr GA	++ Ca F9 Cl FS RI
2	17.6	20.3	QG SO Ep Fe gr SP F9 FS GA Cl	++ do rb RI
3	0	0	ge SU QS	++ QR SO GA gr RI
4	0	0	SP QR GE LR	++ QS RI
5	0	0	QS gr GA	++ SP ge QG QR RI
6	0	0	do QG QR	++ LR gr NR RI
7	0	0	GE LR Ca F9 ge NR GA FS rb Ep	++ do SU SP RI
8	0	0	ge SP Fe	++ FS Py SU GE Cl G LR NR RI

Activated variables
++ = Center point
GA = Gamma log
GE = Geohm log or single point resistance
LR = Lateral resistivity log
NR = Normal resistivity log
SO = Sonic log
SP = Self potential
SU = Susceptibility log
QT = Temperature
QG = Vertical temperature gradient
QR = Borehole fluid resistivity
QS = Salinity
F9 = Fracture zone freq.0-90 deg.
S9 = Single fracture freq.0-90 deg.
FS = Total fracture freq.0-90 deg.
Ca = Calcite
Fe = Fe-oxide
Hm = Hematite
Py = Pyrite
Ep = Epidote
Cl = Chlorite
gr = Granite
ge = Greenstone
do = Dolerite
rb = Lithological contact
RI = Radar intensity
HC = Hydraulic conductivity

Table 4.5 Components from PLS-analysis of data from the boreholes KKL06 and KKL08-KKL14 at the Klipperås study site, including radar intensity, fracture minerals, and variables considered to be related to water flow.

Comp.	Explained variance X	Y	Negative		Positive
1	80.5	79.5	QG	++	Ca Cl RI
2	19.5	20.5	QG Ep QS Fe	++	QR RI
3	0	0	QR	++	QT QS RI
4	0	0	QS Ca QT	++	QR Py RI
5	0	0	Py	++	RI
6	0	0	Ep	++	QS Ca Py RI
7	0	0	Cl QG QS	++	Fe QT Ep RI
8	0	0	Fe	++	Hm QG RI

Activated variables
++ = Center point
QT = Temperature
QG = Vertical temperature gradient
QR = Borehole fluid resistivity
QS = Salinity
F9 = Fracture zone freq.0-90 deg.
S9 = Single fracture freq.0-90 deg.
FS = Total fracture freq.0-90 deg.
Ca = Calcite
Fe = Fe-oxide
Hm = Hematite
Py = Pyrite
Ep = Epidote
Cl = Chlorite
RI = Radar intensity

4.4 PLS2-ANALYSIS OF THE DATA FROM KLIPPERÅS.

PLS2 analysis allows input of more than one dependent variable into the Y-block, compared to the PLS analysis. In this case the angles of radar reflections to borehole was put into the Y-block in form of six classes, or variables, c.f. Table 3.1. The radar intensity was put into the X-block as one independent variable amongst the others. The variables and the components are presented in Table 4.6.

The variable plots show that the PLS2 analysis gives a structural analysis where the radar intensity, as expected, exhibits the best correlation to radar angles in component 1 and 2. In component 1 the radar angles are well clustered on the positive side of the centre, together with high radar intensity. Also, on the positive side of the centre in component 2 radar angles are clustered together with high radar intensity. However, A9 which represents radar angles between 61-90 degrees to borehole axis, diverge from the other radar angles by being situated on the negative side of the centre. The reason for this can be that angles almost perpendicular to borehole axis exhibit very weak radar intensities, if any at all. In the remaining components the radar intensity can be found close to the centre point, thereby indicating that the components do not describe properties of interest for radar intensity.

Table 4.6 Components from PLS2-analysis of data from the boreholes at the Klipperås study site.

Comp.	Explained variance X	Explained variance Y	Negative	Positive
1	19.2	10.2	GE NR LR GA gr ++	A9 F9 FS A2 A6 A3 RI A4
2	14.1	8.6	FS F9 ge S9 do A9 ++	gr GA GE A2 A3 LR NR A6 RI A4 A1
3	11.6	6.0	A2 A9 A6 ge ++	gr QG F9 GA FS A3 A4 SO
4	11.6	5.7	A2 QR SP ge ++	do QS A9
5	8.0	5.5	A4 QS S9 ++	SP QG rb F9 A6 A9 QR do A3
6	6.8	5.5	A4 QR SU ++	A2 QS QG A1
7	7.3	5.3	A6 gr SO A4 ++	LR QG SU A3
8	4.1	5.5	A4 NR GE ge QG rb LR ++	gr A2 A3

Activated variables

++ = Center point
GA = Gamma log
GE = Geohm log or single point resistance
LR = Lateral resistivity log
NR = Normal resistivity log
SO = Sonic log
SP = Self potential
SU = Susceptibility log
QT = Temperature
QG = Vertical temperature gradient
QR = Borehole fluid resistivity
QS = Salinity
F9 = Fracture zone freq.0-90 deg.
S9 = Single fracture freq.0-90 deg.
FS = Total fracture freq.0-90 deg.
Ca = Calcite
Fe = Fe-oxide
Hm = Hematite
Py = Pyrite
Ep = Epidote
Cl = Chlorite
gr = Granite
ge = Greenstone
do = Dolerite
rb = Lithological contact
RI = Radar intensity
A1 = Radar angle 0-10 deg.
A2 = Radar angle 11-20 deg.
A3 = Radar angle 21-30 deg.
A4 = Radar angle 31-45 deg.
A6 = Radar angle 46-60 deg.
A9 = Radar angle 61-90 deg.
HC = Hydraulic conductivity

4.5 COMPARISON WITH PREVIOUS INTERPRETATION OF RADAR DATA FROM KLIPPERÅS.

In the report by Carlsten et al. (1987) it is stated that 112 out of 175 interpreted radar reflections are connected with changes in lithology. Also, fracturing is a very common feature associated with the contacts between different rock types, which causes an increase in strength of the radar reflections. The borehole radar detects 52 % of mapped greenstone, 24 % of mapped pegmatite/aplite, 22 % of porphyry and 73 % of mapped mafic dykes.

63 out of 175 interpreted radar reflections are connected with other features such as fracture zones, clay filled fractures, shear zones, altered fractures, mylonites etc. All geologically or geophysically interpreted zones or features associated with the zones are detected by the borehole radar (Carlsten et al. 1987).

The PLS-analysis supports the statement by Carlsten et al. (1987) that most of the radar reflections are associated with different lithological contacts. The first two components which describe the strongest correlation of features to radar intensity in the PLS-analysis show that highly fractured and low fractured lithological contacts, preferably with dolerite and greenstone, are associated with high radar intensity. The first component describes highly fractured lithological contacts at dolerite and greenstone. The second component describes lithological contacts at dolerite which are low fractured.

The result from the SIMCA analysis supports the statement that a majority of the radar reflecting structures are coupled together with low resistivity.

5 FINNSJÖN STUDY SITE.

5.1 GEOLOGICAL OVERVIEW OF FINNSJÖN.

A geological description of the Finnsjön study site is presented in Olkiewicz et al. (1979) and Ahlbom et al. (1986 and 1987). The distribution of rock types in four of the six investigated boreholes is summarized in Table 5.1, together with abbreviations used in SIMCA analysis. The location of the main zones and the boreholes is presented in Fig. 5.1.

The major rock type is a grey, pink or red granodiorite, fine to medium grained showing weak foliation. The colour is connected to the fracture frequency and degree of tectonization, i.e. red rock is associated with high fracture frequency and/or tectonization. It should be noted that the percentage of red granodiorite, tectonite and mylonite is overestimated, since only the tectonized parts of the boreholes KFI05 and KFI06 have been remapped with a computerized core logging system (Ahlbom et al., 1986).

Other mapped rock types are young granite (late-orogenic), pegmatite, aplite, and xenoliths of leptite and basic rock.

Deformed rock intervals consisting of tectonized and mylonitized rock occur in the boreholes. The term tectonite is used for a rock which is strongly affected by cataclastic to mylonitic transitional deformation.

A subhorizontal zone situated within a flat area was the main target for the performed geological investigations. The zone is a shear zone, about 100 meters wide, comprising a network of slip systems enveloping blocks of less deformed rock. Repeated reactivation of the zone has ocurred along the most deformed parts. The salinity content of the groundwater within the study site increases abruptly at the subhorizontal zone from freshwater above the zone to about 0.8 % salinity (about 5500 mg/l of chlorine) in the upper part of the subhorizontal zone. A computerized piezometric monitoring system has been used to map the groundwater head distribution at the study site. In the western part shallow groundwater and possibly deep saline groundwater is infiltrating into the zone. In the eastern part the groundwater within the zone is exposed to a gradient with a component directed upwards. Probably, part of the groundwater within the subhorizontal zone is discharged into a major

subvertical zone in the area, the Brändan zone, which intersects the subhorizontal zone (Ahlbom et al., 1987).

Radar measurements have been performed at several different occasions. The measurements were performed as singlehole radar reflection measurements using a center frequency of 22 MHz. A radar map from borehole KFI10 is presented in Figure 5.2.

From interpretation of the radar maps it can be seen that shear zones striking about N60W having a subvertical dip constitute distinct radar reflectors. Due to the orientation of the boreholes, the shear zones constitute more or less parallel reflections in the radar maps (Fig. 5.2). They are easily located at the ground surface (S. Tirén, private communication). Lithological contacts are easily detected by the borehole radar. Aplites detected by radar with a width of 0.3 m can be traced from the boreholes to the ground surface and 500 m further on the surface. (S. Tirén, private communication). The large zones (Brändan zone and zone 2) are characterized in the radar maps by loss of penetration of the radar waves.

Table 5.1 Rock type distribution in the boreholes KFI09 and KFI10 and the remapped parts of KFI05 and KFI06 at the Finnsjön study site.

Rock type	Percentage	Abbreviations used in SIMCA
Grey granite (granodiorite)	25.6	gg
Pink granite (granodiorite)	33.6	pg
Red granite (granodiorite)	29.2	rg
Tectonite	7.2	te
Mylonite	0.5	my
Young granite	0.2	ry
Pegmatite	1.7	pe
Aplite	0.3	ap
Xenolith	1.7	xe
	100.0	

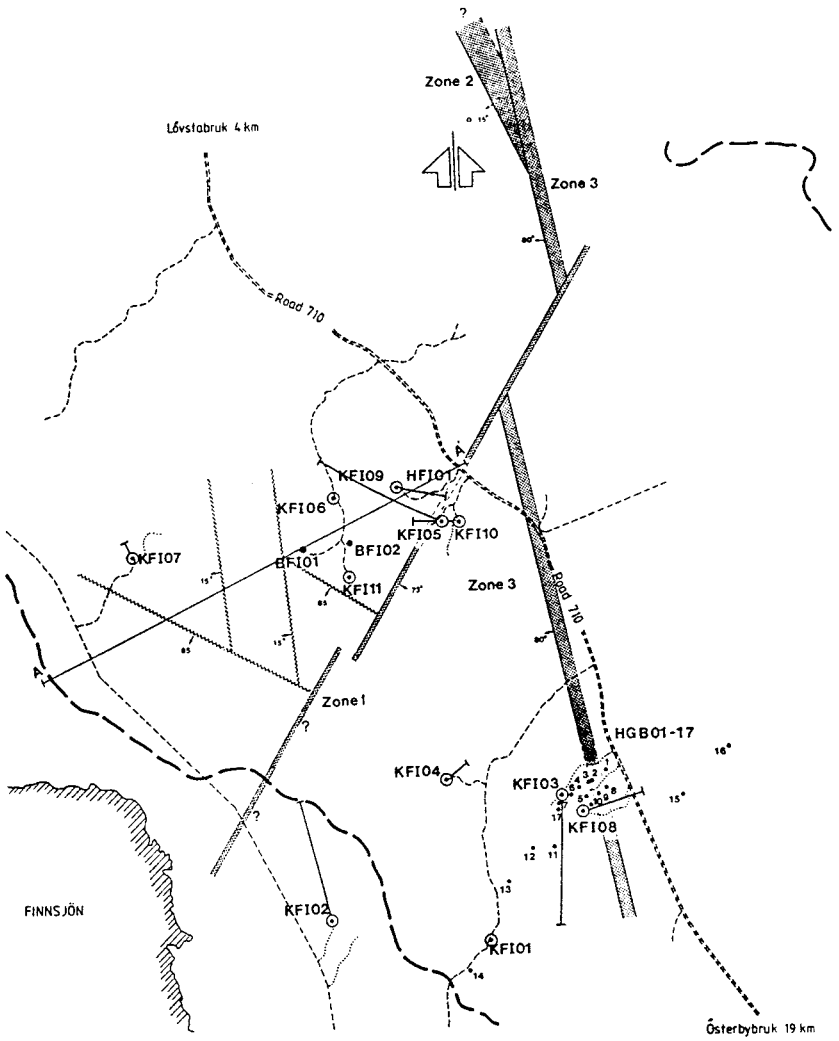

Fig. 5.1 Borehole location and fracture zones within the Finnsjön study site. Zone 1 is the subvertical Brändan zone, and zone 2 is the subhorizontal zone.

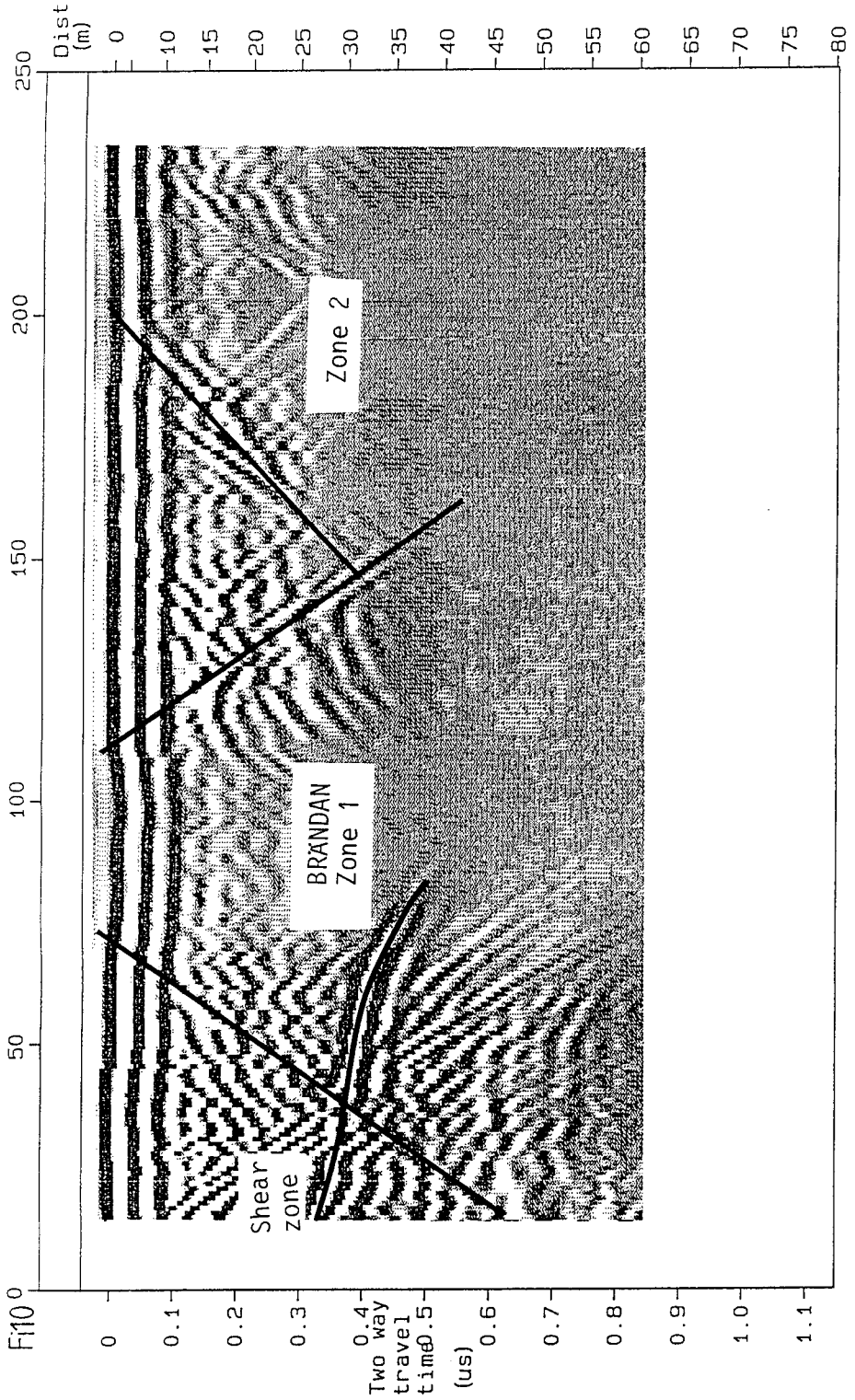

Fig. 5.2 Radar map from the borehole KFI10 at Finnsjön (22 MHz).

5.2 PRINCIPAL COMPONENT ANALYSIS OF THE DATA FROM FINNSJÖN.

The general character of the investigated rock can be described by the components in the Principal Component analysis from the Finnsjö area. The variables and the components are presented in Table 5.2.

The Principal Component analysis shows that variables representing different features of fracturing constitute important variables. The normal resistivity is also an important variable in the analysis, and the presence of the variable lithological contact is abundant in the components. The first component shows that the strongest correlations will result in a distinct division between low fractured, high resistive grey granite on one side, and highly fractured, low resistive red granite on the other side. The high fracturing is represented by single fractures. Hematite and calcite occur at the fractured red granite sections and high gamma ray radiation occurs together with the low fractured grey granite.

Hydraulic conductivity and radar intensity occur together and individually in components of lesser importance. The radar intensity occurs together with fracture zones and lithological contacts at pegmatite. Radar intensity also occurs together with fracture zones and high hydraulic conductivity in one component and together with low fractured lithological contacts in another component. Hydraulic conductivity occurs together with hematite in one component and together with radar intensity in the less significant component described above. Hydraulic conductivity also occurs at fractured lithological contacts.

In essence the strongest correlation in the analysis results in a division between low fractured rock and highly fractured rock.

Table 5.2 Components from the Principal Component analysis of data from the Finnsjön study site.

Comp.	Explained variance	Negative		Positive
1	21.7	gg GA NR	++	Hm Ca rg S9 FS
2	8.2	GE NR Ca	++	pe rb
3	7.1	pg	++	rg F9
4	6.1	HC Hm	++	rb F9 pe RI
5	6.0	pg	++	pe Py rb
6	6.4	Py HC F9 RI	++	Hm pe
7	5.7	pe F9	++	rb Hm RI
8	5.2	Py pe	++	F9 HC rb
9	5.3	rb rg	++	gg FS S9 GA
10	6.2	RI S9 rg GA	++	F9 Hm

Activated variables
++ = Center point
GA = Gamma log
GE = Geohm log or single point resistance
NR = Normal resistivity log
F9 = Fracture zone freq. 0-90 deg.
S9 = Single fracture freq. 0-90 deg.
FS = Total fracture freq. 0-90 deg.
Ca = Calcite
Hm = Hematite
Py = Pyrite
gg = Grey granodiorite
pg = Pink granodiorite
rg = Red granodiorite
pe = Pegmatite
rb = Lithological contact
RI = Radar intensity
HC = Hydraulic conductivity

5.3 PLS-ANALYSIS OF THE DATA FROM FINNSJÖN.

The values of explained variance for the components from the PLS-analysis of data from Finnsjön show that the first three components can be used in the description. The variables and the components are presented in Table 5.3.

The PLS-analysis shows, as the Principal Component analysis, that different features of fracturing are of importance. The strongest correlations give a strict division between low fractured grey granite and highly fractured red granite. The first component also shows that there exists strong correlation between high radar intensity and highly fractured red granite. The fracturing in the red granite is represented by fracture zones and single fractures. The second component shows that strong correlation also exists between high radar intensity and fracture zones in sections with grey granite. High normal resistivity indicates that the fracture zones constitute limited sections surrounded by low fractured rock. The sharp contrast between fracture zones and low fractured surroundings facilitates detection by borehole radar. This correlation is subordinate the correlation between radar intensity and fractured red granite presented in Component 1. The second component also shows that high hydraulic conductivity occurs at sections with highly fractured, red granite. Since radar intensity occurred in the previous component together with almost the same set of variables, it would imply that hydraulic conductivity exhibits a lower degree of correlation towards fractured rock. Fractured lithological contacts show up together with high radar intensity and the mirror point to normal resistivity in the third component.

To sum up the PLS-analysis, it can be said that there exists strong correlation between radar intensity and fracture frequency. Also, somewhat weaker correlation exists between radar intensity and lithological contacts.

Table 5.3 Components from the PLS-analysis of data from the Finnsjön study site.

Comp.	Explained variance X	Y	Negative		Positive
1	14.6	5.9	gg GA	++	S9 rg FS Ca F9 RI
2	16.9	2.9	S9 FS HC rg Hm	++	F9 NR GA gg RI
3	7.6	1.7	GE NR	++	Hm rb RI
4	4.7	1.7	pe rb rg	++	HC RI
5	3.8	1.5	GE gg Hm Py	++	GA pe RI
6	3.5	1.7	GA	++	rb Py NR RI
7	4.4	1.8	pg Ca GE Py pe	++	F9 GA rg HC Hm RI
8	5.6	1.9	rg	++	GE pe pg RI

Activated variables
++ = Center point
GA = Gamma log
GE = Geohm log or single point resistance
NR = Normal resistivity log
F9 = Fracture zone freq. 0-90 deg.
S9 = Single fracture freq. 0-90 deg.
FS = Total fracture freq. 0-90 deg.
Ca = Calcite
Hm = Hematite
Py = Pyrite
gg = Grey granodiorite
pg = Pink granodiorite
rg = Red granodiorite
pe = Pegmatite
rb = Lithological contact
RI = Radar intensity
HC = Hydraulic conductivity

5.4 PLS2-ANALYSIS OF THE DATA FROM FINNSJÖN.

The values of explained variance for the components from the PLS2-analysis of data from the boreholes at Finnsjön, show that only the first two components can be used in the interpretation. It should be noted that the value for the data in the Y-block in the second component is very low. The variables and the components are presented in Table 5.4.

The PLS2-analysis indicates, as the previous analyses, that different features of fracturing and normal resistivity are important variables in the interpretation of the components. The first component shows that hydraulic conductivity and radar intensity have strong correlation to each other and also on a common set of variables consisting of high fracture frequency in red granite. The high fracture frequency is represented in form of single fractures and fracture zones, and the normal resistivity is low. Calcite which is an abundant fracture mineral also occurs at the fractured sections. On the opposite side there is low fractured grey granite together with high normal resistivity. The second component shows hydraulic conductivity and radar intensity on opposite side to each other. High radar intensity occurs at fracture zones and high normal resistivity, which indicates that the fracture zones constitute limited sections surrounded by low fractured rock. The sharp contrast between fracture zones and low fractured surroundings facilitates detection by borehole radar. High hydraulic conductivity occurs on the opposite side at fractured sections in pink granite and the mirror point to normal resistivity indicating low values of resistivity. It should be noted that the amount of data in the Y-block in the second component is small.

Summing up the PLS2-analysis, it can be said that it gives a distinct division between low fractured rock and highly fractured rock. Also, there exists a good correlation between hydraulic conductivity, radar intensity, resistivity, and fracture frequency. It can also be said that high values of the variables mentioned above, except for the resistivity which has low values, occur together in sections with red granite.

Table 5.4 Components from the PLS2-analysis of data from the Finnsjön study site.

Comp.	Explained variance X	Y	Negative		Positive
1	23.5	4.8	gg GA NR	++	F9 S9 rg Ca FS RI HC
2	9.7	0.4	HC S9 pg	++	NR F9 RI
3	4.2	0	HC GE gg	++	rg pe rb Py
4	7.0	0	HC rg	++	pg
5	7.8	0	pe	++	GE pg NR HC
6	4.7	0	HC GE pg	++	Hm pe GA gg
7	6.9	0	HC	++	gg Hm Py
8	6.5	0	Py	++	Hm HC

Activated variables
++ = Center point
GA = Gamma log
GE = Geohm log or single point resistance
NR = Normal resistivity log
F9 = Fracture zone freq. 0-90 deg.
S9 = Single fracture freq. 0-90 deg.
FS = Total fracture freq. 0-90 deg.
Ca = Calcite
Hm = Hematite
Py = Pyrite
gg = Grey granodiorite
pg = Pink granodiorite
rg = Red granodiorite
pe = Pegmatite
rb = Lithological contact
RI = Radar intensity
HC = Hydraulic conductivity

5.5 COMPARISON WITH PREVIOUS INTERPRETATION OF RADAR DATA FROM FINNSJÖN.

The objective of borehole radar investigations in the boreholes at Finnsjön was to identify certain specified zones and to construct a geometric model of the zones at the site. Attempts have therefore not been made in the reports by Ahlbom et al. (1986 and 1987) to identify all radar reflections, only the strongest ones or those of particular interest were considered. From the reports it can be deduced that the radar reflections are equally distributed between shear zones, fracture zones and lithological contacts.

The PLS-analysis from the Finnsjön site shows that the most important variables which correlate with the radar intensity are high fracture frequency in form of fracture zones and single fractures in red granite. Also, individual fracture zones with low hydraulic conductivity located in grey granite and surrounded by low fractured rock is a feature which correlates to high radar intensity. Lithological contacts do not occur earlier than in component 3. This would indicate that fractured sections are more easily detected in the boreholes from Finnsjön, than for instance Klipperås. The amount of lithological contacts in the boreholes is high, but this is caused by the fact that the variable lithological contact mainly consists of transitions between red, pink and grey granite. Such transitions are difficult to detect by borehole radar since they are not distinct and do not constitute a sharp contrast in the electrical properties of the rock.

6 SALTSJÖTUNNEL SITE.

6.1 GEOLOGICAL OVERVIEW OF SALTSJÖTUNNEL.

The geological description of the boreholes at the Saltsjötunnel site is presented by Andersson et al. (1987). The overall distribution of rock types in the boreholes according to the core mapping is summarized in Table 6.1, together with abbreviations used in the SIMCA analysis of the Saltsjötunnel site.

The two dominating rock types are migmatite and granite. The alternations between migmatite and granite in the boreholes are numerous. Grey migmatite gneiss is the dominating rocktype, i.e. a veined and rather coarse-grained gneiss. The origin is presumably a greywacke. According to regional mapping, the strike of the internal structure of the migmatite in the investigation area is NNW and the dip is 80-85 degrees towards E. The granite is grey, fine to medium grained and is of the Stockholm type, i.e. homogeneous and shows only weak foliation. Pegmatite occurs as a number of narrow sections in the boreholes.

The location of the boreholes is shown in Fig. 6.1.

The radar has for this investigation been applied in three different modes; singlehole reflection, crosshole reflection, and crosshole tomography. Singlehole reflection measurements and crosshole measurement were made with the center frequency 22 and 60 MHz. Data for the crosshole reflection were obtained from the crosshole tomography measurement.

The model produced by the radar results have in general been in agreement with the result of geological, geophysical, and hydrogeological borehole investigations. The combined interpretation reveals two sets: the first set is adjoined with lithological variations in the bedrock striking roughly N-S with a more or less vertical dip. The second set is subhorizontal and constitute the most prominent fracture zones striking NW with a dip 35 degrees towards NE. The combined interpretation resulted in a model comprising three dominating subhorizontal zones. The three subhorizontal zones are interpreted to be the most dominating fracture zones within the investigated area. A radar map from borehole KST01 is presented in Figure 6.2.

Table 6.1 Rock type distribution in the boreholes KST01 and KST02 at the Saltsjötunnel site.

Rock type	Percentage	Abbreviations used in SIMCA
Migmatite	53.8	mi
Granite	43.3	gr
Pegmatite	2.9	pe
	100.0	

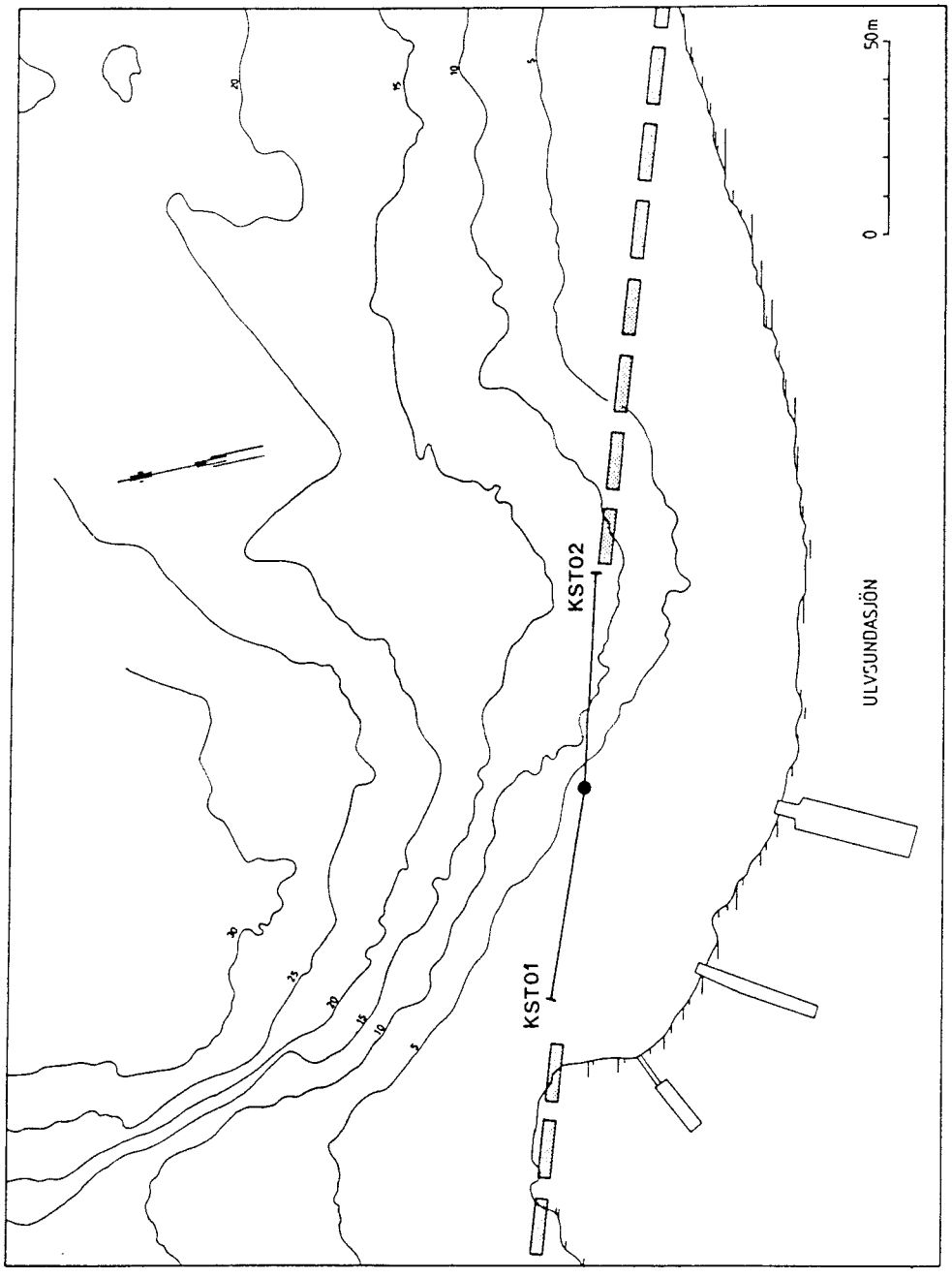

Fig. 6.1 Borehole locations within the Saltsjötunnel study site.

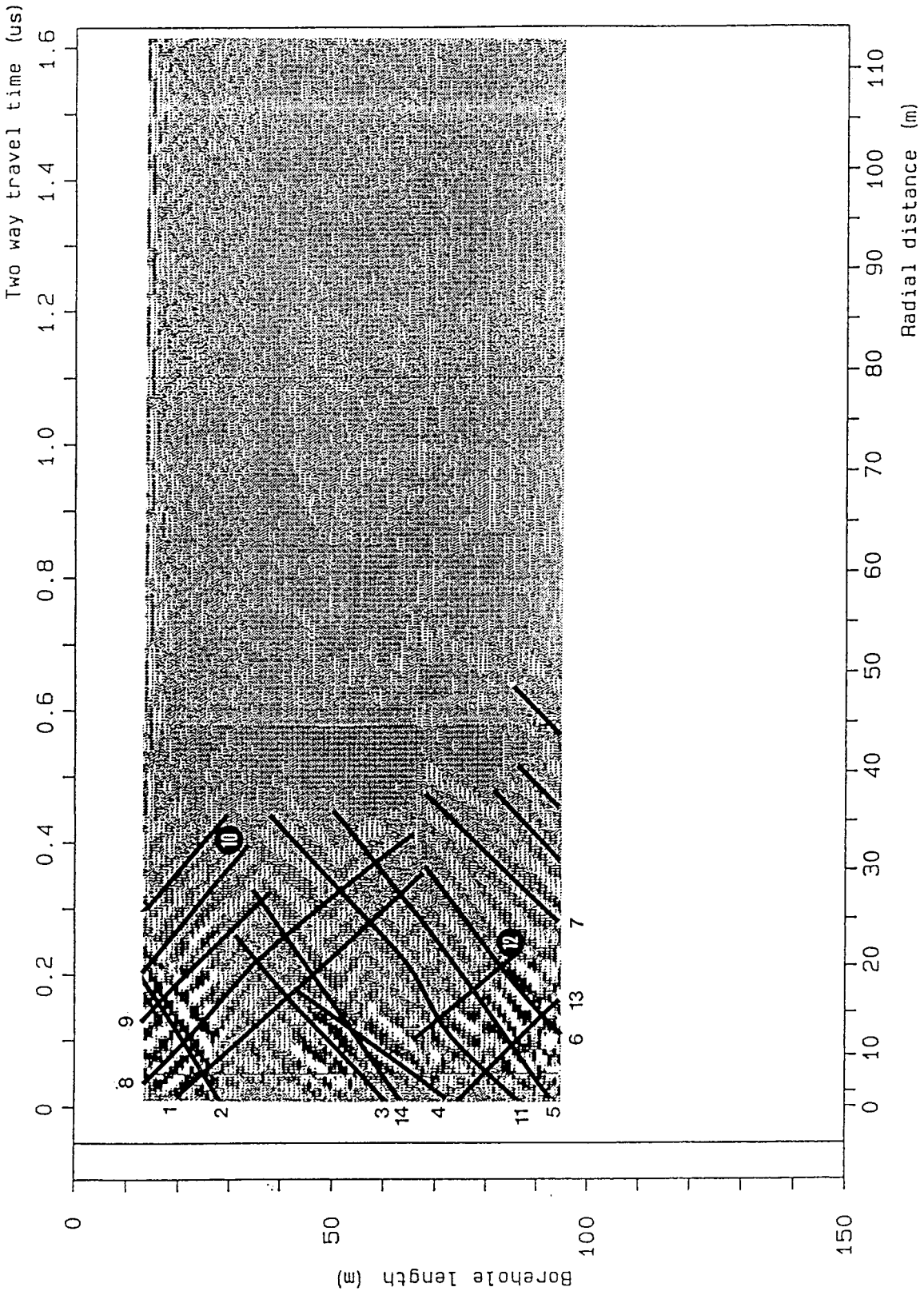

Fig. 6.2 Radar map from the borehole KST01 with a center frequency of 22 MHz.

6.2 PRINCIPAL COMPONENT ANALYSIS OF DATA FROM THE SALTSJÖTUNNEL.

The Principal Component analysis of data from the boreholes at the Saltsjötunnel site shows that the general character of the rock is described. The variables and the components are presented in Table 6.2.

From the Principal Component analysis it can be seen that different features of fracturing are of importance in the interpretation of the components. The first component exhibits a distinct division between low fractured and highly fractured rock. The fracturing is represented in form of fracture zones and the resistivity is low. Chlorite and calcite are present in the fractured sections probably due to their abundance in fractures. The presence of Fe-oxide in the sections might be an indication of waterflow in the fractures. Radar intensity occurs together with single fractures and migmatite in one of the significant components, hence showing strong correlation. Lithological contacts, both fractured and low fractured, are a frequently recurring variable in the components showing strong correlation to radar intensity. Hydraulic conductivity has a relatively low degree of correlation compared to the variables mentioned above. When hydraulic conductivity first occurs in the 5th component, it is together with high normal resistivity in migmatite and the presence of Fe-oxide. The high resistivity implies low fractured rock. One interpretation is that high hydraulic conductivity occurs at individual fractures in migmatite.

The summary of the Principal Component analysis is that it shows a distinct division between low fractured and highly fractured rock. High radar intensity occurs at an early stage at fractured sections in migmatite. High radar intensity also occurs at both low fractured and highly fractured lithological contacts. Hydraulic conductivity has a low degree of correlation to other variables.

Table 6.2 Components from the Principal Component analysis of data from the boreholes at the Saltsjötunnel site.

Comp.	Explained variance	Negative		Positive
1	24.0	NR GE	++	Ca Fe Cl FS F9
2	14.4	mi RI Py S9	++	GA gr
3	7.1	S9 Py	++	GE rb RI pe
4	6.8	Fe RI GA	++	NR Py S9 GE pe Ca rb
5	6.5	NR HC GE Fe mi	++	gr S9 rb RI
6	5.4	GE Ca	++	pe Py
7	5.5	rb	++	Ca Fe RI pe
8	5.8	HC	++	Py
9	5.0	GA	++	gr HC
10	5.5	Ca mi	++	RI NR S9 Fe

Activated variables
++ = Center point
GA = Gamma log
GE = Geohm log or single point resistance
NR = Normal resistivity log
F9 = Fracture zone freq. 0-90 deg.
S9 = Single fracture freq. 0-90 deg.
FS = Total fracture freq. 0-90 deg.
Ca = Calcite
Fe = Fe-oxide
Py = Pyrite
Cl = Chlorite
mi = Migmatite
gr = Granite
pe = Pegmatite
rb = Lithological contact
RI = Radar intensity
HC = Hydraulic conductivity

6.3 PLS-ANALYSIS OF THE DATA FROM SALTSJÖTUNNEL.

The values of explained variance for the different components indicate that three components can be used in the interpretation. The variables and the components are presented in Table 6.3.

The PLS-analysis shows that the strongest correlations result in a division between low fractured, high resistive granite and highly fractured, low resistive migmatite. High radar intensity occurs together with the highly fractured migmatite. In this analysis, as well as the Principal Component analysis, variables representing different features of fracturing and resistivity are of importance. In contrast to the Principal Component analysis, hydraulic conductivity occurs at an early stage in the analysis. Here it occurs together with high fracture frequency in form of fracture zones, and certain fracture minerals, including Fe-oxide. Fe-oxide is supposed to be present in fractures with waterflow. Even the third component exhibits a division between low fractured and highly fractured rock. In this case the low fractured rock is constituted by migmatite and the highly fractured rock by granite. It is of interest to notice that high radar intensity occurs not only together with fractured migmatite but also with fractured granite, even if the amount of such sections are lower.

To sum up the PLS-analysis it can be said that high radar intensity occurs firstly at sections with fractured migmatite and secondly fractured granite. Hydraulic conductivity occurs at fracture zones containing Fe-oxide as fracture mineral. Lithological contacts do not show up at all in the usable components.

Table 6.3 Components from the PLS-analysis of data from the boreholes at the Saltsjötunnel site.

Comp.	Explained variance X	Y	Negative		Positive
1	12.4	19.4	gr GA NR	++	mi RI
2	15.4	6.2	FS Cl F9 Fe HC Ca	++	RI
3	15.0	3.4	NR mi	++	gr FS Ca Cl F9 RI
4	2.9	2.2	rb Fe F9 NR	++	S9 HC Py RI
5	2.3	1.5	Ca S9	++	GE Fe RI
6	4.0	1.3	GE	++	rb S9 RI
7	0.6	1.3	rb	++	RI
8	5.5	1.3	GA	++	GE rb Ca RI

Activated variables
++ = Center point
GA = Gamma log
GE = Geohm log or single point resistance
NR = Normal resistivity log
F9 = Fracture zone freq. 0-90 deg.
S9 = Single fracture freq. 0-90 deg.
FS = Total fracture freq. 0-90 deg.
Ca = Calcite
Fe = Fe-oxide
Py = Pyrite
Cl = Chlorite
mi = Migmatite
gr = Granite
pe = Pegmatite
rb = Lithological contact
RI = Radar intensity
HC = Hydraulic conductivity

6.4 PLS2-ANALYSIS OF THE DATA FROM SALTSJÖTUNNEL.

The given values of explained variance for the components of the PLS2-analysis of the boreholes from Klipperås show that the first three components can be used. The variables and the components are presented in Table 6.4.

Since the PLS2-method correlates all active variables to hydraulic conductivity and radar intensity, is it of interest to establish that the two variables never occur at the same side in the first three components, i.e. hydraulic conductivity and radar intensity do not jointly correlate to a set of variables. In this analysis, as well as the Principal Component analysis and the PLS-analysis, there are correlations which result in a division between low fractured, high resistive granite and highly fractured, low resistive migmatite. Variables representing different features of fracturing and resistivity are of importance in the analysis. The content of the components is on the whole similar to the components in the PLS-analysis. However, some variables have been included and some excluded in the PLS2-analysis. The first component shows that the strongest correlations give fractured migmatite together with high radar intensity on one side of the component and low fractured granite together with hydraulic conductivity on the opposite side. The presence of high hydraulic conductivity on the low fractured side might be explained by waterflow in individual fractures in the granite. The analysis also shows that high radar intensity occurs at low fractured lithological contacts and at fracture zones in general. This is in agreement with the Principal Component analysis. The second component shows that high hydraulic conductivity occurs in sections with high fracture frequency.

Summing up the PLS2-analysis it can be said that it shows a similar pattern as the PLS-analysis. High radar intensity occurs at low resistive, fractured sections in migmatite, low fractured lithological contacts, and low resistive, fracture zones in general. High hydraulic conductivity occurs at individual fractures and in sections with high fracture frequency. It should be noted that hydraulic conductivity and radar intensity never occur on the same side in the components.

Table 6.4 Components from PLS2-analysis of data from the boreholes at the Saltsjötunnel site.

Comp.	Explained variance X	Y	Negative		Positive
1	11.6	12.3	gr GA NR HC	++	mi RI
2	17.8	5.2	HC FS Cl F9 Fe Ca	++	rb RI
3	14.1	3.9	NR	++	F9 RI
4	1.0	2.9	HC rb	++	GE RI
5	5.7	0	Fe RI	++	Py HC
6	5.0	2.0	HC GE Ca	++	RI Fe Py
7	5.3	1.4	rb GA	++	HC pe RI
8	7.1	1.1	GA	++	rb S9 RI

Activated variables
++ = Center point
GA = Gamma log
GE = Geohm log or single point resistance
NR = Normal resistivity log
F9 = Fracture zone freq. 0-90 deg.
S9 = Single fracture freq. 0-90 deg.
FS = Total fracture freq. 0-90 deg.
Ca = Calcite
Fe = Fe-oxide
Py = Pyrite
Cl = Chlorite
mi = Migmatite
gr = Granite
pe = Pegmatite
rb = Lithological contact
RI = Radar intensity
HC = Hydraulic conductivity

6.5 COMPARISON WITH PREVIOUS INTERPRETATION OF RADAR DATA FROM SALTSJÖTUNNEL.

In Andersson et al. (1987), it was stated that most of the single hole radar reflections seem to be correlated to lithological contacts. Two sets of main structures were interpreted at the site. The lithological contacts between migmatite, granite, and pegmatite constitute vertical structures in the rock mass and are often accompanied by a somewhat higher fracture frequency. Also, the geophysical logs supported this interpretation. However, the hydraulic conductivity is in general not very high in connection to the lithological contacts. The vertical set of lithological contacts was not considered as very prominent in the rock mass. The other set of structures at the site is connected to a high degree of tectonization and fracturing. In this set lithological variations seem to play a minor role. The sections representing this set in the boreholes exhibit the largest geophysical anomalies encountered in the boreholes. The singlehole radar reflections representing the same set are rather weak. It should be kept in mind that the poor radar response can be caused by the large angle of the set relative borehole axis which is unfavorable for obtaining strong radar reflections. Also, the penetration of radar waves at the site was low due to high attenuation.

The PLS-analysis of data from the boreholes shows that high radar intensity firstly occurs in fractured migmatite. This indicates that the radar intensity in the first component might be coupled to the vertical lithological structures. The second component shows the radar intensity alone, and does not describe any features correlated to the radar intensity. However, there is a negative correlation to high hydraulic conductivity and a few other variables. The high hydraulic conductivity values in the boreholes was interpreted to occur mainly at the subhorizontal fracture zones and the variables correlating with hydraulic conductivity can describe features connected to the subhorizontal fracture zones. In the third component high radar intensity occurs together with fracture zones in granite. The variable set in this component is very similar to the variable set occurring together with hydraulic conductivity in component 2. In component 2 the variable set was interpreted to be connected with the subhorizontal fracture zones and it can possibly be connected to the same zones in component 3.

The SIMCA analysis from Saltsjötunnel shows that

borehole radar at the site is sensitive to fracture frequency and changes in lithology.

7 STRIPA

7.1 GEOLOGICAL OVERVIEW OF STRIPA.

A geological description of the Crosshole (Small scale) site in the Stripa mine is presented by Carlsten et al. (1985). The overall distribution of rock types in the boreholes F2, F3, and F4, which have been investigated in this report is summarized in Table 7.1, together with abbreviations used in the SIMCA analysis.

The site is situated within a granitic pluton which outcrops in a supracrustal belt. Due to the relatively mild tectonism since the intrusion, the granite is generally unfoliated. The Stripa granite is grey to reddish and fine to medium grained. The granite is also a relatively uraniferous rock. Pegmatite occurs in the boreholes as a number of rather narrow dykes. Aplite and quartz veins also occur as a few very narrow dykes.

Deformed rock intervals consisting of tectonized, brecciated and mylonitized rock occur rather frequently in the boreholes. Alteration occurs within the deformed intervals or in discrete zones in the undeformed granite. Alteration have been observed as red colouring of the rock mass. Fractures with open cavities partly or totally filled with idiomorphic calcite crystals is a common feature in the deformed sections.

Six major units were interpreted in the geological model of the Crosshole site. The units have a similar strike to NE-NNE and a steep dip toward ESE or WNW. Two of the units namely 1 and C have a dip toward WNW and the rest of the units toward ESE. Unit E constitutes the front of a tectonized and brecciated red-stained granite and unit F also constitutes a part of this tectonized rock mass. Units E and F are followed by other probably subparallel units not reached by the boreholes, except for the 300 m long borehole E1 (Carlsten et al., 1985).

The major units generally constitute the more fractured parts of the boreholes. However, the degree of fracturing for each unit exhibits a large variation between the boreholes. Thus, the fracturing varies along the extension of the units. The fractures within the major units often have the dominating direction more or less subparallel with extension of the units (Carlsten et al., 1985).

Table 7.1 Rock type distribution in the boreholes F2, F3, and F4 at the Crosshole site in Stripa.

Rock type	Percentage	Abbreviations used in SIMCA
Granite (and tectonized)	99.9	gr te
Pegmatite and quartz vein	0.1	pe qv
	100.0	

The borehole radar, seismic, and hydraulic investigations performed at the site have caused some changes in the above mentioned geological model of the Crosshole site (Olsson, Black, Cosma, and Pihl, 1987b). The location of the boreholes is presented in Figure 7.1.

The radar measurements in Stripa have been performed in two different modes, singlehole radar reflection measurement and crosshole radar reflection measurement. Two center frequencies was used, 22 MHz and 60 MHz. Data from the crosshole measurement was used as input data for tomographic analysis. A radar map from singlehole reflection measurement in part of borehole F2 is presented in Figure 7.2.

A three dimensional model describing the geometry of fracture zones has been constructed of the experimental site in the Stripa Mine (Fig. 7.3). The model is based on results from singlehole reflection, crosshole reflection, and crosshole tomography. Four major zones have been identified and also some zones of smaller magnitude. The zones are found to be roughly planar but there are undulations from the average plane. Variations in thickness and electrical properties of the zones have also been noticed. The zones identified at the site belong to two different sets with different orientation. The fracture zones within each set have roughly the same orientation.

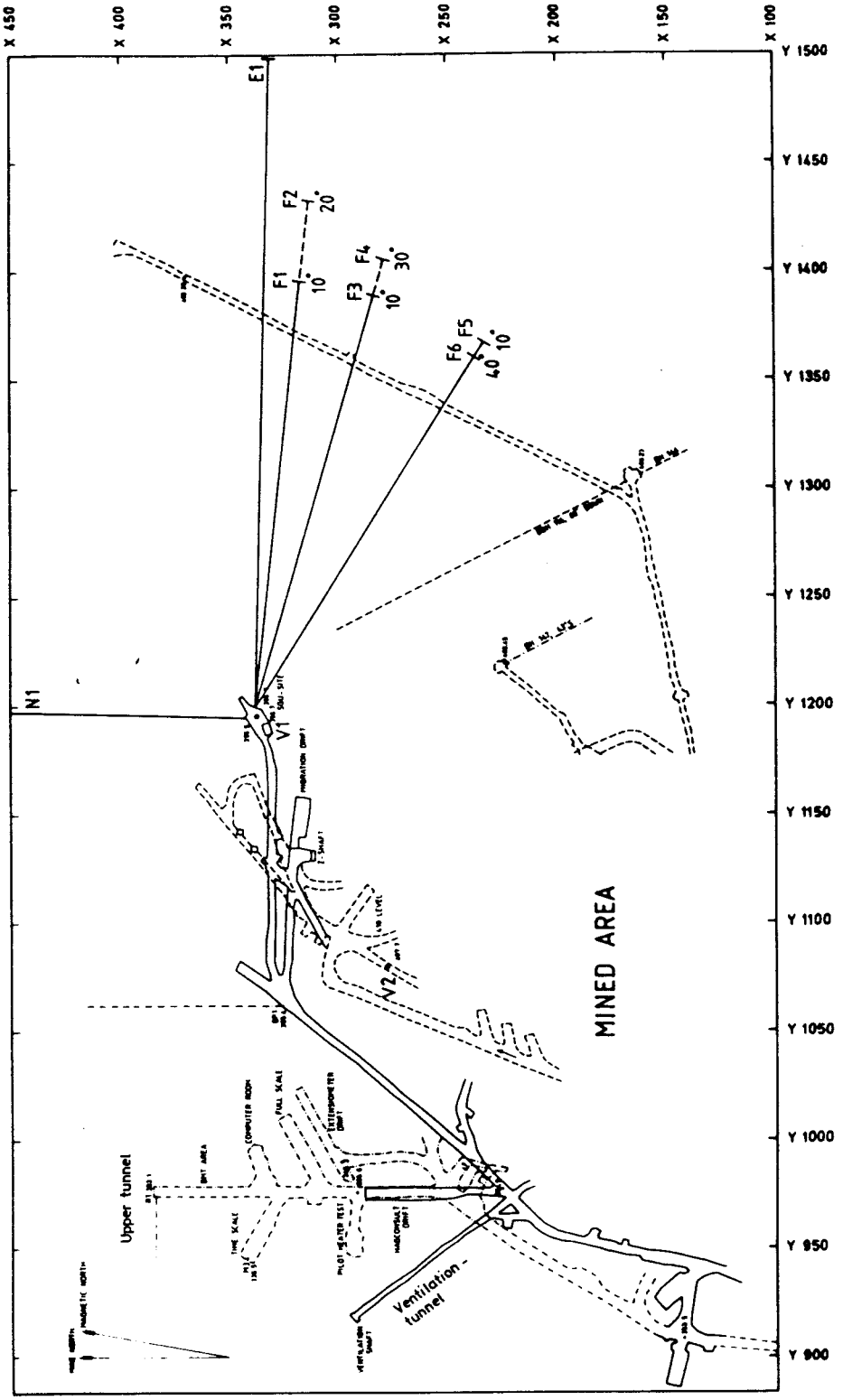

Fig. 7.1 Borehole location at the Stripa site.

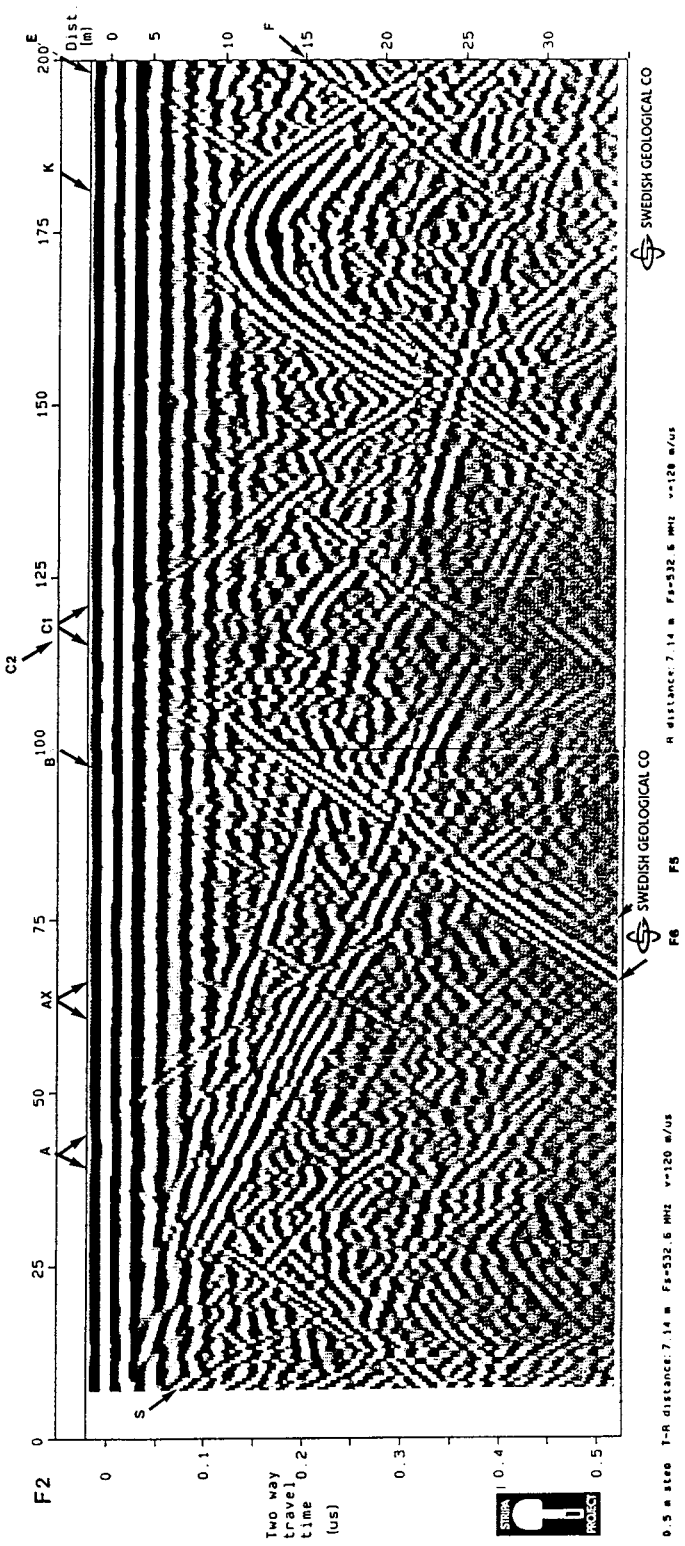

Fig 7.2 Radar map from the borehole F2, 0-200 m, at the Crosshole site in Stripa with a center frequency of 22 MHz.

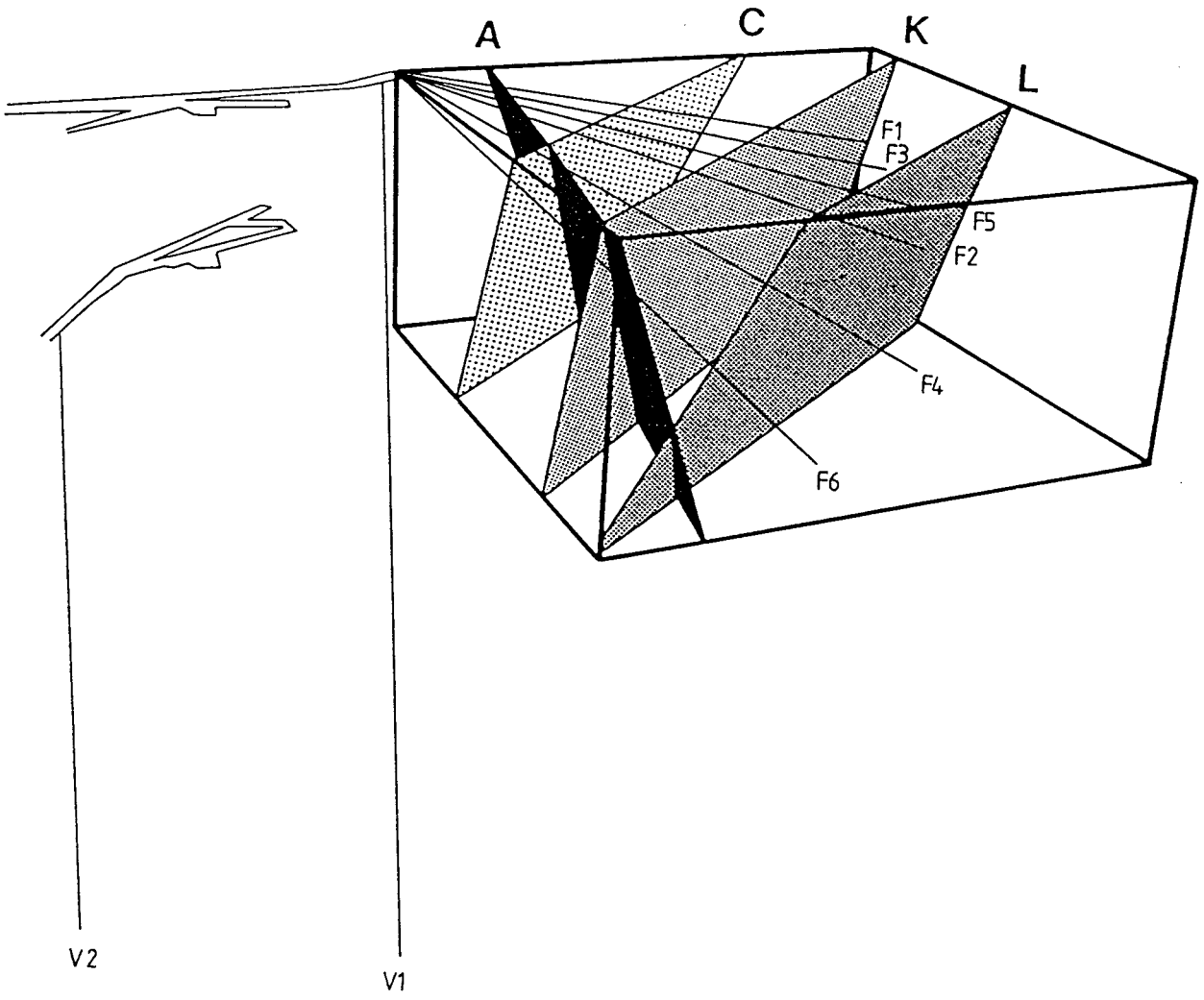

Fig. 7.3 The basic model of the Crosshole site showing the four major fracture zones.

7.2 PRINCIPAL COMPONENT ANALYSIS OF THE DATA FROM STRIPA.

The Principal Component analysis gives a description of the general character of the investigated rock in Stripa. The active variables differ somewhat from the other sites in this investigation by having only one active rock type variable, which is granite. The core mapping data of the boreholes in Stripa is not stored in the SKB-database as data from the other investigated sites, instead it is kept at SGAB on floppy discs. Several attempts where made to create SIMCA compatible files, but without success. Epidote was the only fracture mineral that was possible to read from the data discs and hence the only fracture mineral included in the analysis. The variables and the components are presented in Table 7.2.

The Principal Component analysis shows that variables representing different features of fracturing together with normal and lateral resistivity, hydraulic conductivity, lithological contacts, and radar intensity are most important in the components. It should be noted, as mentioned above, that there is only one rock type present in the data, namely granite and that the lithological contacts constitute changes between tectonized and untectonized granite. The analysis shows that the strongest correlations will result in a division between low fractured, high resistive granite and highly fractured, low resistive granite. High fracture frequency, represented by fracture zones and single fractures, correlates with high hydraulic conductivity and high radar intensity. High hydraulic conductivity also occurs at lithological contacts and fracture zones.

To sum up the Principal Component analysis it can be said that there is a distinct division between low fractured, high resistive granite and highly fractured, low resistive granite which is accompanied with high hydraulic conductivity and high radar intensity.

Table 7.2 Components from the Principal Component analysis of data from the boreholes at the crosshole site in Stripa.

Comp.	Explained variance	Negative		Positive
1	21.6	NR GE LR	++	RI SO S9 HC SP F9 Ep FS
2	16.0	GA GE	++	SP
3	9.9	Ep LR F9 NR FS	++	rb HC
4	8.5	SO RI F9	++	S9 SU
5	6.8	HC F9	++	rb
6	6.7	SO S9	++	RI
7	6.2	RI S9	++	SU F9 rb
8	5.3	HC rb	++	SO RI SU
9	6.8	S9 Ep	++	HC SU SO
10	5.8	Ep	++	SP F9 FS

Activated variables
++ = Center point
GA = Gamma log
GE = Geohm log or single point resistance
LR = Lateral resistivity log
NR = Normal resistivity log
SO = Sonic log
SP = Self potential
SU = Susceptibility log
F9 = Fracture zone freq.0-90 deg.
S9 = Single fracture freq.0-90 deg.
FS = Total fracture freq.0-90 deg.
Ep = Epidote
gr = Granite
rb = Lithological contact
RI = Radar intensity
HC = Hydraulic conductivity

7.3 PLS-ANALYSIS OF THE DATA FROM STRIPA.

The values of explained variance from the PLS-analysis indicate that the first three components can be used in the description. The variables and the components are presented in Table 7.3.

The PLS-analysis shows, as was the case for the Principal Component analysis, that the strongest correlations result in a division between low fractured granite and highly fractured granite. High radar intensity and high hydraulic conductivity correlate together on a common set of variables consisting of high fracture frequency in form of fracture zones and single fractures, epidote, and high sonic. On this side the resistivity is low. All variables indicate fracturing. Epidote is an abundant fracture mineral in the boreholes. On the opposite side there is low fractured granite with high resistivity. The component indicates that a good correlation exists between hydraulic conductivity and radar intensity. High radar intensity also occurs at lithological contacts in Component 2. It can not be interpreted with any accuracy whether the lithological contacts are sealed or fractured in this component.

The summary of the PLS-analysis is that there is a distinct division between low fractured granite and highly fractured granite. The analysis also shows that there exists a good correlation between radar intensity and hydraulic conductivity at the highly fractured sections.

Table 7.3 Components from the PLS-analysis of data from the boreholes at the crosshole site in Stripa.

Comp.	Explained variance X	Y	Negative		Positive
1	21.8	13.6	NR LR GE GA	++	S9 SO F9 HC Ep FS RI
2	7.4	3.9	SP S9 NR SU	++	GE rb GA RI
3	11.3	2.2	GA GE SU	++	SP RI
4	8.2	2.0	SO SP	++	FS RI
5	4.9	1.8	Ep F9 NR FS rb	++	SO RI
6	8.2	1.5	HC rb S9	++	F9 Ep SO RI
7	4.0	1.6	F9 FS LR	++	rb SU RI
8	2.9	1.5	rb SU SO	++	HC RI

Activated variables
++ = Center point
GA = Gamma log
GE = Geohm log or single point resistance
LR = Lateral resistivity log
NR = Normal resistivity log
SO = Sonic log
SP = Self potential
SU = Susceptibility log
F9 = Fracture zone freq.0-90 deg.
S9 = Single fracture freq.0-90 deg.
FS = Total fracture freq.0-90 deg.
Ep = Epidote
gr = Granite
rb = Lithological contact
RI = Radar intensity
HC = Hydraulic conductivity

7.4 PLS2-ANALYSIS OF THE DATA FROM STRIPA.

According to the values of explained variance can the first three components in the PLS2-analysis of data from the boreholes in Stripa be used. The variables and the components are presented in Table 7.4.

The PLS2-analysis exhibits a similar division between low fractured granite and highly fractured granite as was the case in the previous Principal Component and PLS-analysis. High radar intensity and high hydraulic conductivity both correlate on a common set of variables consisting of high fracture frequency, fracture zones, single fractures, and epidote. Also, the resistivity is low at these sections. On the opposite side there is low fractured granite with high resistivity. The third component shows that radar intensity and hydraulic conductivity together correlate with lithological contacts. It is difficult to gather from the variable set whether the lithological contacts are fractured or not. High radar intensity also correlates with individual fracture zones, indicated by the presence of high resistivity on the same side. High hydraulic conductivity also occurs at generally fractured sections.

To sum up the PLS2-analysis it can be said that the strongest correlations result in a similar division between low fractured granite and highly fractured granite, as was the case in the previous principal component and PLS-analysis. The PLS2-analysis also shows good correlation between hydraulic conductivity, radar intensity, and fracture frequency.

Table 7.4 Components from the PLS2-analysis of data from the boreholes at the crosshole site in Stripa.

Comp.	Explained variance X	Y	Negative		Positive
1	21.4	16.2	NR LR GE	++	S9 Ep F9 FS RI HC
2	9.9	3.9	HC GA SU	++	F9 LR NR Ep SO SP RI
3	8.5	2.0	SP S9 LR	++	GE HC rb GA RI
4	14.6	1.8	GE GA	++	SP RI HC
5	7.2	2.0	SO	++	LR F9 FS HC RI
6	10.1	1.5	HC	++	SU S9 RI rb
7	6.8	1.4	Ep F9	++	SO HC
8	3.6	0	HC	++	F9 FS

Activated variables
++ = Center point
GA = Gamma log
GE = Geohm log or single point resistance
LR = Lateral resistivity log
NR = Normal resistivity log
SO = Sonic log
SP = Self potential
SU = Susceptibility log
F9 = Fracture zone freq.0-90 deg.
S9 = Single fracture freq.0-90 deg.
FS = Total fracture freq.0-90 deg.
Ep = Epidote
gr = Granite
rb = Lithological contact
RI = Radar intensity
HC = Hydraulic conductivity

7.5 COMPARISON WITH PREVIOUS INTERPRETATION OF RADAR DATA FROM STRIPA.

In Olsson et al. (1987) an attempt was made to compare radar features with single borehole hydraulic conductivity results. The conclusion was that the single borehole reflection radar identifies more features of interest than the single borehole hydraulic testing. If the number of radar features are reduced by a weighting procedure in which the intensity of the radar reflections is used, there is a good correlation achieved between radar identified features having high intensity and hydraulically conductive zones. The poor correlation of unweighted data, i.e. also radar reflections with low intensity, suggests that many of the features seen by single borehole radar are hydraulically insignificant.

The PLS2- and PLS-analyses of the data from the three boreholes in Stripa show that high intensity of the borehole radar is associated with low resistive sections with high hydraulic conductivity, a fact which supports the result by Olsson et al. (1987). The PLS-analysis also shows that high radar intensity occurs at sections with lithological contacts, i.e. between tectonized and untectonized granite. The PLS2-analysis shows that radar reflections occur at fractured sections and lithological contacts having high hydraulic conductivity.

8 ÄVRÖ STUDY SITE.

8.1 GEOLOGICAL OVERVIEW OF ÄVRÖ.

The geological description of Ävrö is presented in Carlsten et al. (1986) and Gentzschein et al. (1987). The distribution of rock types in the boreholes KAV01, KAV02 and KAV03 is presented in Table 8.1, together with abbreviations used in the SIMCA analysis. Borehole KAV02 is not included in the SIMCA investigation, since it was not radar measured, core logged, or geophysically logged at the time for this report.

The dominating rock type in the three boreholes is granite, which is normally greyish red to reddish grey, fine to medium grained, and partly exhibiting a weak foliation. Aplite, pegmatite, porphyry, and mafic rock (metabasite) occur as dykes in the rock mass. A mixture of hybrid rock and tectonite also occurs in the boreholes. Tectonite is a rock which is impossible to define the origin to. The hybrid rock is mostly fine grained, varying in colour from dark grey to red, appearing partly as metabasite, partly as granite, or as a mixture of both.

The location of the boreholes is shown in Figure 8.1.

The borehole radar measurement were performed at two different occasions during 1985 and 1987. The center frequency used in the singlehole radar reflection measurement was 22 MHz. An example of a radar map including the major fracture zone of interest from part of the borehole KAV01 is presented in Figure 8.2, and a cross section is presented in Figure 8.3. The radar measurements indicates tectonized rock, fracture zones, mafic dykes, and sections with strong contrast in resistivity. The presence of saline water in the boreholes results in a significant reduction of radar wave penetration.

Table 8.1 Rock type distribution in the boreholes KAV01, KAV02 and KAV03 at the Ävrö study site.

Rock type	Percentage	Abbreviations used in SIMCA
Granite	88.0	gr
Aplite	1.6	ap
Pegmatite	0.2	pe
Mafic	3.2	ba
Porphyry	1.5	vg
Mixture of hybrid and tectonite	5.0	ur te
Core loss	0.5	
	100.0	

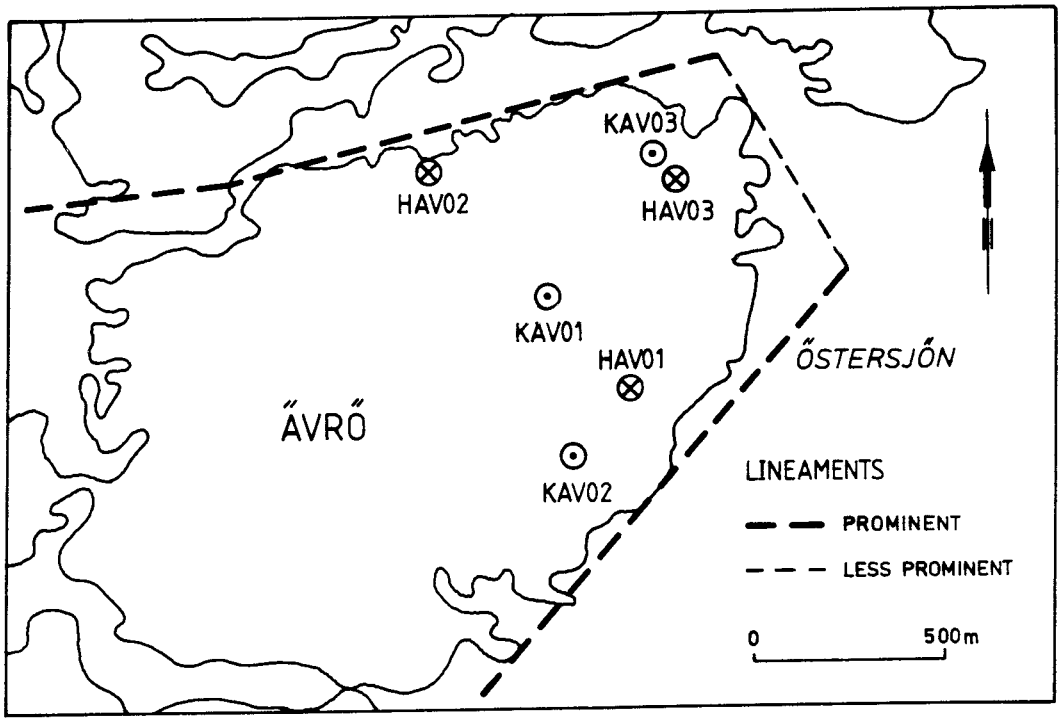

Fig. 8.1 Location of the boreholes within the Ävrö study site.

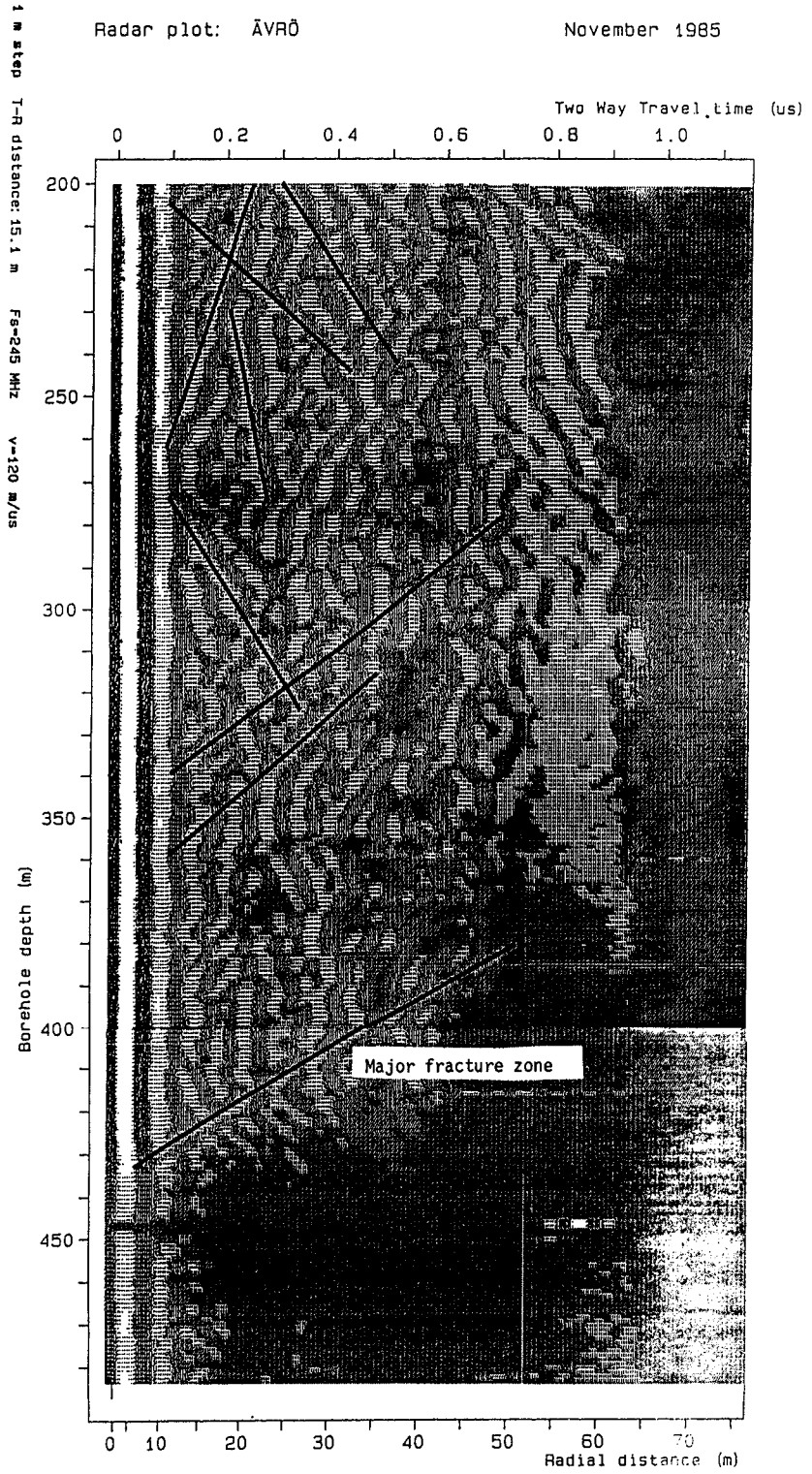

Fig. 8.2 Radar map from the section 200-480 m in the borehole KAV01 at Ävrö with a center frequency of 22 MHz.

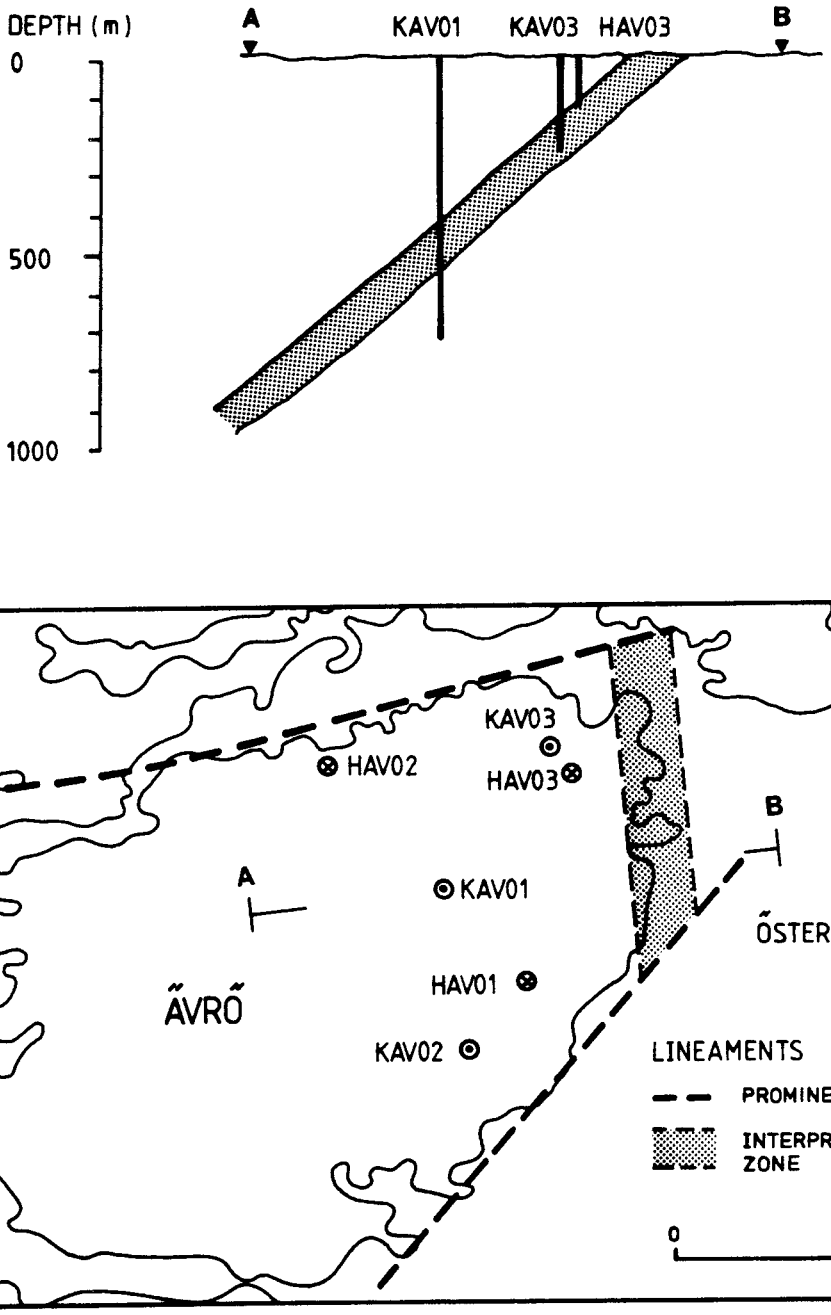

Fig. 8.3 Tentative interpretation of the extension of the major fracture zone encountered in borehole KAV01.

8.2 PRINCIPAL COMPONENT ANALYSIS OF THE DATA FROM ÄVRÖ.

The Principal Component analysis gives a description of the general character of the investigated rock at Ävrö. The variables and the components are presented in Table 8.2.

Values of explained variance show that only six components can be used in the description. Variables representing different features of fracturing together with lateral and normal resistivity and single point resistance are of importance in the Principal Component analysis. The strongest correlations result in a division between low fractured, high resistive rock and highly fractured, low resistive rock. High fracture frequency, fracture zones, and crushed zones occur together at one side of Component 1, and the resistivity is also low at this side. Hematite is also present at the fractured sections. Radar intensity occurs firstly in the third component together with granite, hematite and self potential log. Conclusions about the character of the granite sections are difficult to draw on basis of the variable set and the mirror points to the set on the opposite side. Hydraulic conductivity never shows up in the usable components.

The summary of the Principal Component analysis is that it shows a distinct division between low fractured, high resistive rock and highly fractured, low resistive rock.

Table 8.2 Components from the Principal Component analysis of data from the Ävrö study site.

Comp.	Explained variance	Negative		Positive
1	15.9	FS SP C9 F9 Hm	++	SU GE NR LR
2	10.5	gr Cl Fe Ca	++	F9 Hm NR GA rb te
3	6.8	Hm RI gr SP	++	SU Fe Ca Cl
4	5.6	GE	++	ur
5	4.8	vg	++	rb GA ap
6	4.6	te F9 Hm gr	++	S9
7	0	HC	++	
8	0		++	HC
9	0	ba	++	RI ep vg
10	0	Ep	++	RI

Activated variables
++ = Center point
GA = Gamma log
GE = Geohm log or single point resistance
LR = Lateral resistivity log
NR = Normal resistivity log
SP = Self potential
SU = Susceptibility log
F9 = Fracture zone freq.0-90 deg.
S9 = Single fracture freq.0-90 deg.
C9 = Fracture frequency in crushed zones, 0-90 deg.
FS = Total fracture freq.0-90 deg.
Ca = Calcite
Fe = Fe-oxide
Hm = Hematite
Py = Pyrite
Ep = Epidote
Cl = Chlorite
gr = Granite
ba = Basite (mafic)
vg = Porphyry
te = Tectonite
ur = Mixture of hybrid and tectonite (unknown rock)
ap = Aplite
rb = Lithological contact
RI = Radar intensity
HC = Hydraulic conductivity

8.3 PLS-ANALYSIS OF THE DATA FROM ÄVRÖ.

Values of explained variance for the components from the PLS-analysis of data from Ävrö show that three components can be used. The variables and the components are presented in Table 8.3.

The PLS-analysis indicates that the most important variables seem to be different features of fracturing together with lateral and normal resistivity. The analysis shows that the strongest correlations result in a division between low fractured rock and highly fractured rock, as was the case for the Principal Component analysis. High radar intensity occurs at the sections with high fracture frequency, crushed zones, hematite and high self potential. The mirror points to lateral and normal resistivity exhibit low values at these sections. Next component shows that high radar intensity occurs at sections with generally low fractured granite. It is difficult to conclude more about the features of the granite. The third component shows that high radar intensity occurs at fractured sections with low resistivity. According to Tullborg et al. (1986), might the presence of the fracture mineral Fe-oxide be an indication of waterflow. The presence of chlorite and calcite might be due to high fracturing. Hydraulic conductivity exhibits poor correlations to the important variables, and do not show up in the three usable components.

A summary of the PLS-analysis is that there is a distinct division between low fractured, high resistive rock and highly fractured, low resistive rock. Radar intensity correlates with fracture frequency and low resistivity.

Table 8.3 Components from the PLS-analysis of data from the Ävrö study site.

Comp.	Explained variance X	Y	Negative	Positive
1	10.4	6.6	LR NR SU ++	C9 Hm FS SP RI
2	12.6	3.5	Cl ba FS Fe Ca C9 F9 ur ++	gr RI
3	7.9	2.1	NR ba SP ur ++	SU Fe Cl Ca RI
4	4.2	1.9	gr Cl Fe ++	ba ur Py SU RI
5	7.8	1.5	rb NR vg ap te F9 GA ++	gr RI
6	3.7	1.5	gr Py S9 ++ F9 te GE NR rb	HC ap ba GA RI
7	1.5	1.5	GE ++	S9 Py vg HC RI
8	1.3	1.5	te S9 Cl ++	HC FS C9 RI

Activated variables
++ = Center point
GA = Gamma log
GE = Geohm log or single point resistance
LR = Lateral resistivity log
NR = Normal resistivity log
SP = Self potential
SU = Susceptibility log
F9 = Fracture zone freq.0-90 deg.
S9 = Single fracture freq.0-90 deg.
C9 = Fracture frequency in crushed zones, 0-90 deg.
FS = Total fracture freq.0-90 deg.
Ca = Calcite
Fe = Fe-oxide
Hm = Hematite
Py = Pyrite
Ep = Epidote
Cl = Chlorite
gr = Granite
ba = Basite (mafic)
vg = Porphyry
te = Tectonite
ur = Mixture of hybrid and tectonite (unknown rock)
ap = Aplite
rb = Lithological contact
RI = Radar intensity
HC = Hydraulic conductivity

8.4 PLS2-ANALYSIS OF THE DATA FROM ÄVRÖ.

Three components can be used in the description of PLS2-analysis of data from Ävrö, according to values of explained variance. The variables and the components are presented in Table 8.4.

The PLS2-analysis exhibits a similar pattern of the components as the previous Principal Component analysis and PLS-analysis. Different features of fracturing, resistivity, and lithological contact are variables of importance in the analysis. The strongest correlations result in a division between low fractured rock and highly fractured rock. High radar intensity occurs at the fractured side together with high fracture frequency, crushed zones, hematite, and high self potential. The mirror point to lateral resistivity indicates low values together with high radar intensity. High radar intensity also occurs at granite sections with high hydraulic conductivity in Component 2. Component 3 shows that radar intensity occurs at lithological contacts at aplite and tectonite. Hydraulic conductivity occurs together with high resistivity on the opposite side to radar intensity in the first and most important component. This indicates that there is high hydraulic conductivity at low fractured sections in the rock. One explanation might be the presence of individual hydraulically conductive fractures in these sections. Hydraulic conductivity also occurs together with radar intensity in Component 2, as mentioned above. This show that there exists a correlation between hydraulic conductivity and radar intensity, even if the correlation is not the strongest one in the PLS2-analysis. High hydraulic conductivity also occurs at sections with granite in general.

To sum up the PLS2-analysis, it can be said that it exhibits a division between low fractured and highly fractured rock. High radar intensity correlates very well with fracture frequency and low resistivity. Radar intensity correlates with a lesser degree with hydraulic conductivity and lithological contacts.

Table 8.4 Components from the PLS2-analysis of data from the Ävrö study site.

Comp.	Explained variance X	Y	Negative		Positive
1	12.4	5.5	HC LR	++	C9 Hm FS SP RI
2	10.9	3.8	ur ba	++	HC gr RI
3	7.8	2.6	HC gr	++	SU rb te ap GA RI
4	4.3	2.4	HC NR rb	++	Ep Fe Ca Cl RI
5	3.4	2.0	HC	++	rb Ca Fe Cl
6	8.0	1.6	Py NR gr	++	RI Cl FS C9 Fe HC
7	2.2	1.6	Ca ba F9	++	S9 GA ur RI HC
8	3.1	1.4	GE GA	++	rb SU vg HC RI

Activated variables
++ = Center point
GA = Gamma log
GE = Geohm log or single point resistance
LR = Lateral resistivity log
NR = Normal resistivity log
SP = Self potential
SU = Susceptibility log
F9 = Fracture zone freq.0-90 deg.
S9 = Single fracture freq.0-90 deg.
C9 = Fracture frequency in crushed zones, 0-90 deg.
FS = Total fracture freq.0-90 deg.
Ca = Calcite
Fe = Fe-oxide
Hm = Hematite
Py = Pyrite
Ep = Epidote
Cl = Chlorite
gr = Granite
ba = Basite (mafic)
vg = Porphyry
te = Tectonite
ur = Mixture of hybrid and tectonite (unknown rock)
ap = Aplite
rb = Lithological contact
RI = Radar intensity
HC = Hydraulic conductivity

8.5 COMPARISON WITH PREVIOUS INTERPRETATION OF RADAR DATA FROM ÄVRÖ.

The radar investigation at the Ävrö boreholes KAV01 and KAV03 was performed at two separate occasions. The first radar measurement in KAV01 between 0 - 502 m was evaluated by Carlsten et al. (1986) and the second radar measurement in KAV01 between 502 - 744 m and in KAV03 was evaluated by Gentzschein et al. (1987). The purpose of both reports were to establish the orientation of a fracture zone encountered between 418 - 578 m in borehole KAV01. A detailed study of the kind of features which were detected by the borehole radar were not made except for the interpretation of the major units. A comparison between the rock logs and the list with intersections of radar reflections in the boreholes shows that there is an equal distribution of interpreted radar reflectors between lithological contacts and fractured sections.

The PLS-analysis of data from the boreholes at Ävrö shows that in the first component high radar intensity occurs together with highly fractured and crushed sections. However, the component does not incorporate hydraulic conductivity. This indicates that of the radar detected sections in the boreholes at Ävrö, highly fractured sections constitute the largest group. In the second component high radar intensity occurs together with granite and hydraulic conductivity. This component does not show the character of the geological features connected to radar intensity, except that they are hydraulically conductive. In general, hydraulic conductivity does not show a very good correlation to any of the parameters measured in the Ävrö boreholes.

9 PHYSICAL PROPERTIES OF CORE SAMPLES FROM THE BOREHOLES KFI09, KFI11, KKL02, AND F2.

Measurements of the high frequency electrical properties of core samples have been performed in order to relate the values of the dielectric constant and electric conductivity obtained from in situ measurements to those obtained from core samples. The core samples also provide a means to relate the electrical properties of the samples to other observable properties of the core such as fracture minerals and rock type. However, measurements on core samples have some inherent limitations due to the fact that measurements can only be made on intact rock samples. For example, fracture zones will always be under-represented in core sample data sets. Thus, it is natural that the data obtained in situ will have a greater spread in values compared to the data obtained from core samples.

For this study a total of 80 samples have been taken from the boreholes KFI09 (25 samples), KFI11 (25 samples), and KKL02 (30 samples). In addition data from measurements on core samples from borehole F2 in the Stripa mine has been used in the analysis (Magnusson et. al., 1987). This provided data on electromagnetic properties from a set of 149 samples which are analyzed below.

The measurements of the electrical properties of the core samples were made by the department of Applied Geophysics at the University of Luleå, Sweden. The procedures for preparation of the samples and the measurement technique is described by Sherman (1983) and Magnusson et. al. (1987). Measurement of the dielectric constant and the electric conductivity were made at five different frequencies; 0.025, 1, 5, 20, and 70 MHz. The porosity of the samples have also been measured in order to relate the electrical properties to the water content of the rock. The complete set of results are presented in Appendix D.

A few samples have been excluded from the analysis for the respective frequencies. The number of excluded samples are listed in Table 9.1. The samples were generally excluded on the basis that it had been not possible to measure their electrical properties with the technique applied. The excluded samples generally had very high porosities with porosity values were in the range 6-22%, which is very high for crystalline rock. The high porosity has probably led to anomalous electric properties outside the range of the measuring apparatus.

Table 9.1 Number of measurements used in the analysis for each frequency.

Frequency MHz	Excluded samples	Used samples
0.025	4	145
1	4	145
5	7	142
20	7	142
70	7	142

A SIMCA analysis was attempted on the data set listed in Appendix D together with additional information available from the corresponding locations in the boreholes. This included core log data (fracture minerals, rock types, etc.), geophysical logs, and hydraulic tests. In this case the SIMCA analysis met with limited success. The basic reason was the limited number of samples in relation to the number of parameters used in the analysis.

In order to reduce the number of parameters separate SIMCA analyses were made with restricted sets of parameters. Three separate analyses were made with different sets of parameters included in each analysis. The electrical properties were included as parameters in all analyses while fracture minerals, fracture frequency, and rock type parameters were included one at a time in each of the three analyses. A good correlation was found between high electric conductivity, dielectric constant, and density for all three analyses. The analysis including the fracture mineral parameters gave a good correlation of chlorite and iron stained fractures with high electric conductivity and dielectric constant. The analysis including the fracture frequency parameters gave a moderate correlation of electrical properties to total fracture frequency and the occurrence of single fractures. In the analysis including rock types a negative correlation was found between electric properties and grey granite. This implies that dielectric constant and conductivity have low values in grey granite.

There is plenty of experimental and theoretical evidence that the electrical properties of rock essentially are a function of porosity and the electrical properties of the pore fluid. This is under the assumption that the rock does not contain electrically conductive minerals. An empirical relation was established by Archie (1942)

$$\sigma = a\ \sigma_w \Phi^m$$

where

σ = formation conductivity
σ_w = pore fluid conductivity
Φ = porosity
a = dimensionless parameter close to 1
m = cementation factor, normally in the range 1 to 2.2.

Archie's law is valid for low frequencies (actually static currents) and a more complex equation has been derived by Sen et.al. (1981) which is valid for all frequencies. The low frequency limit of Sen's equation yields Archie's law. The correlation of electrical properties and porosity of the core samples have been analyzed to study the validity of equations derived by Archie and Sen et.al.

A crossplot of the dielectric constant versus the porosity of the samples is shown in Figure 9.1. A general trend of increasing dielectric constant with porosity can be observed. There are a few samples which have porosities above 2% but a relatively low dielectric constant compared to the rest of the samples. These high porosity samples come from borehole F2 in Stripa and they consist of intensely altered samples of granite (Magnusson, Carlsten, and Olsson, 1987). The large spread in the data points give rise to a poor correlation between dielectric constant and porosity with regression coefficients in the range 0.07 to 0.43 (Table 9.2). Table 9.2 includes the regression data for all frequencies and there is a poor correlation for all frequencies. A correlation analysis was also made for all samples classified as granite, these points are marked with an "x" in Figure 9.1, and this resulted in a considerable improvement of the correlation coefficients (Table 9.3). Correlation coefficients are now in the range 0.41 to 0.61, which must be considered as fair. From the table we observe that the dielectric constant decreases with frequency. This is also demonstrated in Figure 9.2 which shows the average dielectric constant of the granite samples as a function of frequency. There is also a decrease in standard deviation with frequency.

Table 9.3 shows that the parameter "B" decreases with frequency. This implies smaller changes in dielectric constant with porosity as frequency increases. There is a drastic change for frequencies lower than 1 Mhz, but this is outside the frequency range of interest for radar applications. A comparison of data from the different sites is made in Table 9.4.

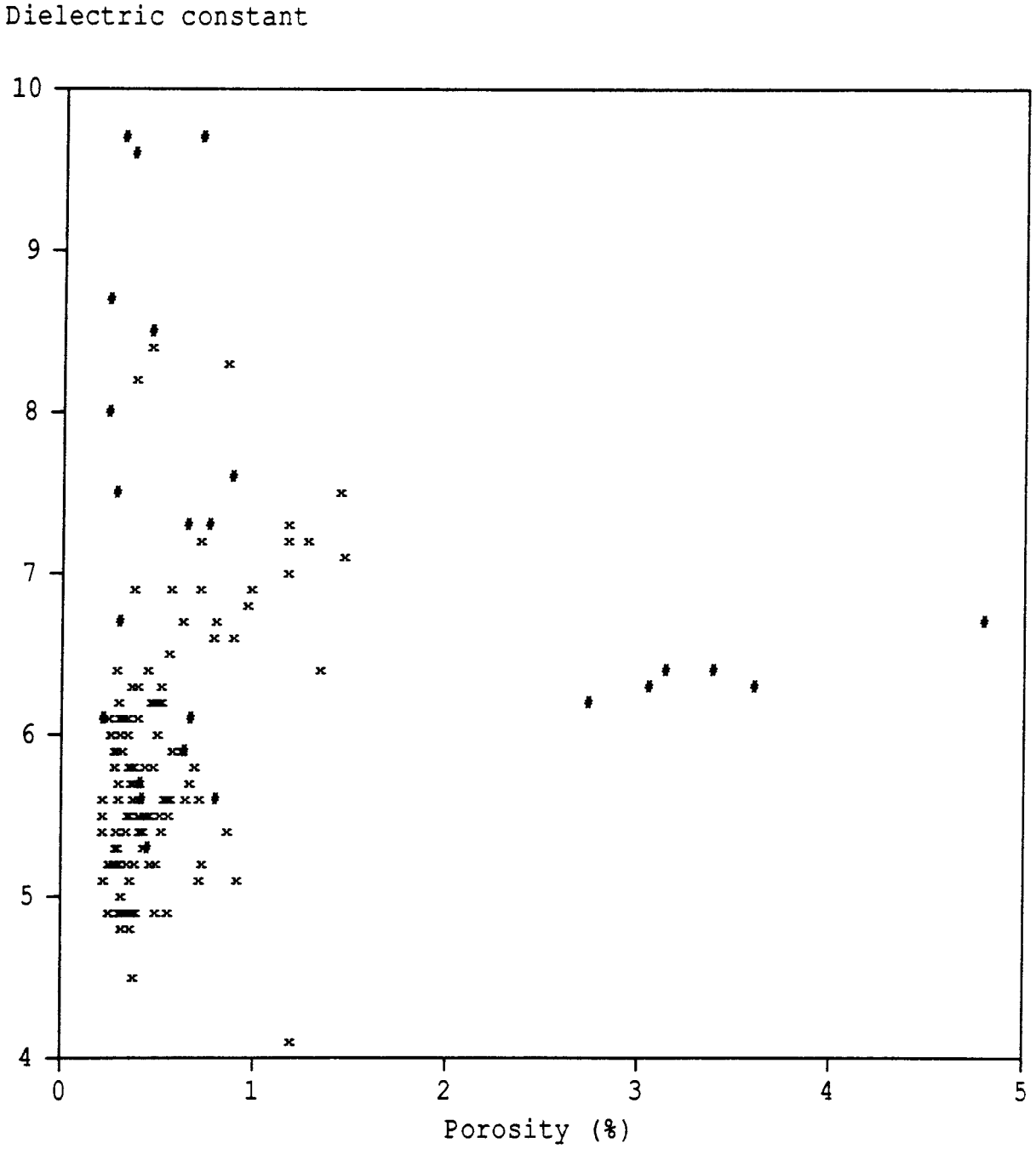

Figure 9.1 Crossplot of dielectric constant at a frequency of 20 MHz versus porosity. x = samples classified as granite are indicated, # = other rock types.

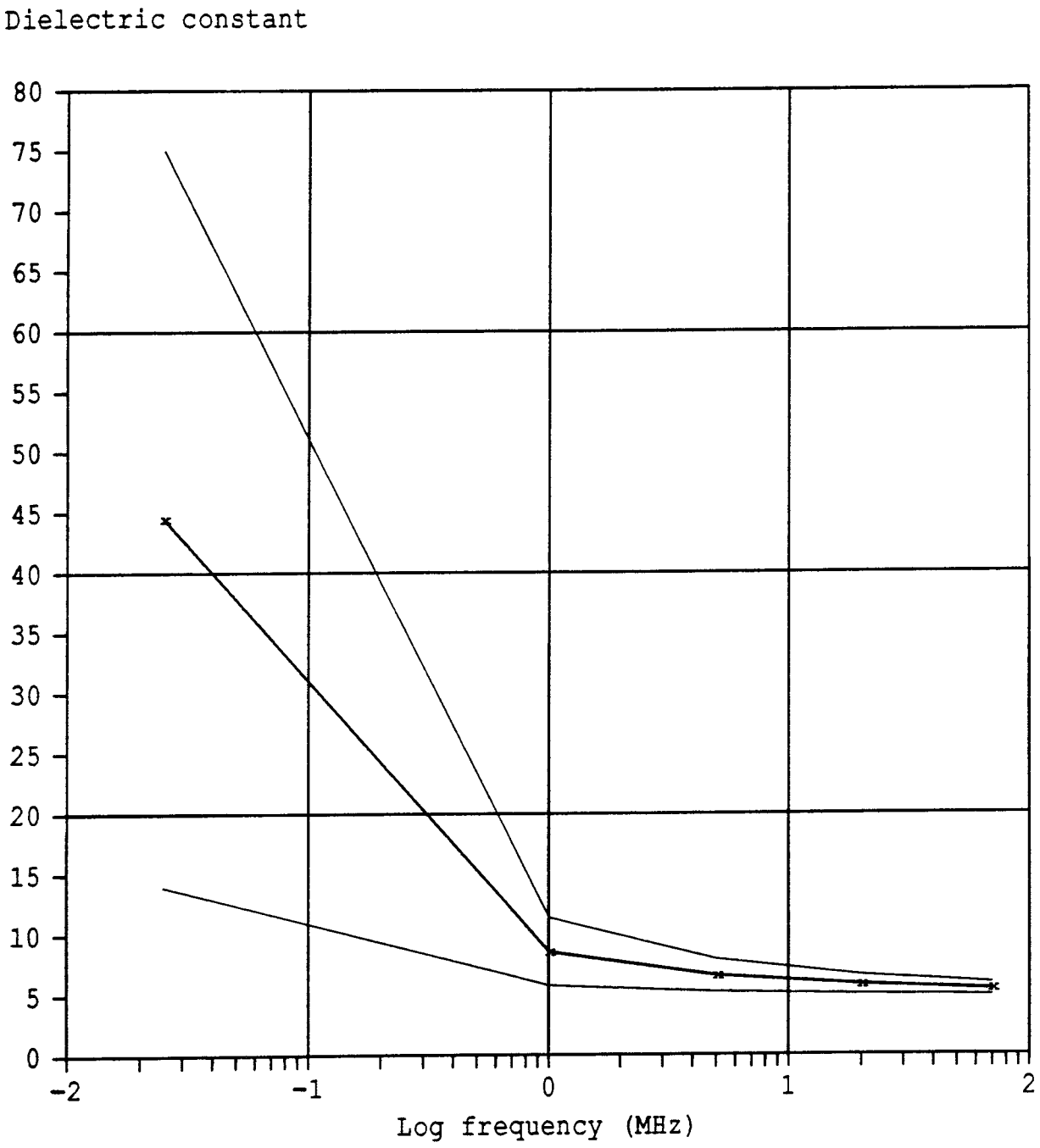

Figure 9.2 Average dielectric constant as a function of frequency for samples classified as granite. Thin lines indicate the standard deviation.

Table 9.2 Results from linear regression of dielectric constant versus porosity. All samples. $\varepsilon_r = A + B * \Phi$.

Frequency MHz	A	B	r	$\langle\varepsilon_r\rangle$	$\langle\Phi\rangle$
0.025	35.05	20.01	0.43	47.11	0.61
1	9.15	0.43	0.07	9.41	
5	6.63	0.42	0.17	6.89	
20	5.84	0.27	0.18	6.01	
70	5.45	0.24	0.21	5.60	

Table 9.3 Results from linear regression of dielectric constant versus porosity. Samples classified as granite. $\varepsilon_r = A + B * \Phi$.

Frequency MHz	A	B	r	$\langle\varepsilon_r\rangle$	$\langle\Phi\rangle$
0.025	11.05	68.18	0.61	44.52	0.49
1	5.83	5.62	0.55	8.59	
5	5.25	2.68	0.54	6.58	
20	5.15	1.32	0.46	5.80	
70	5.03	0.81	0.41	5.43	

Table 9.4 Results from linear regression of dielectric constant versus porosity. Data from all samples measured at 20 MHz separated into sites. $\varepsilon_r = A + B * \Phi$.

Site	A	B	r	$\langle\varepsilon_r\rangle$	$\langle\Phi\rangle$
Stripa	5.18	0.37	0.57	5.45	0.72
Klipperås	5.98	1.52	0.14	6.54	0.36
Finnsjön	5.95	1.07	0.46	6.56	0.58
All	5.84	0.27	0.18	6.01	0.61

The crossplot of electric conductivity versus porosity is shown in Figure 9.3. The high porosity samples from Stripa are outside of the general cluster also in this case. The regression coefficients are approximately 0.4 (Table 9.5) for all frequencies except the lowest one if all samples

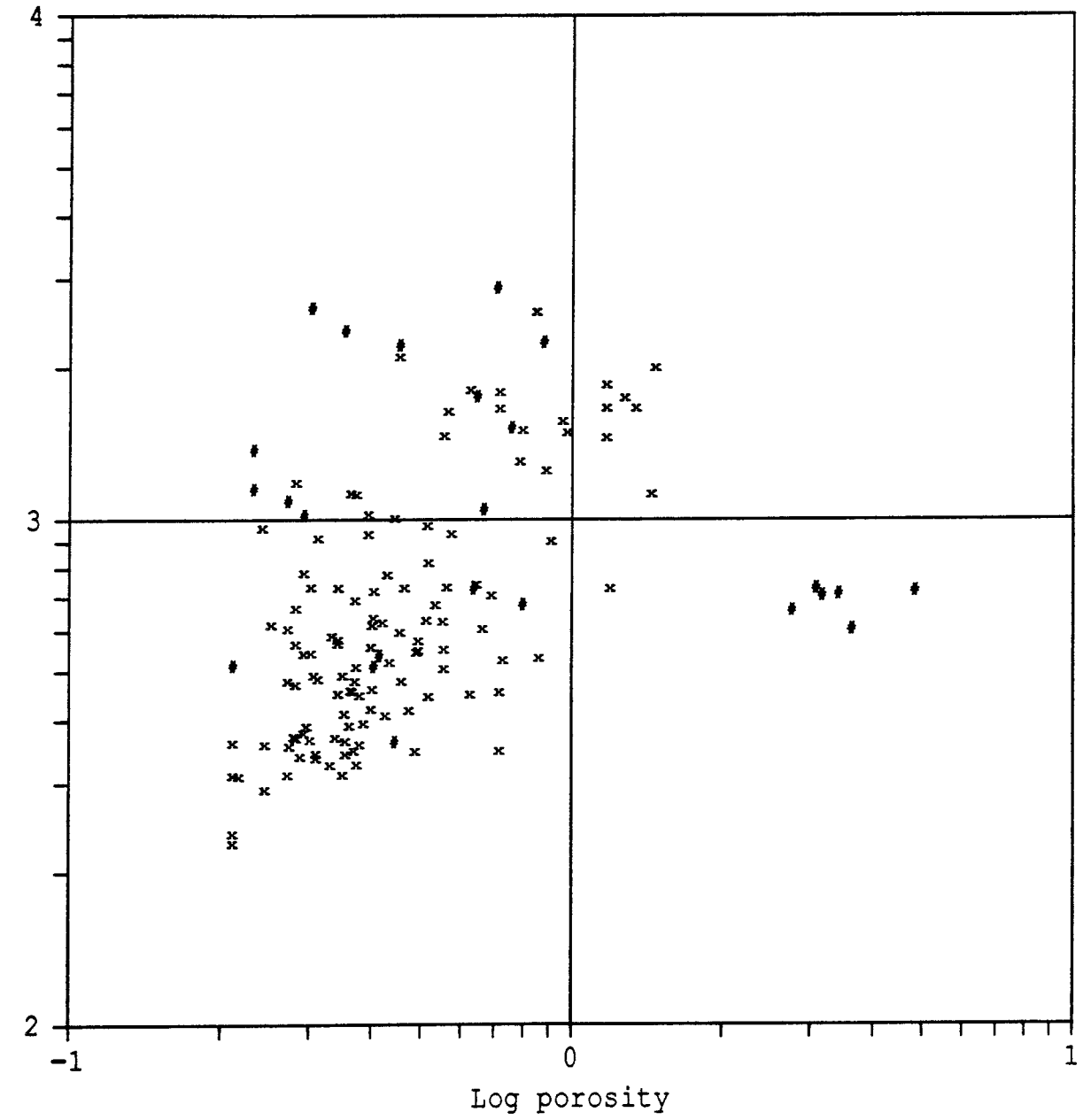

Figure 9.3 Crossplot of electric conductivity at a frequency of 20 MHz versus porosity. x = samples classified as granite are indicated, # = other rock types.

are included. If only the granite samples are considered the regression coefficients become approximately 0.6 (Table 9.6). The exclusion of the non-granitic samples changes the value of the cementation factor from approximately 0.4 to 0.8. If the lowest frequency is excluded the cementation factor may be considered as frequency independent. A cementation factor of 0.8 is lower than the value of 1.5 which is expected based on the theoretical analysis by Sen et.al. (1981). We also find an increase in the average conductivity with frequency (Figure 9.4) which was not predicted by Sen et.al. (1981). The conductivity is proportional to frequency raised to the power 0.44.

Table 9.7 shows a comparison of the conductivity data for the three sites. On the average the highest conductivities are found in Finnsjön and this is also the site where the smallest radar range (50-60 m) has been obtained. Average conductivities from Stripa and Klipperås are comparable as well as the obtained radar ranges (100-120 m). This demonstrates that core sample data on high frequency electric properties are a good predictor of in situ radar performance.

The core sample data show a good correlation between electric conductivity and porosity which roughly follows Archie's law. The cementation factor is lower compared to what could be theoretically expected. A further study of this discrepancy is clearly worth while. The correlation between dielectric constant and porosity is poorer but this could be due to the smaller relative accuracy in the dielectric constant data. The nongranitic samples showed a poor correlation to porosity and this indicates that other factors significant for the high frequency electric properties exist.

The overall correlation of the electric parameters to porosity supports the general conclusion drawn from the SIMCA analysis that radar reflexes mainly are caused by fracture zones.

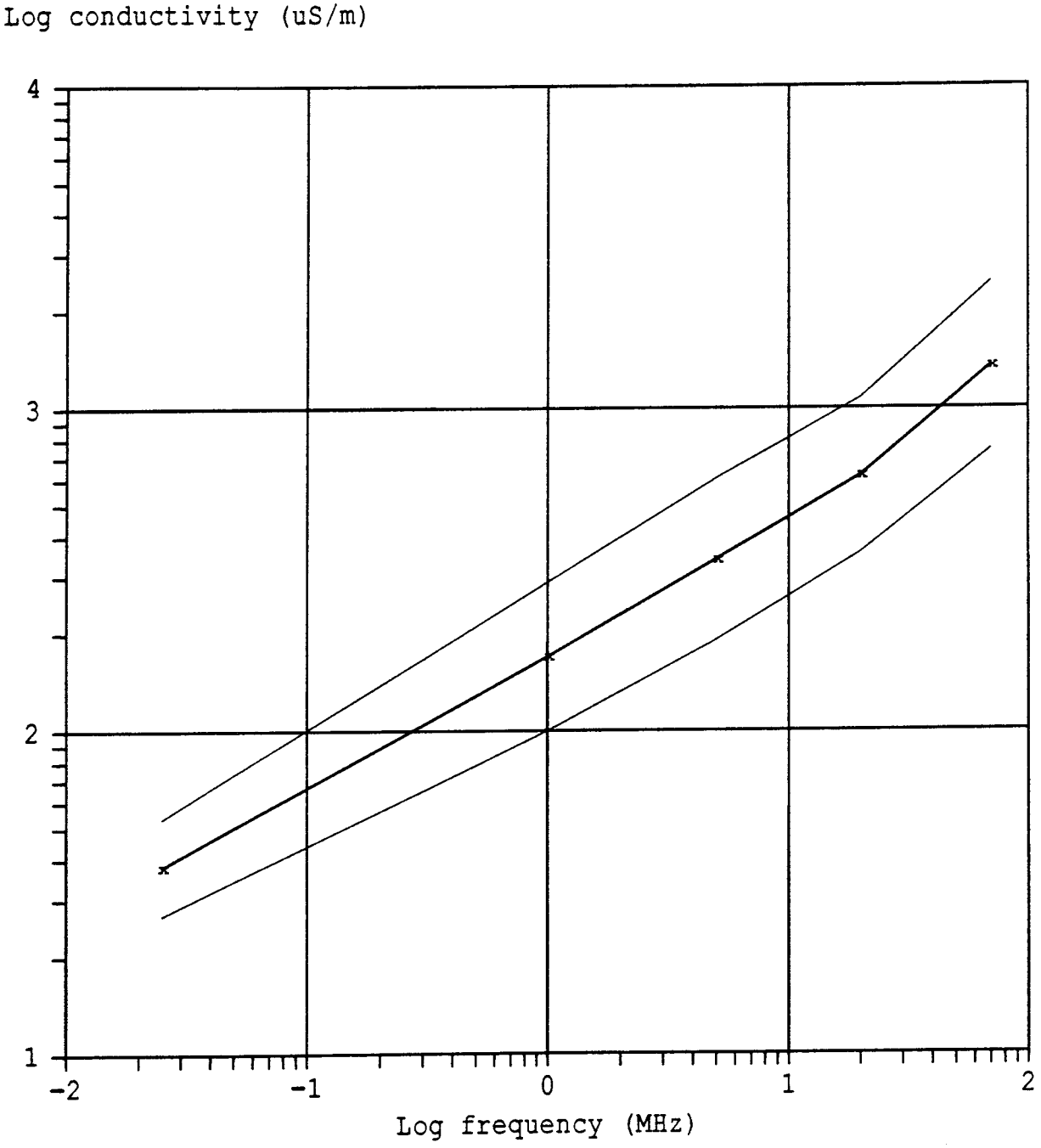

Figure 9.4 Average electric conductivity as a function of frequency for samples classified as granite. Thin lines indicate the standard deviation.

Table 9.5 Results from linear regression of log conductivity versus log porosity. All samples. $\log(\sigma) = A + m * \log(\Phi)$.

Frequency MHz	A	m	r	$\langle\log(\sigma)\rangle$	$\langle\Phi\rangle$
0.025	1.72	0.43	0.62	1.57	0.61
1	2.38	0.35	0.44	2.26	
5	2.69	0.39	0.40	2.57	
20	2.96	0.39	0.41	2.83	
70	3.29	0.38	0.37	3.17	

Table 9.6 Results from linear regression of log conductivity versus log porosity. Samples classified as granite. $\log(\sigma) = A + m * \log(\Phi)$.

Frequency MHz	A	m	r	$\langle\log(\sigma)\rangle$	$\langle\Phi\rangle$
0.025	1.68	0.27	0.35	1.58	0.49
1	2.47	0.68	0.59	2.23	
5	2.79	0.75	0.59	2.53	
20	3.08	0.80	0.67	2.79	
70	3.43	0.83	0.64	3.13	

Table 9.7 Results from linear regression of log conductivity versus log porosity. Data from all samples measured at 20 MHz separated into sites. $\log(\sigma) = A + m * \log(\Phi)$.

Site	A	m	r	$\langle\log(\sigma)\rangle$	$\langle\Phi\rangle$
Stripa	2.80	0.31	0.61	2.71	0.72
Klipperås	3.08	0.60	0.30	2.80	0.36
Finnsjön	3.21	0.63	0.69	3.02	0.58
All	2.96	0.39	0.41	2.83	0.61

10 DISCUSSION

10.1 EXPERIENCES FROM USE OF THE SIMCA METHOD

Multivariate data analysis (SIMCA) has been performed with data from 23 boreholes at Klipperås, Finnsjön, Saltsjötunnel, Stripa and Ävrö. A total amount of 90000 data was included in the SIMCA analyses. The purpose was to study the correlation between borehole radar measurements and other geophysical, geological, and hydrological parameters.

The primary target was to give a clearer picture of what structures borehole radar is able to detect and the relevance to water transport through the rock of these structures.

For the data modelling two different algorithms available in the SIMCA software was used. One for Principal Component analysis and one for Partial Least Squares regression analysis (PLS and PLS2).

The **Principal Component analysis** gives a general description of the data in terms of relations between measured variables. It also works as an indicator of the accuracy of the input of data. In the Principal Component analysis it is possible to quantify the correlation between the strongest variables and to define those variables.

The **PLS analysis** gives information about the correlation of one selected variable to the other variables. In our case radar intensity was compared to the other variables. The PLS analysis of radar intensity worked satisfactorily at all sites.

The **PLS2 analysis** gives information about the correlation of two or more variables to the remaining variables. In our case PLS2 analysis was made to correlate radar intensity and hydraulic conductivity to the remaining variables. The hydraulic conductivity data from Klipperås was not included in the SIMCA analysis. Instead a PLS2 analysis was made on Klipperås data with radar angles and radar intensity as correlation variables.

The basic model used in the SIMCA analysis comprises 65 different variables. It was possible to use 35 of these variables, but a smaller number was used in most analyses due to differences in the number of mapped rock types, fracture minerals and in some cases missing geophysical logs.

This study has shown that only some variables are suitable to use in a SIMCA analysis of this type. These are the following geophysical logs: natural gamma log, single point resistance log, lateral resistivity log, normal resistivity log, sonic log, self potential log, and susceptibility log. Parameters from the geological core log which are suitable are fracture zones, single fractures, crushed zones, and the total fracture frequency. Fracture minerals and all rock types can also be used as variables. The variable lithological contact was created from the geological core log and turned out to be a very useful variable. Finally, hydraulic conductivity could be used where the data had sufficient resolution. This depended on the section length used at the hydraulic conductivity measurements. For hydraulic conductivity data to be suitable for a SIMCA analysis the section length should be two meter or less.

Attempts were made to use the following parameters in the SIMCA-analyses, but generally they were found to have little relevance to the problem. The parameters temperature log (QT), vertical temperature log (QG), borehole fluid resistivity (QR), and salinity of borehole fluid (QS) were not included. Normally, there is an increase in temperature with depth in a borehole which gives the temperature gradient a constant background value. The temperature gradient might increase or decrease at locations with water flow in or out of the borehole, due to a number of factors such as the relative temperature of in- or outflowing water to the borehole fluid and the direction of flow in the borehole. Hence water flow may cause both positive and negative temperature gradient anomalies. This makes the correlation with other variables quite spurious and difficult to interpret. The same type of discussion can be applied to borehole fluid resistivity and the salinity of the borehole fluid, two variables which are closely related to each other. These variables may also be high or low at locations of waterflow. Twelve variables containing different features of fracturing were excluded from the study since they contain data on the angle of fractures to borehole axis. The angle to borehole axis was not considered relevant for this study. The variable vertical depth (ZZ) was not used since borehole radar is not considered to be depth dependent. The 7 variables containing geophysical measurements on core samples were not used in the study because there were only a few measurements in every cored borehole. The 6 variables containing radar angles were not used. They were considered to be without interest in this study which did not

include geometrical correlation of features at the sites.

In almost all SIMCA analyses in this study, variables connected to properties of the borehole fluid were excluded for reasons mentioned above. The character of these variables make correlation with other variables spurious and difficult to interpret. It is therefore of interest to compare results of a PLS-analysis including the borehole fluid parameters to a PLS-analysis where these parameters have been excluded. Data from Stripa were selected as an example and the results of these PLS-analyses are presented in Tables 10.1 and 10.2 and Figure 10.1.

There are no dramatic changes in the variables contained in component 1 between the PLS-analysis excluding borehole fluid parameters and the PLS-analysis including these parameters. Two variables disappear when the borehole fluid parameters are excluded, both belong to the excluded group, and only one variable is added to component 1, namely single fractures (S9), but this variable exhibits a weak correlation to radar intensity in this component. The hydraulic conductivity is one of the variables with the strongest correlation to radar intensity when the borehole fluid parameters are excluded while inclusion of these variables leads to a reduced correlation between radar intensity and hydraulic conductivity. There are greater changes in component 2 between the two PLS-analyses than there are in component 1. All four variables connected to borehole fluid are of course excluded in the new analysis. Also, lateral resistivity (LR), fracture zones (F9), and hydraulic conductivity (HC) are absent as variables of importance in component 2 in the analysis excluding the borehole fluid parameters, while two variables are added, namely single fractures (S9) and susceptibility (SU). There are also changes in the position of variables between the two analyses. Lithological contact (rb), for example, correlates stronger to radar intensity if borehole fluid parameters are excluded. There are much greater changes in component 3 than the first two components. Five variables were excluded or are absent as variables of importance when excluding the borehole fluid parameters. These are salinity (QS), temperature (QT), lithological contact (rb), single fractures (S9), and fracture frequency (FS). Two variables are added, gamma (GA) and single point resistance (GE). Only three variables are retained between the two analyses, susceptibility (SU), self potential (SP), and of course radar intensity (RI).

Table 10.1 Components from PLS-analysis of data from the boreholes at the crosshole site in Stripa with variables connected to borehole fluid **excluded**.

Comp.	Explained variance X	Y	Negative		Positive
1	21.8	13.6	NR LR GE GA	++	S9 SO F9 HC Ep FS RI
2	7.4	3.9	SP S9 NR SU	++	GE rb GA RI
3	11.3	2.2	GA GE SU	++	SP RI
4	8.2	2.0	SO SP	++	FS RI
5	4.9	1.8	Ep F9 NR FS rb	++	SO RI
6	8.2	1.5	HC rb S9	++	F9 Ep SO RI
7	4.0	1.6	F9 FS LR	++	rb SU RI
8	2.9	1.5	rb SU SO	++	HC RI

Table 10.2 Components from PLS-analysis of data from the boreholes at the crosshole site in Stripa with variables connected to borehole fluid **included**.

Comp.	Explained variance X	Y	Negative		Positive
1	21.8	12.9	NR GE LR QR GA	++	HC SP SO QS F9 Ep FS RI
2	20.4	4.7	SP QS NR LR QT	++	F9 HC rb QG GE QR GA RI
3	8.1	4.6	S9 SU FS	++	SP rb QS QT RI
4	4.3	3.0	SO	++	SU FS S9 LR RI
5	2.9	1.9	Ep F9 NR rb FS	++	HC SO RI
6	6.4	1.2	rb HC S9	++	SO Ep F9 RI
7	2.9	1.5	HC NR GE	++	rb SU QG RI
8	3.7	1.6	QG F9 HC	++	S9 rb RI

A

B

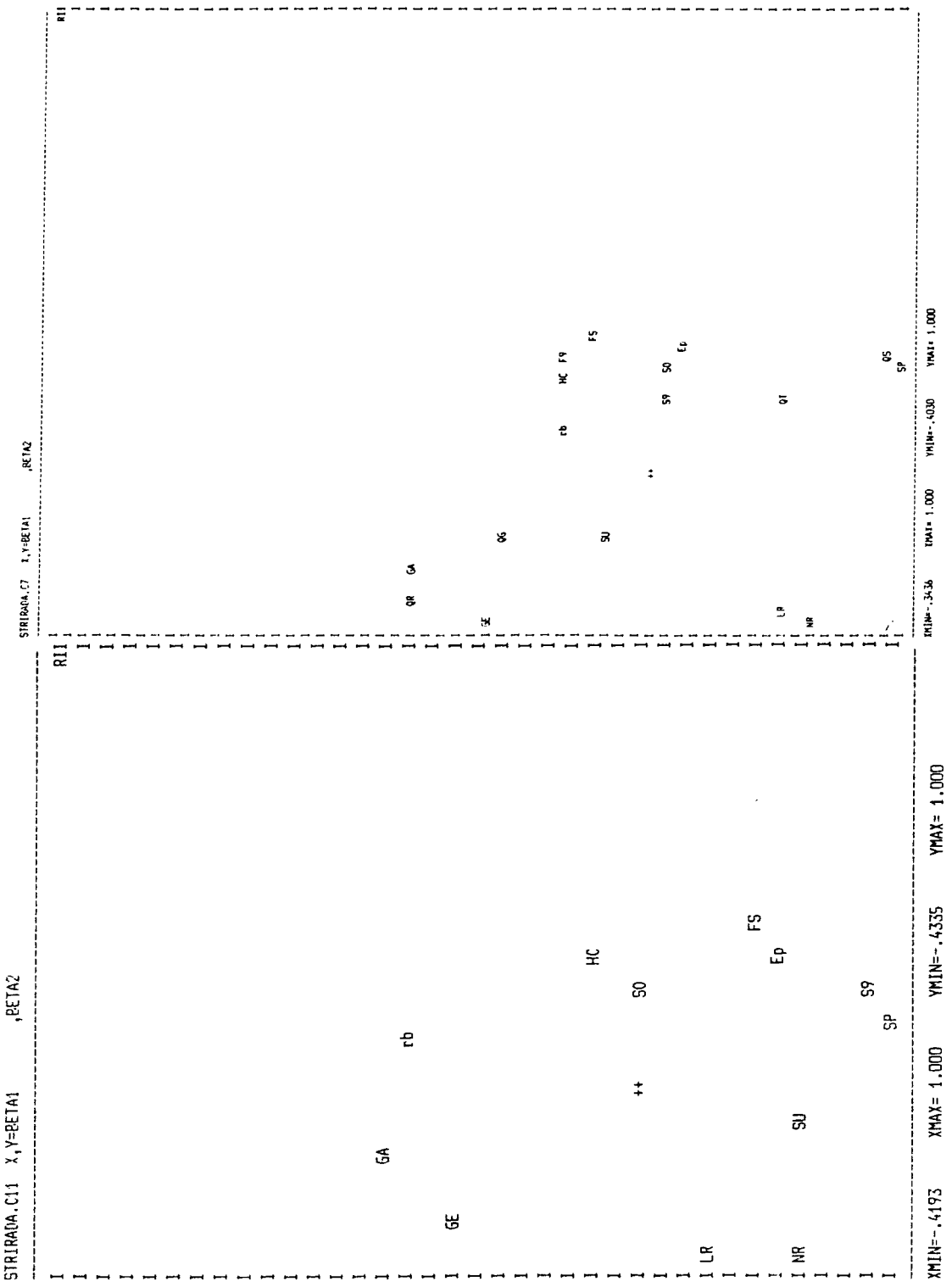

Fig. 10.1 Variable plots with principal components from the PLS-analysis of data from Stripa.
a. Variables connected to borehole fluid are **included**.
b. Variables connected to borehole fluid are **excluded**.

Table 10.3 Components from the Principal Component analysis of data from the boreholes at the crosshole site in Stripa with variables connected to borehole fluid **excluded.**

Comp.	Explained variance	Negative		Positive
1	21.6	NR GE LR	++	RI SO S9 HC SP F9 Ep FS
2	16.0	GA GE	++	SP
3	9.9	Ep LR F9 NR FS	++	rb HC
4	8.5	SO RI F9	++	S9 SU
5	6.8	HC F9	++	rb
6	6.7	SO S9	++	RI
7	6.2	RI S9	++	SU F9 rb
8	5.3	HC rb	++	SO RI SU
9	6.8	S9 Ep	++	HC SU SO
10	5.8	Ep	++	SP F9 FS

Table 10.4 Components from the Principal Component analysis of data from the boreholes at the crosshole site in Stripa with variables connected to borehole fluid **included.**

Comp	Explained variance	Negative		Positive
1	26.4	QR GA GE QG	++	QT SP QS
2	17.0	NR LR	++	SO RI Ep S9 HC F9 FS
3	8.3	Ep LR F9 NR FS	++	rb QG HC
4	7.3	SO GA RI GE QT	++	QG S9 SU
5	6.0	F9 QG QT	++	SO rb S9
6	5.4	HC SO	++	RI rb
7	4.6	RI HC S9	++	F9 QG rb SO
8	4.1	QT S9	++	NR LR SO HC
9	4.1	HC rb Ep	++	S9 QG SO RI
10	3.3	SU	++	FS S9 QG

The Principal Component analyses exhibit a somewhat different pattern. Component 1 in the analysis including the borehole fluid parameters is dominated by these parameters, cf. Tables 10.3 and 10.4. When excluding the borehole fluid parameters component 1 describes features of the rock, i.e. low fractured rock on one side and highly fractured rock on the other side together with high radar intensity and high hydraulic conductivity. This component is almost equal to component 2 in the analysis including the borehole fluid parameters. By excluding the borehole fluid parameters there is a stronger correlation of features connected to the rock.

Three different PLS-analyses were performed on the data from Klipperås. The purpose was to investigate the correlation of fracture minerals to other variables. The first analysis contained all variables except hydraulic conductivity, properties of the borehole fluid, and fracture minerals. The second analysis included the same variable set and in addition it also included borehole fluid properties and fracture minerals. The third analysis only contained fracture minerals and borehole fluid properties while all other variables were excluded.

A comparison of component 1 in the first (Table 10.5) and second (Table 10.6) PLS-analyses shows that there is a change from fractured lithological contacts at dolerite and greenstone correlating with high radar intensity to fracture zones with calcite and chlorite correlating with high radar intensity. Component 2 in the first and second PLS-analysis does not exhibit much of a change in the variables which correlate with high radar intensity. In both analyses low fractured lithological contacts at dolerite correlate with high radar intensity. The only change is that high normal resistivity and high susceptibility disappears as variables of importance in the second analysis. However, one interesting feature can be observed on the negative side of the component. Fe-oxide occurs in the second analysis together with fracture zones, high fracture frequency, and high temperature gradient. The presence of Fe-oxide might be an indication of waterflow. Component 3 in the first and second PLS-analysis does not show much change with respect to radar intensity either. High sonic travel times and high gamma radiation occur together with granite in both cases. The third analysis (Table 10.7) gives negative correlation of high radar intensity with temperature gradient in component 1. As mentioned above, low temperature gradient, as well as high temperature gradient, might indicate waterflow. Calcite and chlorite correlate with high radar intensity, which is also indicated in the second PLS-analysis.

The influence of single variables on the data set seems to play a minor role for the first and strongest components in the SIMCA-analysis. The description above shows that removal of one or several variables does not affect the analysis significantly. Only components with small amounts of data show dramatic changes. In the Principal Component method this can be of importance, because in this method more components than the first three strongest are of interest. In the PLS-method it is not as important, because only the first few and strongest components are useful.

Table 10.5 Components from PLS-analysis of data from the boreholes at the Klipperås study site. All variables except fracture minerals.

Comp.	Explained variance X	Y	Negative		Positive
1	26.8	9.8	NR GE LR gr GA	++	do rb ge F9 FS RI
2	8.8	6.7	SP ge FS S9 SO F9	++	NR SU do rb RI
3	12.9	5.6	SU ge do NR LR GE	++	SO GA gr RI
4	7.1	5.5	SO do	++	S9 NR RI
5	7.5	5.5	rb ge	++	RI
6	5.4	5.5	SU S9	++	NR rb SO RI
7	5.7	5.4	SP ge	++	S9 RI
8	5.1	5.5	SO LR	++	SP RI

Table 10.6 Components from PLS-analysis of data from the boreholes KKL06 and KKL08-KKL14 at Klipperås, including all variables and fracture minerals.

Comp.	Explained variance X	Y	Negative		Positive
1	82.4	79.7	NR GE LR gr GA	++	Ca F9 Cl FS RI
2	17.6	20.3	QG SO Ep Fe gr SP F9 FS GA Cl	++	do rb RI
3	0	0	ge SU QS	++	QR SO GA gr RI
4	0	0	SP QR GE LR	++	QS RI
5	0	0	QS gr GA	++	SP ge QG QR RI
6	0	0	do QG QR	++	LR gr NR RI
7	0	0	GE LR Ca F9 ge NR GA FS rb Ep	++	do SU SP RI
8	0	0	ge SP Fe	++	FS Py SU GE Cl G LR NR RI

Table 10.7 Components from PLS-analysis of data from the boreholes KKL06 and KKL08-KKL14 at Klipperås, including radar intensity, fracture minerals, and variables considered to be related to waterflow.

Comp.	Explained variance X	Y	Negative		Positive
1	80.5	79.5	QG	++	Ca Cl RI
2	19.5	20.5	QG Ep QS Fe	++	QR RI
3	0	0	QR	++	QT QS RI
4	0	0	QS Ca QT	++	QR Py RI
5	0	0	Py	++	RI
6	0	0	Ep	++	QS Ca Py RI
7	0	0	Cl QG QS	++	Fe QT Ep RI
8	0	0	Fe	++	Hm QG RI

10.2 COMPARISON OF SIMCA RESULTS FROM THE SITES

A comparison has been made of the results from the SIMCA-analysis of data from the different sites to see what general conclusions can be drawn concerning the causes of radar reflections.

The first and hence most important component of the Principal Component analysis has the same character at all five sites. It gives a description of rock quality where parameters which indicate fracturing occur on the positive side and parameters indicative of competent rock on the negative side. This may be interpreted as if fracturing is the most important characteristic of all sites. Actually this is not surprising considering that the sites generally have been selected on the basis that they should be relatively homogeneous, in particular with respect to rock type. It is thus natural that fracturing is the major source of anomalies.

The variables which show the strongest correlation seem to be fracture frequency (FS), different features of fracturing (S9, F9, and C9), and the resistivity logs (LR and NR). The strong correlation is expected since the first component describes low fractured and fractured rock at all sites, and as high normal and lateral resistivity is a strong indicator of low fractured rock. There is, of course, a negative correlation between the geophysical variables and the fracture frequency in the first components. The single point resistance (GE) is also a variable which exhibits strong correlation. It occurs in the first component at all sites except Finnsjön. The strong correlation is expected since single point resistance is connected with homogeneous rock. The gamma log (GA) is also a variable which exhibits strong correlation and occurs in component 1 at Klipperås and Finnsjön. Gamma is associated with acid rock, such as granite, and the granite at these two sites seems to be low fractured since gamma occurs together with lateral and normal resistivity.

The PLS-analysis shows variables which are strongly correlated to the radar intensity. In the PLS-analysis, as in the Principal Component analysis, the first component describes the strongest and highest degree of correlation between the variables. At all sites, except for the Saltsjötunnel, high radar intensity in component 1 exhibits a strong correlation to high fracture frequency and also to different geophysical logs associated with fracturing. This indicates that the borehole radar detects fractured sections in different environments. However, at the Saltsjötunnel radar intensity is

correlated with migmatite having low resistivity, indicating that the migmatite is fractured. At all sites, except Ävrö, there is a strong negative correlation to gamma radiation which occurs on the opposite side to radar intensity in the first component. There is a strong negative correlation between radar intensity and the resistivity logs (LR and NR) at all sites except Finnsjön where resistivity does not occur in the first component. The mirror points to normal resistivity and lateral resistivity implies low resistivity together with radar intensity. This is expected since high lateral and normal resistivity values normally are associated with low fractured rock and radar intensity normally is associated with high fracturing. The single point resistance (GE) also shows a negative correlation to radar intensity in Klipperås and Stripa. This is also expected since single point resistance is connected with homogeneous rock, in this case low fractured granite.

Prior to this study lithological contact (rb) were thought to be one of the more important features associated with high radar intensity. However, the PLS-analyses show that the variable lithological contact occurs in the first component at only one site, namely Klipperås. This is in good agreement with the conclusions made by Carlsten et al. (1987) concerning the radar investigation in Klipperås. The results from the other sites indicate that lithological contacts exhibits a lower degree of correlation than was expected.

Hydraulic conductivity (HC) is another variable which is interesting concerning its correlation to radar intensity. Hydraulic conductivity was not included in the SIMCA analysis at Klipperås due to the large section lengths. Hydraulic conductivity in the PLS-analyses occurs in component 1 at one site only, namely Stripa where it occurs together with radar intensity and high fracturing. The correlation between radar intensity and hydraulic conductivity, according to the PLS-analyses, is very good in Stripa and poor at the sites Finnsjön, Saltsjötunnel, and Ävrö.

The presence of fracture minerals, especially Fe-oxide (Fe), and its correlation to radar intensity is also of interest. There is an hypothesis that presence of Fe-oxide in fractures is an indicator of waterflow and it is of interest to investigate if there exists any correlation between radar intensity and Fe-oxide. As mentioned in chapter 3, Fe-oxide was mapped in the cores from Ävrö, Saltsjötunnel site, and in a number of boreholes at Klipperås. A special PLS-analysis was made with emphasis put on fracture

minerals in the boreholes at Klipperås. Fe-oxide occurs in the second component in Klipperås together with high temperature gradient (QG) which might indicate waterflow, high fracture frequency (FS and F9), and high sonic (SO) which indicate fractured rock. On the opposite side there is radar intensity together with lithological contacts at dolerite. In this case there has been no hydraulic data which could have been used in the analysis. Hence, the Klipperås data do not provide a basis for conclusions concerning the correlation of either Fe-oxide or radar intensity to waterflow.

In the PLS-analysis from Saltsjötunnel and Ävrö site Fe-oxide occurs already in component 2 from both sites but on the opposite side to radar intensity. Fe-oxide is associated with high fracturing in both components. In component 2 from the Saltsjötunnel hydraulic conductivity occurs together with Fe-oxide on the same side. In component 3 from Ävrö Fe-oxide occurs together with high radar intensity. The presence of Fe-oxide in the boreholes seems to be associated with high fracture frequency. Based on this data no general conclusions can be made with respect to the presence of Fe-oxide and its correlation to hydraulic conductivity or radar intensity.

The PLS2-analysis performed at all sites, except Klipperås, was made in order to show correlation of measured variables to both hydraulic conductivity and radar intensity. Two of the investigated sites, Finnsjön and Stripa, exhibit a very good correlation between hydraulic conductivity and radar intensity. Variables which correlate well with hydraulic conductivity and radar intensity on the same side of the component center are high fracture frequency (FS), fracture zones (F9), and single fractures (S9), and the mirror points to resistivity indicate low values. Hydraulic conductivity and radar intensity are separated from each other in component 2 at both sites and they occur on each side of the centre, thus they correlate with different variables. Hydraulic conductivity correlates with low lateral and normal resistivity, and radar intensity correlates with fracture zones. The fracture zones are probably isolated and surrounded by low fractured rock, which is indicated by high lateral and normal resistivity. Hydraulic conductivity and radar intensity occur together again in components with lower degree of correlation. In the components from the other two sites, Saltsjötunnel and Ävrö, hydraulic conductivity and radar intensity are separated from each other already in the first components. In the Saltsjötunnel they do not occur together in the usable components. At Ävrö hydraulic conductivity and radar intensity

occur together in component 2 and there they are correlated with the variables granite (gr), i.e. the component does not show much of interest except that hydraulic conductivity and radar intensity occur together at sections within granite.

10.3 SUMMARY CONCLUSIONS

Summarizing the results discussed in chapter 10.1 we find that there are no great changes in the most important components from the PLS-analyses when the borehole fluid parameters are excluded. The variables which correlate to radar intensity are unchanged, but the correlation becomes more distinct. The Principal Component analysis exhibits greater changes when the borehole fluid parameters are excluded. This is due to that the Principal Component analysis in the first component shows variables which have the strongest correlation to each other, while the PLS-analysis shows the variables which have the strongest correlation to radar intensity. The strong correlation is actually due to physical relations between the borehole fluid parameters, which do not depend on the rock. Hence, they show up in the first component in the Principal Component analysis. When the borehole fluid parameters are excluded correlations related to rock properties become apparent.

Concluding the results discussed in chapter 10.2 we find that Principal Component, PLS, and PLS2 analysis all show similar pattern where the strongest correlations result in a division between low fractured and highly fractured rock. Furthermore, PLS-analysis shows that high radar intensity correlates with variables on the highly fractured side. The PLS2-analysis shows that hydraulic conductivity and radar intensity at Stripa and Finnsjön act together and exhibit a high degree of correlation in sections with high fracturing. However, it is impossible to draw firm conclusions from the PLS2-analysis of Ävrö and Saltsjötunnel data regarding hydraulic conductivity and radar intensity, except that these parameters do not correlate well with a common set of variables.

Variables which exhibit strongest correlation in the SIMCA analysis are fracture frequency, different features of fracturing, lateral and normal resistivity, gamma, and single point resistance.

Some improvements can be made in order to simplify the use of the SIMCA-method. Instead of using the temperature gradient directly with its negative and positive anomalies, it should be better to take the magnitude of the gradient and use as a variable in the analysis. Since the SIMCA-method has shown to be sensitive for too much missing values in the data set, it is desirable that core mapping is performed continuously along the total length of boreholes in order to have a complete data set from the boreholes. An effort should be made to use the same or an equivalent set of fracture minerals in the core mapping at the different sites, especially with respect to clay minerals. The use of one code for clay minerals in the core log is desirable for the purpose of making SIMCA-analysis of the correlation of clay filled fractures and zones against other parameters. Concerning the hydraulic conductivity the use of a section length of two meters or less should simplify the use of the hydraulic data in the SIMCA-method. The quantification of radar intensity could be refined if one takes the relation between radar intensity and the angle to borehole axis of the structure causing the reflection into account.

The SIMCA method has proven to be a useful tool in the work to quantify the correlation between radar intensity and other geophysical, geological, and hydraulical borehole parameters. The best result with respect to radar intensity was received with the PLS analysis of the data. The combined result from Principal Component analysis, PLS, and PLS2 shows that borehole radar primarily detects fractured sections and both sealed and fractured lithological contacts. The correlation between radar and hydraulic conductivity varies between the different sites. This implies that borehole radar can not be used directly as an indicator of permeable zones in the rock. Radar should be seen as an indicator of potentially permeable zones while the hydraulic properties of these zones have to be obtained by other means. However, in some cases geologic conditions might be favorable and radar will be a good indicator of permeable zones (e.g. Stripa). The great advantage of the radar method compared to other borehole methods is that it gives geometric information about structures at considerable distances from the boreholes.

ACKNOWLEDGEMENTS

Ove Persson has provided invaluable assistance in the collection, preparation and filing of the data sets that have been used for the SIMCA analysis.

REFERENCES

Agmalm, G., 1985. Parametermätningar på borrkärneprover och jämförelse med borrhålsloggning från Stripa gruva. University of Luleå report 1985:020 E, Luleå, Sweden. (In swedish).

Ahlbom, K., Andersson, P., Ekman, L., Gustafsson, E., Smellie, J. and Tullborg, E-L., 1986. Preliminary investigations of fracture zones in the Brändan area, Finnsjön study site. SKB TR 86-05, SKB, Stockholm, Sweden.

Ahlbom. K., Andersson, P., Ekman, L. and Tirén, S., 1987. Extended preliminary investigations of fracture zones in the Brändan area, Finnsjön study site. SGAB IRAP 87354, Uppsala, Sweden.

Andersson, J-E., Andersson, P., Carlsten, S., Falk, L., Olsson, O. and Stråhle, A., 1987. Combined interpretation of geophysical, geological, hydrological and radar investigations in the boreholes ST 1 and ST 2 at the Saltsjötunnel. SKB TR 87-14, SKB, Stockholm, Sweden.

Andersson, J.-E. and Lindqvist, L., 1988. Prediction of hydraulic conductivity and conductive fracture frequency by multivariate analysis of data from the Klipperås study site. (in print).

Andersson, J.-E., Ekman, L. and Winberg, A., 1988. Detailed investigations of fracture zones in the Brändan area Finnsjön study site. Single hole water injection tests in detailed sections. Analysis of the conductive fracture frequency. SKB AR 88-08, SKB, Stockholm, Sweden.

Carlsten, S., Magnusson, K-Å. and Olsson, O., 1985a. Crosshole Investigations - Description of the small scale site. Stripa project TR 85-05, SKB, Stockholm, Sweden.

Carlsten, S. and Stråhle, A., 1985b. Crosshole investigations - Compilation of core log data from F1 - F6. Stripa project IR 85-13, SKB, Stockholm, Sweden.

Carlsten, S., Magnusson, K-Å. and Ahlbom, K., 1986a. Reconnaissance study of a fracture zone at Ävrö. SKB AR 86-15, SKB, Stockholm, Sweden.

Carlsten, S. and Melkersson, K., 1986b. Fracture zone project - Core log and technical data for borehole Ä 1. SKB AR 86-18, SKB, Stockholm, Sweden.

Carlsten, S., Olsson, O., Sehlstedt, S. and Stenberg, L., 1987. Radar measurements performed at the Klipperås study site. SKB TR 87-01, SKB, Stockholm, Sweden.

Esbensen, K., Lundholm, I., Lindqvist, L., Nisca, D. and Wold, S., 1985. Geokemi och dataanalys. Integrated exploration using multivariate modelling of geochemical and petrophysical data. SGAB PRAP 85091, SGAB, Luleå, Sweden.

Esbensen, K., Lindqvist, L., Lundholm, I., Nisca, D. and Wold, S., 1987. Multivariate Modelling of Geochemical and Geophysical Exploration Data. Chemometrics and Intelligent Laboratory Systems, vol 2, 14 p.

Esbensen, K. and Martens, H., 1987. Predicting Oil-Well Permeability and Porosity from Wire-Line Petrophysical Logs - A Feasibility Study Using Partial Least Square Regression. Chemometrics and Intelligent Laboratory Systems, vol 2, 11 p.

Gentzschein, B., Nilsson, G. and Stenberg, L., 1987. Preliminary investigations of fracture zones at Ävrö - Results of investigations performed July 1986 - May 1987. (in print).

Lindqvist, L. and Lundholm, I., 1985. Effektivare prospektering med hjälp av dataanalys (In swedish). Jernkontorets Annaler, nr 4/85.

Lindqvist, L., Lundholm, I., Nisca, D., Esbensen, K. and Wold, S., 1987. Multivariate geochemical modelling and integration with petrophysical data. Journal of Geochemical Exploration, 29, pp 279-294, Elsevier Science Publishers B.V., Amsterdam, Netherlands.

Magnusson, K-Å., Carlsten, S. and Olsson, O., 1987. Crosshole Investigations - Physical properties of core samples from boreholes F 1 and F 2. Stripa project TR 87-10, SKB, Stockholm, Sweden.

Olkiewicz, A., Scherman, S. and Kornfält, K.-A., 1979. Supplementary bedrock investigations in the Finnsjön and Karlshamn areas (In swedish). KBS Technical Report 79-05, KBS, Stockholm, Sweden.

Olkiewicz, A. and Stejskal, V., 1986. Geological and tectonic description of the Klipperås study site. SKB TR 86-06, SKB Stockholm, Sweden.

Olsson, O. and Sandberg, E., 1984. Crosshole investigations - Preliminary design of a new borehole radar system. Stripa project IR 84-04, SKB, Stockholm, Sweden.

Olsson, O., Falk, L., Forslund, O., Lundmark, L. and Sandberg, E., 1987a. Crosshole Investigations - Results from borehole radar investigations. Stripa project TR 87-11, SKB, Stockholm, Sweden.

Olsson, O., Black, J., Cosma, C. and Pihl, J., 1987b. Crosshole Investigations - Final report. Stripa project TR 87-16, SKB, Stockholm, Sweden.

Olsson, O., Eriksson, J., Falk, L. and Sandberg, E., 1988. Site characterization and validation - Borehole radar investigations, Stage I. SGAB IR 88 233. Uppsala, Sweden.

Sehlstedt, S. and Stenberg, L., 1986. Geophysical investigations at the Klipperås study site. SKB TR 86-07, Stockholm, Sweden.

SIMCA - 3F, User's manual, version 0.4, 1985. Swedish Geological company and University of Umeå, Chemometric research group. Sherman, M. M., 1983. The determination of cementation exponents using high frequency dielectric measurements. The Log Analyst.

Tullborg, E-L., 1986. Fissure fillings from the Klipperås study site. SKB TR 86-10, SKB, Stockholm, Sweden.

Wold, S., Carlsson, R., Edlund, U., Albano, C., Hellberg, S., Johansson, E. and Sjöström, M., 1983. Optimering och analys av flerdimensionella data (In swedish). Kemisk tidskrift nr 14.

Wold; S., Esbensen, K. and Geladi, P., 1987. Principal Component Analysis. Chemometrics and Intelligent Laboratory Systems, vol. 2, 15 p.

Wold, S., 1985. En bild säger mer än tusen siffror. (In swedish). Forskning och framsteg, nr 5.

APPENDICES:

Appendix A: Boreholes included in the SIMCA investigations.

Appendix B: Status of the variables from the investigated sites.

Appendix C: Variable plots from Principal Component analysis, PLS, and PLS2 analysis of data from the investigated sites.

Appendix D: Measurements on core samples from the boreholes KFI09, KFI11, and F2.

APPENDIX A

BOREHOLES INCLUDED IN THE SIMCA INVESTIGATION.

SITE	BOREHOLE	BOREHOLE LENGTH USED IN SIMCA
KLIPPERÅS	KKL01	5.5 - 527.5
	KKL02	15.5 - 915.5
	KKL04	9.5 - 189.5
	KKL06	8.5 - 791.5
	KKL08	9.5 - 249.5
	KKL09	6.5 - 784.5
	KKL10	7.5 - 181.5
	KKL12	5.5 - 717.5
	KKL13	25.5 - 684.5
	KKL14	11.5 - 691.5
FINNSJÖN	KFI05	11.5 - 265.5
	KFI06	154.5 - 303.5
	KFI07	248.5 - 453.5
	KFI09	1.5 - 367.5
	KFI10	1.5 - 69.5
	KFI11	21.5 - 382.5
SALTSJÖTUNNEL	KST01	1.5 - 98.5
	KST02	1.5 - 102.5
STRIPA	F2	13.5 - 163.5
	F3	4.5 - 194.5
	F4	4.5 - 244.5
ÄVRÖ	KAV01	1.5 - 736.5
	KAV03	1.5 - 240.5

APPENDIX B

STATUS OF THE VARIABLES FROM THE INVESTIGATED SITES.

VARIABLE		KLIPPERÅS	FINNSJÖN	SALTSJÖ-TUNNEL	STRIPA	ÄVRÖ
1	GA	X	X	X	X	X
2	GE	X	X	X	X	X
3	LR	X	M	M	X	X
4	NR	X	X	X	X	X
5	SO	X	M	M	X	M
6	SP	X	M	M	X	X
7	SU	X	M	M	X	X
8	QT	(X)	0	0	0	0
9	QG	(X)	0	0	0	0
10	QR	(X)	0	0	0	0
11	QS	(X)	0	0	0	0
12	F0	0	0	0	0	0
13	S0	0	0	0	0	0
14	F1	0	0	0	0	0
15	S1	0	0	0	0	0
16	F3	0	0	0	0	0
17	S3	0	0	0	0	0
18	F4	0	0	0	0	0
19	S4	0	0	0	0	0
20	F6	0	0	0	0	0
21	S6	0	0	0	0	0
22	F7	0	0	0	0	0
23	S7	0	0	0	0	0
24	F9	X	X	X	X	X
25	S9	X	X	X	X	X
26	C9	X	X	X	X	X
27	FS	X	X	X	X	X
28	Ca	(X)	X	X	M	X
29	Fe	(X)	M	X	M	X
30	Hm	(X)	X	M	M	X
31	Py	(X)	X	X	M	X
32	Ep	(X)	M	M	X	X
33	Cl	(X)	M	X	M	X
34		gr	(mb)	mi	gr	gr
35		ge	pe	gr	(pe)	ba
36		(pp)	(ap)	pe	(br)	vg
37		(qp)	(my)	0	(qv)	te
38		(qd)	(te)	0	0	ur
39		(ap)	gg	0	0	ap
40		(pe)	pg	0	0	(pe)
41		do	rg	0	0	0
42		(gn)	(ry)	0	0	0

APPENDIX B Continued.

VARIABLE		KLIPPERÅS	FINNSJÖN	SALTSJÖ-TUNNEL	STRIPA	ÄVRÖ
43		(am)	(xe)	0	0	0
44		0	(av)	0	0	0
45		0	0	0	0	0
46		0	0	0	0	0
47		0	0	0	0	0
48		0	0	0	0	0
49	rb	X	X	X	X	X
50	ZZ	0	0	0	0	0
51	De	0	0	0	0	0
52	Po	0	0	0	0	0
53	Su	0	0	0	0	0
54	Qv	0	0	0	0	0
55	Re	0	0	0	0	0
56	Rs	0	0	0	0	0
57	Ip	0	0	0	0	0
58	RI	X	X	X	X	X
59	A1	(X)	0	0	0	0
60	A2	(X)	0	0	0	0
61	A3	(X)	0	0	0	0
62	A4	(X)	0	0	0	0
63	A6	(X)	0	0	0	0
64	A9	(X)	0	0	0	0
65	HC	0	X	X	X	X

X = activated in the SIMCA-analysis.
0 = not activated in the SIMCA-analysis.
M = missing in the boreholes.
(X) = missing in some of the boreholes or activated in a special analysis.
xx = denotes different rock types, for explanation see respective chapter.
(xx) = denotes rock type which has become inactive during the process of deleting outliers.

APPENDIX C

VARIABLE PLOTS FROM PRINCIPAL COMPONENT ANALYSIS, PLS, AND PLS2 ANALYSIS OF DATA FROM THE INVESTIGATED SITES.

EXPLANATION TO FIGURES:

Component 1 is always plotted along the horizontal (short) axis and the remaining components are always plotted along the vertical (long) axis.

FIGURE	COMPONENT BETA 1/BETA X	OVERLAPPING POINTS
C.3	BETA 6	NR over GE
C.6	BETA 3	LR over GE
C.7	BETA 4	gr over GA
C.8	BETA 6	LR over GE
C.18	BETA 3	NR over LR
C.35	BETA 2	Cl over FS
C.36	BETA 5	Cl over F9
C.37	BETA 6	Cl over F9
C.38	BETA 9	Cl over F9
C.47	BETA 8	pe over F9
C.51	BETA 8	F9 over SP
C.53	BETA 2	HC over F9
	BETA 3	Ep over F9
C.57	BETA 2	NR over LR
C.61	BETA 3	Cl over Ca
C.62	BETA 4	Fe over Ca
		Cl over Fe
		gr over GA
	BETA 5	Ep over Ca
C.63	BETA 6	Cl over Fe
	BETA 7	SU over GE
		Fe over Ca
		Ep over Fe
		Cl over Ep
		gr over GA
		ap over S9
C.66	BETA 2	Fe over Ca
	BETA 3	Cl over Fe
		HC over vg
C.67	BETA 4	Cl over Fe
	BETA 5	Cl over Fe
C.68	BETA 6	Hm over FS
		ur over vg
	BETA 7	Cl over Fe
C.72	BETA 6	ur over vg

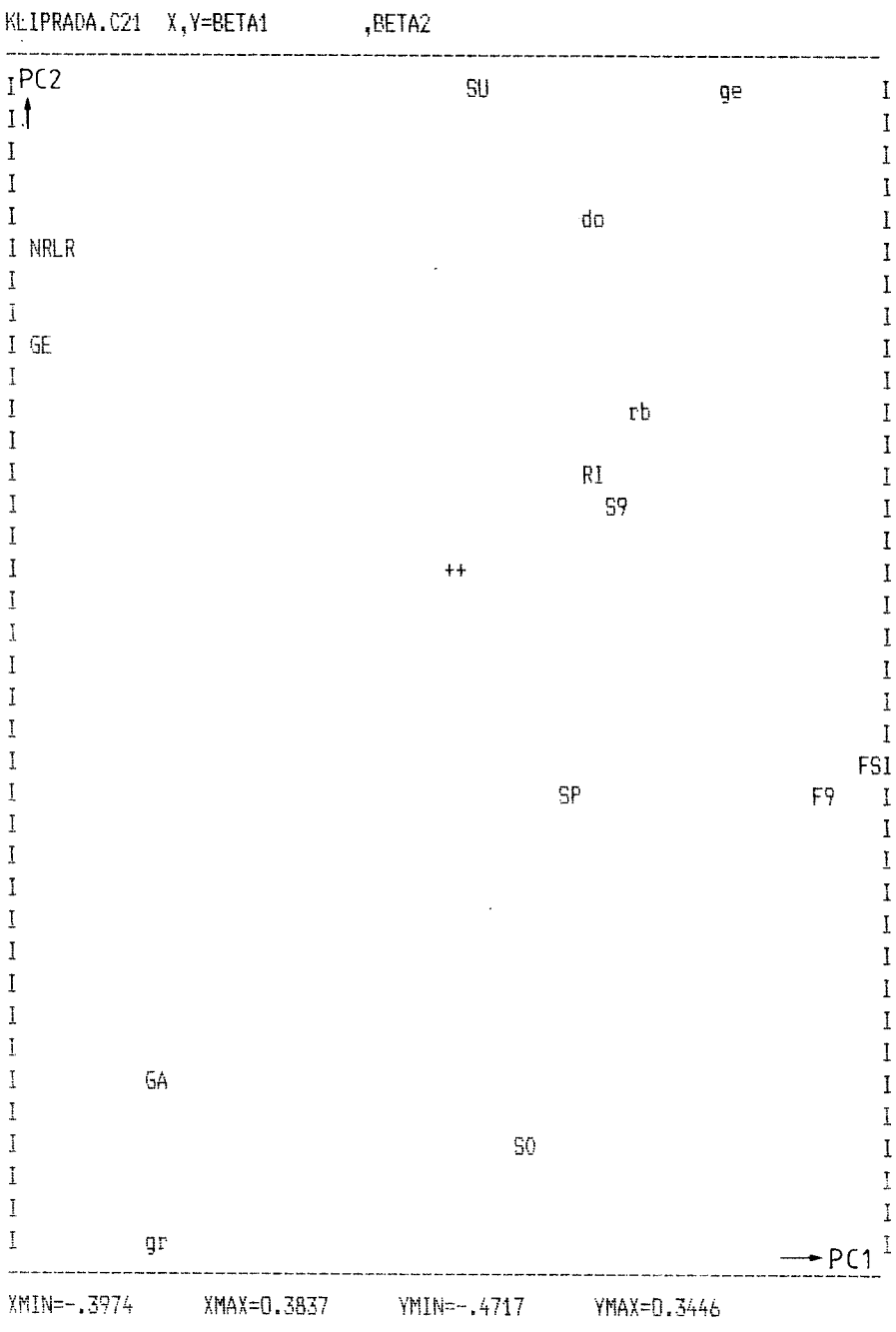

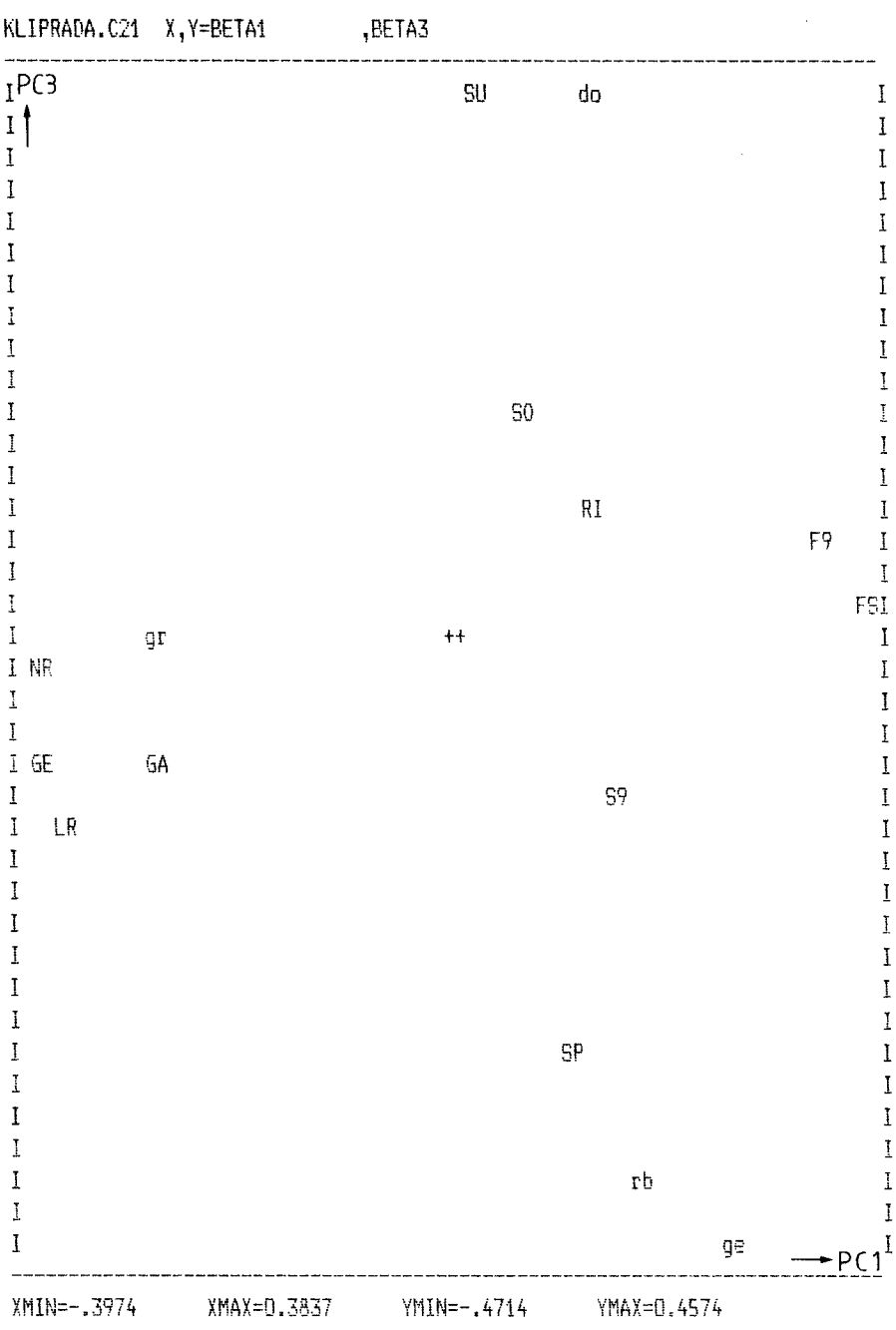

Fig C.1 Variable plots of principal components from PC-analysis of data from Klipperås.

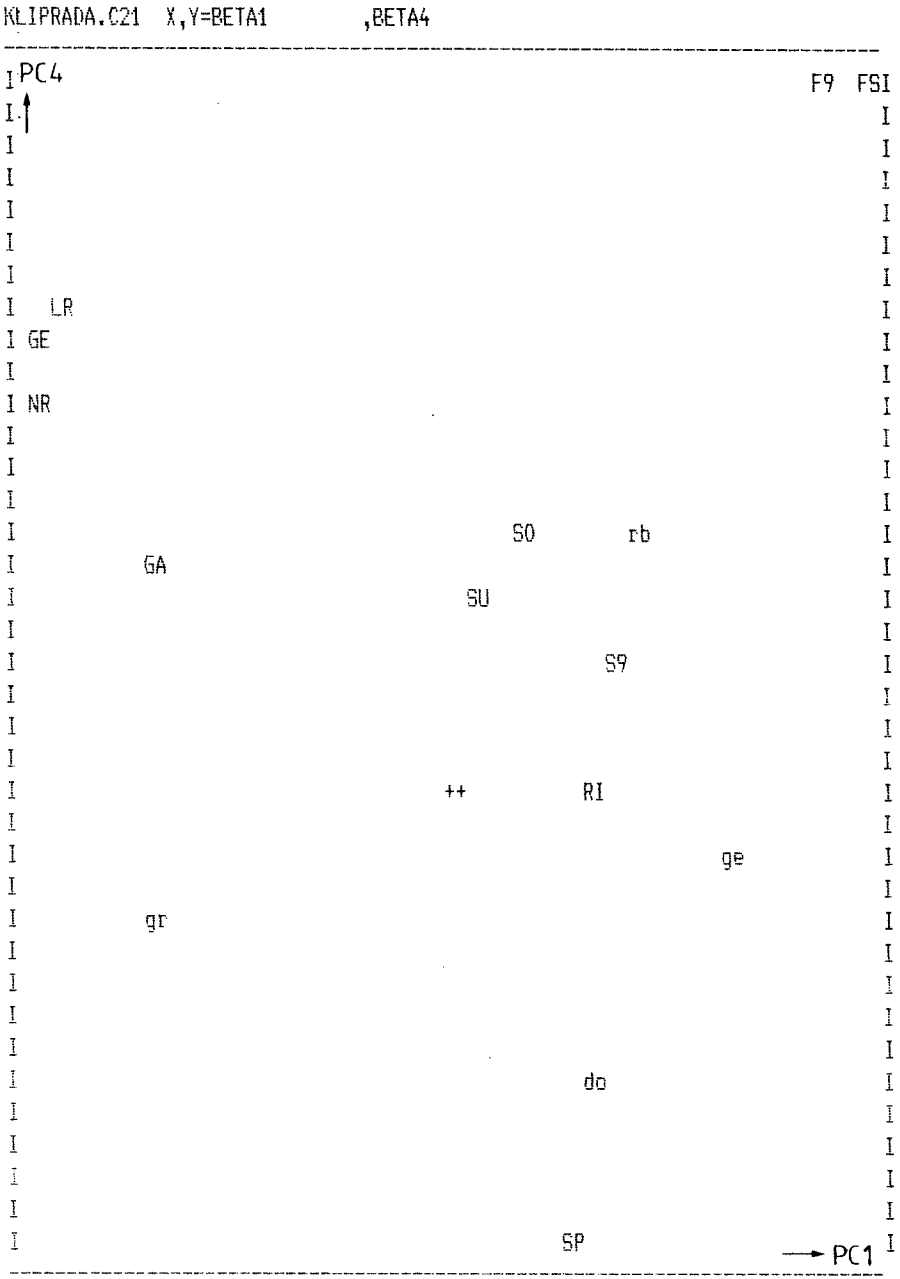

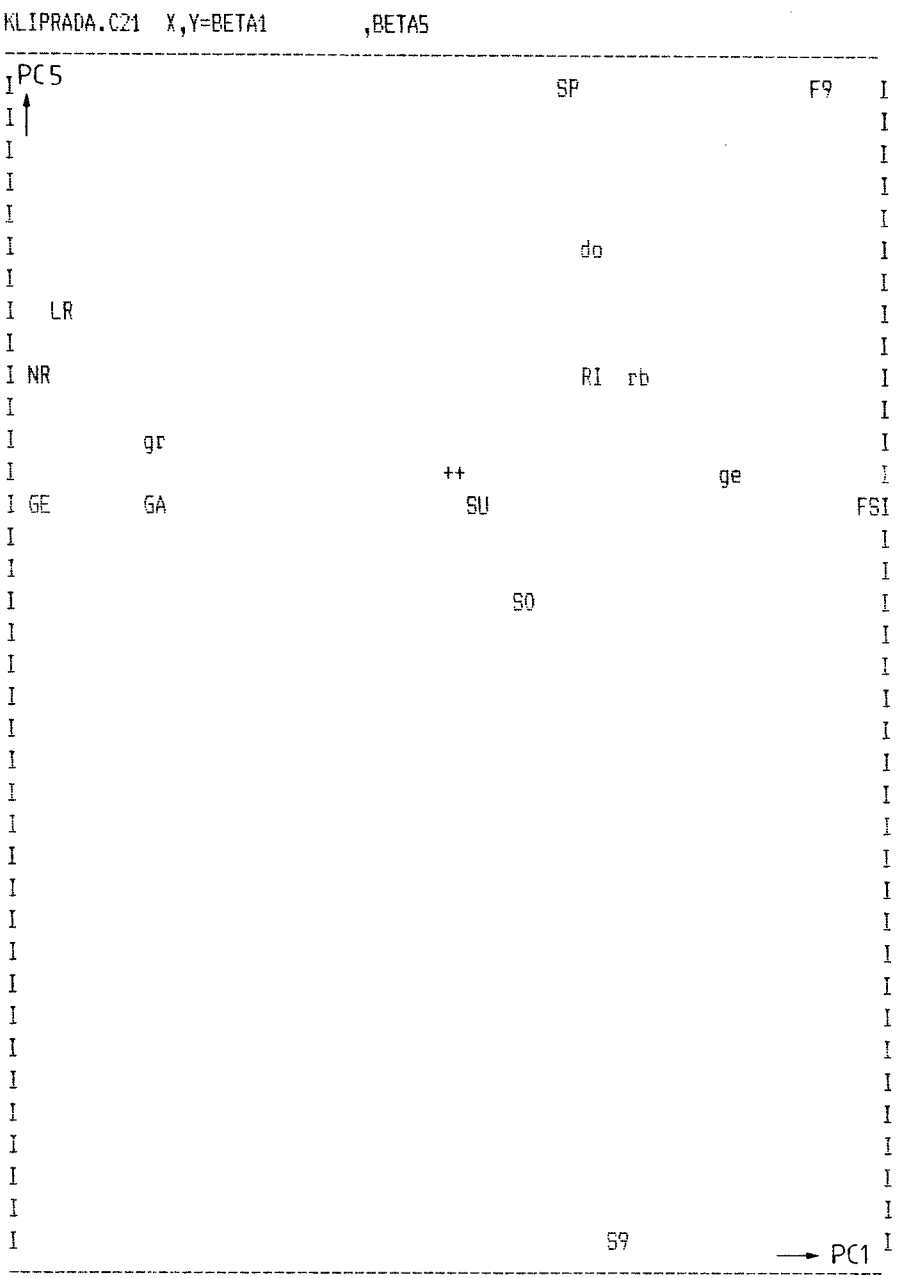

Fig C.2 Variable plots of principal components from PC-analysis of data from Klipperås.

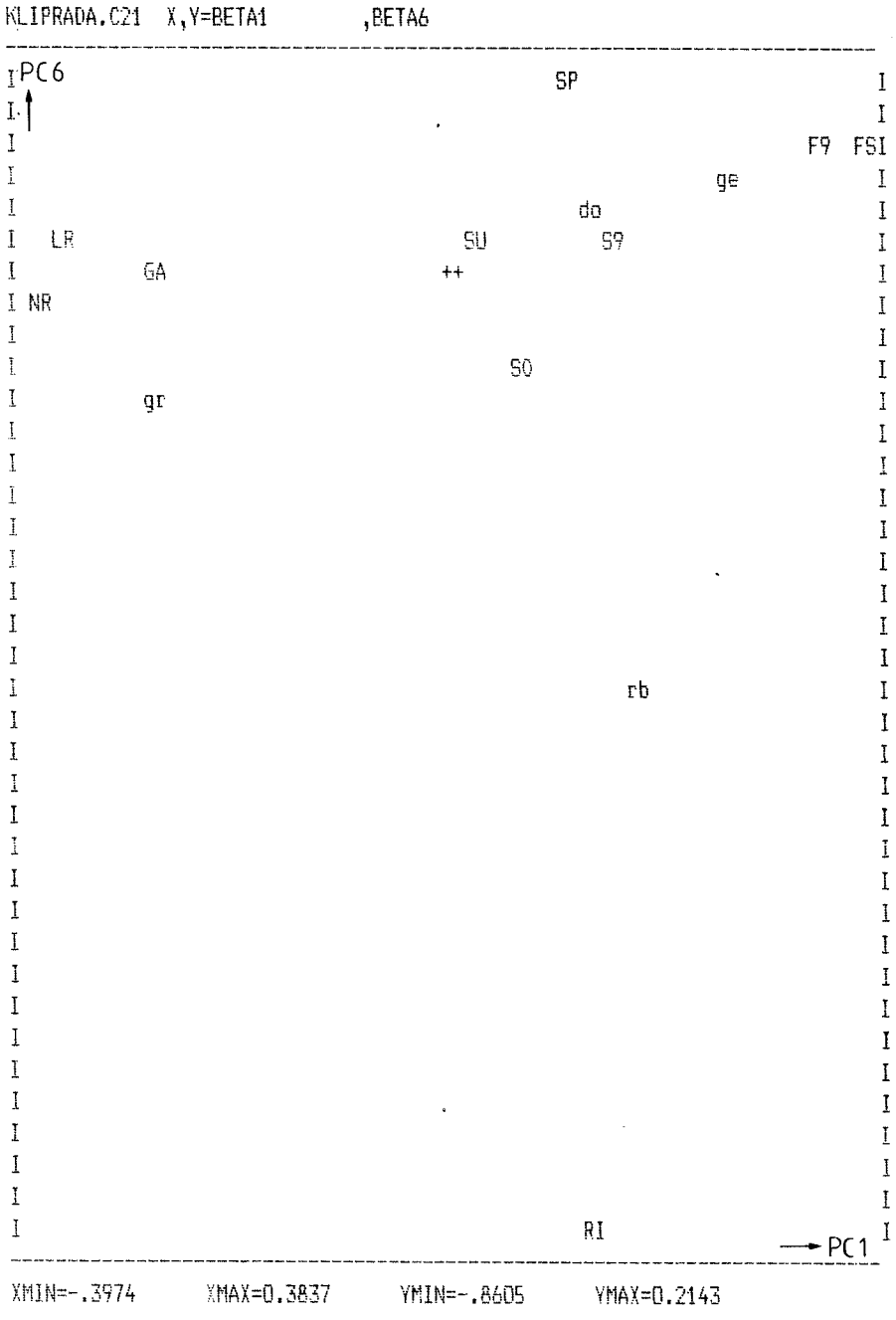

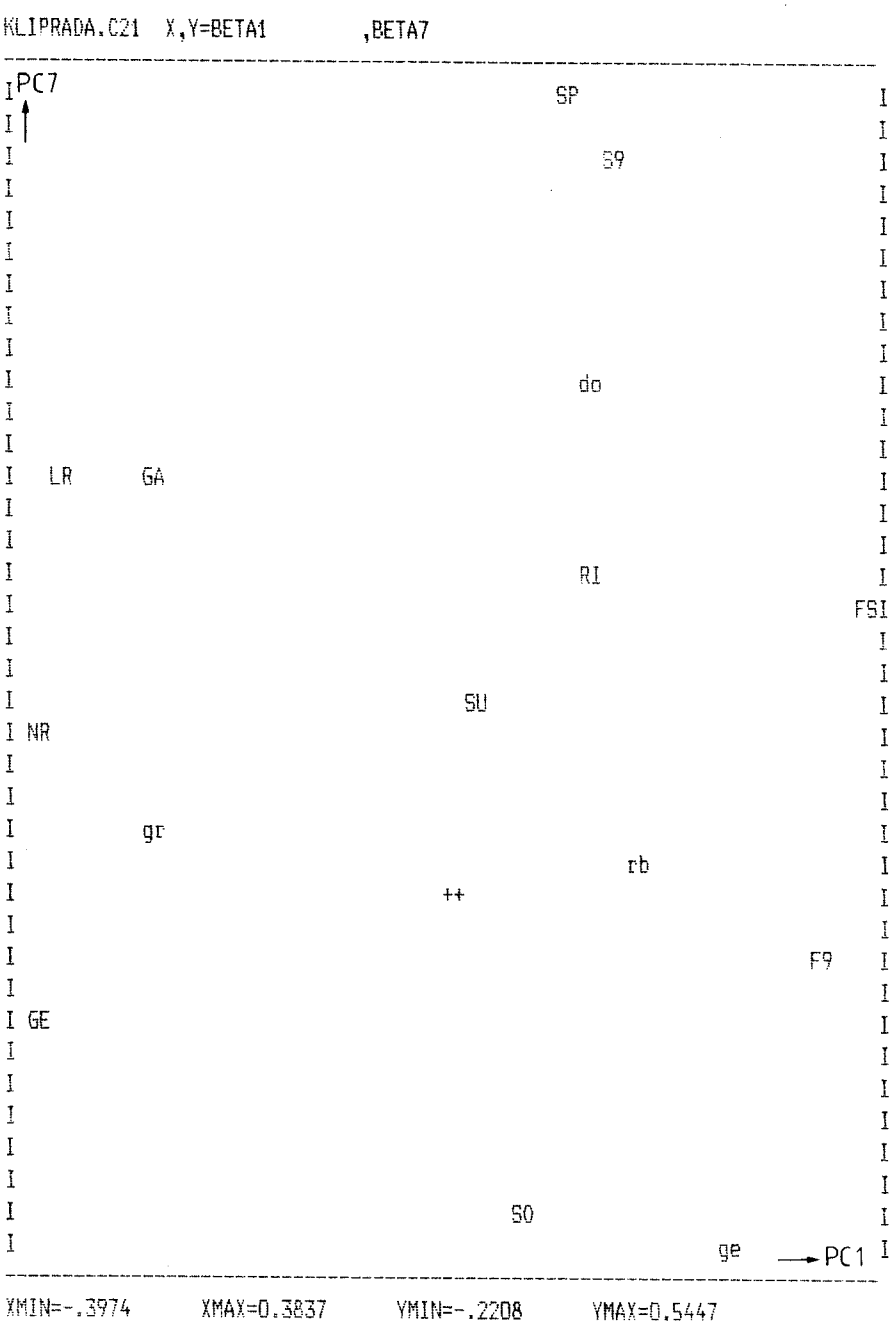

Fig C.3 Variable plots of principal components from PC-analysis of data from Klipperås.

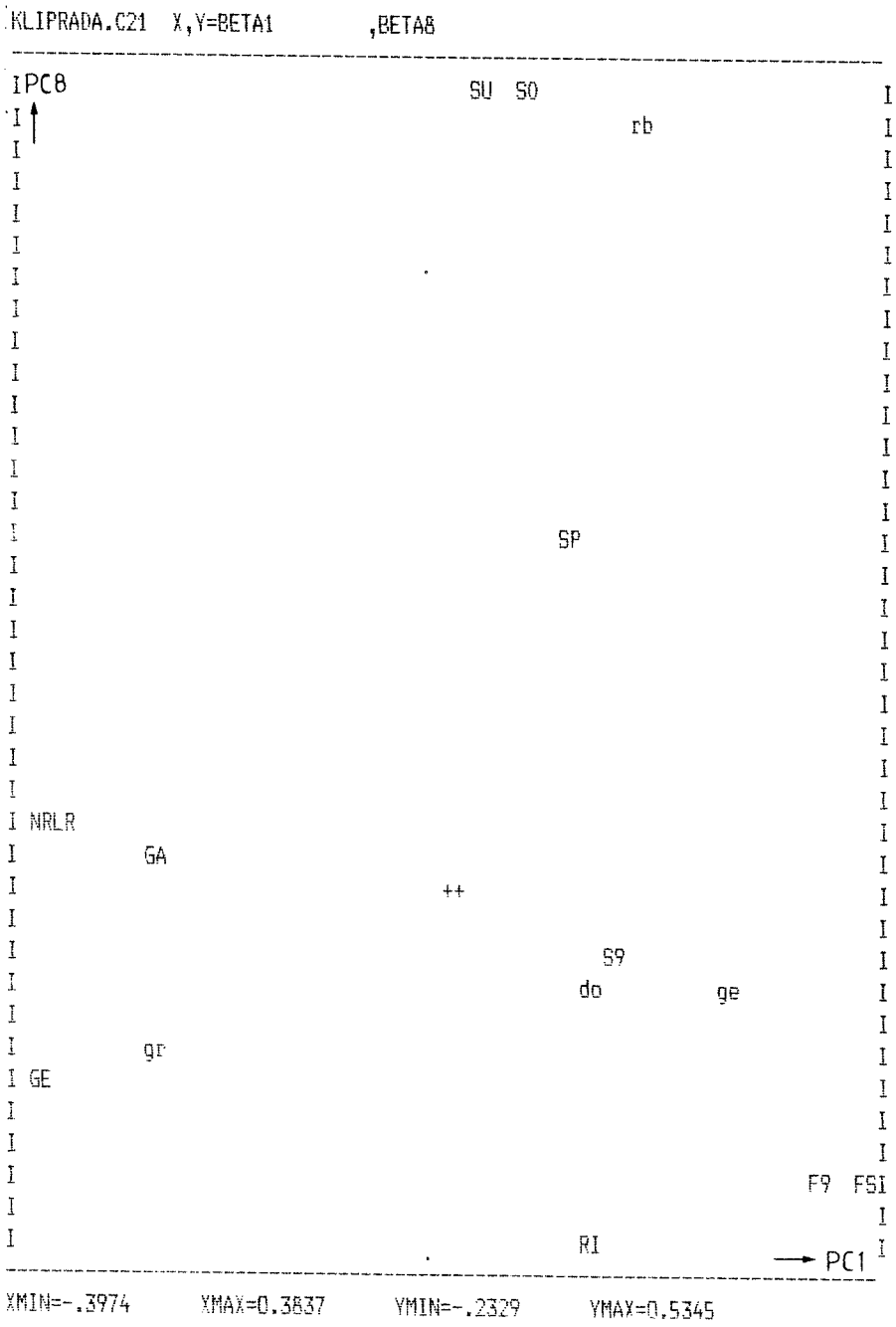

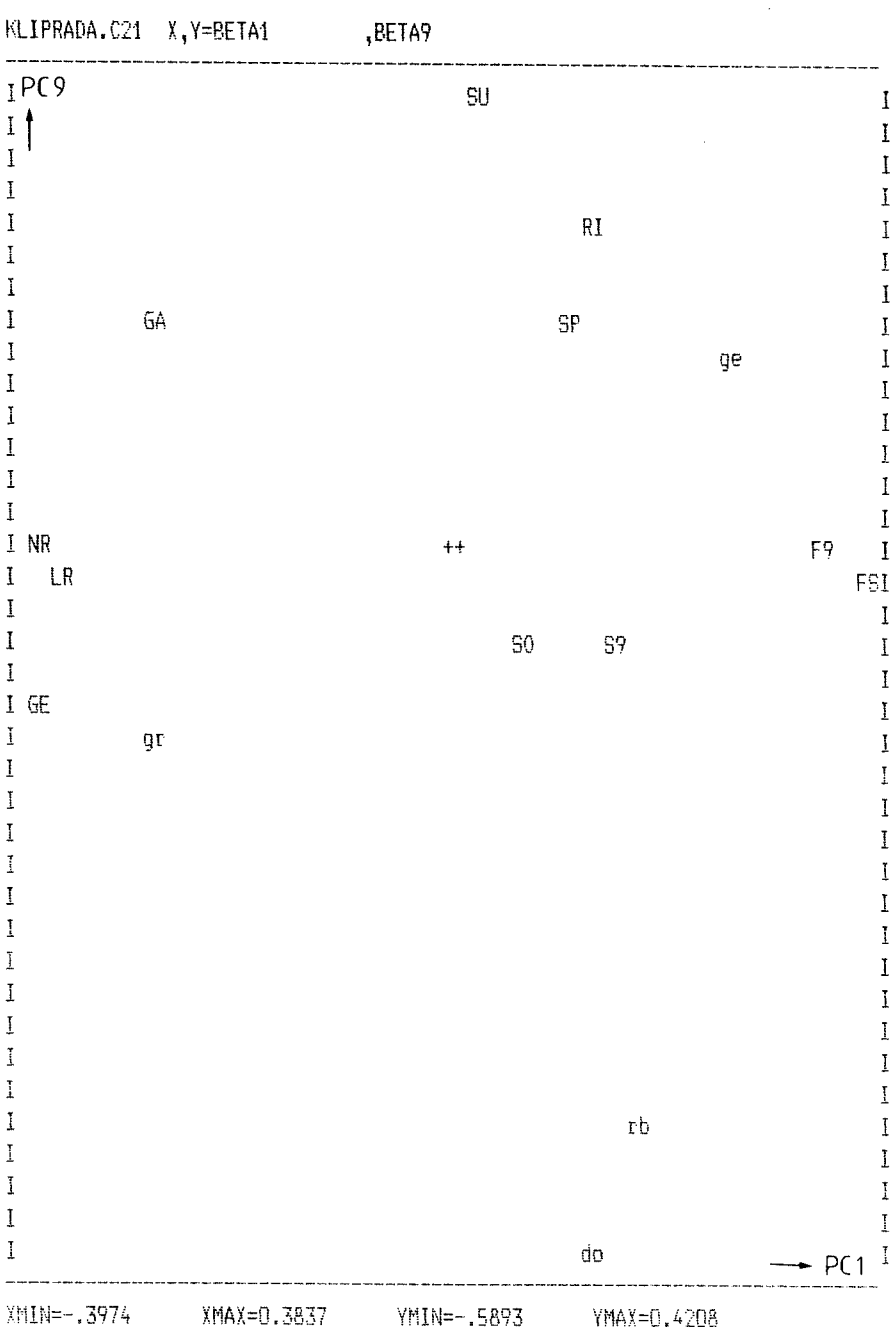

Fig C.4 Variable plots of principal components from PC-analysis of data from Klipperås.

Fig C.5 Variable plots of principal components from PC-analysis of data from Klipperås.

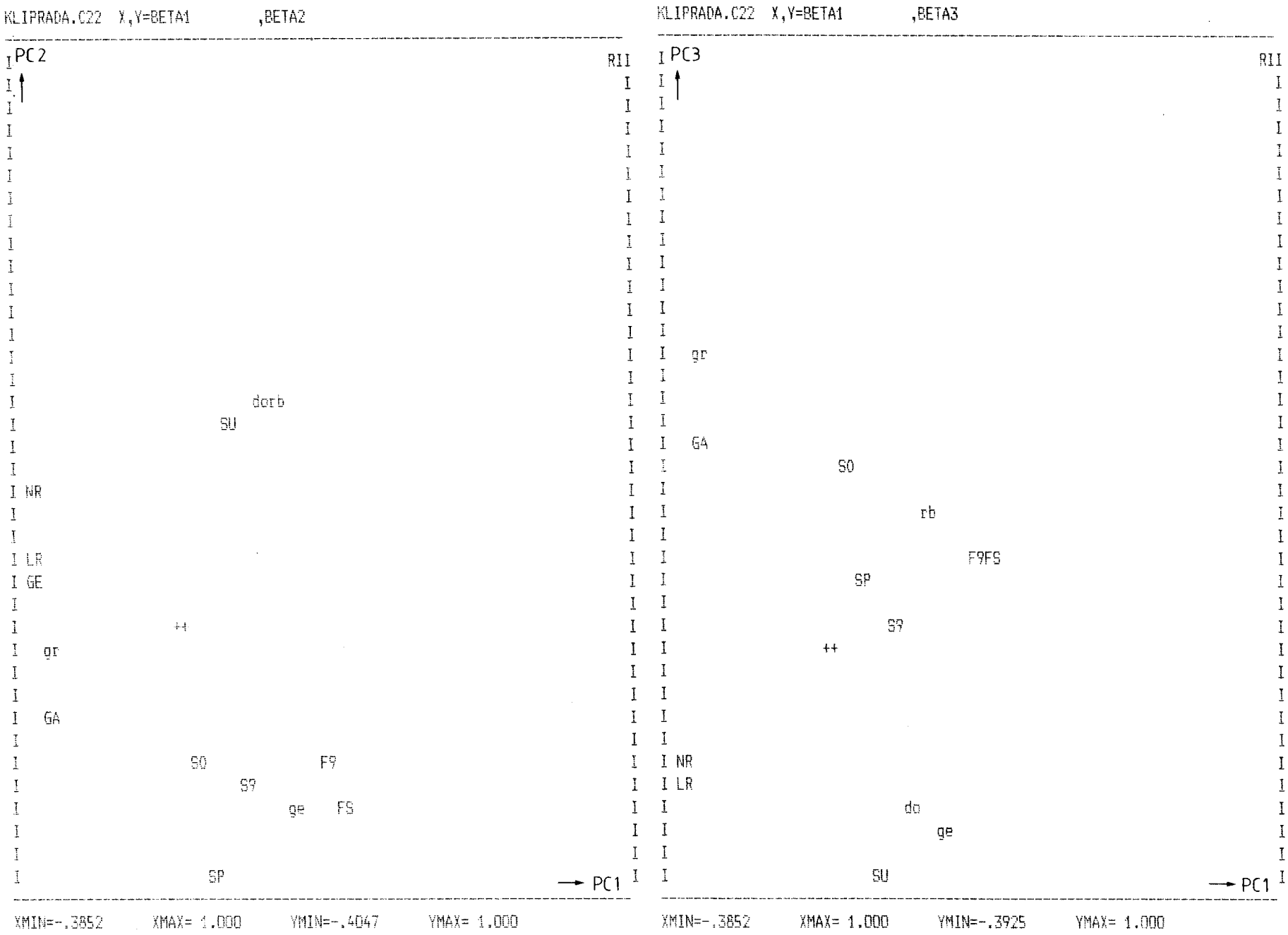

Fig C.6 Variable plots of the principal components from the PLS investigation of data from Klipperås.

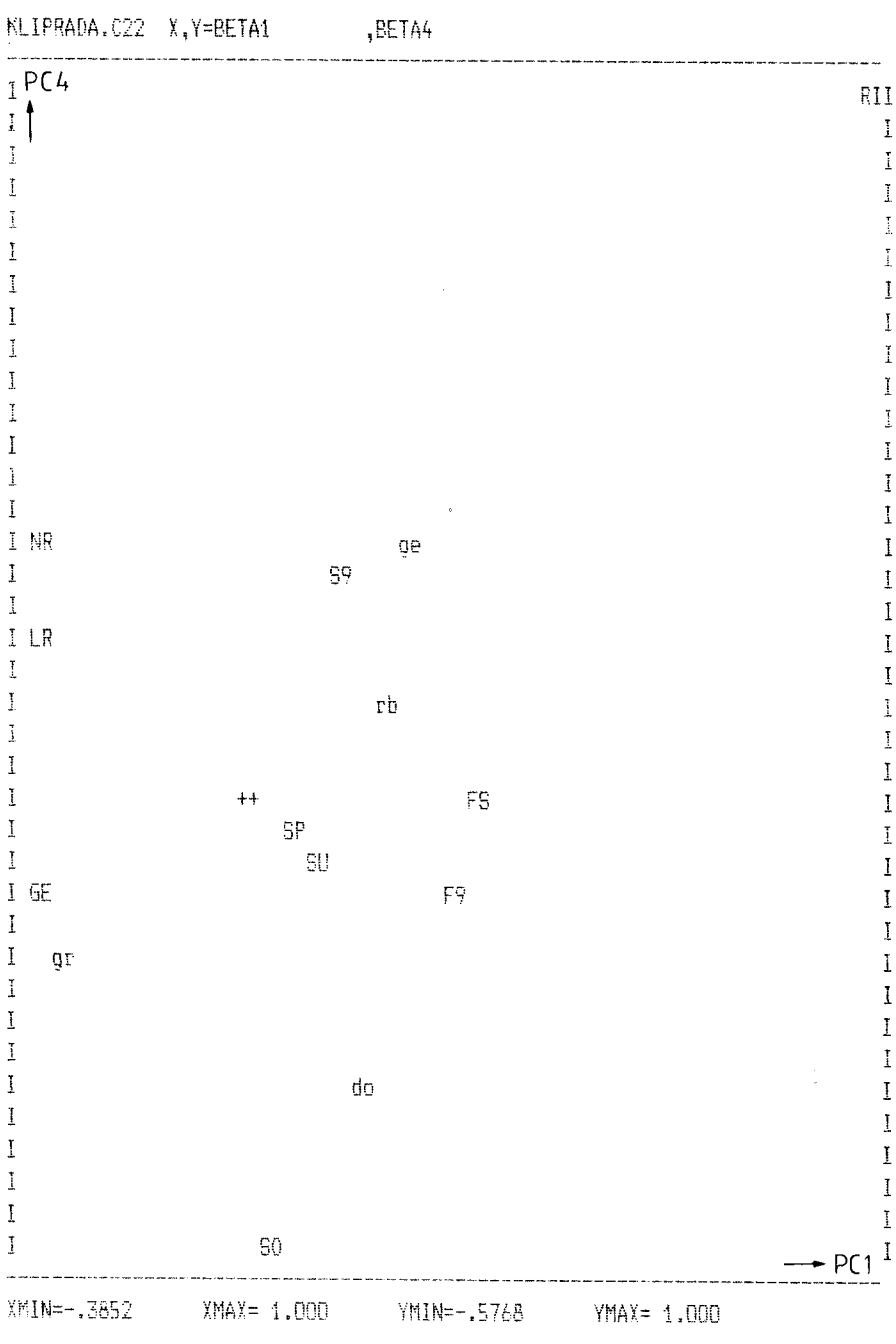

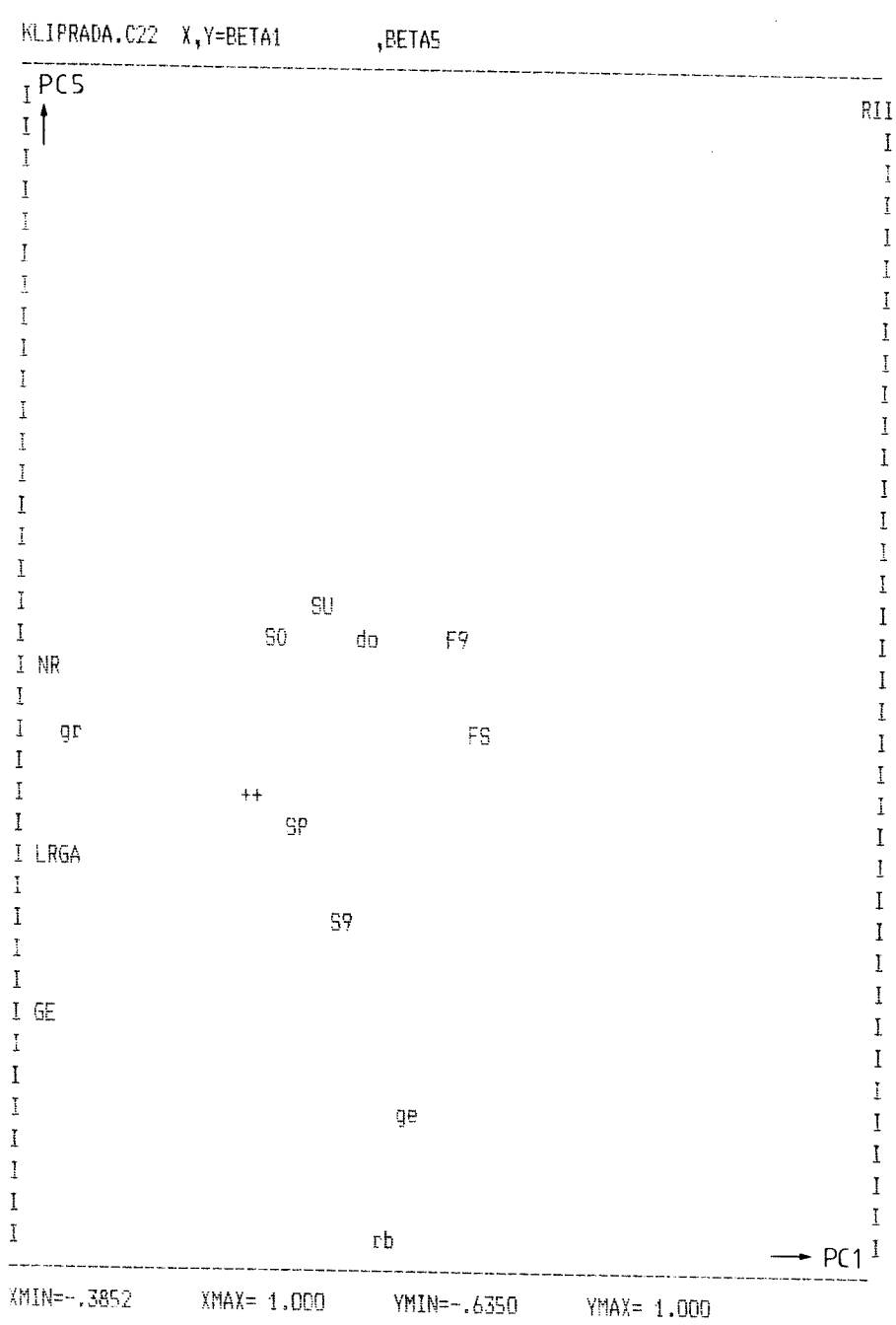

Fig C.7 Variable plots of the principal components from the PLS investigation of data from Klipperås.

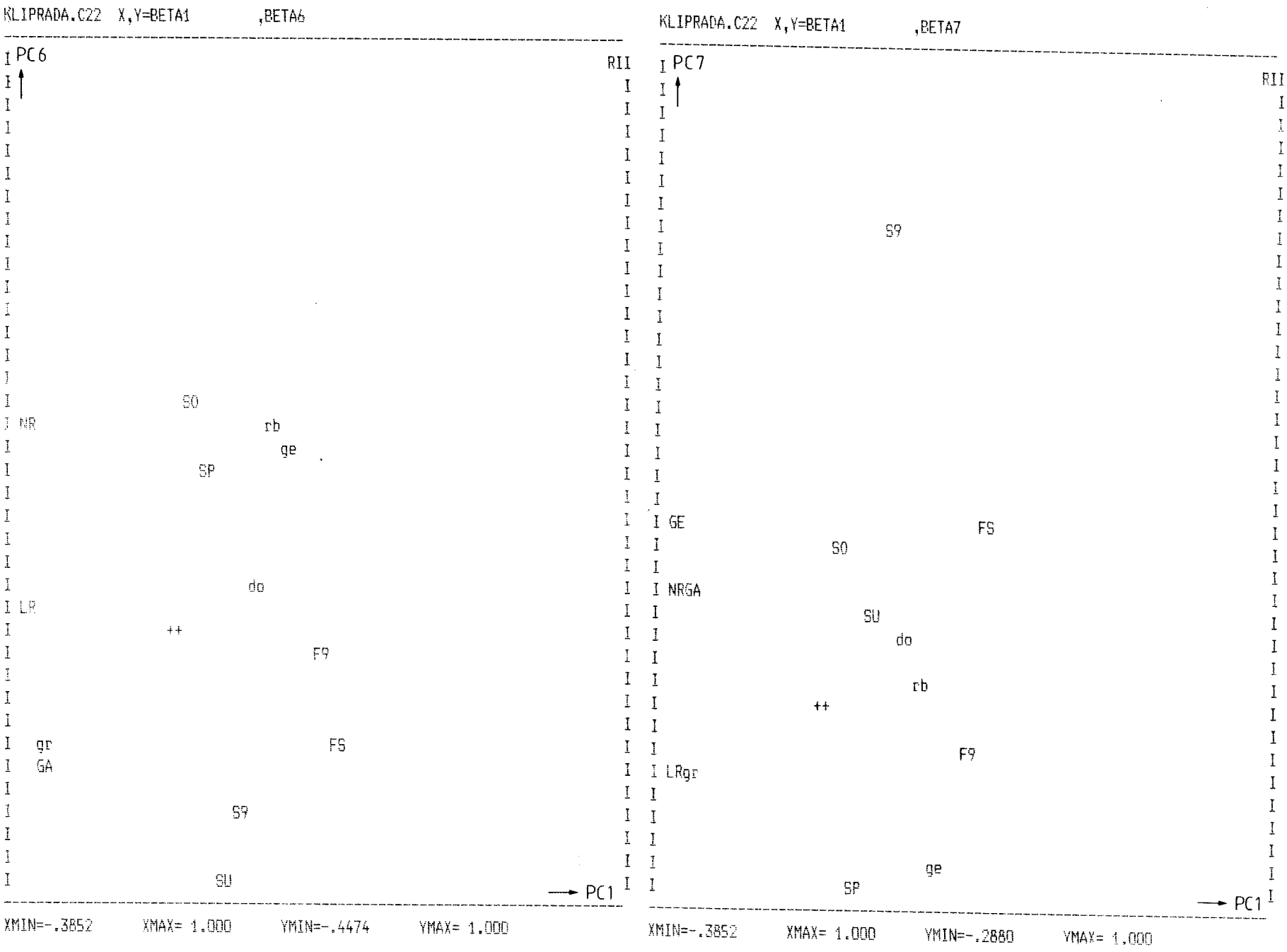

Fig C.8 Variable plots of the principal components from the PLS investigation of data from Klipperås.

Fig C.9 Variable plots of the principal components from the PLS investigation of data from Klipperås.

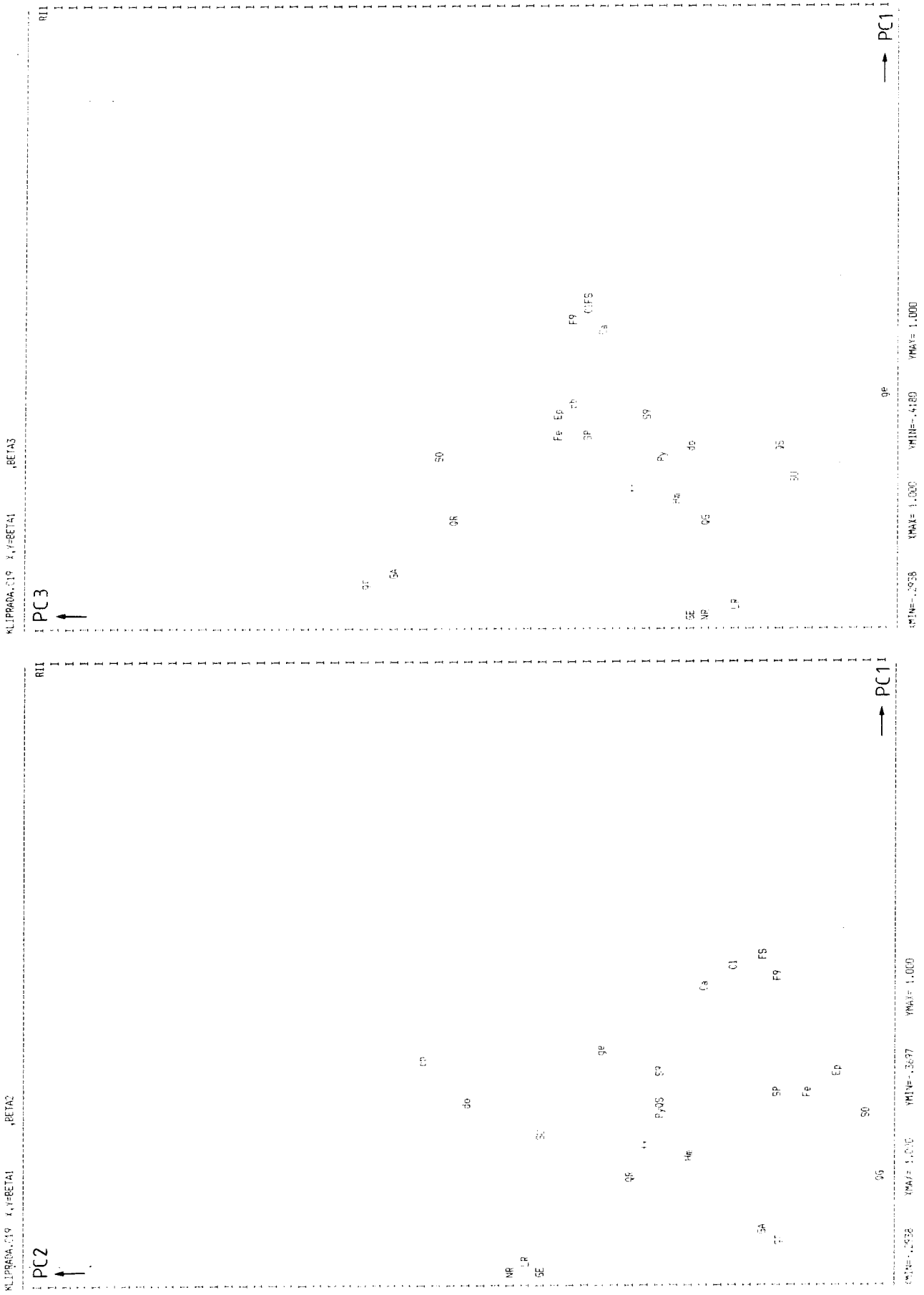

Fig C.10 Variable plots of principal components from the PLS investigation of data from Klipperås, with fracture minerals.

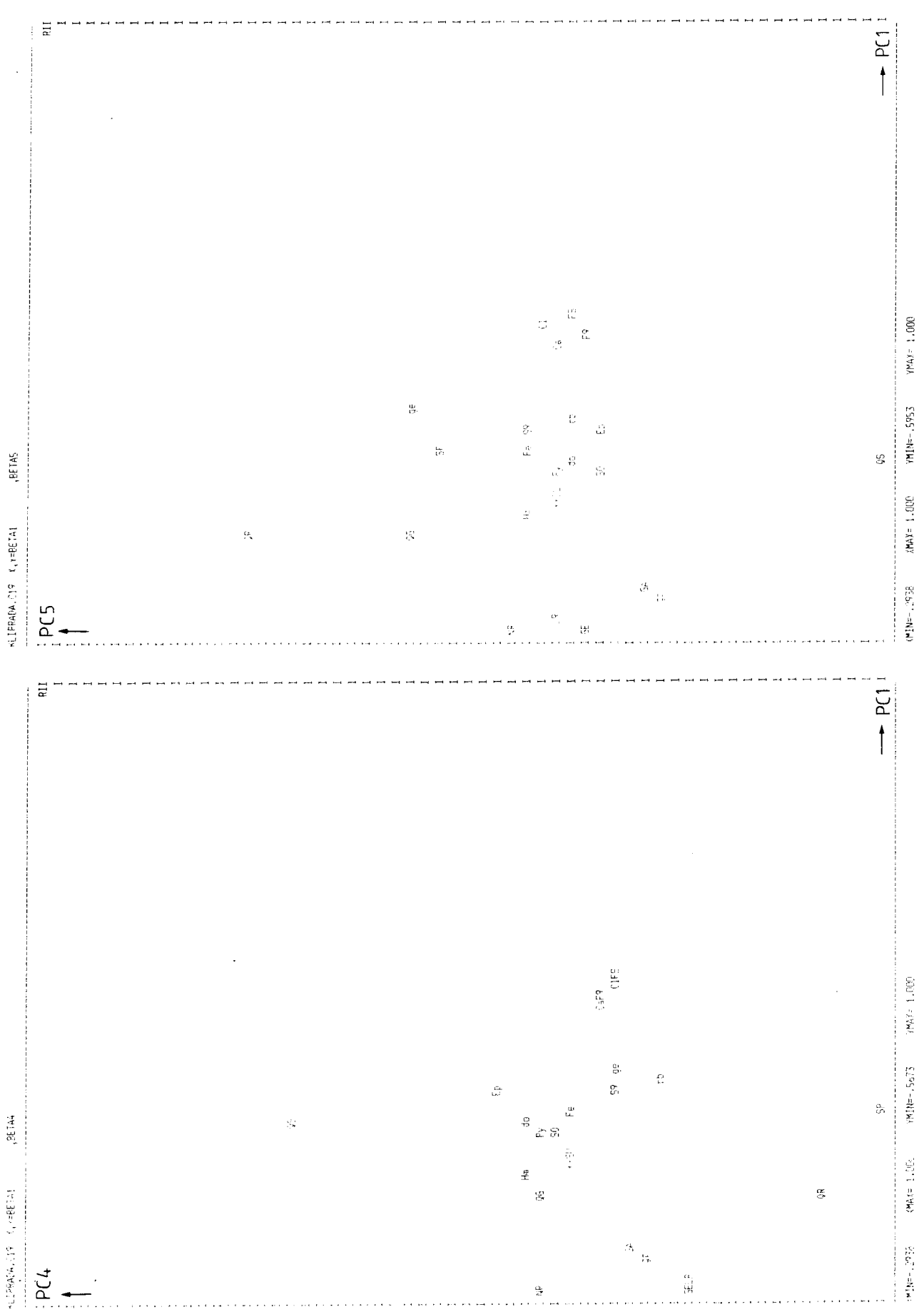

Fig C.11 Variable plots of principal components from the PLS investigation of data from Klipperås, with fracture minerals.

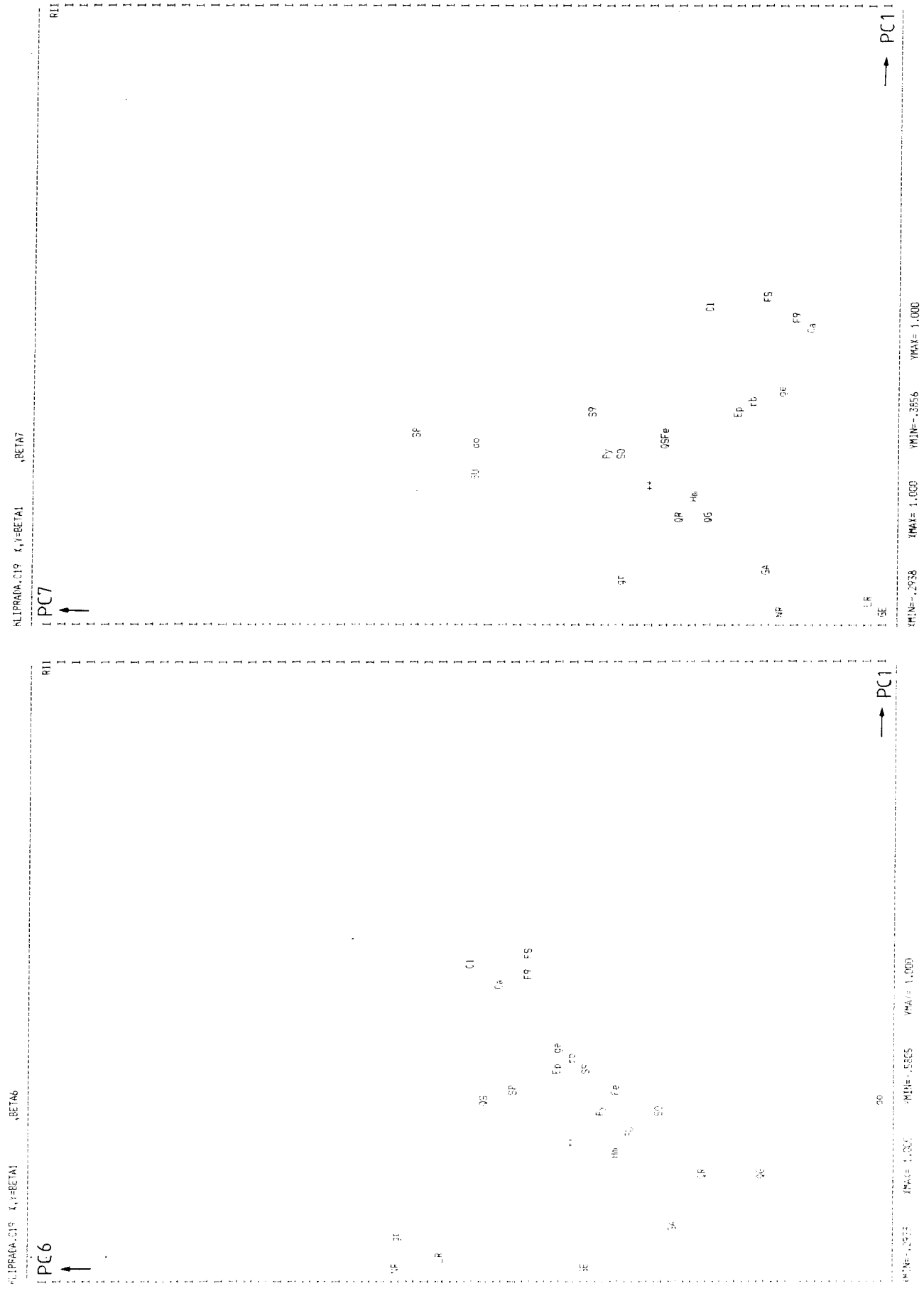

Fig C.12 Variable plots of principal components from the PLS investigation of data from Klipperås, with fracture minerals.

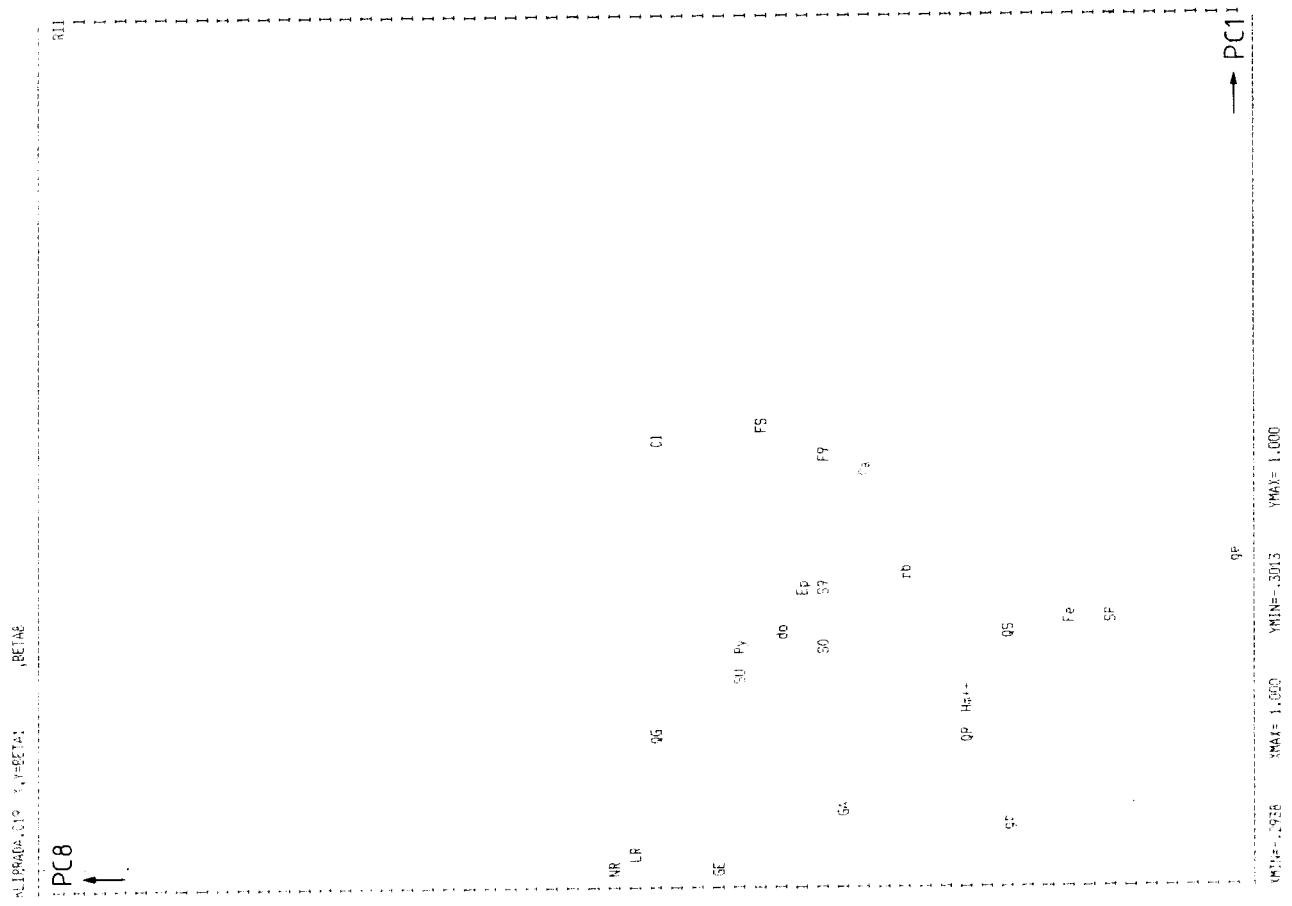

Fig C.13 Variable plots of principal components from the PLS investigation of data from Klipperås, with fracture minerals.

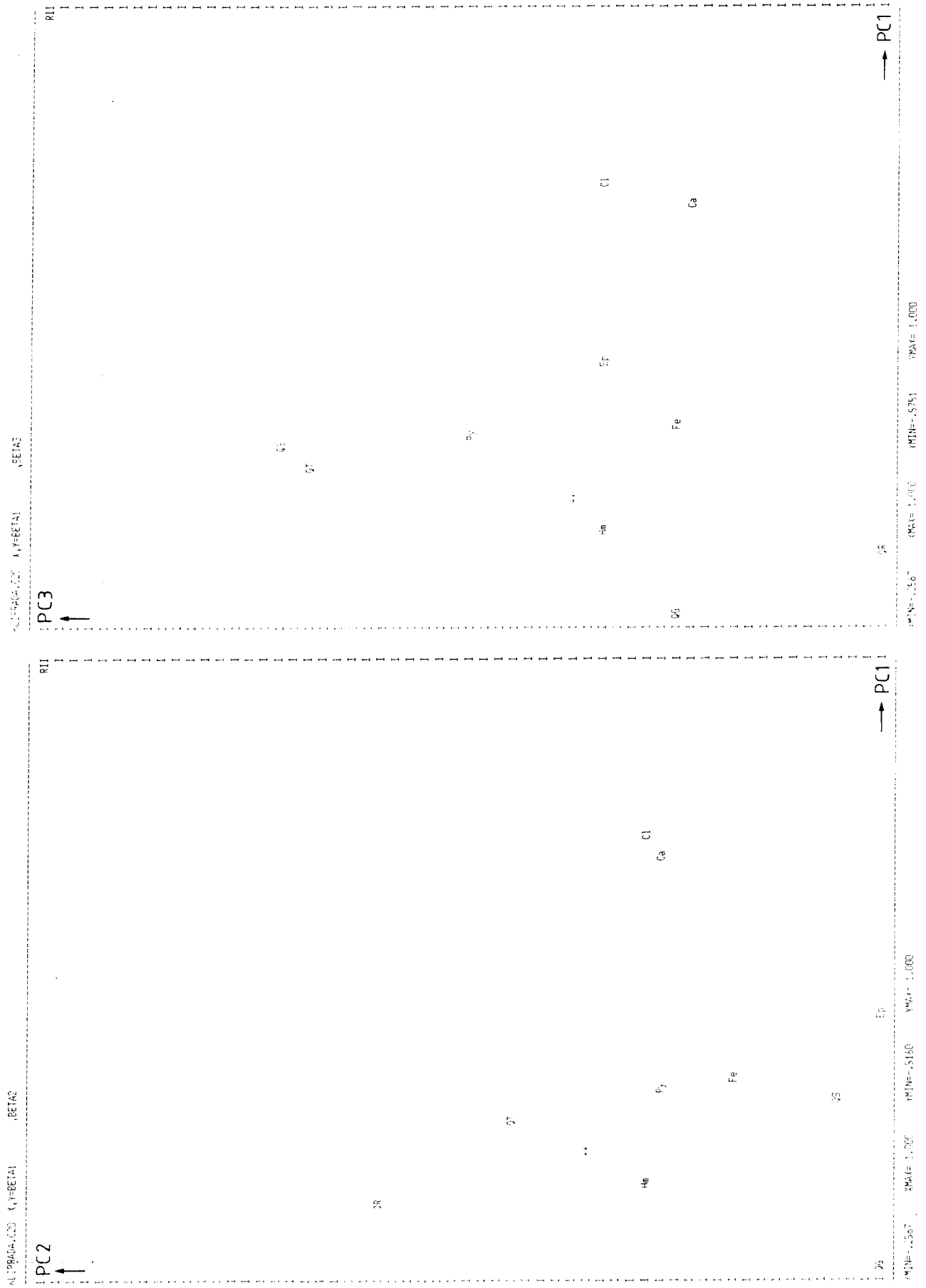

Fig C.14 Variable plots of the principal components from the PLS investigation of data from Klipperås, with fracture minerals and borehole fluid.

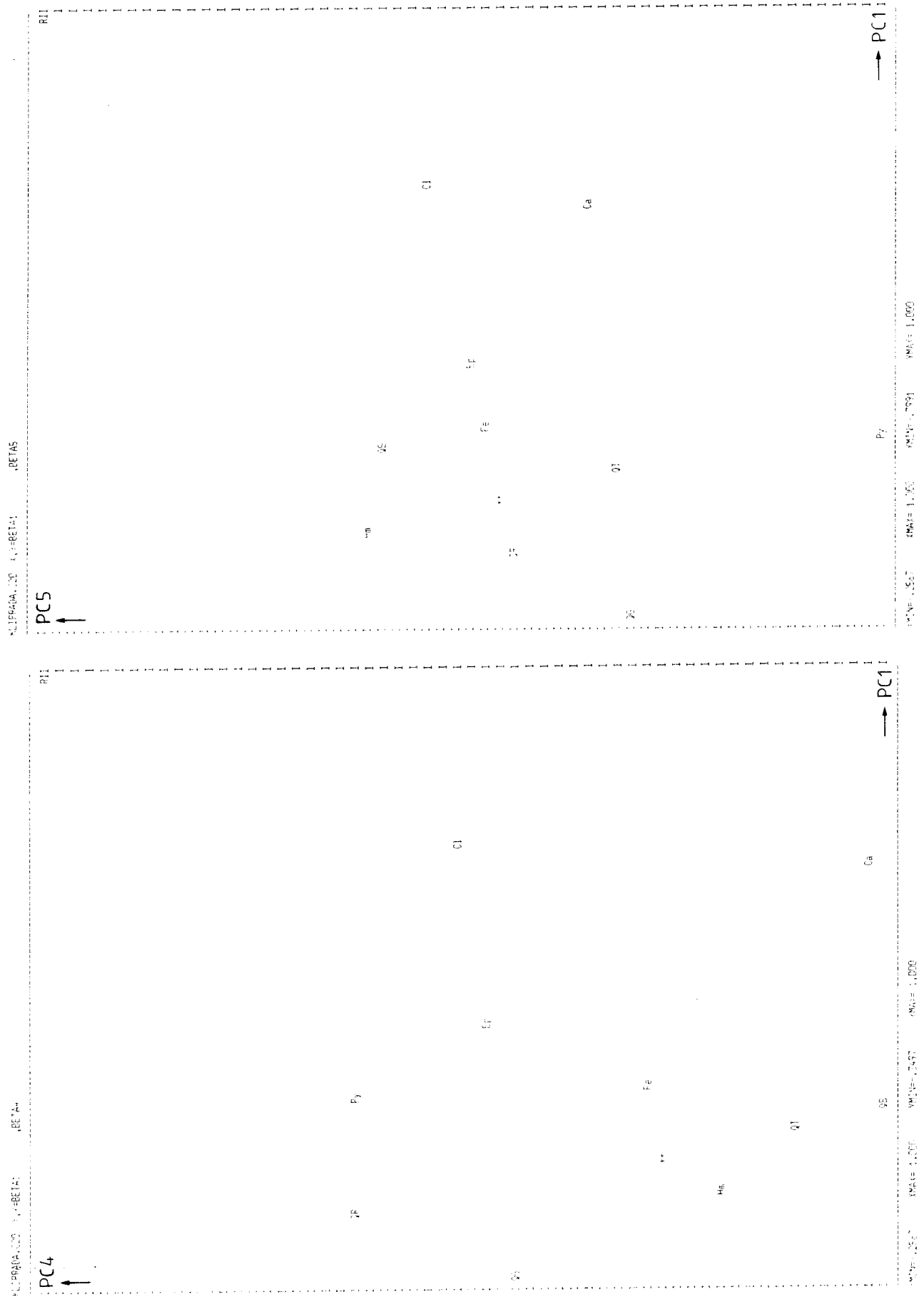

Fig C.15 Variable plots of the principal components from the PLS investigation of data from Klipperås, with fracture minerals and borehole fluid.

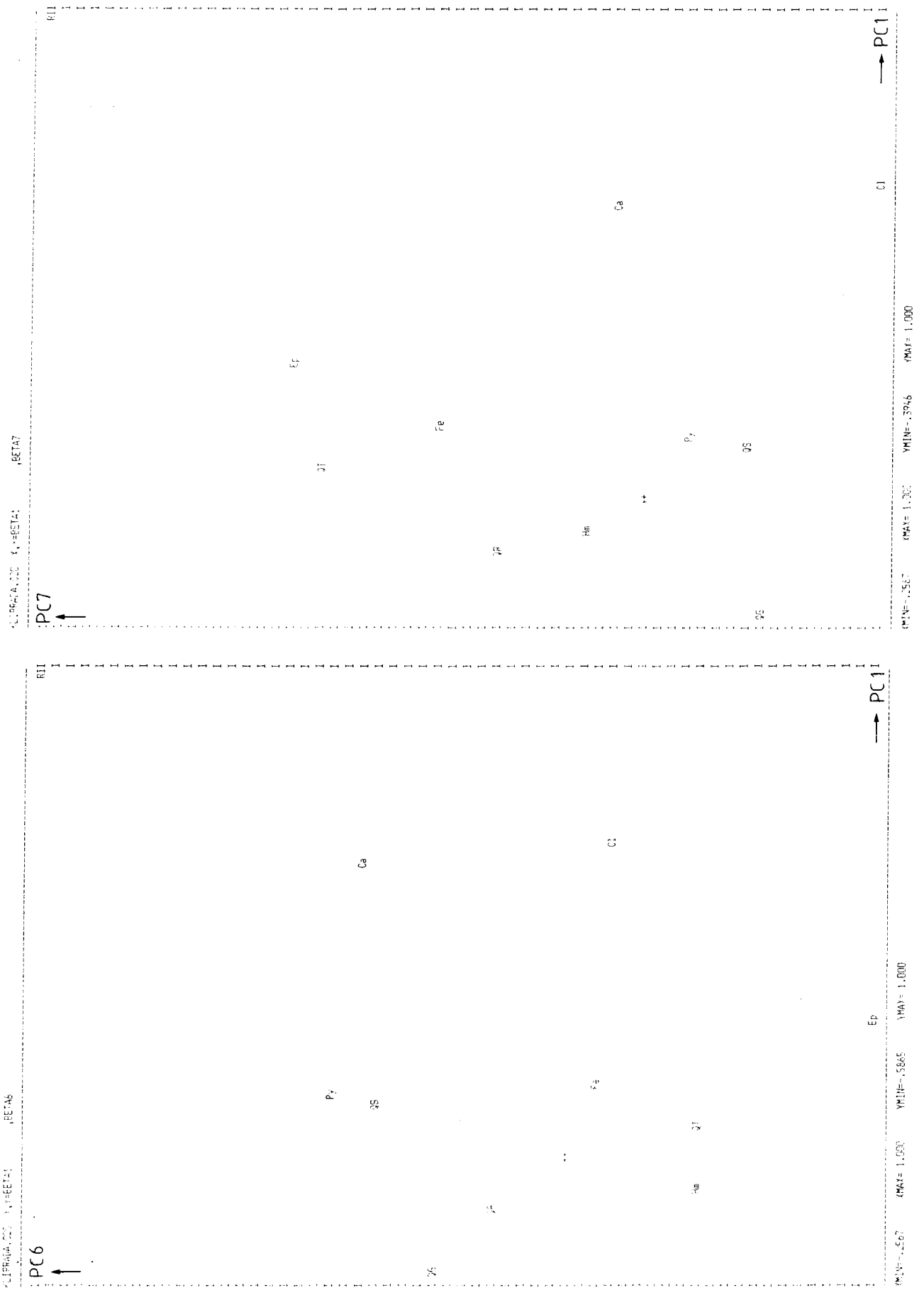

Fig C.16 Variable plots of the principal components from the PLS investigation of data from Klipperås, with fracture minerals and borehole fluid.

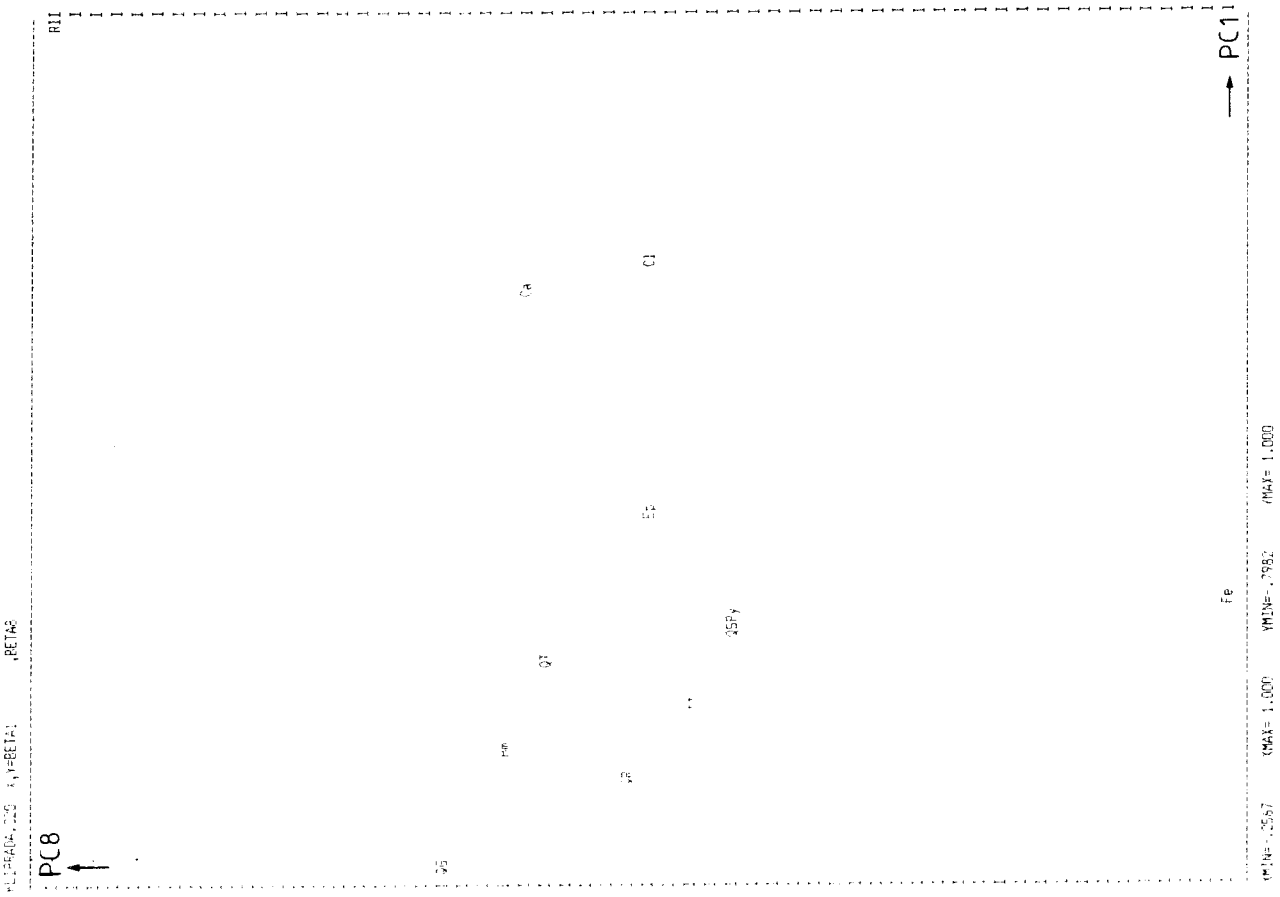

Fig C.17 Variable plots of the principal components from the PLS investigation of data from Klipperås, with fracture minerals and borehole fluid.

Fig C.18 Variable plot of the principal components from the PLS2 investigation of data from Klipperås, with radar angles.

Fig C.19 Variable plot of the principal components from the PLS2 investigation of data from Klipperås, with radar angles.

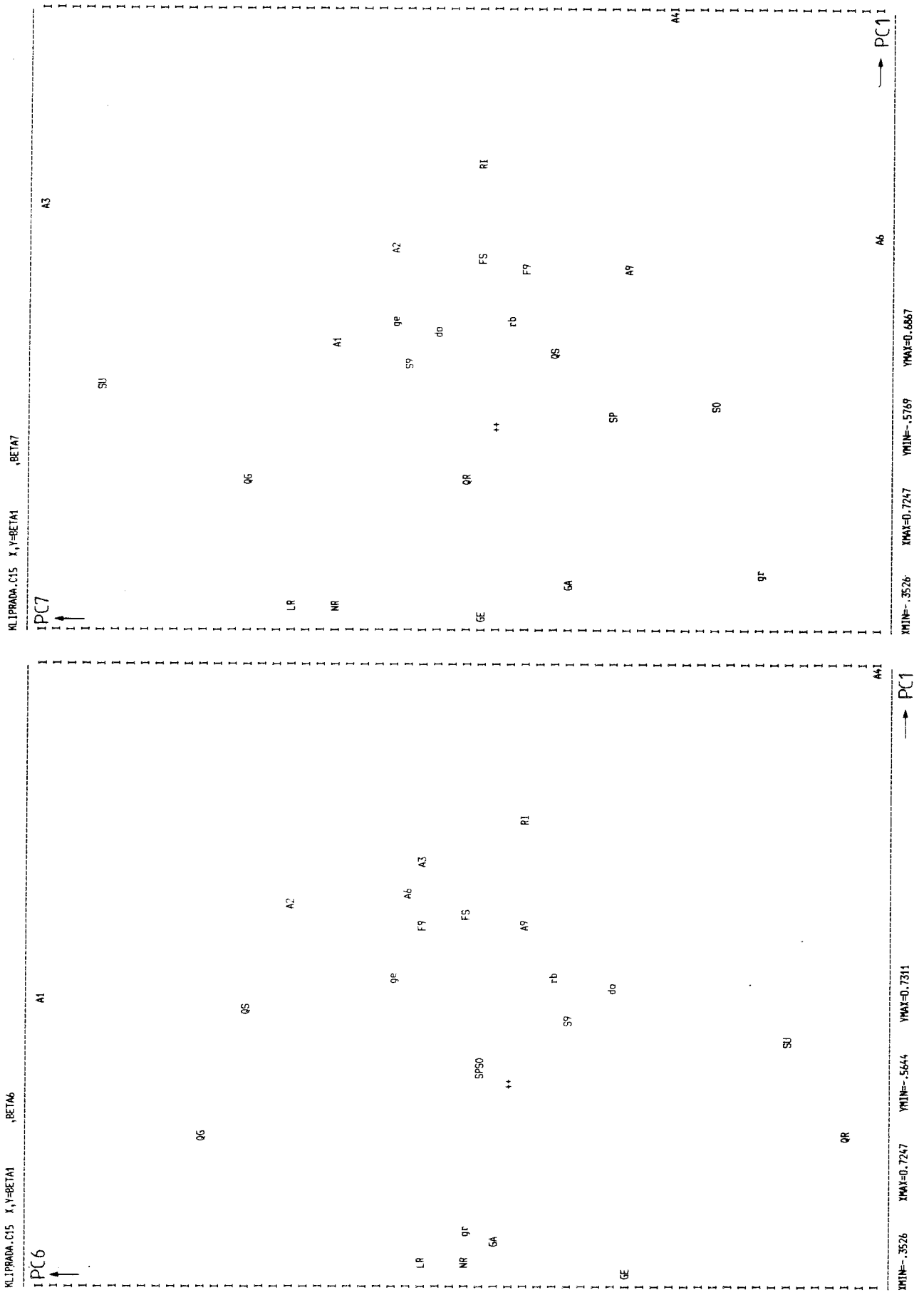

Fig C.20 Variable plot of the principal components from the PLS2 investigation of data from Klipperås, with radar angles.

Fig C.21 Variable plot of the principal components from the PLS2 investigation of data from Klipperås, with radar angles.

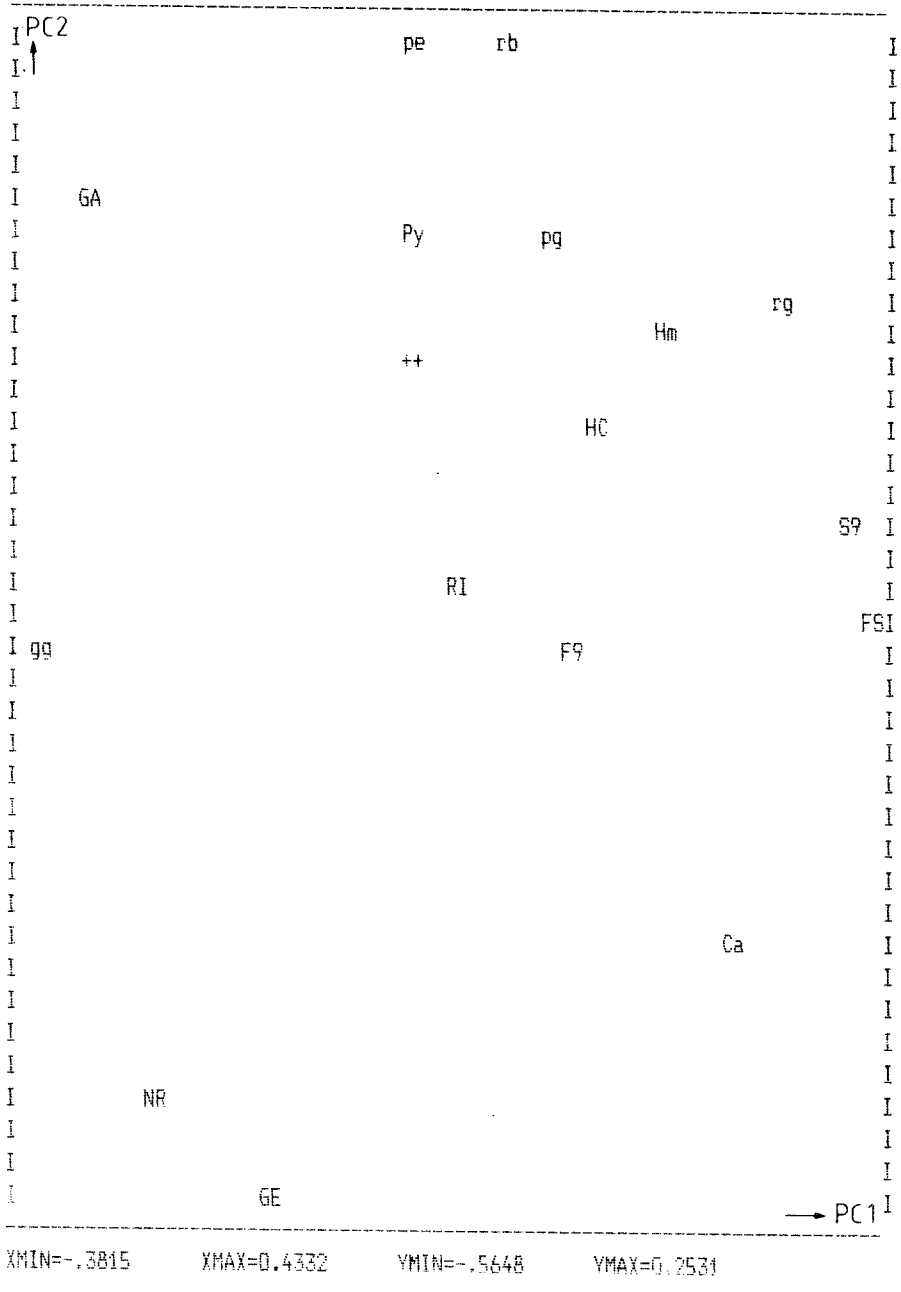

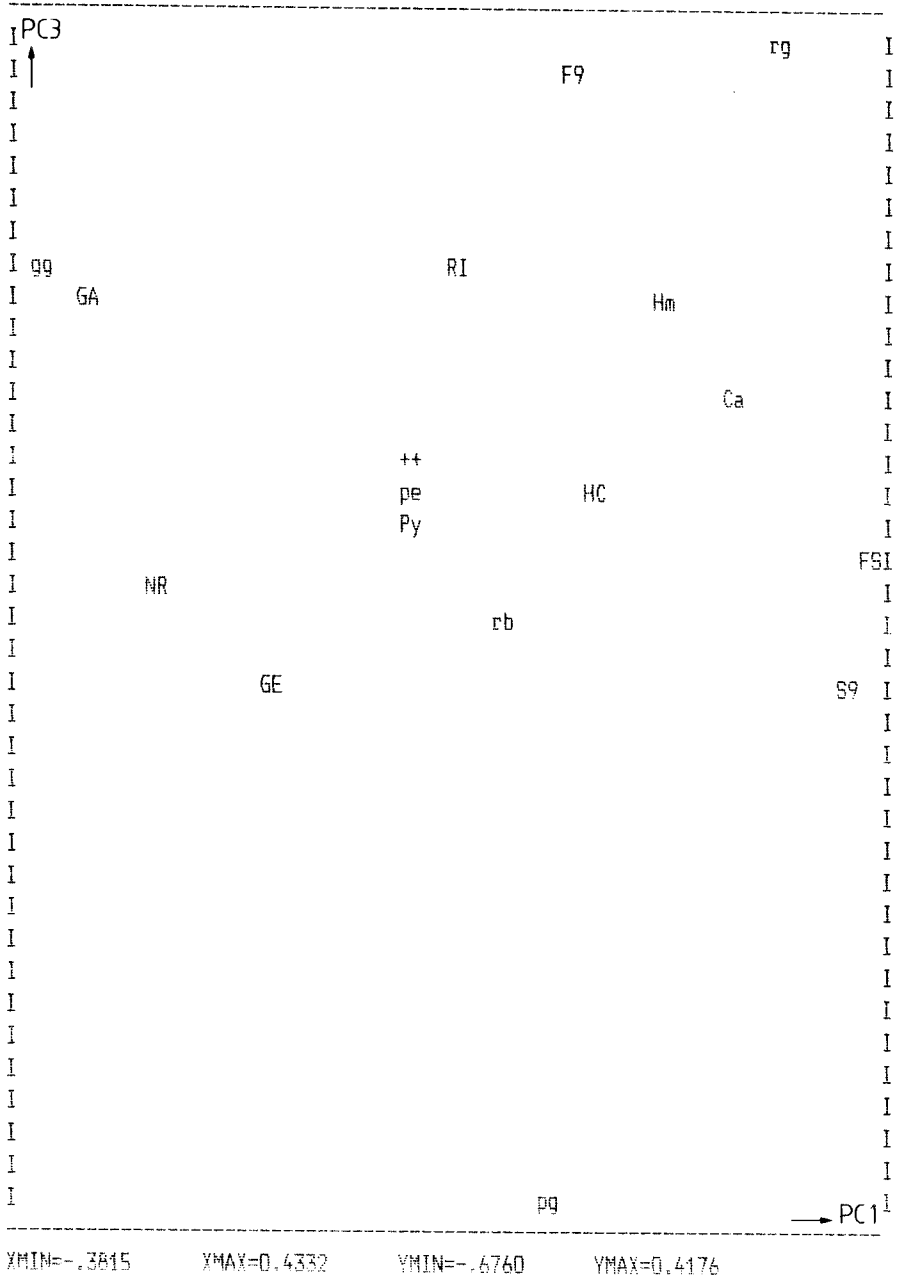

Fig C.22 Variable plots of principal components from PC-analysis of data from Finnsjön.

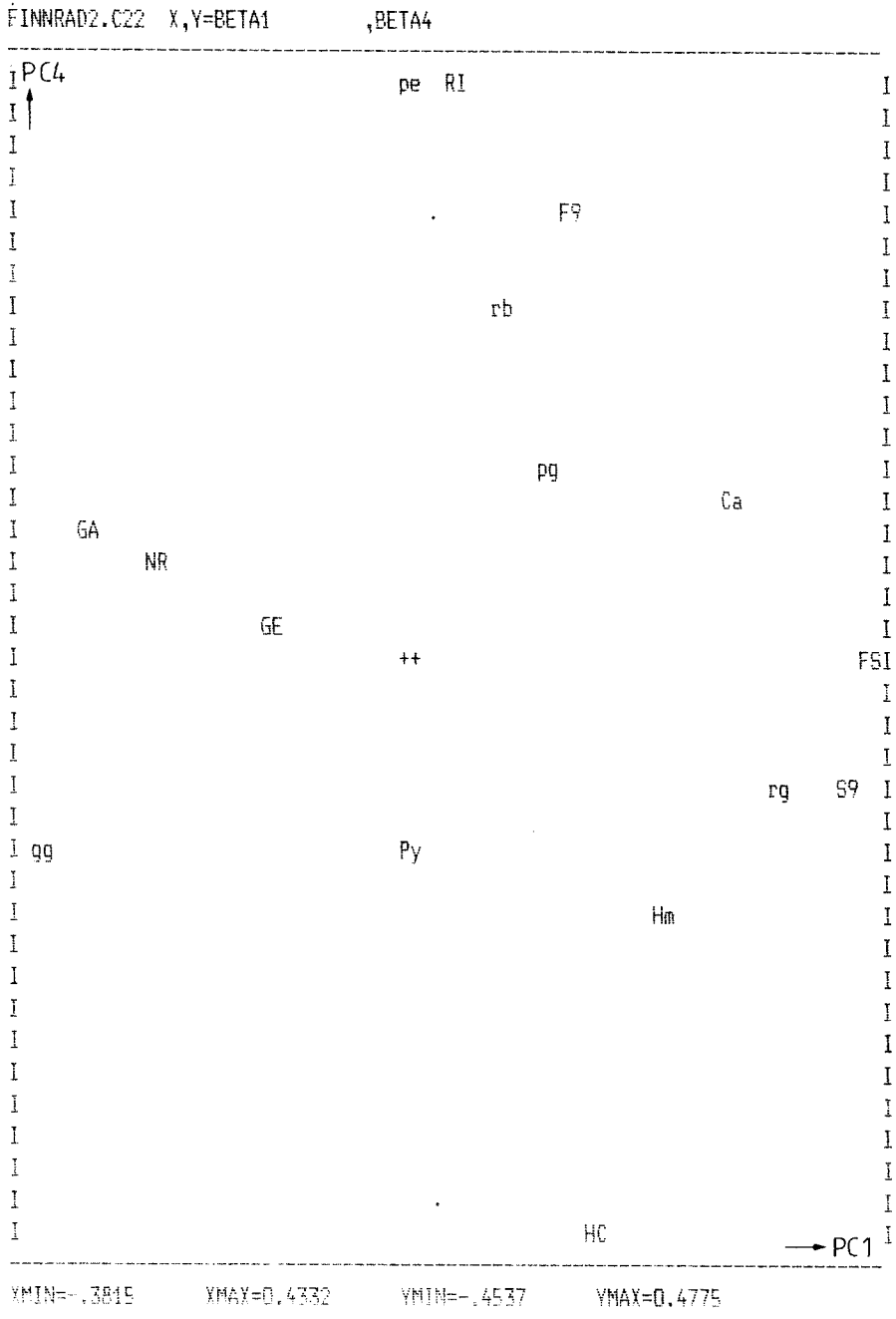

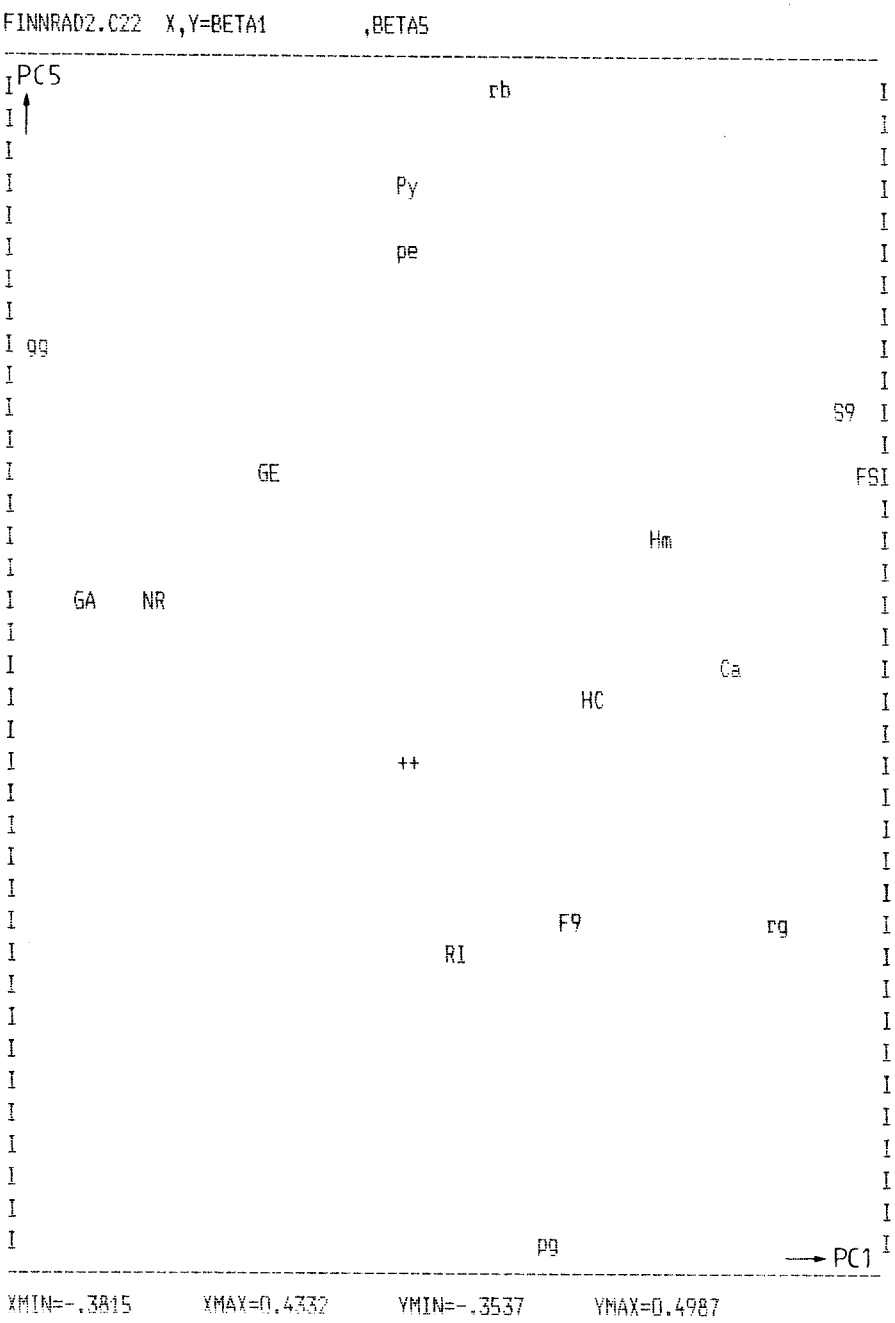

Fig C.23 Variable plots of principal components from PC-analysis of data from Finnsjön.

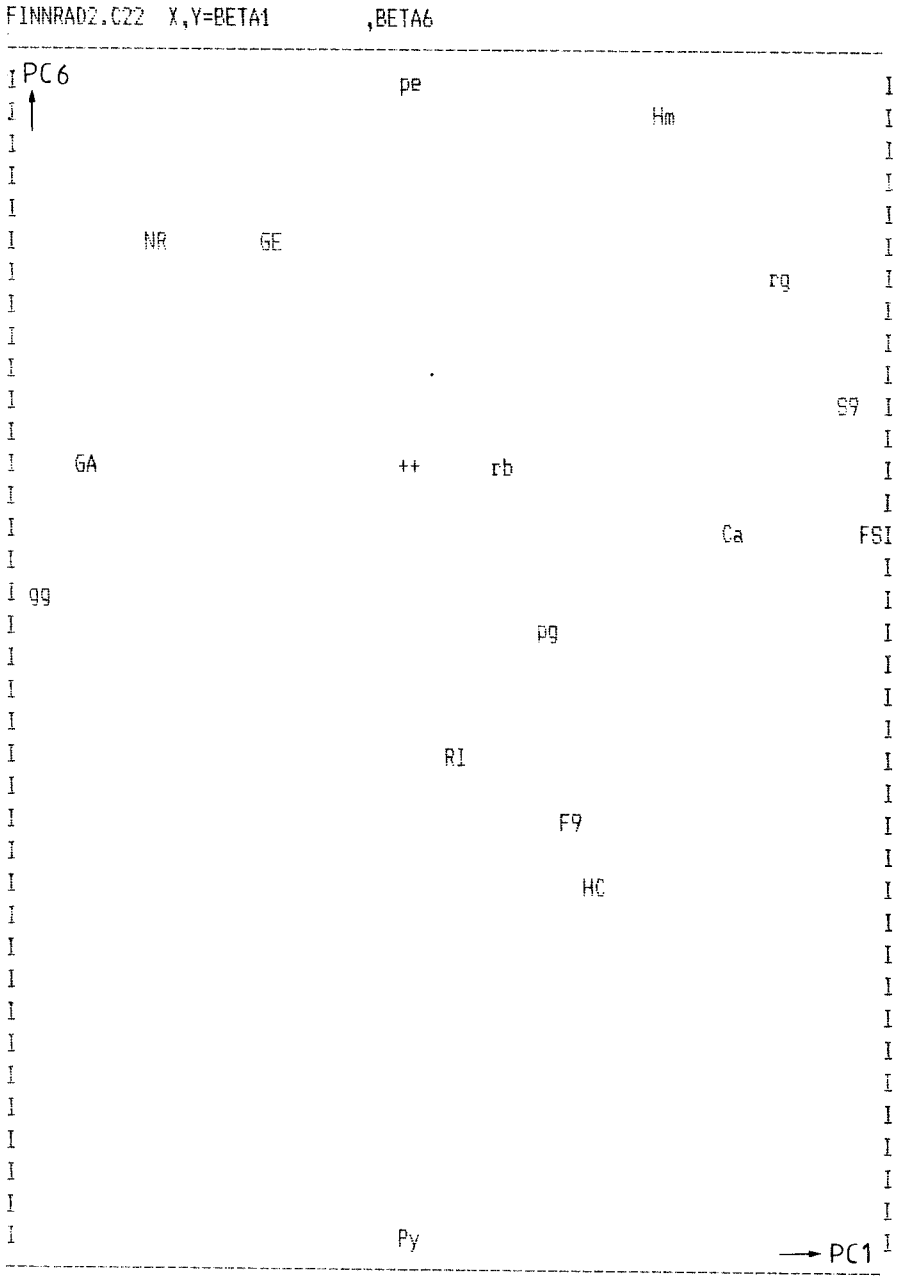

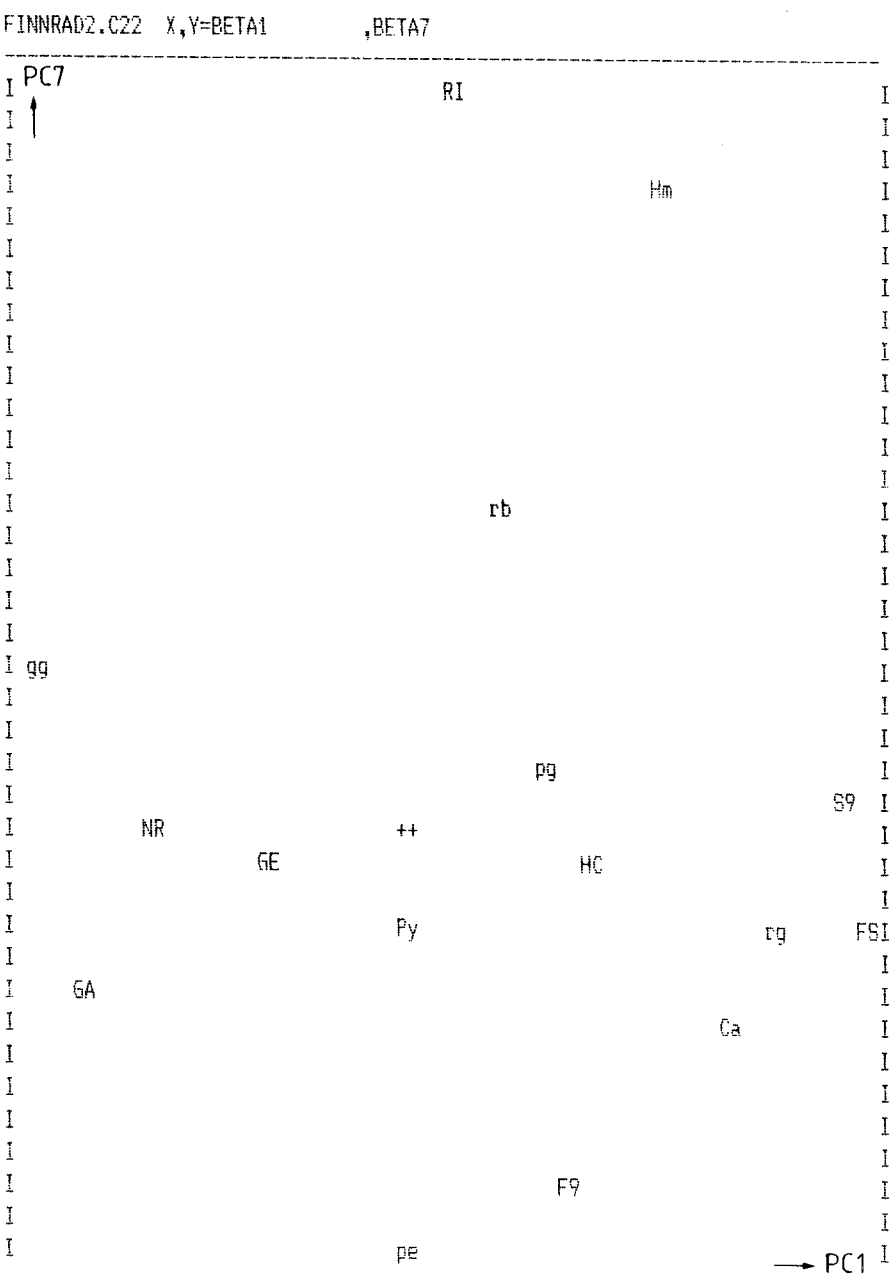

Fig C.24 Variable plots of principal components from PC-analysis of data from Finnsjön.

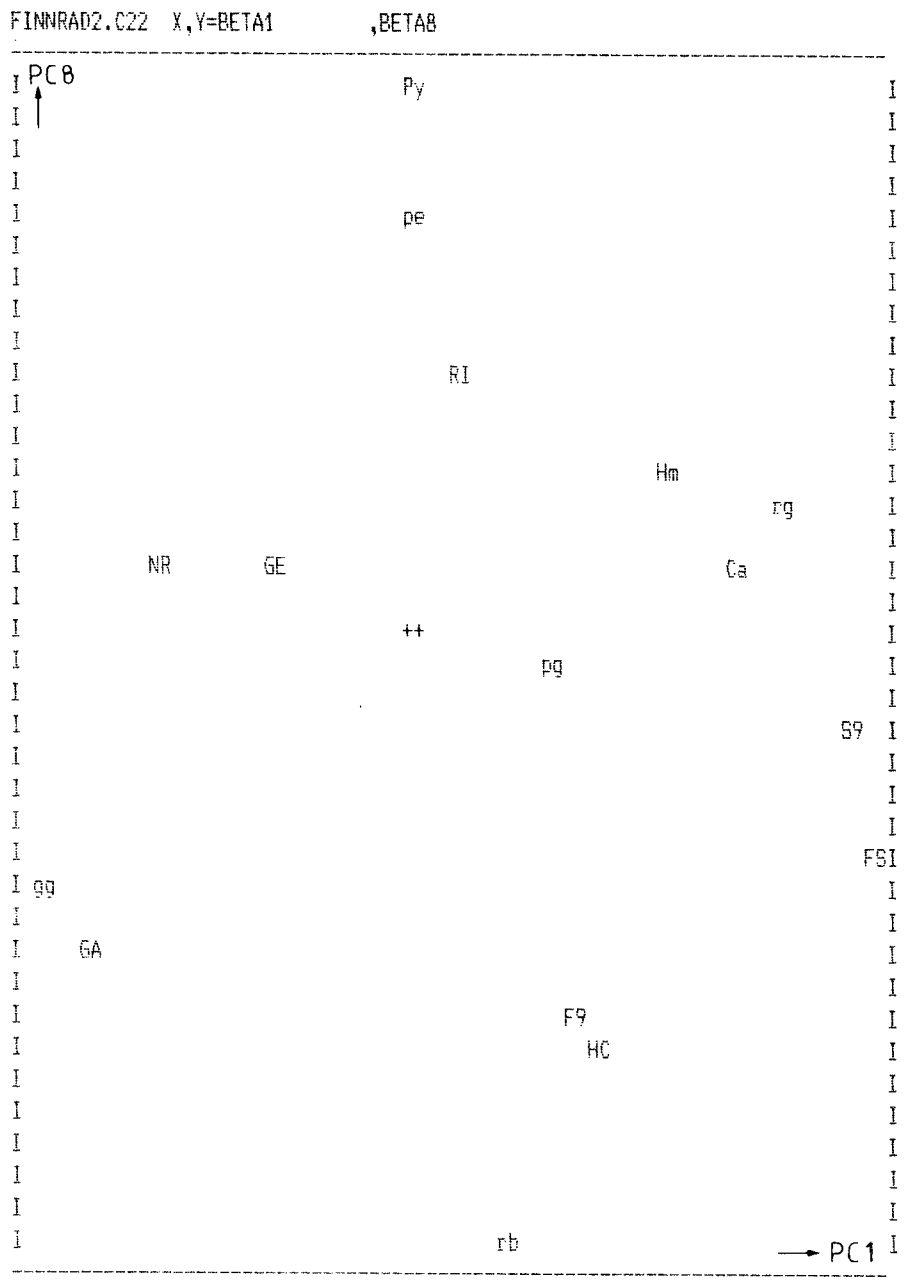

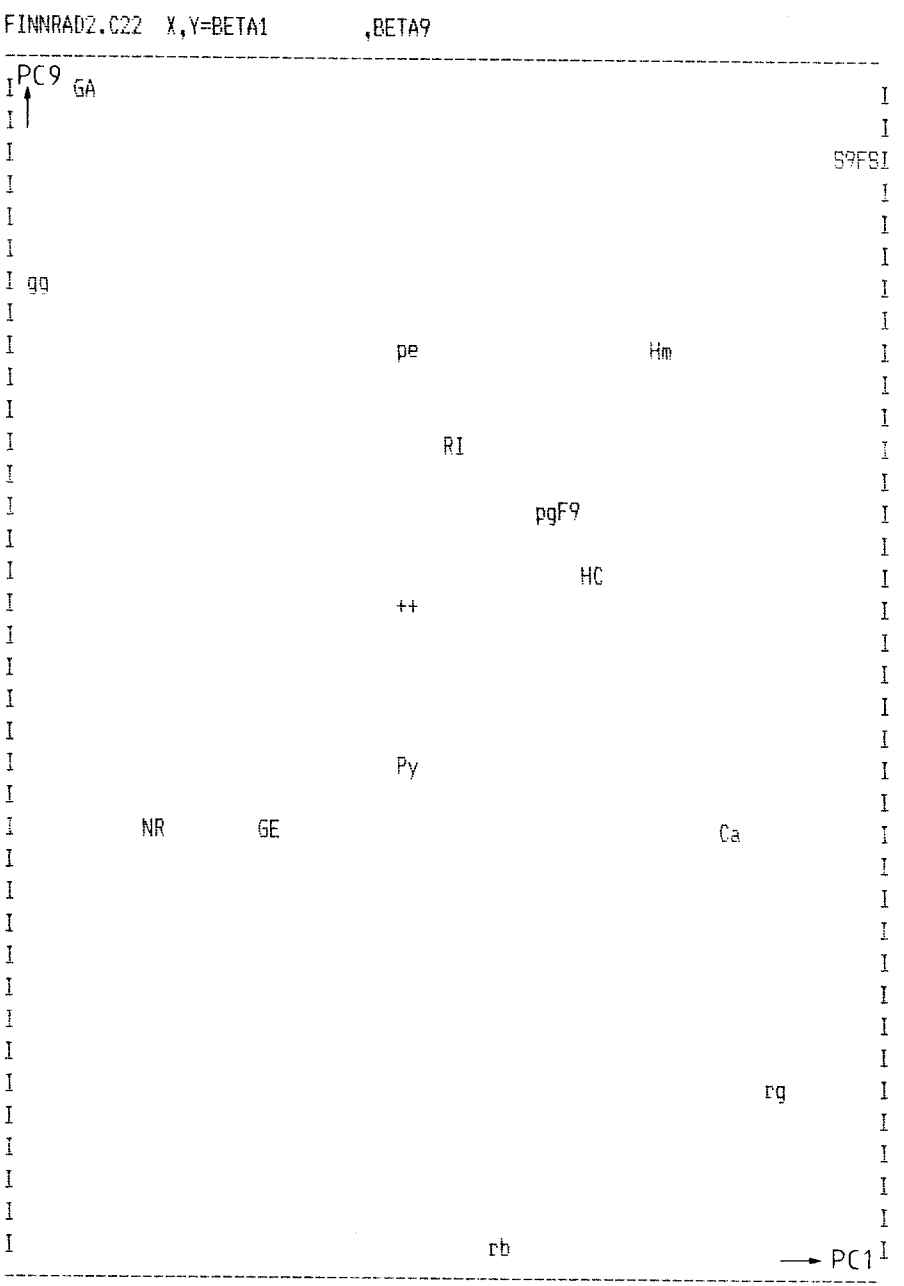

Fig C.25 Variable plots of principal components from PC-analysis of data from Finnsjön.

Fig C.26 Variable plots of principal components from PC-analysis of data from Finnsjön.

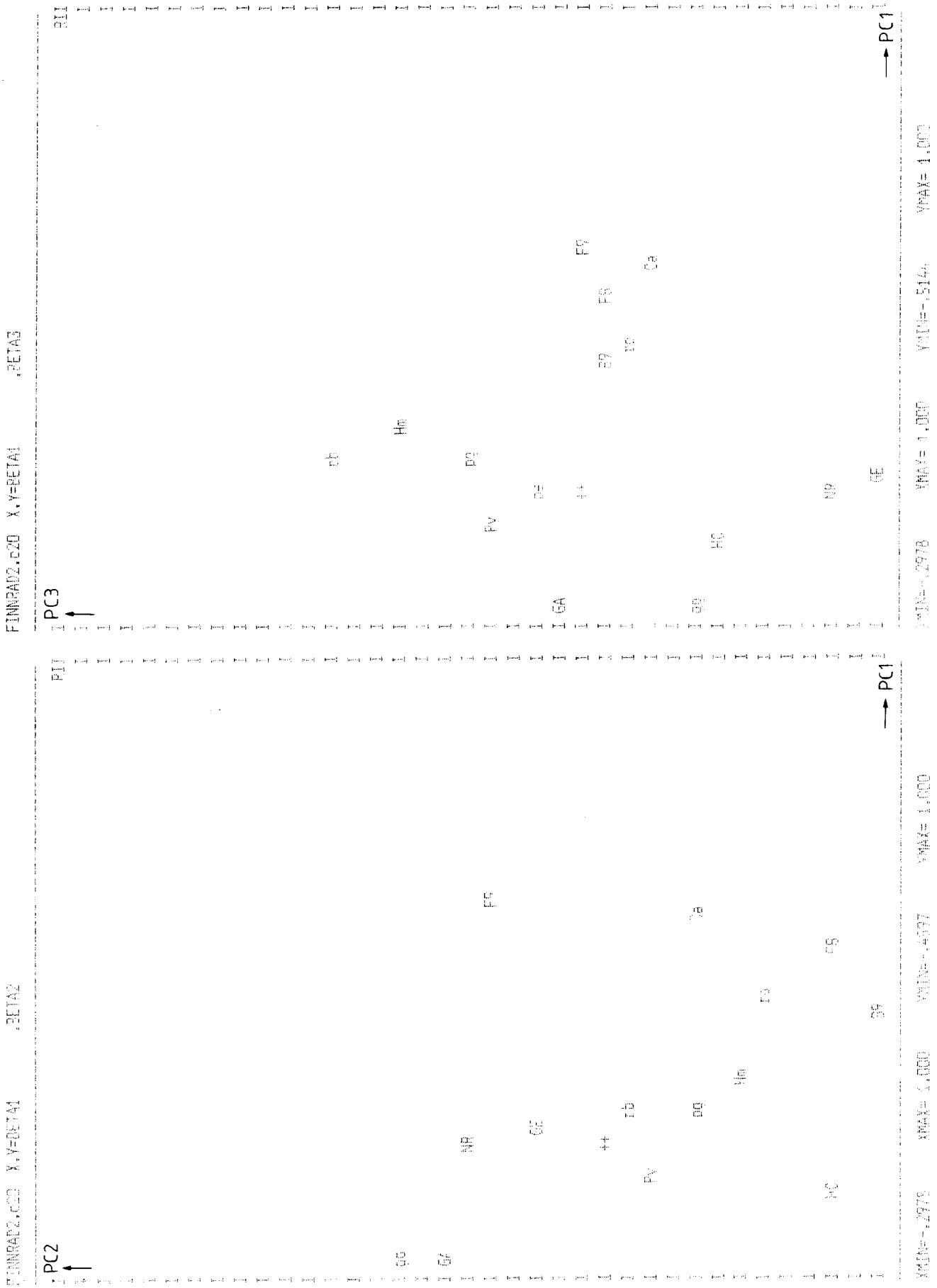

Fig C.27 Variable plots of the principal components from the PLS investigation of data from Finnsjön.

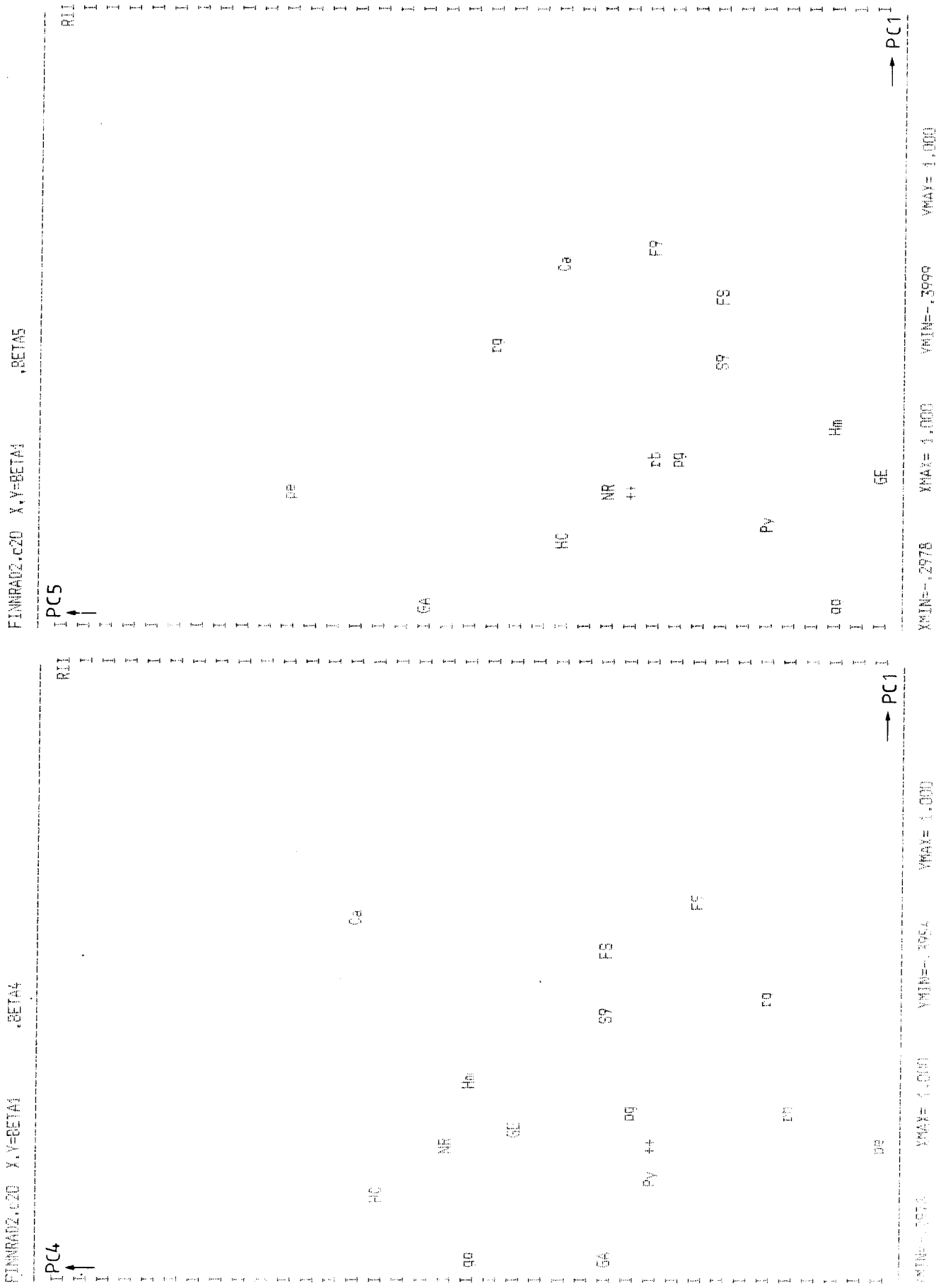

Fig C.28 Variable plots of the principal components from the PLS investigation of data from Finnsjön.

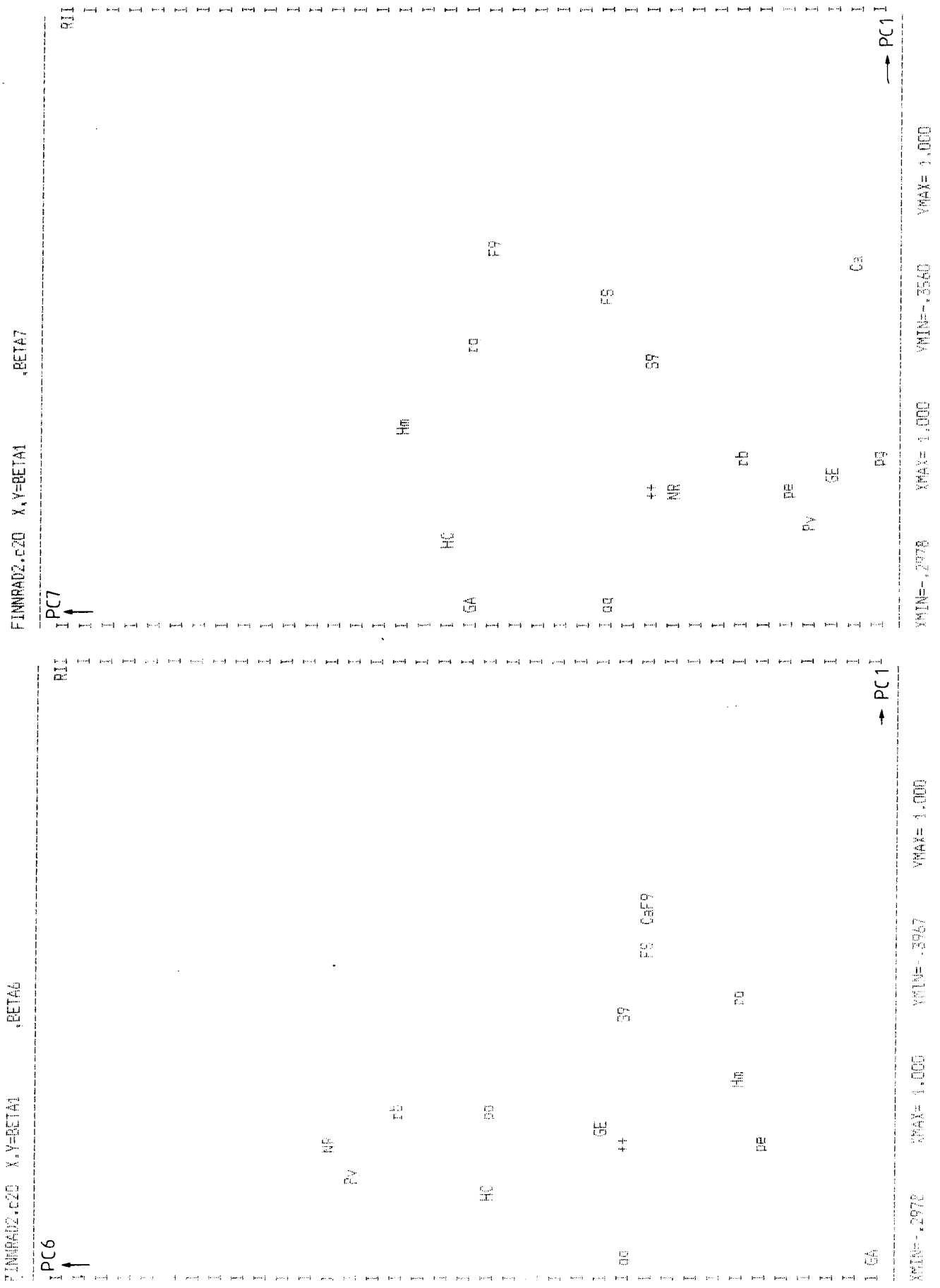

Fig C.29 Variable plots of the principal components from the PLS investigation of data from Finnsjön.

Fig C.30 Variable plots of the principal components from the PLS investigation of data from Finnsjön.

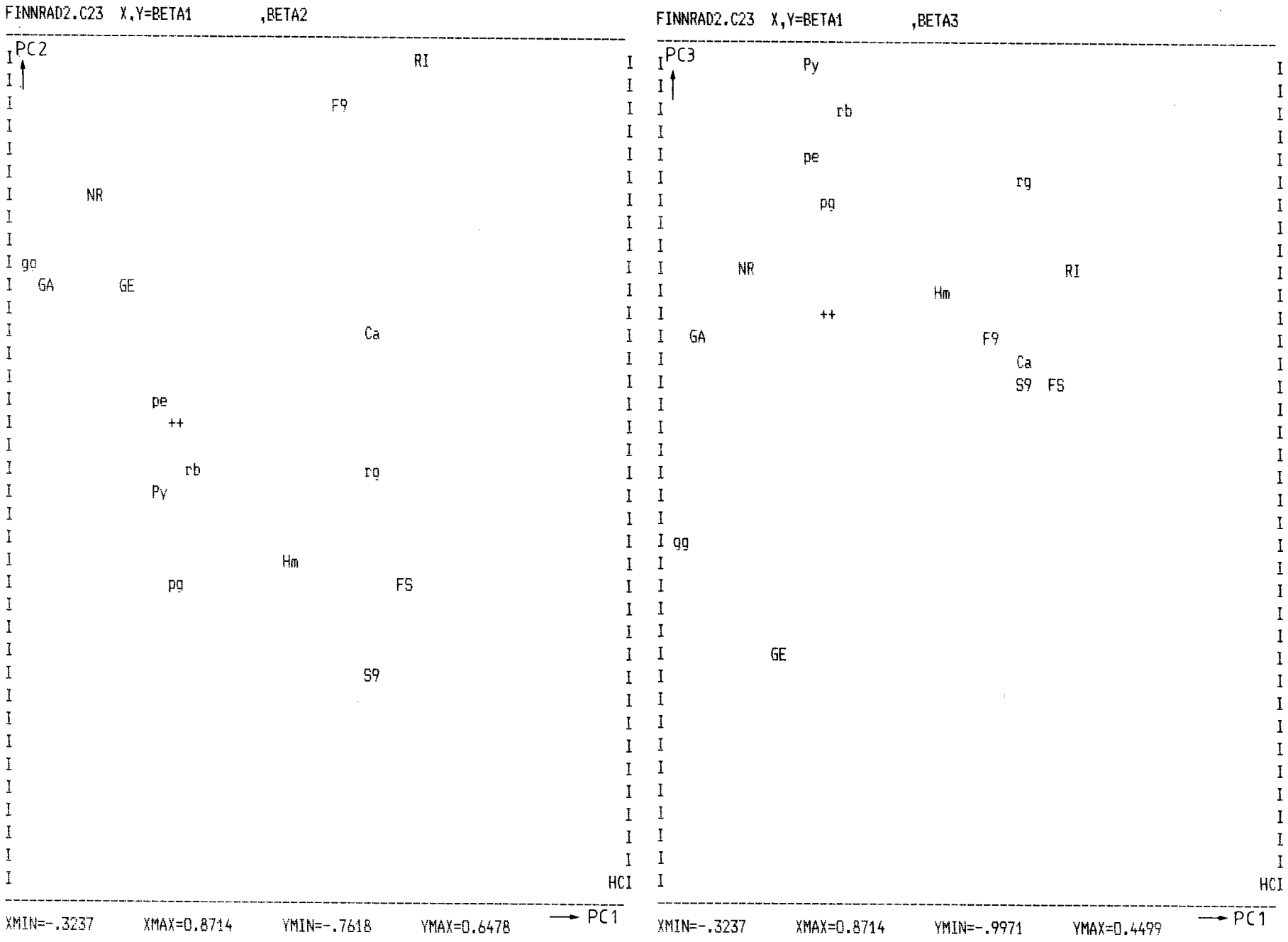

Fig C.31 Variable plot of the principal components from the PLS2 investigation of data from Finnsjön.

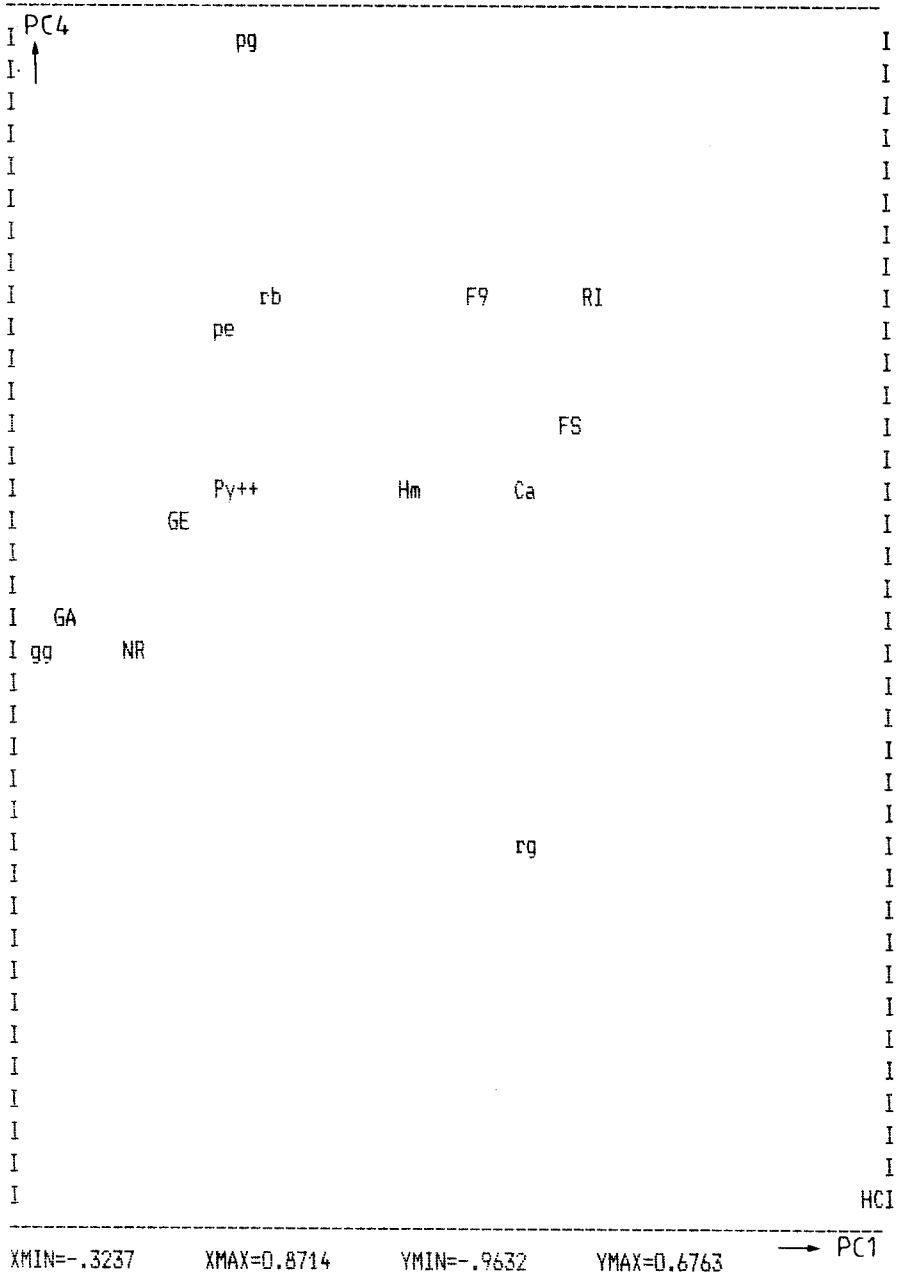

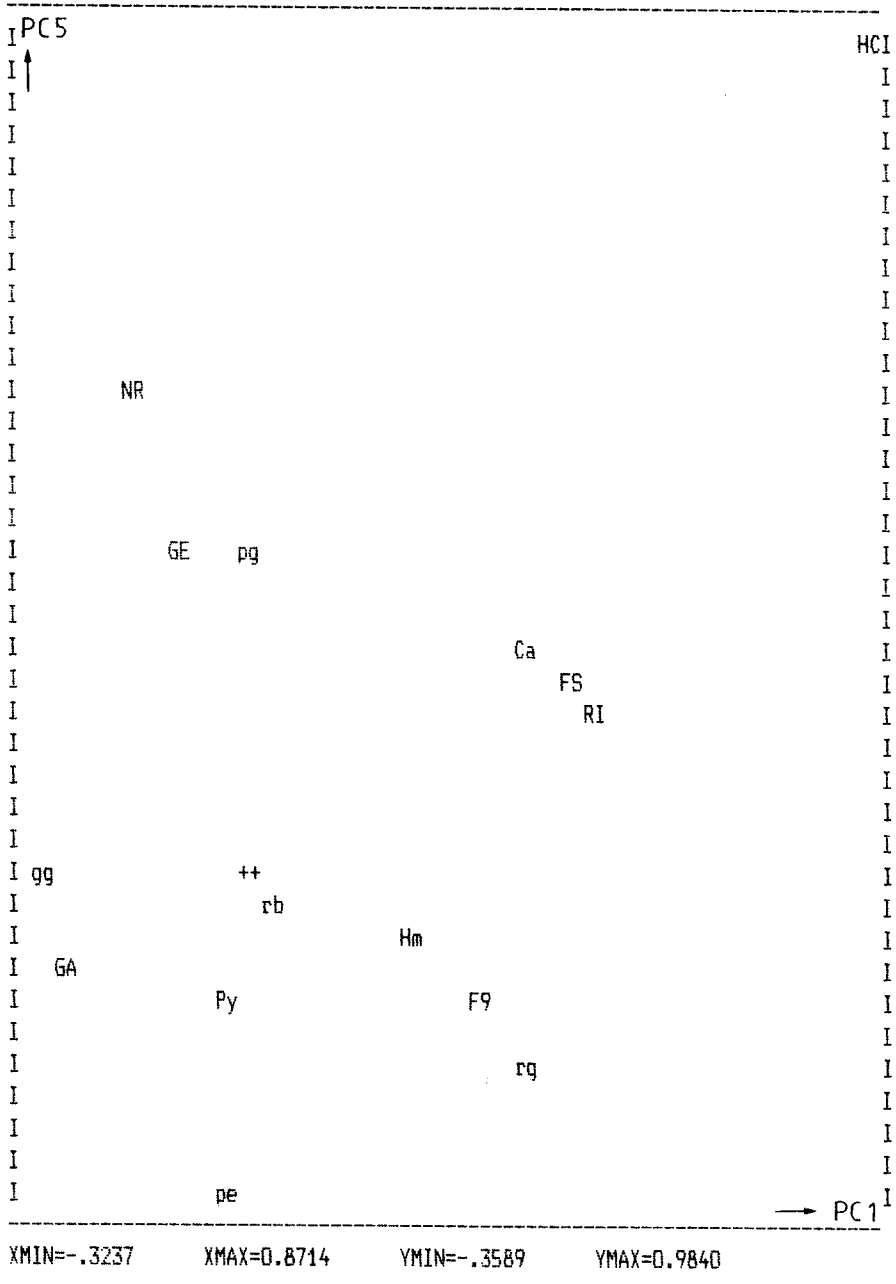

Fig C.32 Variable plot of the principal components from the PLS2 investigation of data from Finnsjön.

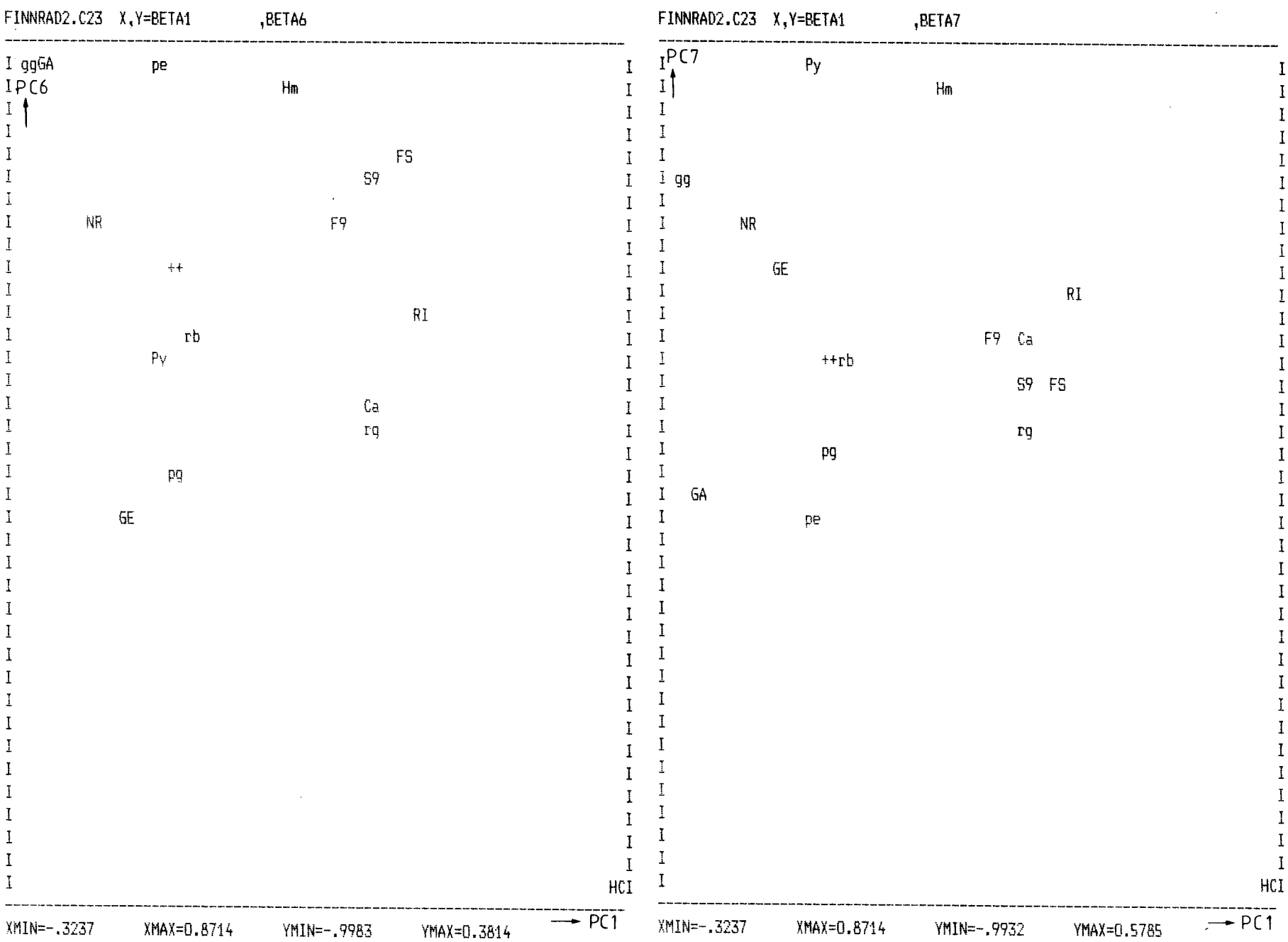

Fig C.33 Variable plot of the principal components from the PLS2 investigation of data from Finnsjön.

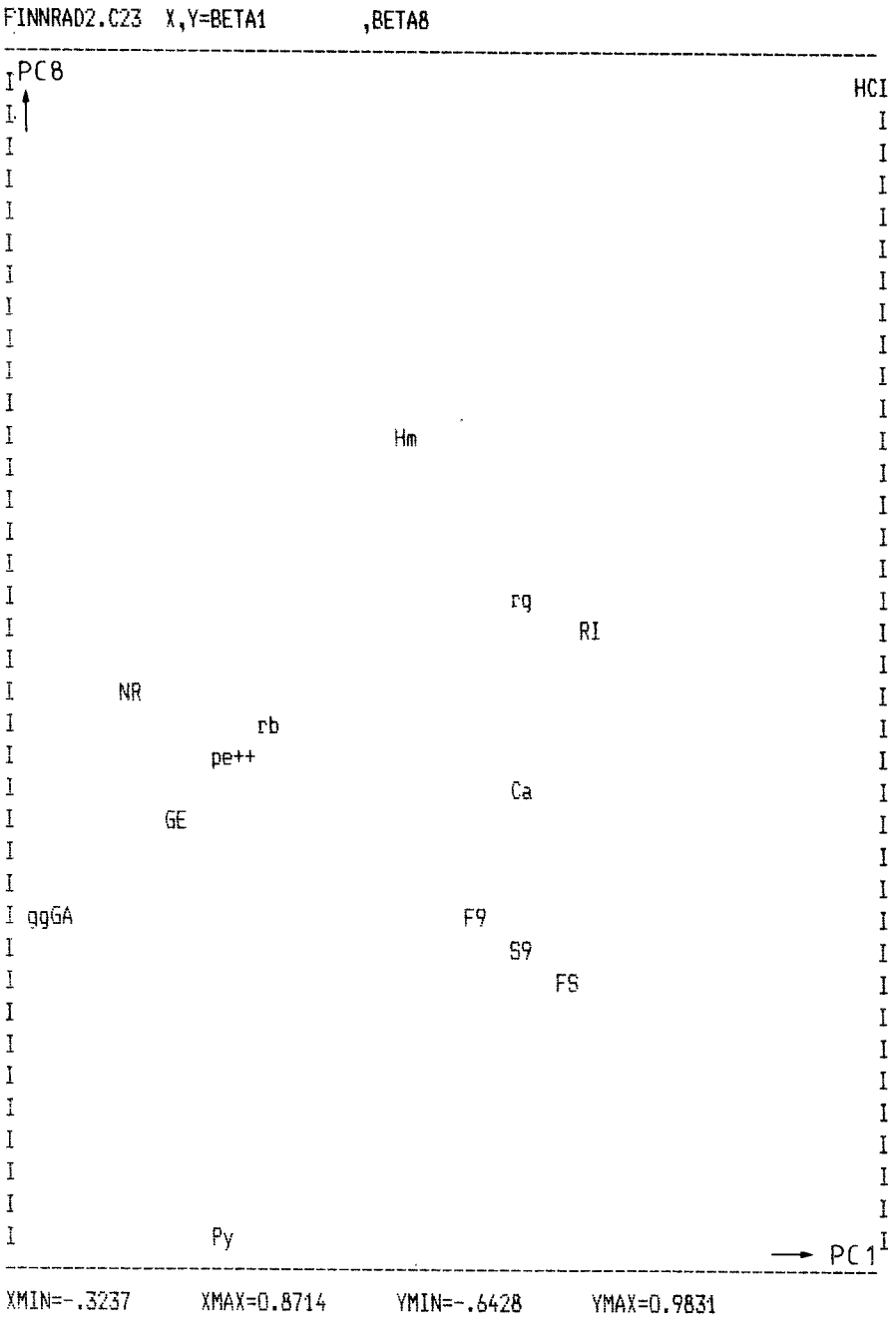

Fig C.34 Variable plot of the principal components from the PLS2 investigation of data from Finnsjön.

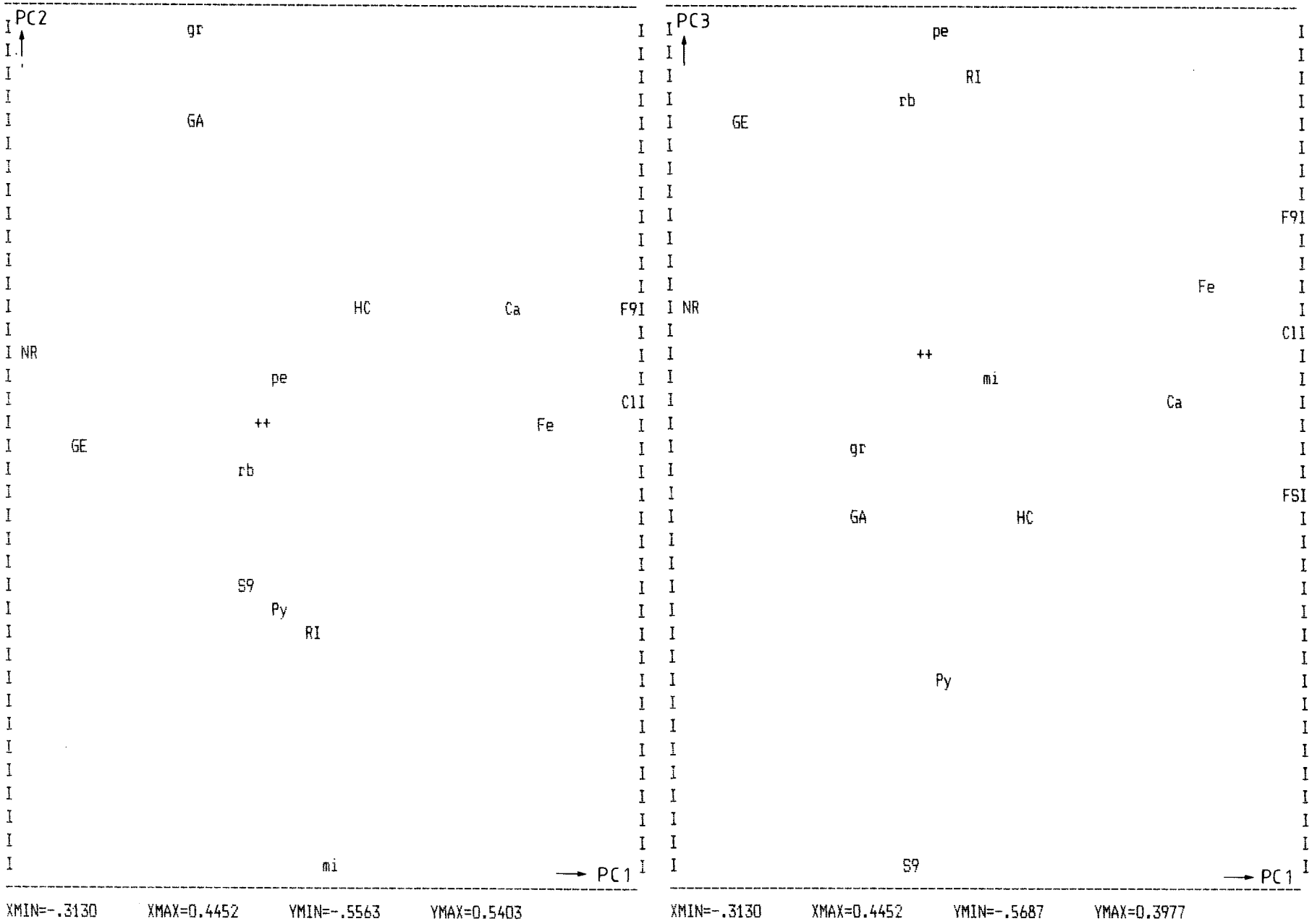

Fig C.35 Variable plots of principal components from PC-analysis of data from Saltsjötunnel.

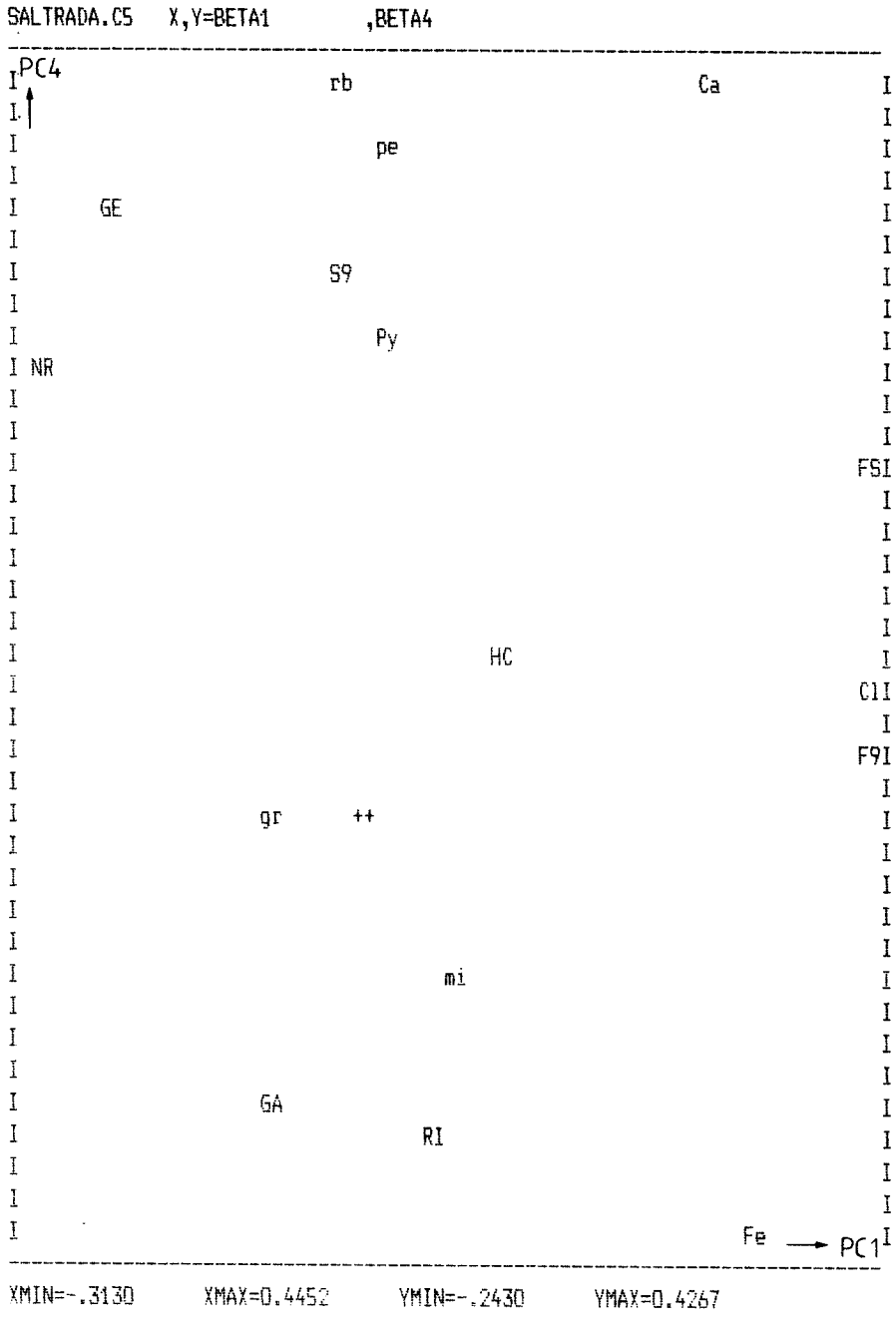

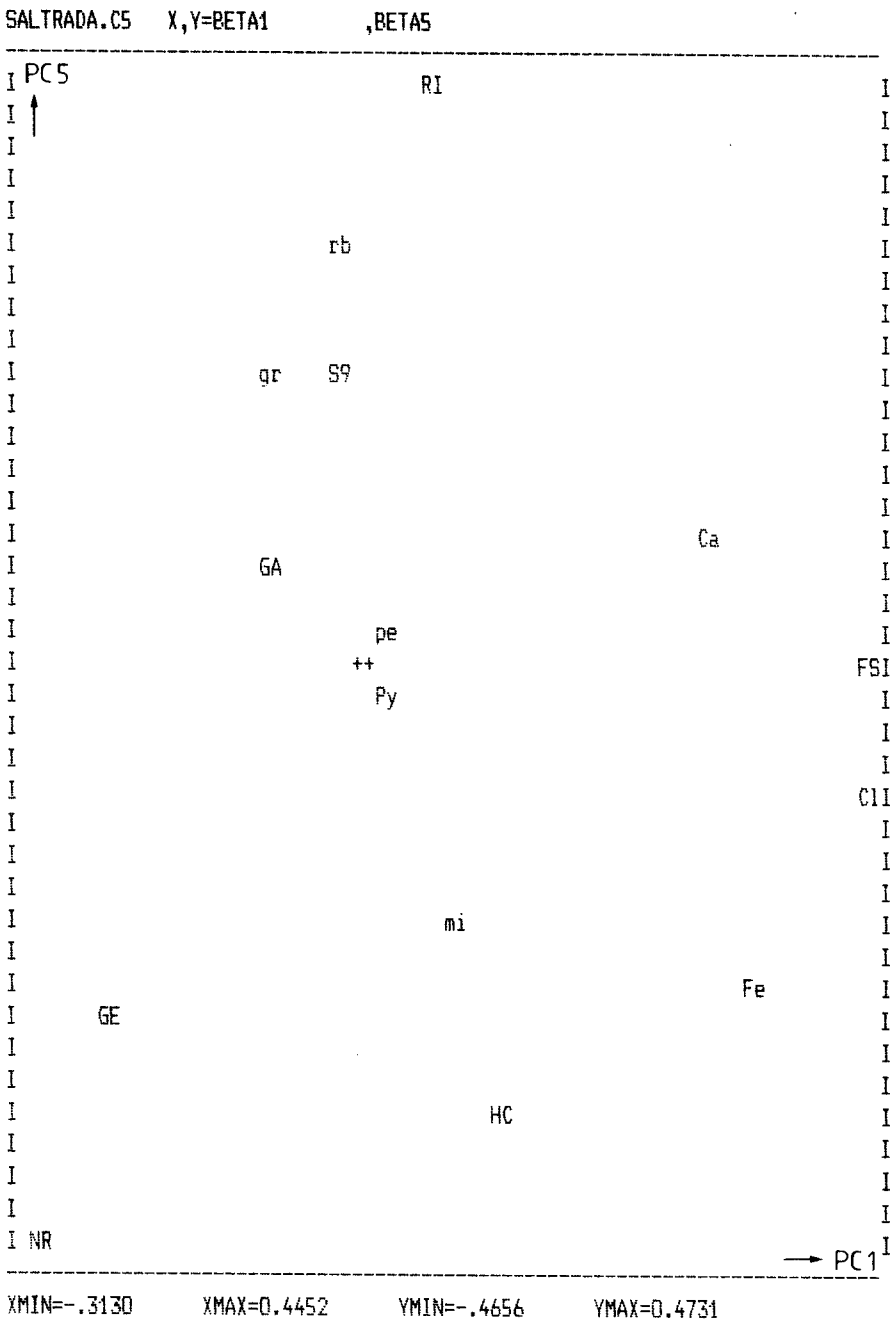

Fig C.36 Variable plots of principal components from PC-analysis of data from Saltsjötunnel.

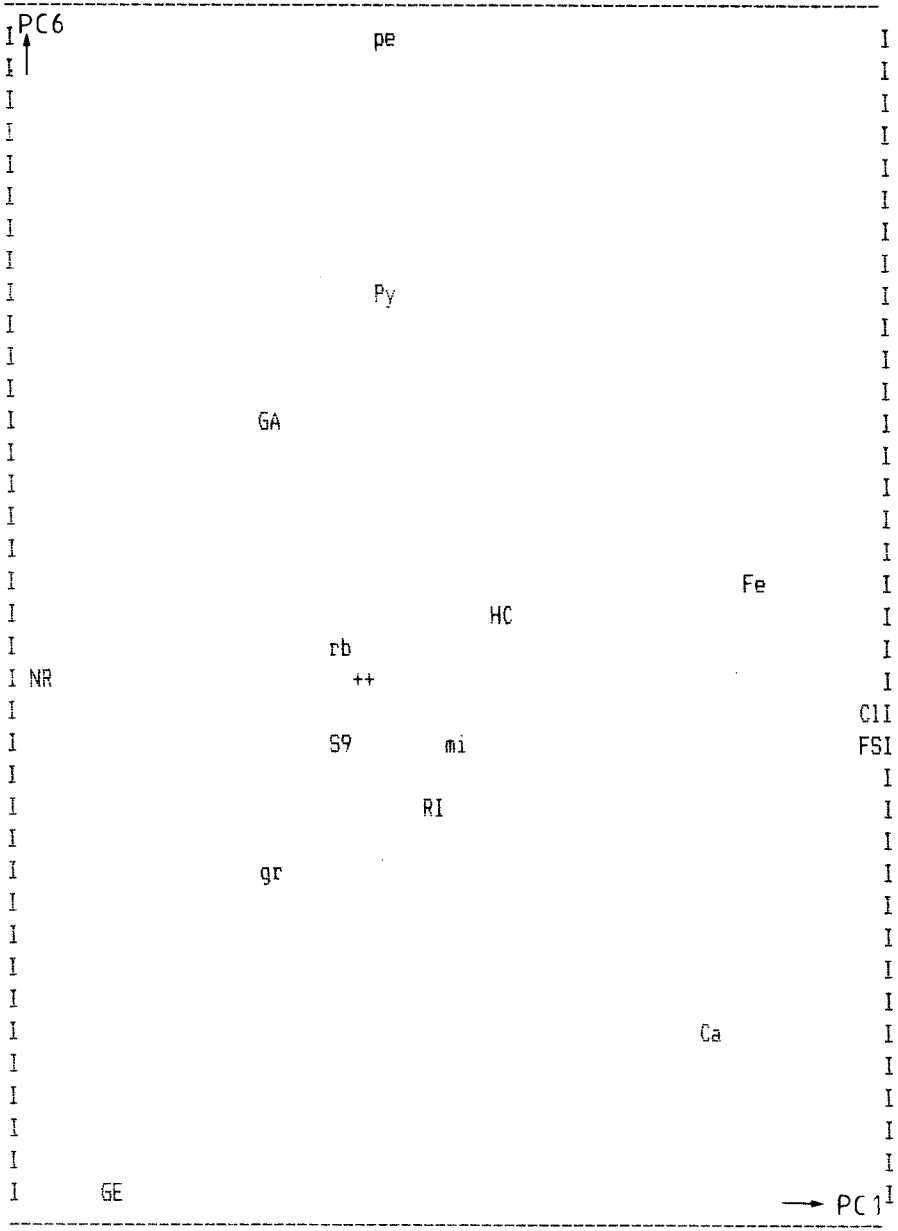

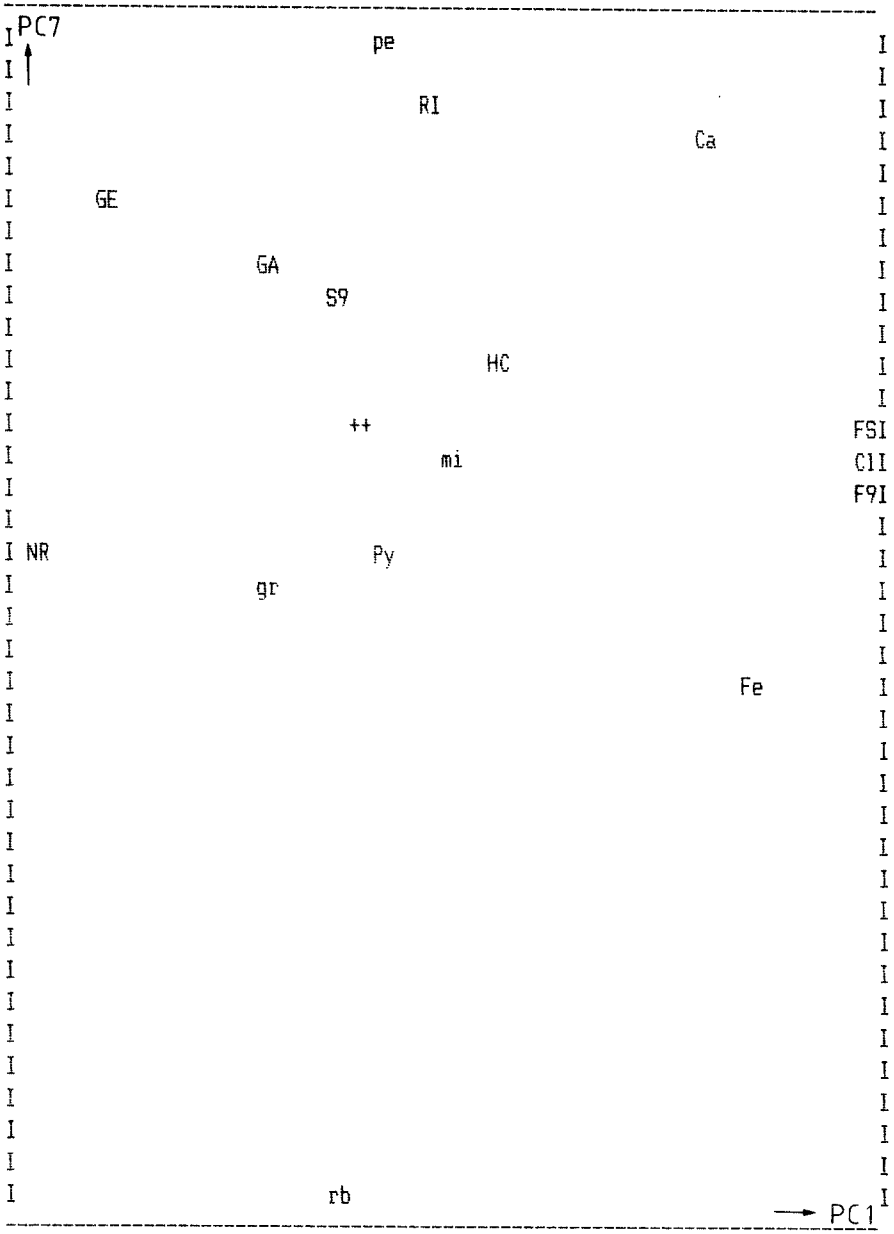

Fig C.37 Variable plots of principal components from PC-analysis of data from Saltsjötunnel.

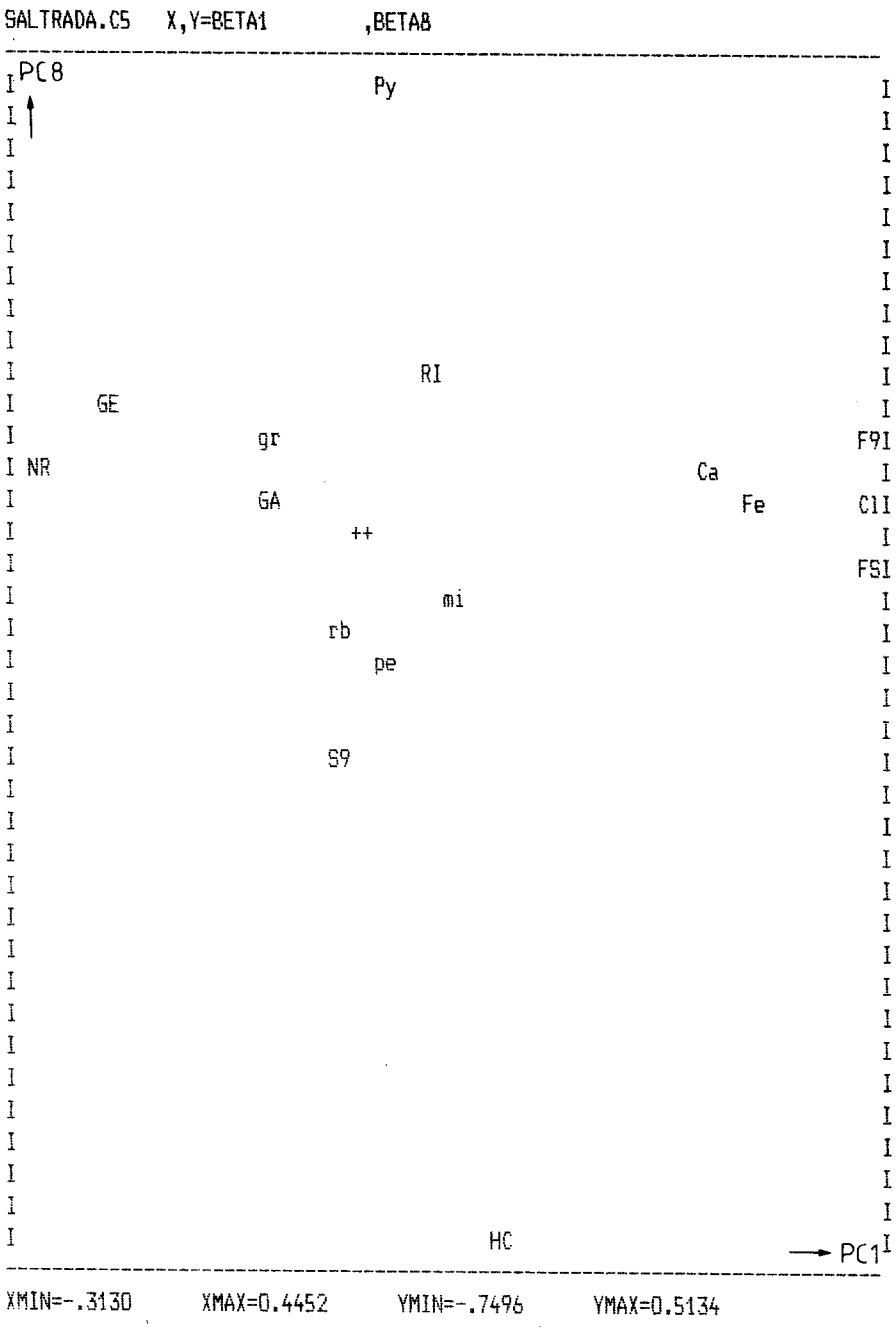

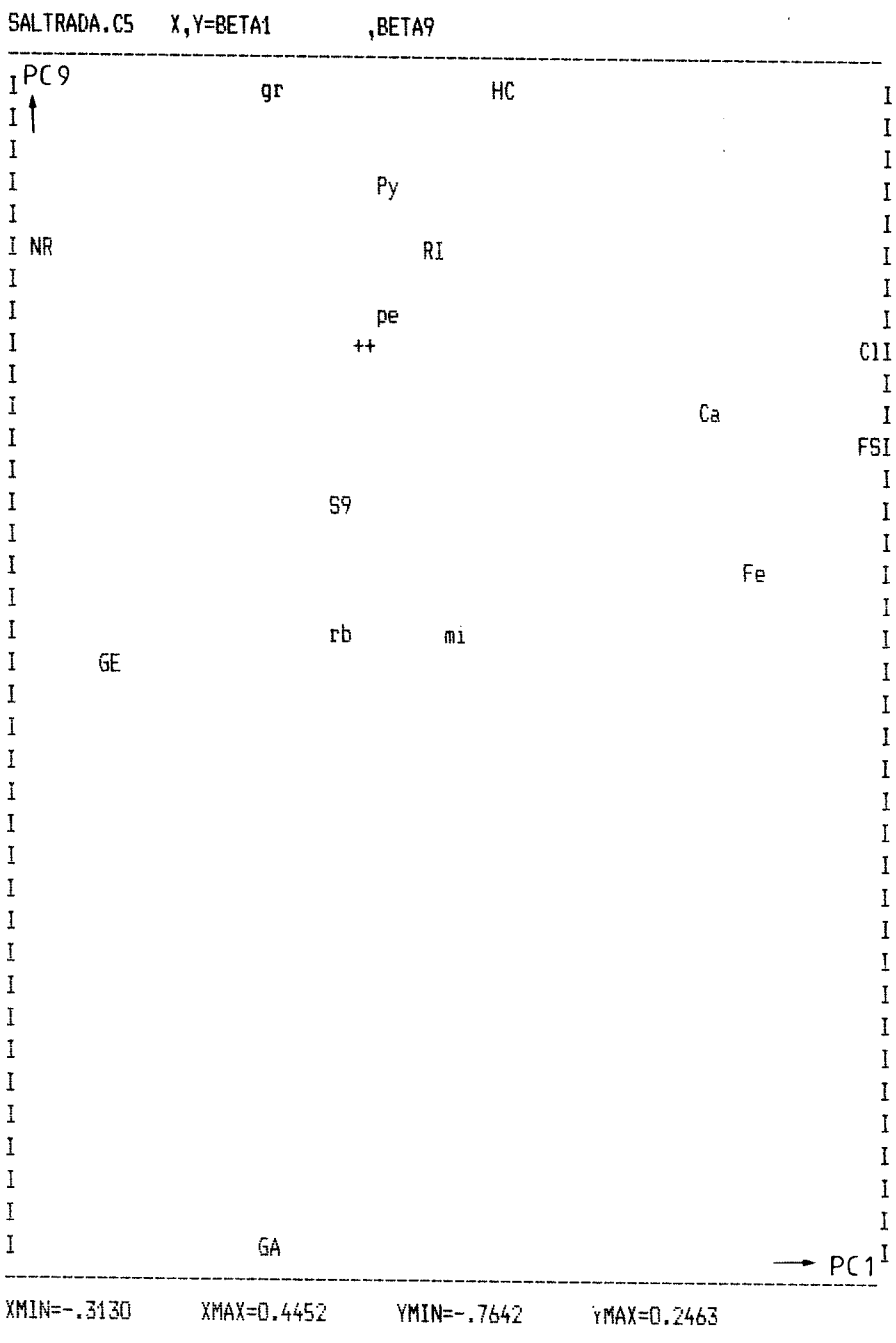

Fig C.38 Variable plots of principal components from PC-analysis of data from Saltsjötunnel.

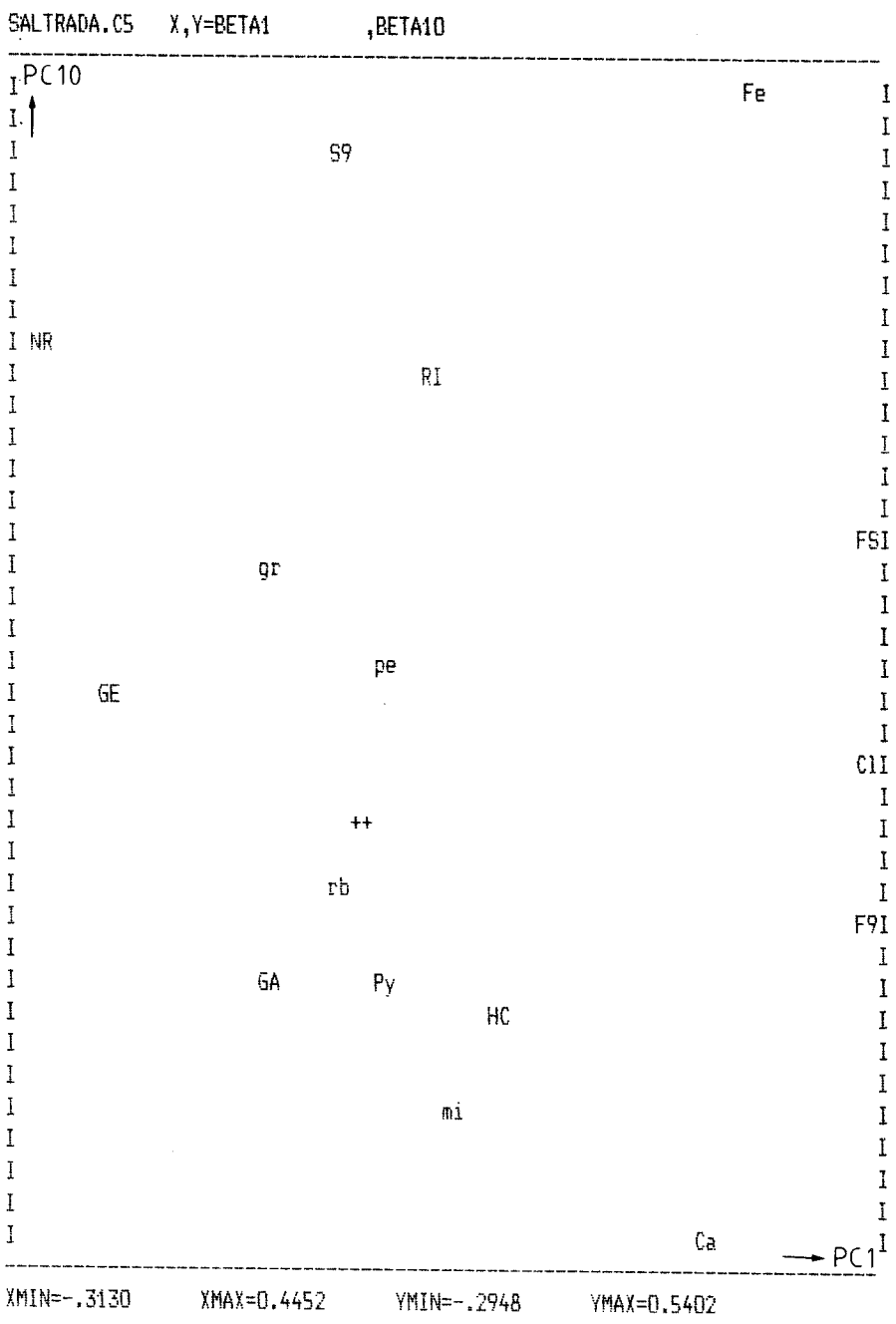

Fig C.39 Variable plots of principal components from PC-analysis of data from Saltsjötunnel.

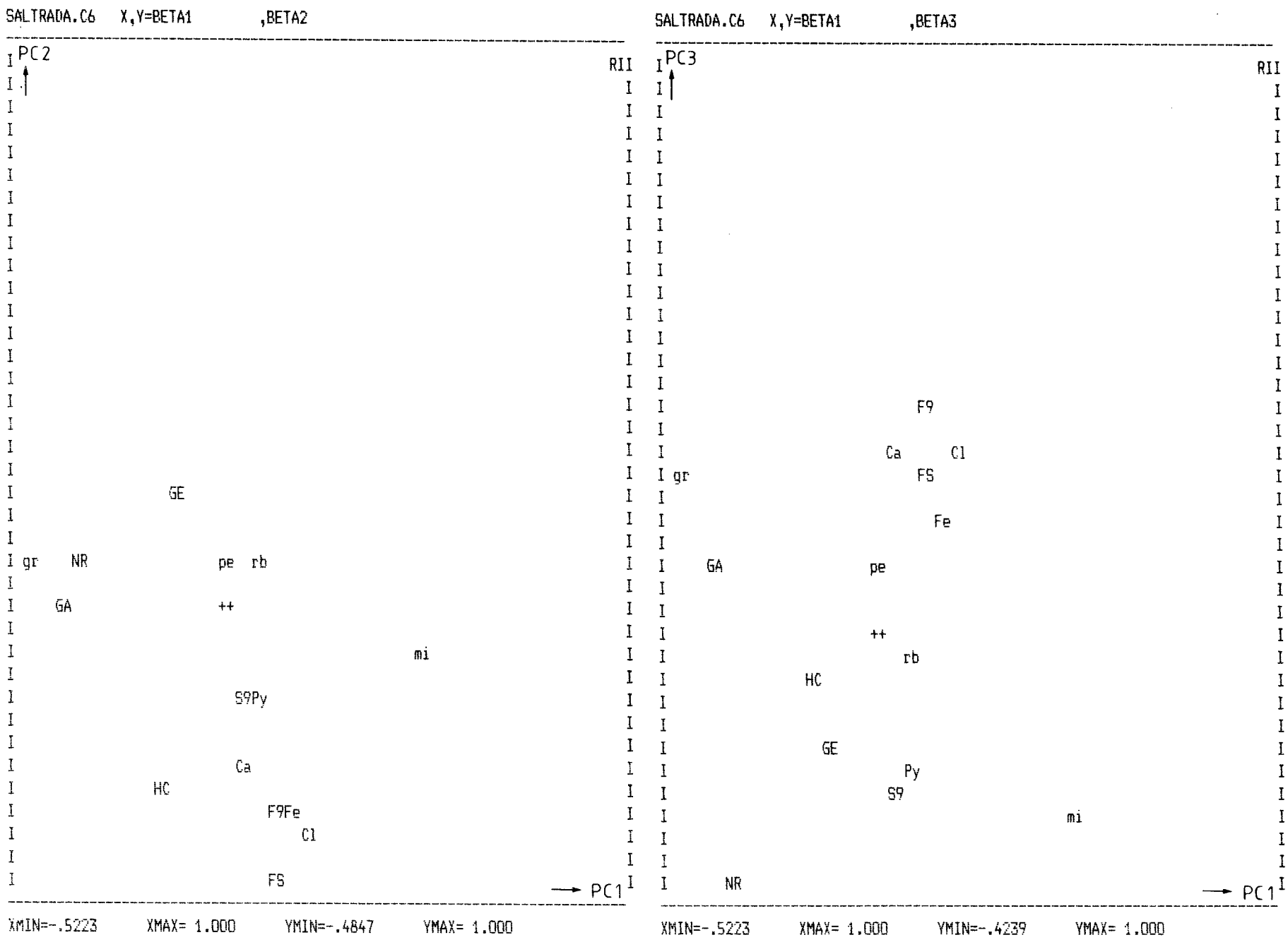

Fig C.40 Variable plots of the principal components from the PLS investigation of data from Saltsjötunnel.

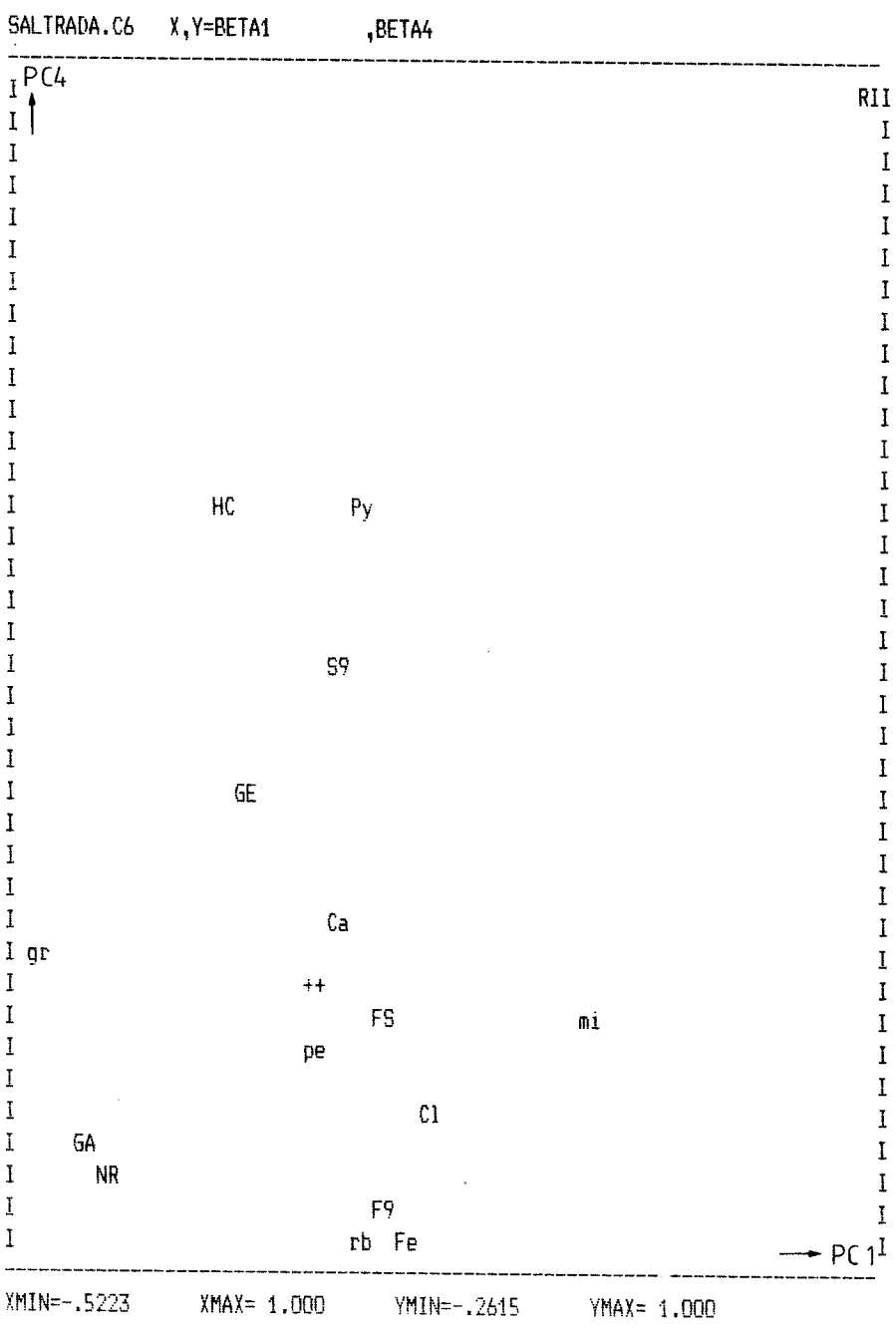

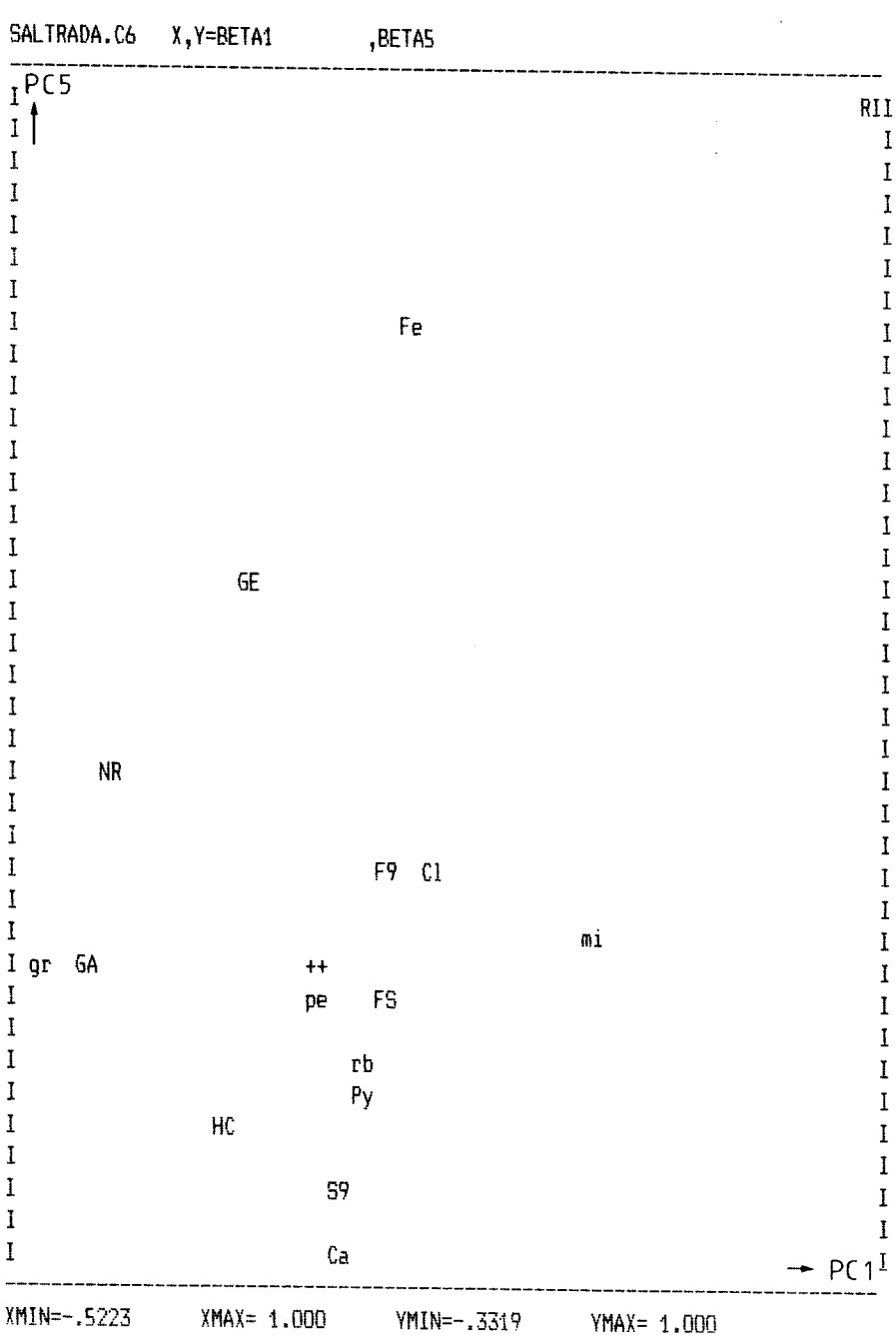

Fig C.41 Variable plots of the principal components from the PLS investigation of data from Saltsjötunnel.

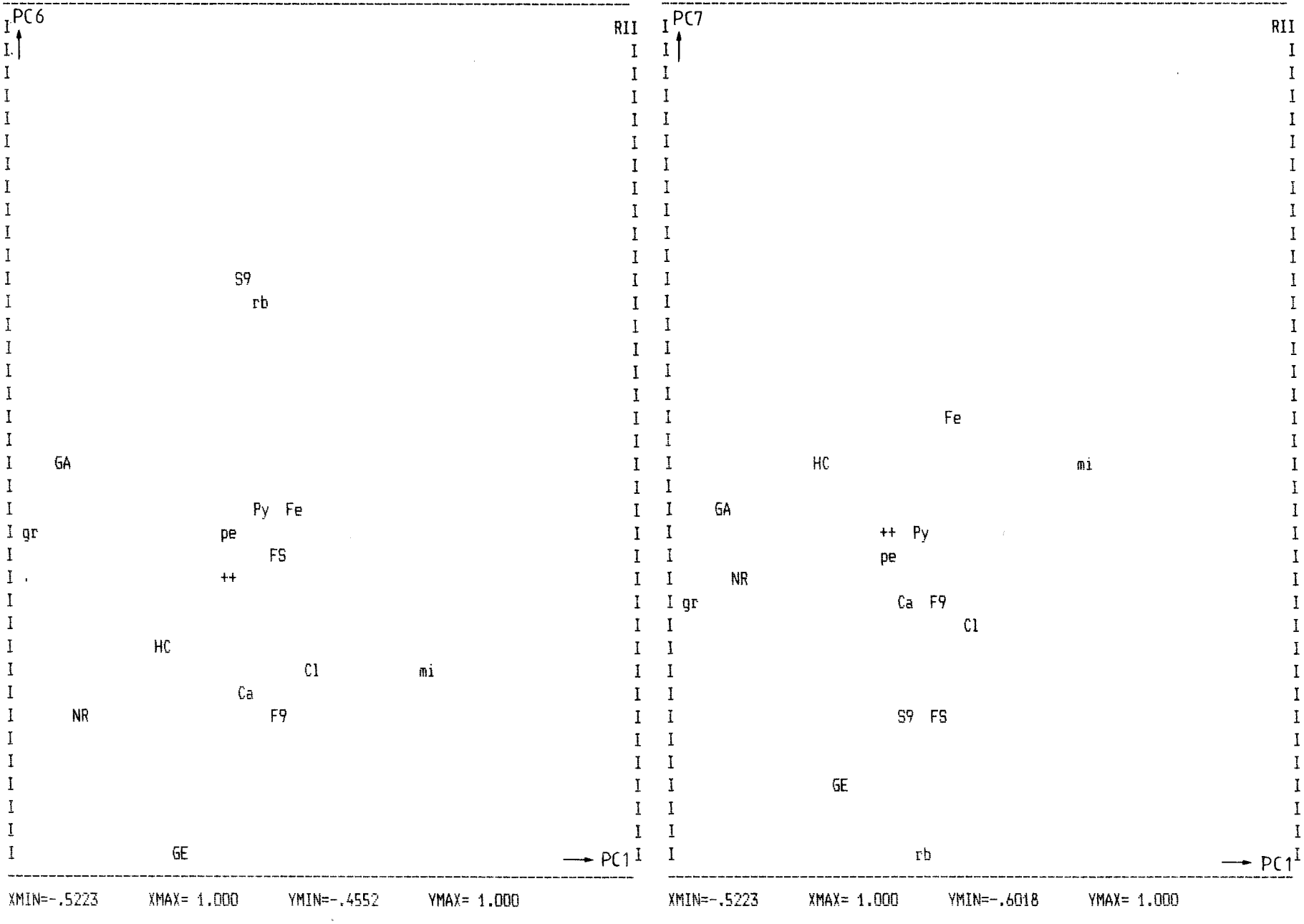

Fig C.42 Variable plots of the principal components from the PLS investigation of data from Saltsjötunnel.

Fig C.43 Variable plots of the principal components from the PLS investigation of data from Saltsjötunnel.

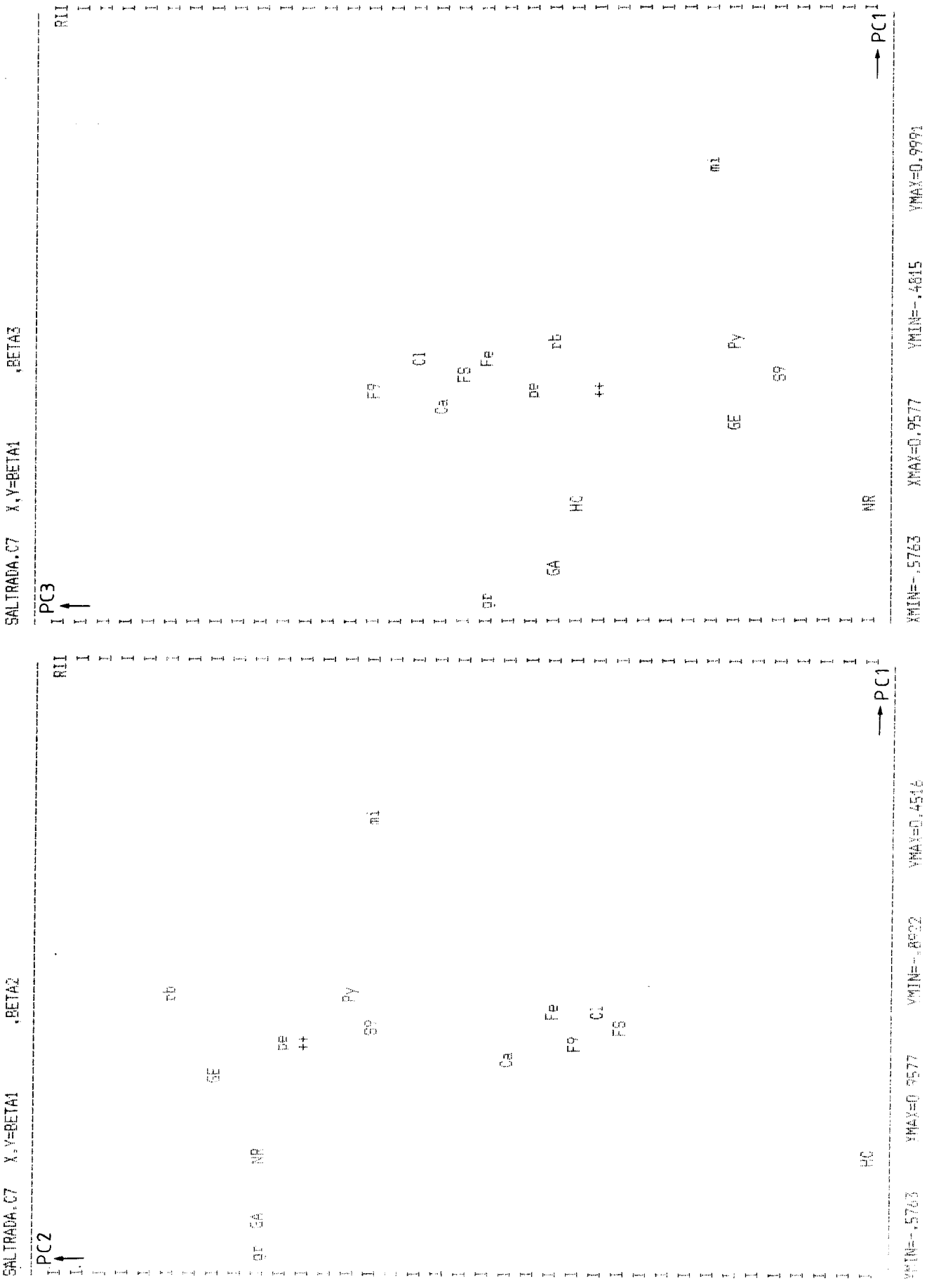

Fig C.44 Variable plot of the principal components from the PLS2 investigation of data from Saltsjötunnel.

Fig C.45 Variable plot of the principal components from the PLS2 investigation of data from Saltsjötunnel.

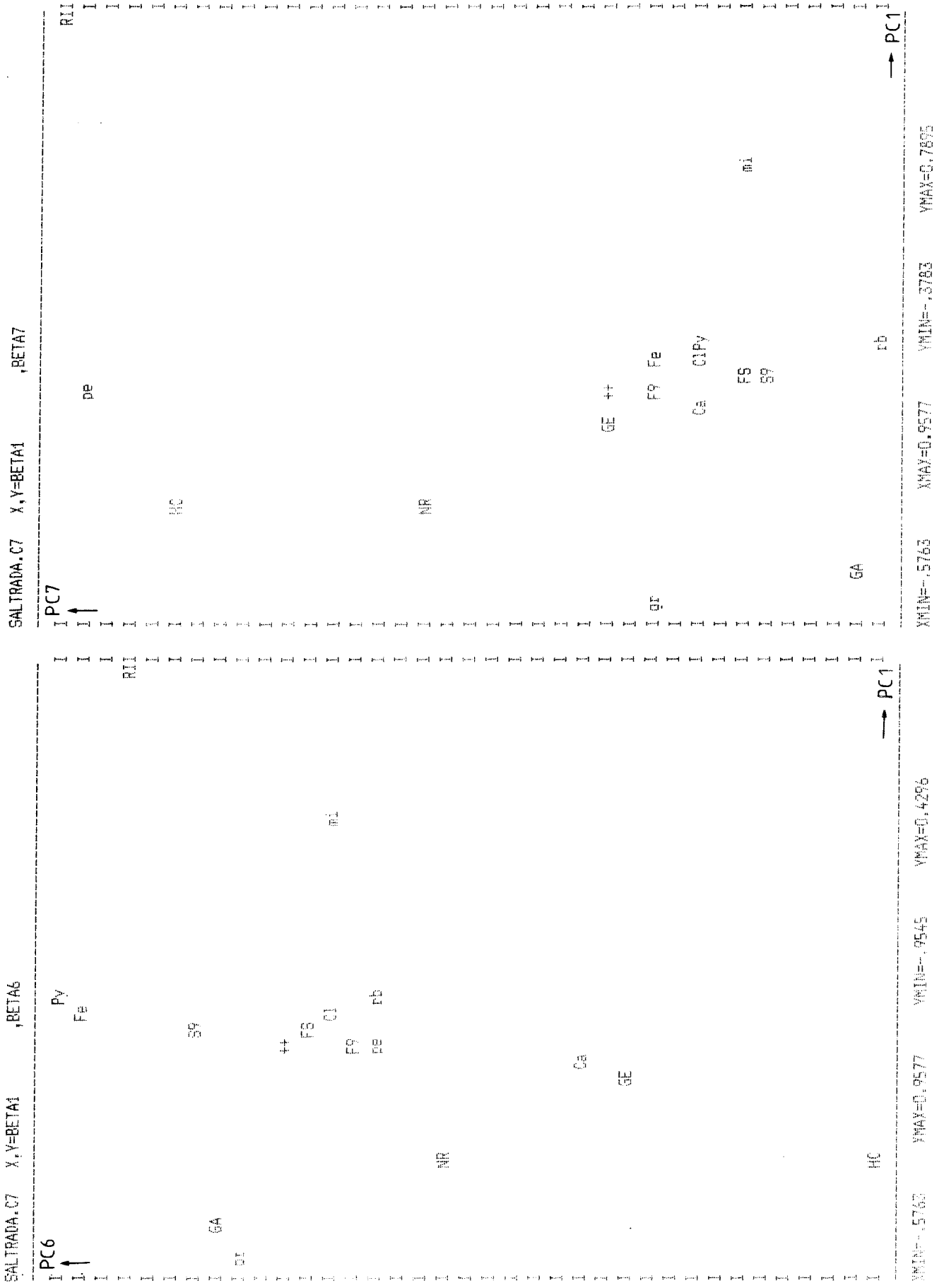

Fig C.46 Variable plot of the principal components from the PLS2 investigation of data from Saltsjötunnel.

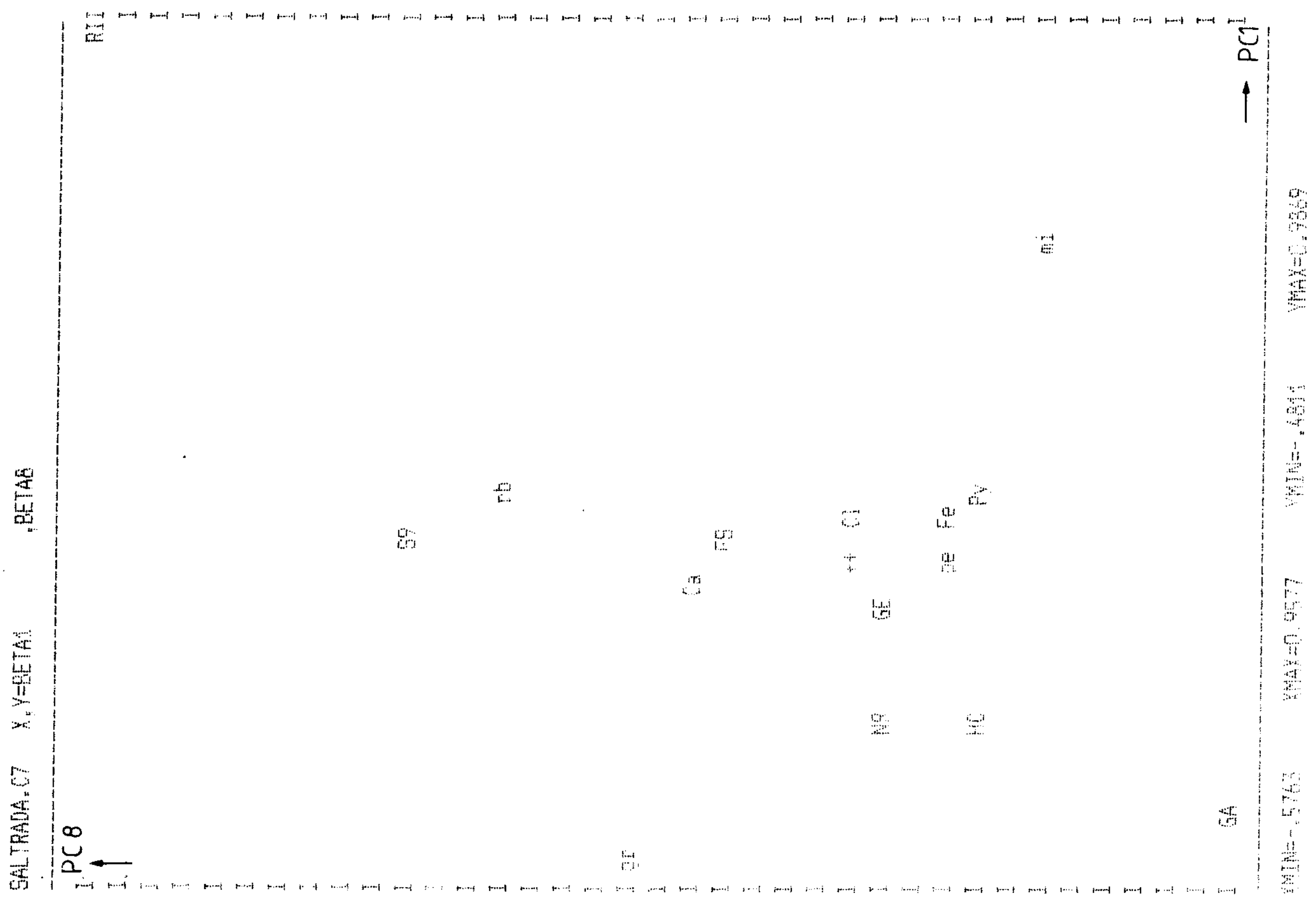

Fig C.47 Variable plot of the principal components from the PLS2 investigation of data from Saltsjötunnel.

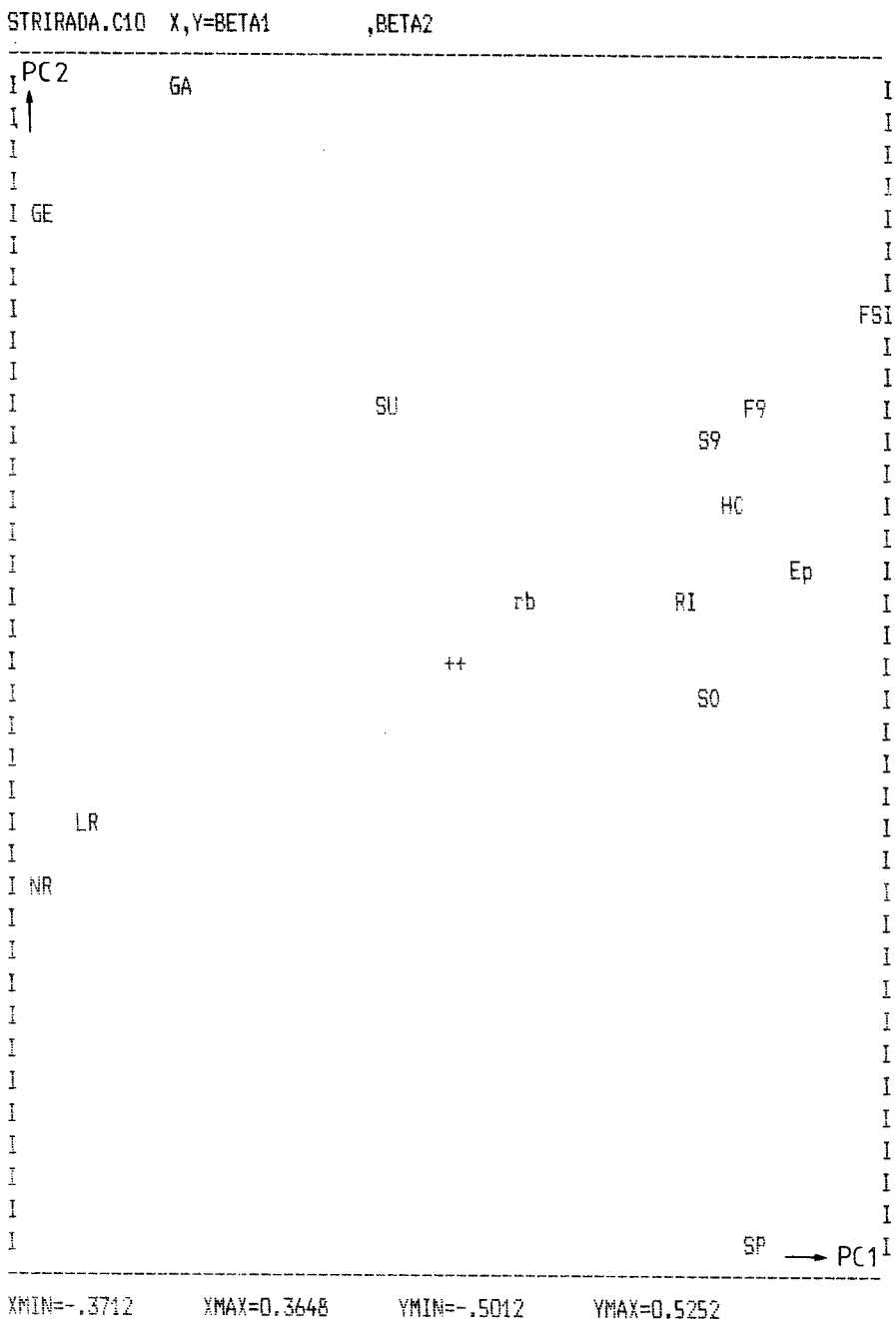

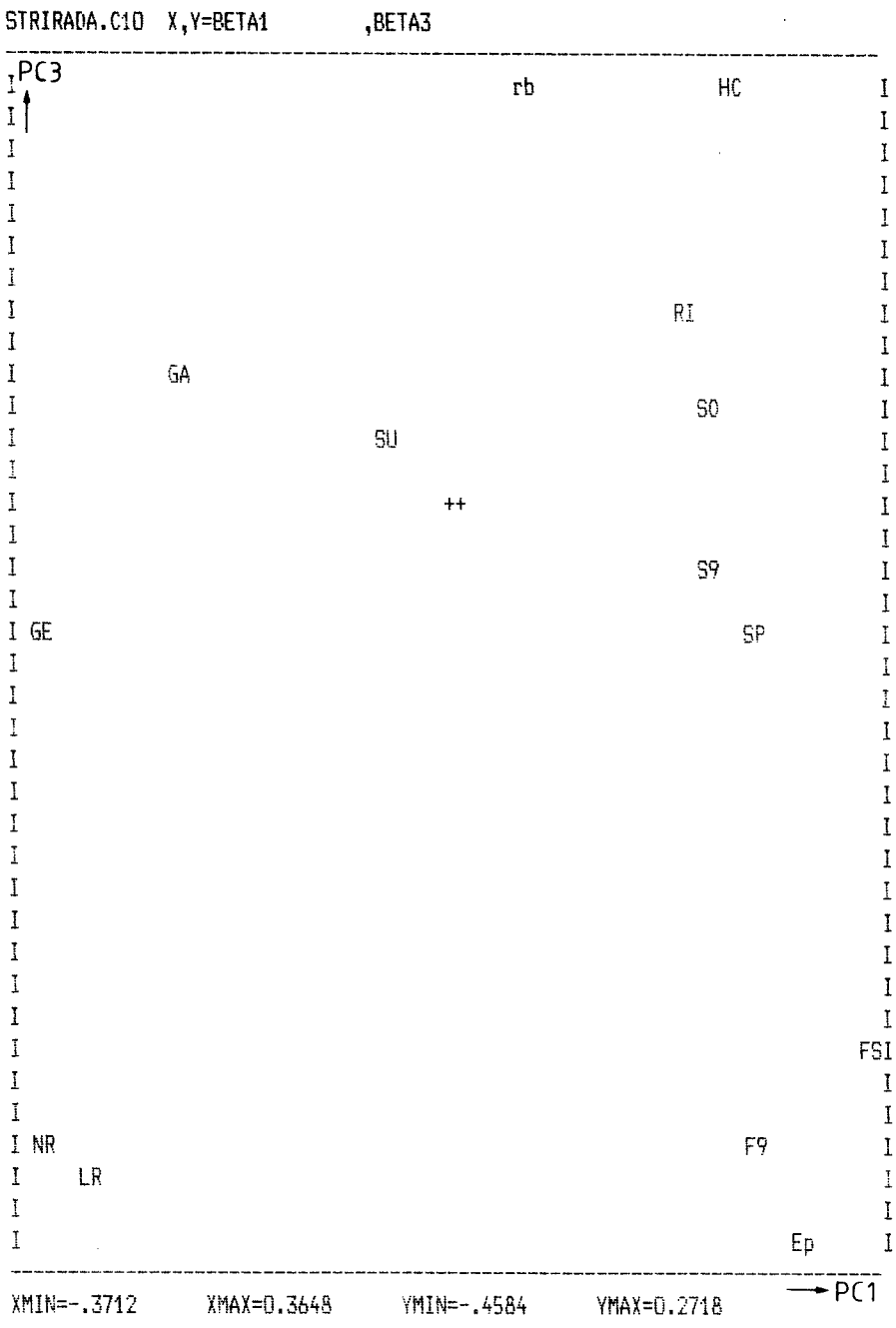

Fig C.48 Variable plots of principal components from PC-analysis of data from Stripa.

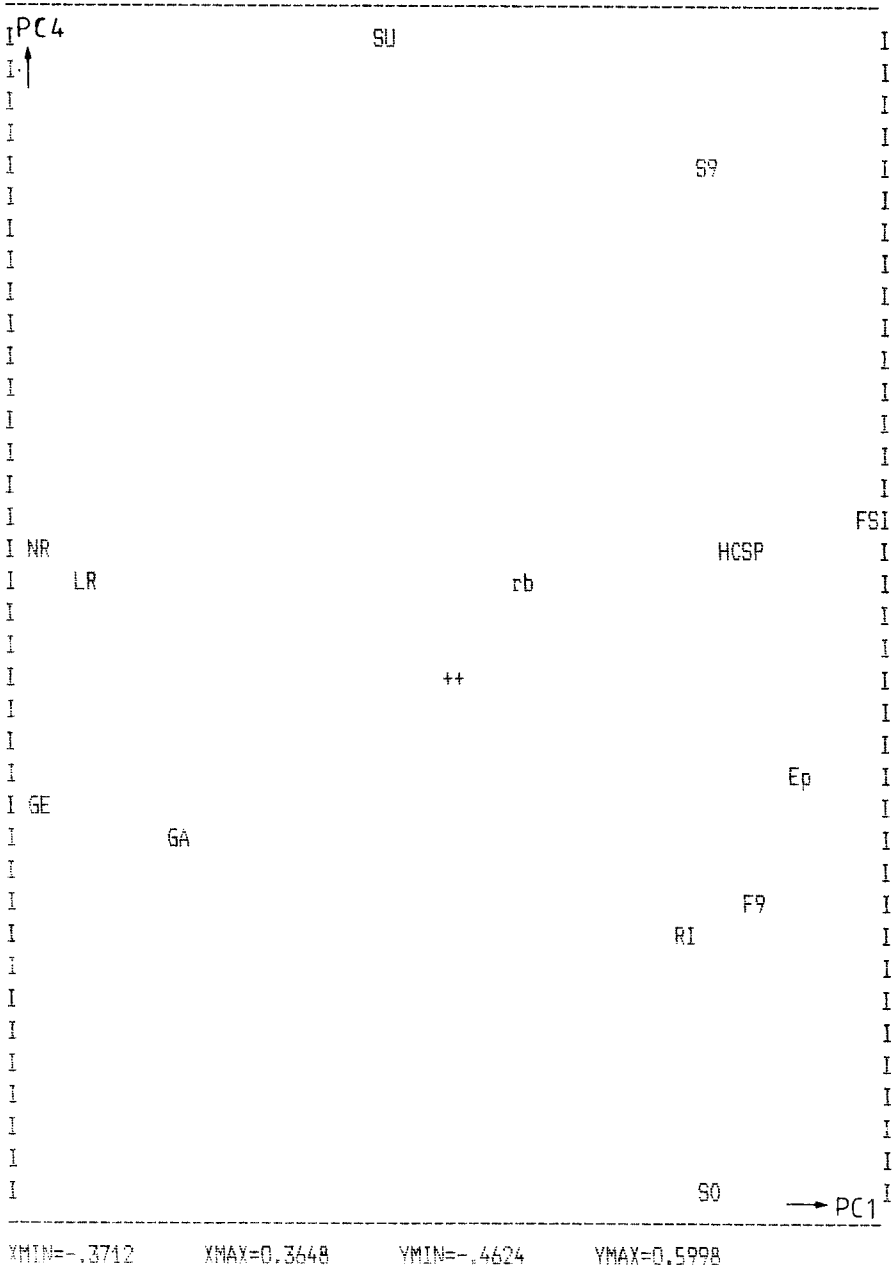

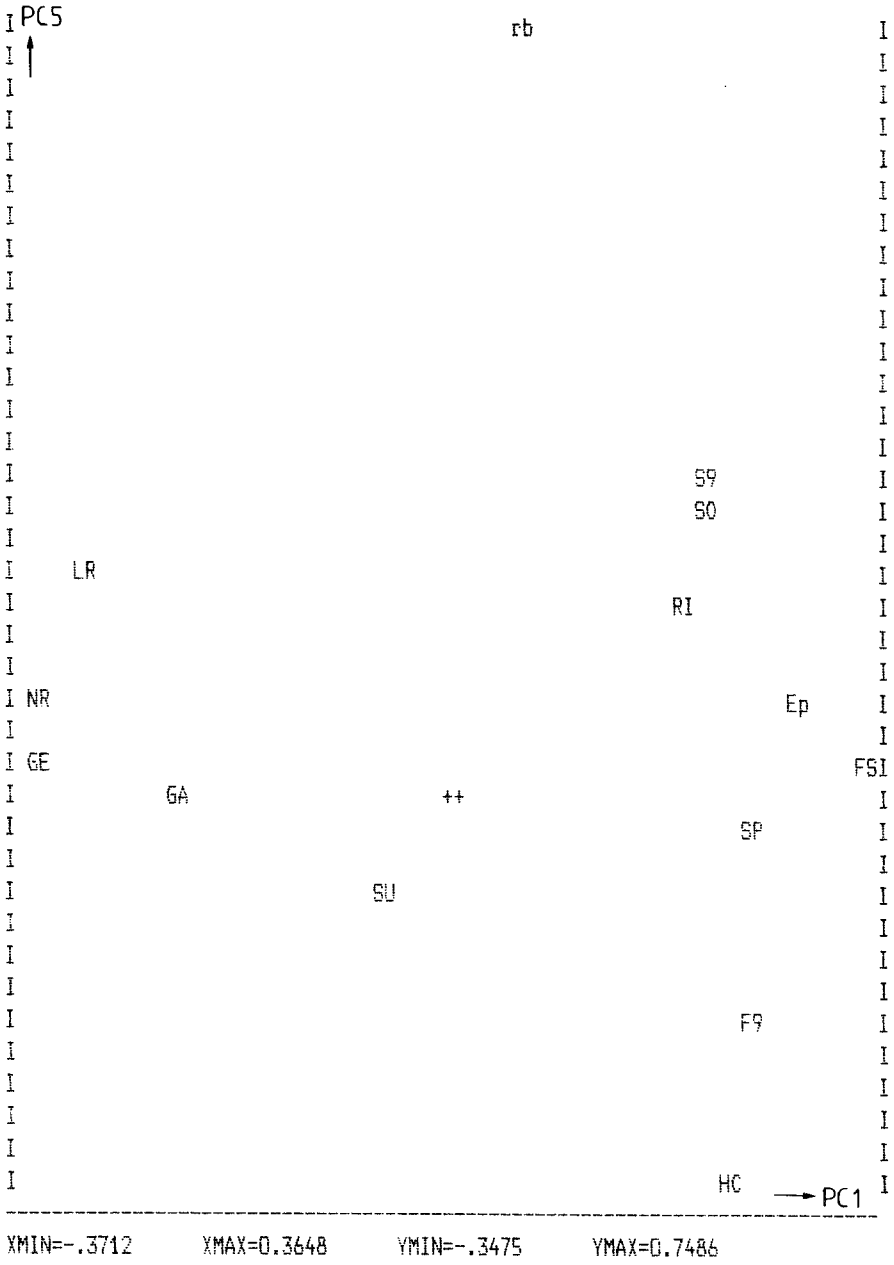

Fig C.49 Variable plots of principal components from PC-analysis of data from Stripa.

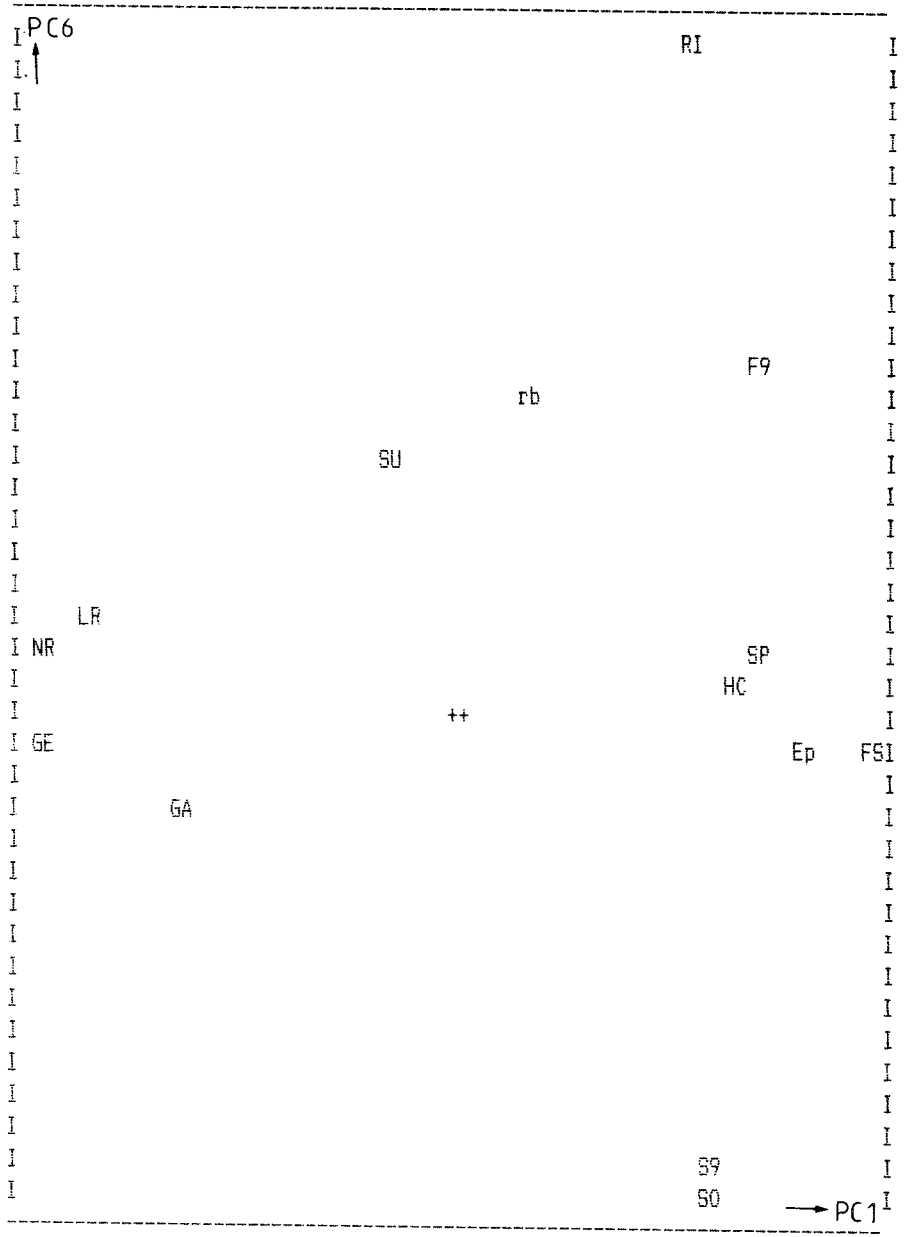

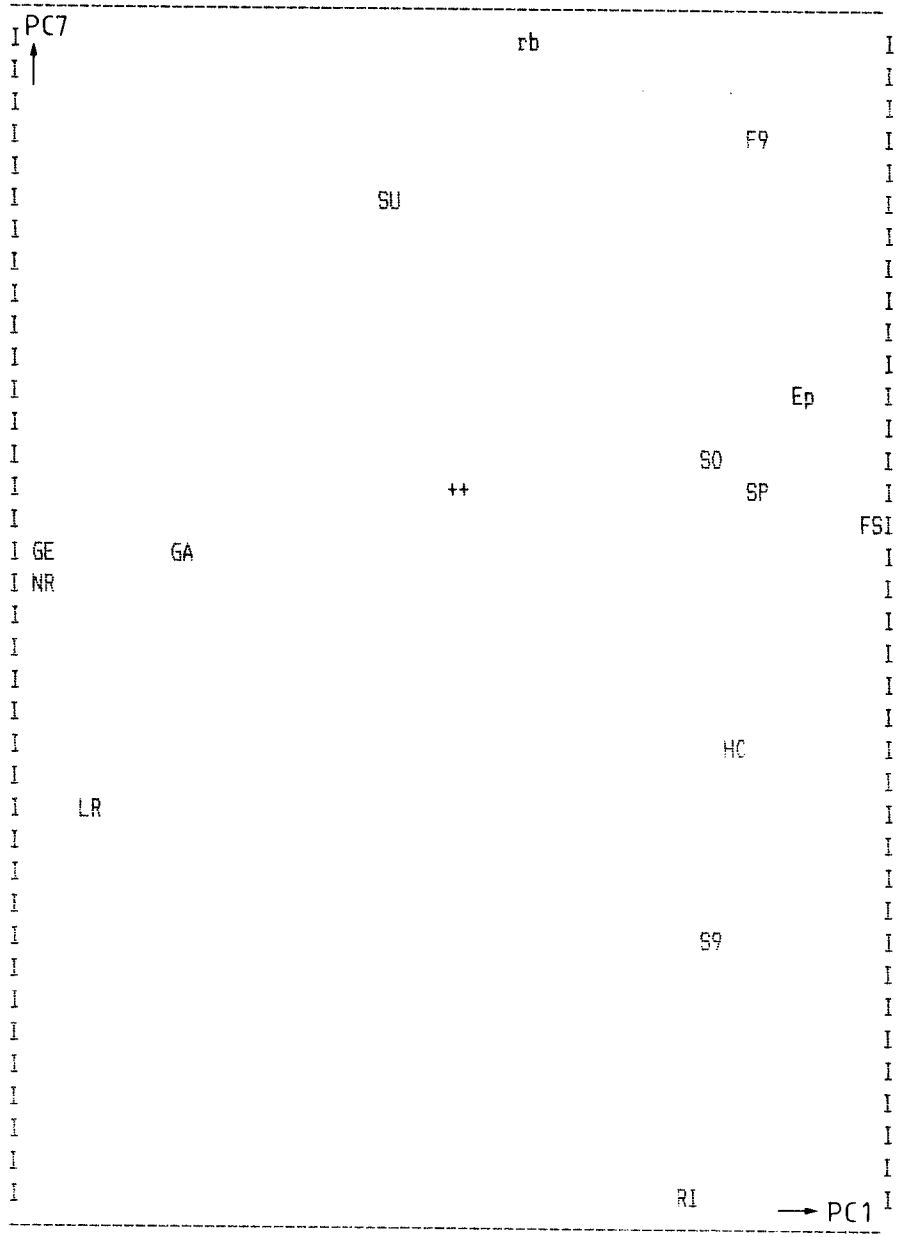

Fig C.50 Variable plots of principal components from PC-analysis of data from Stripa.

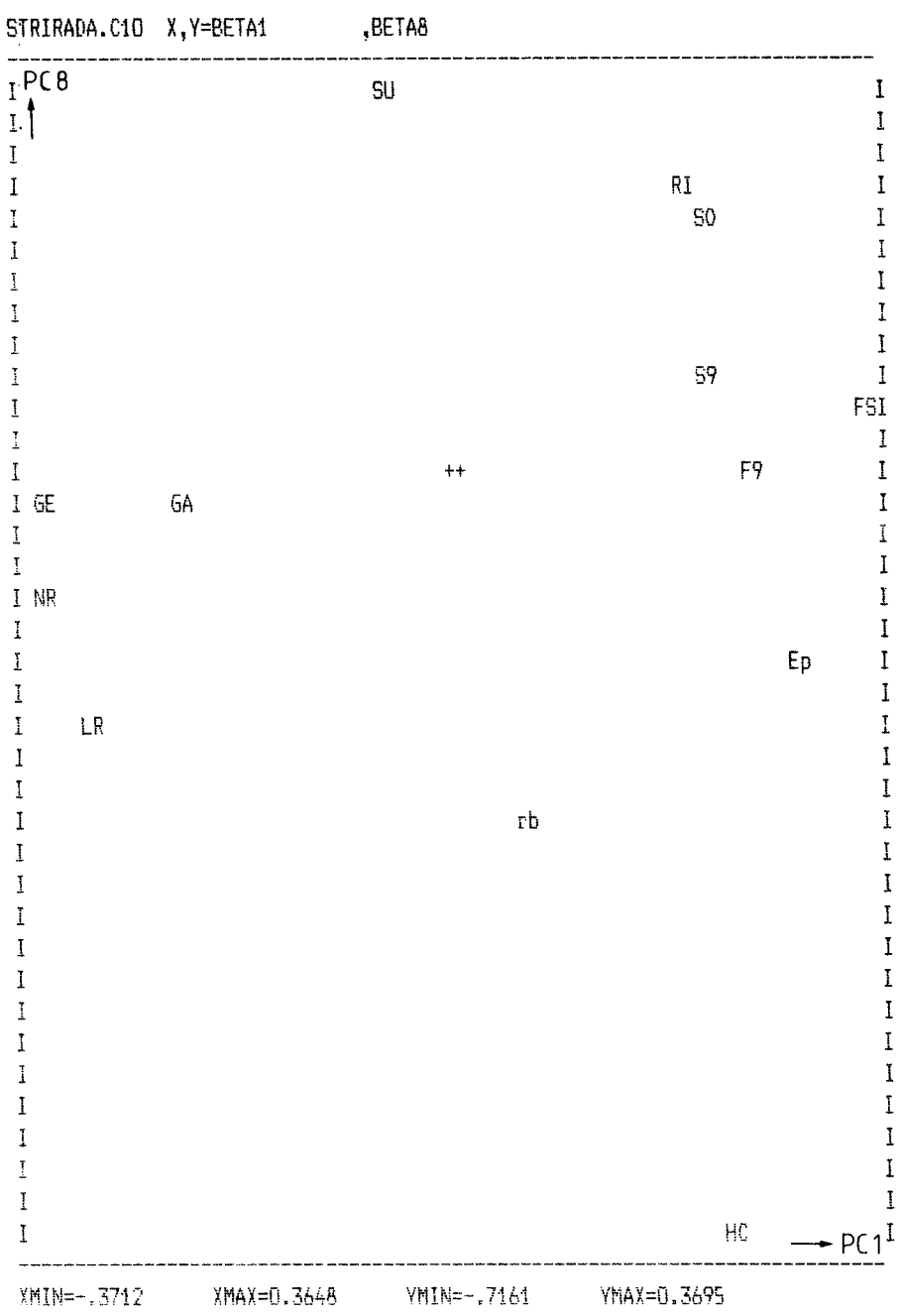

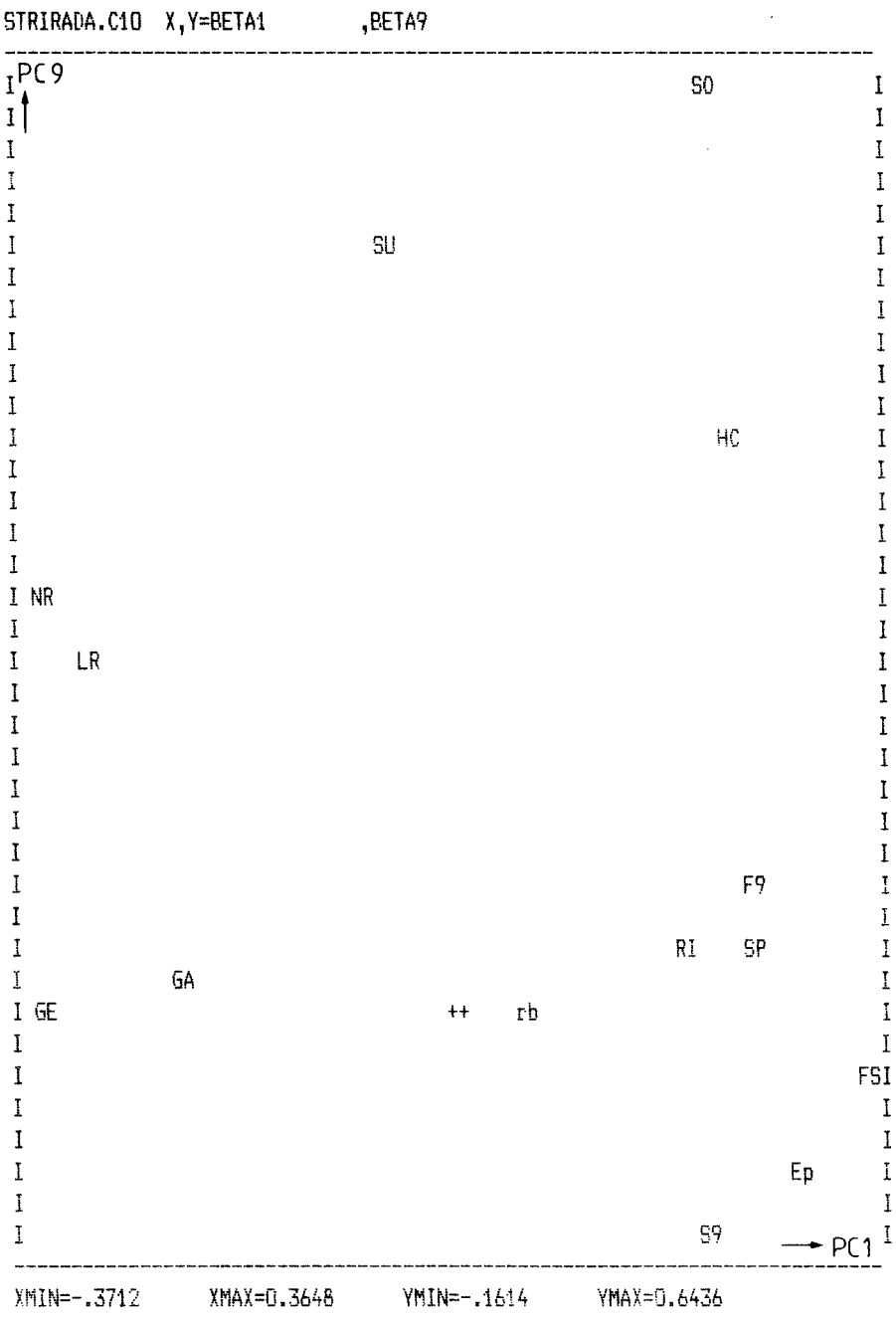

Fig C.51 Variable plots of principal components from PC-analysis of data from Stripa.

Fig C.52 Variable plots of principal components from PC-analysis of data from Stripa.

Fig C.53 Variable plots of the principal components from the PLS investigation of data from Stripa.

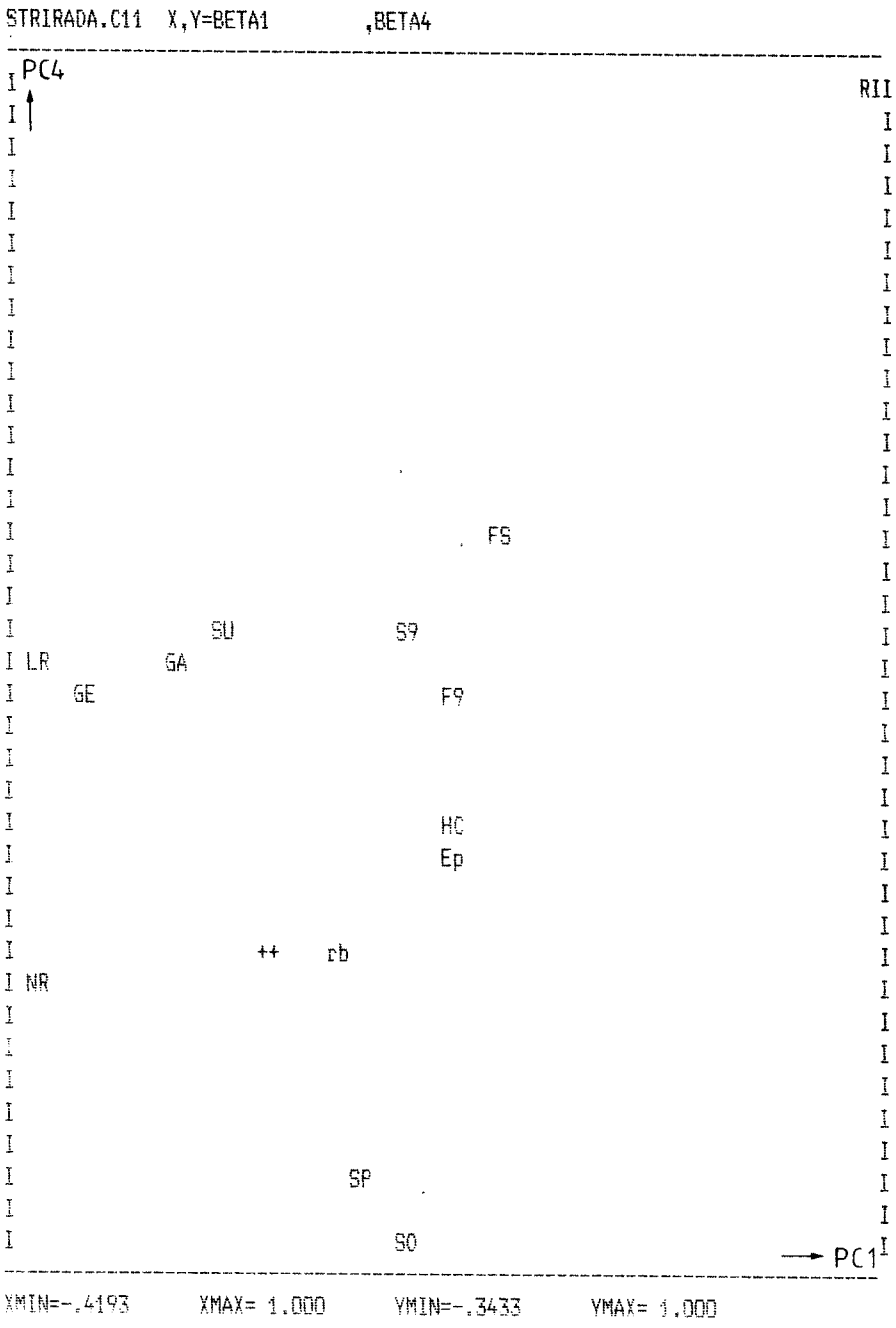

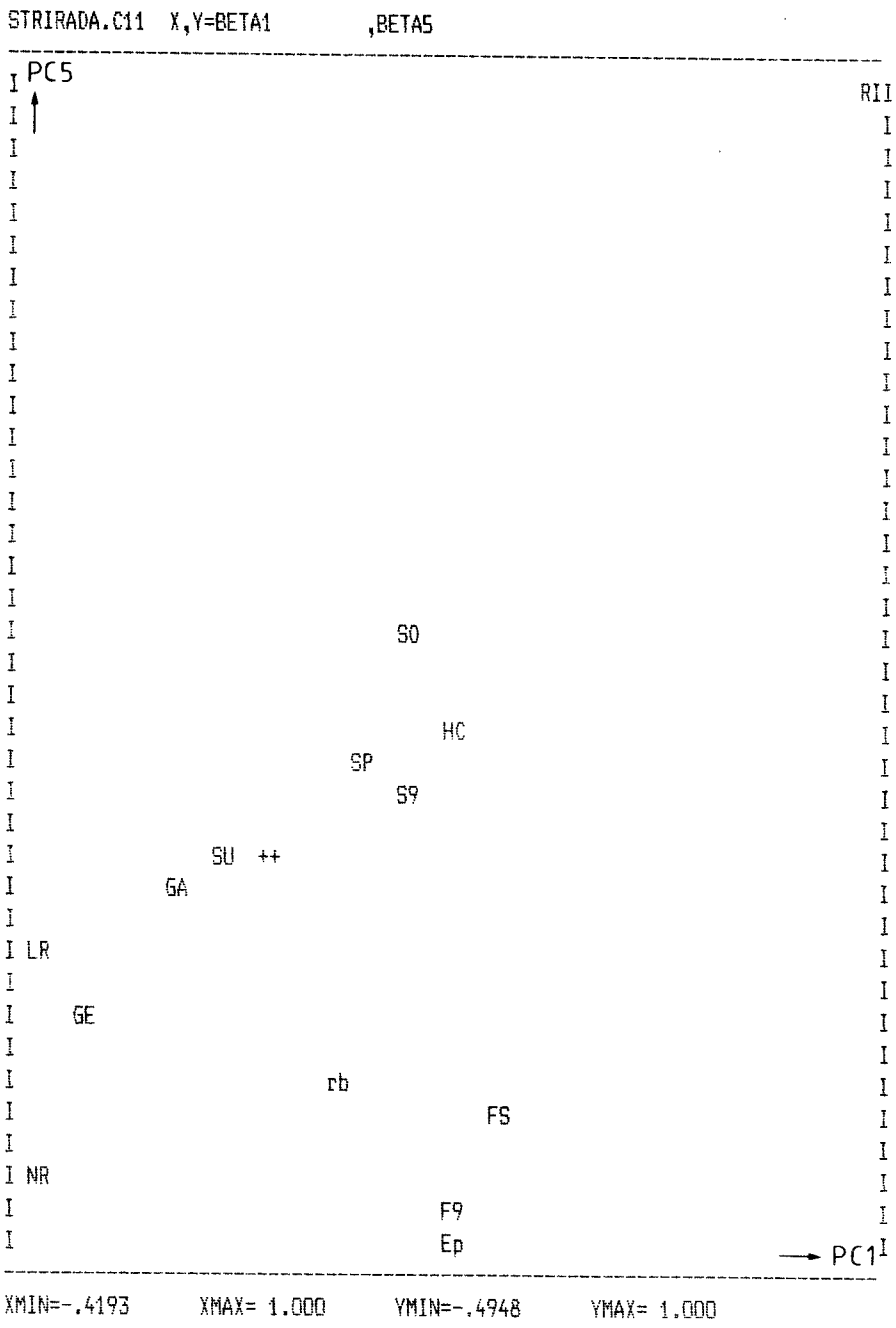

Fig C.54 Variable plots of the principal components from the PLS investigation of data from Stripa.

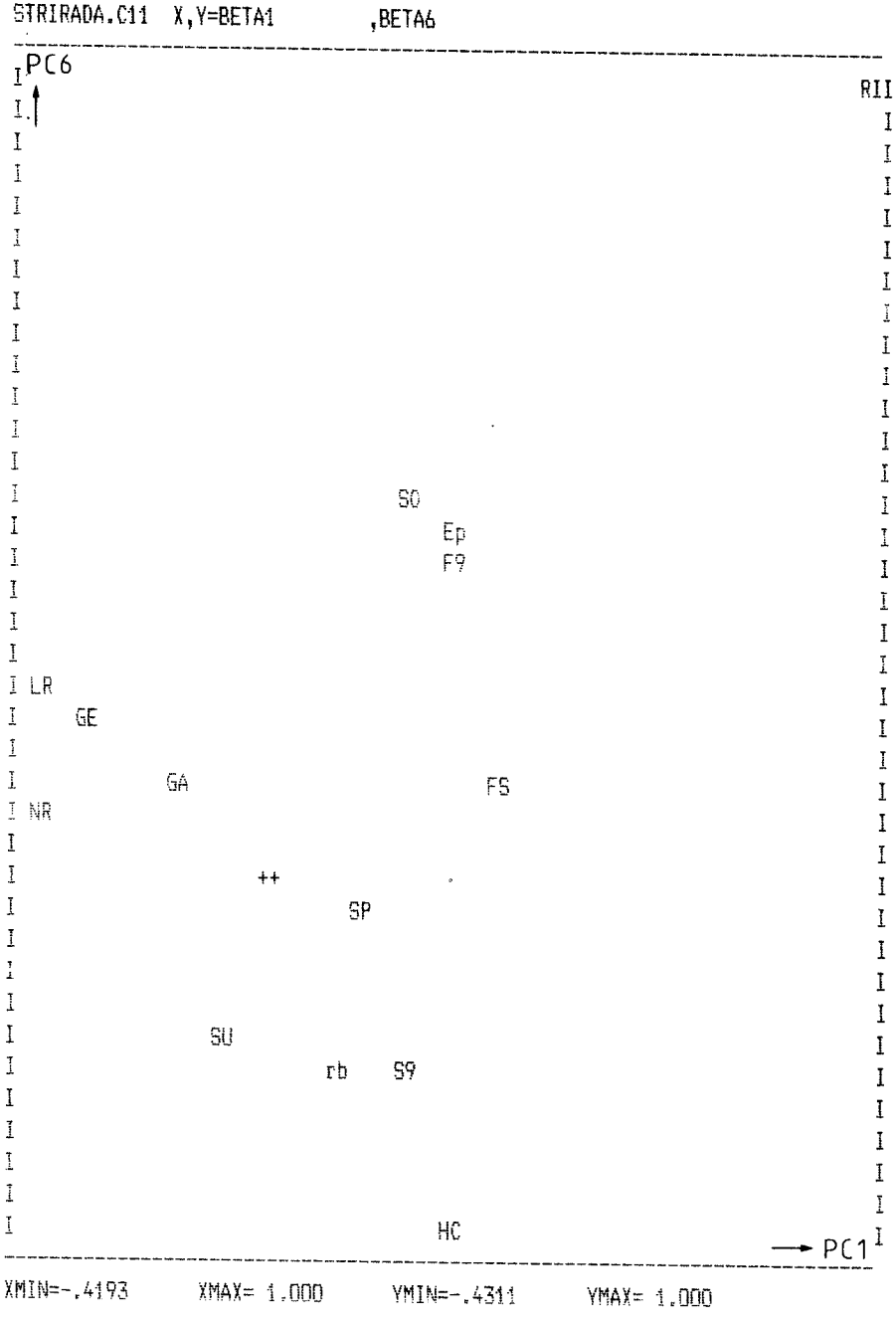

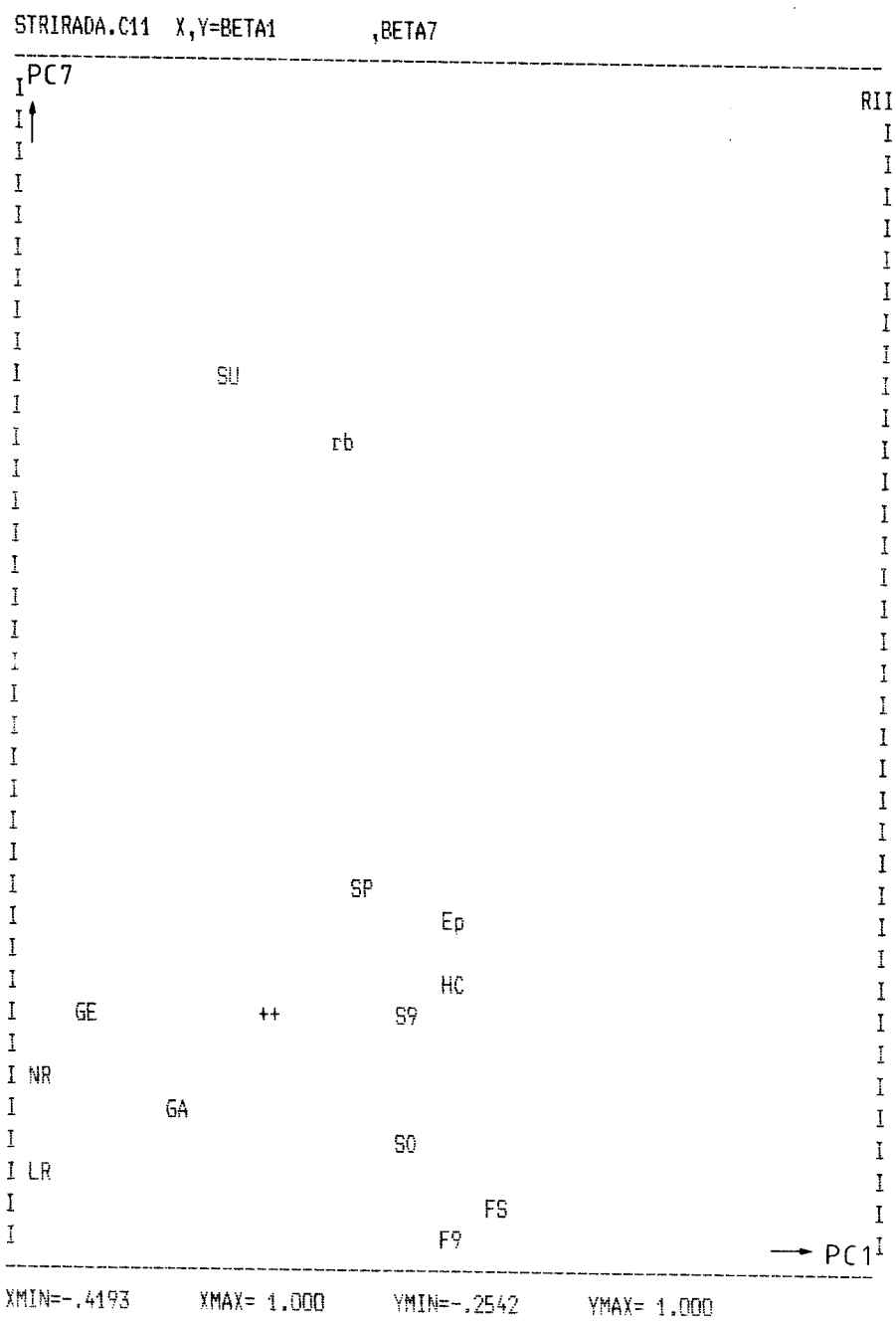

Fig C.55 Variable plots of the principal components from the PLS investigation of data from Stripa.

Fig C.56 Variable plots of the principal components from the PLS investigation of data from Stripa.

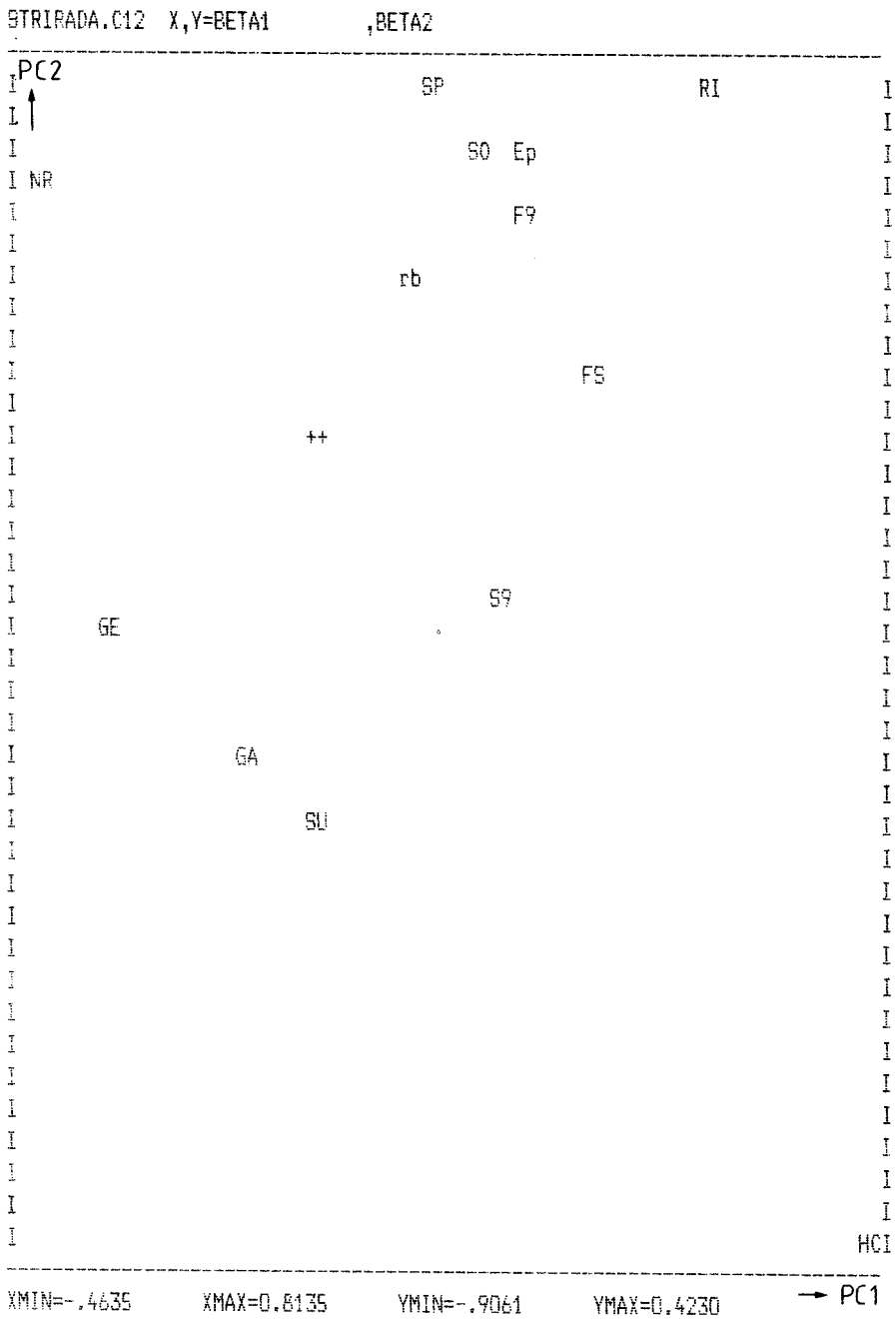

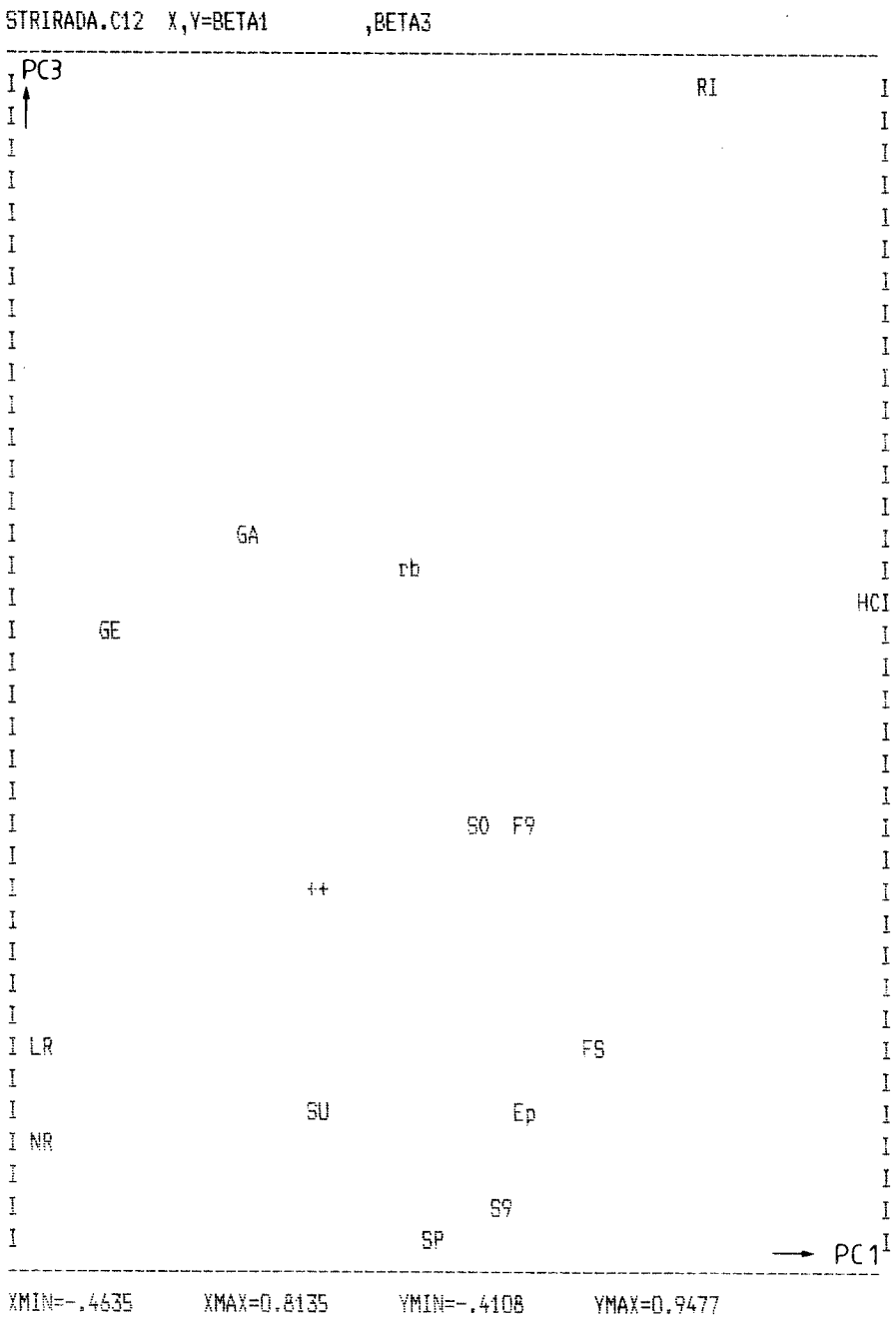

Fig C.57 Variable plot of the principal components from the PLS2 investigation of data from Stripa.

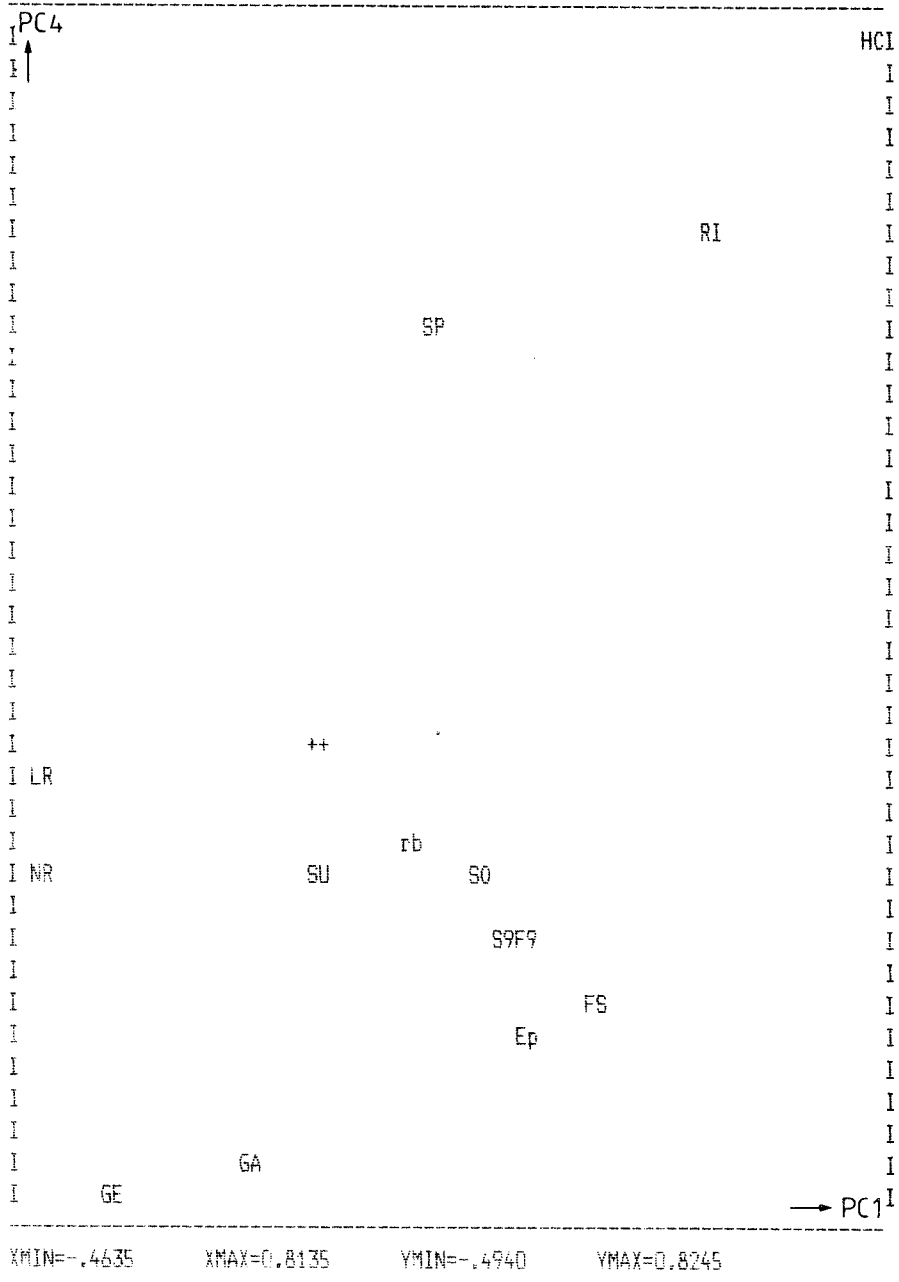

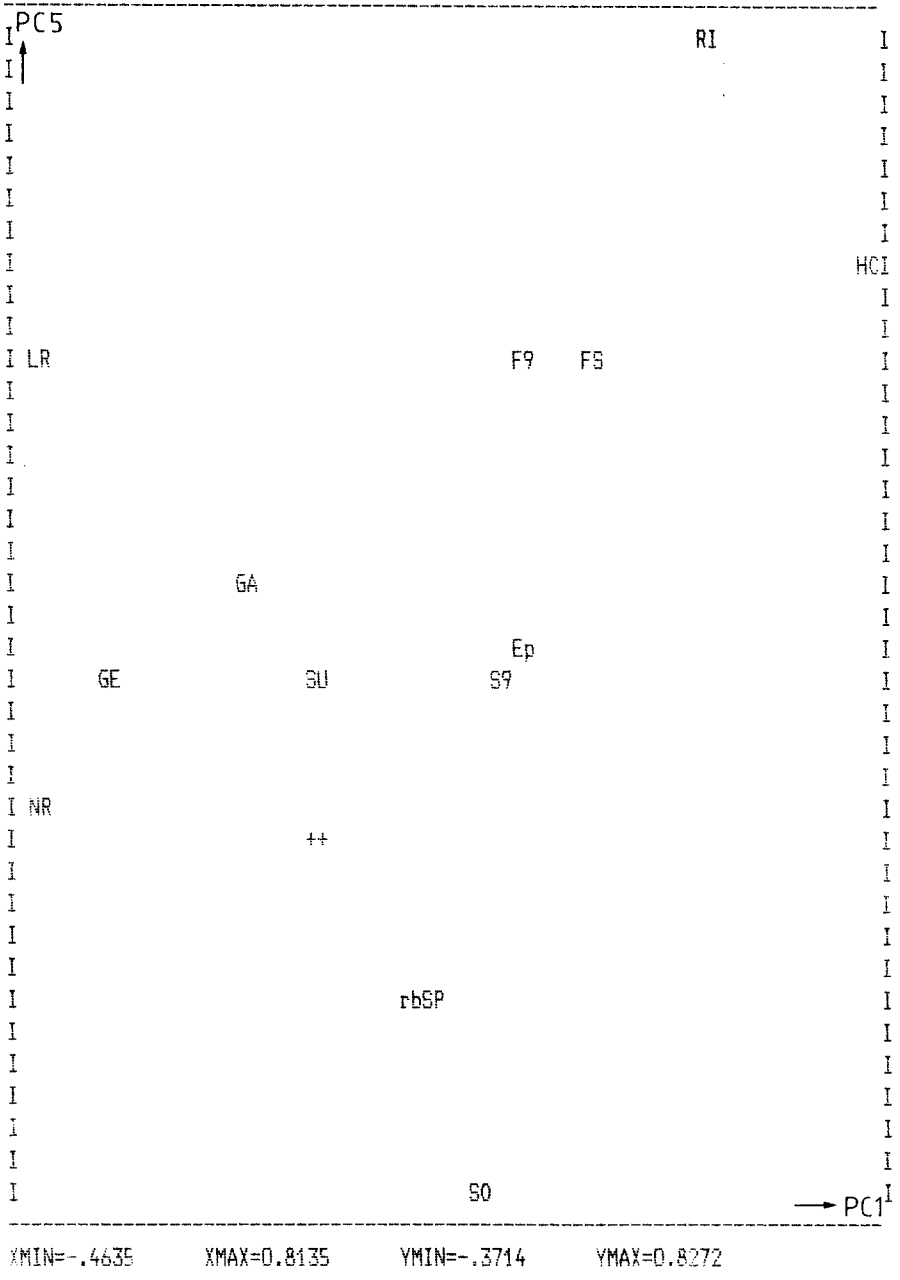

- 19 C.58 Variable plot of the principal components from the PLS2 investigation of data from Stripa.

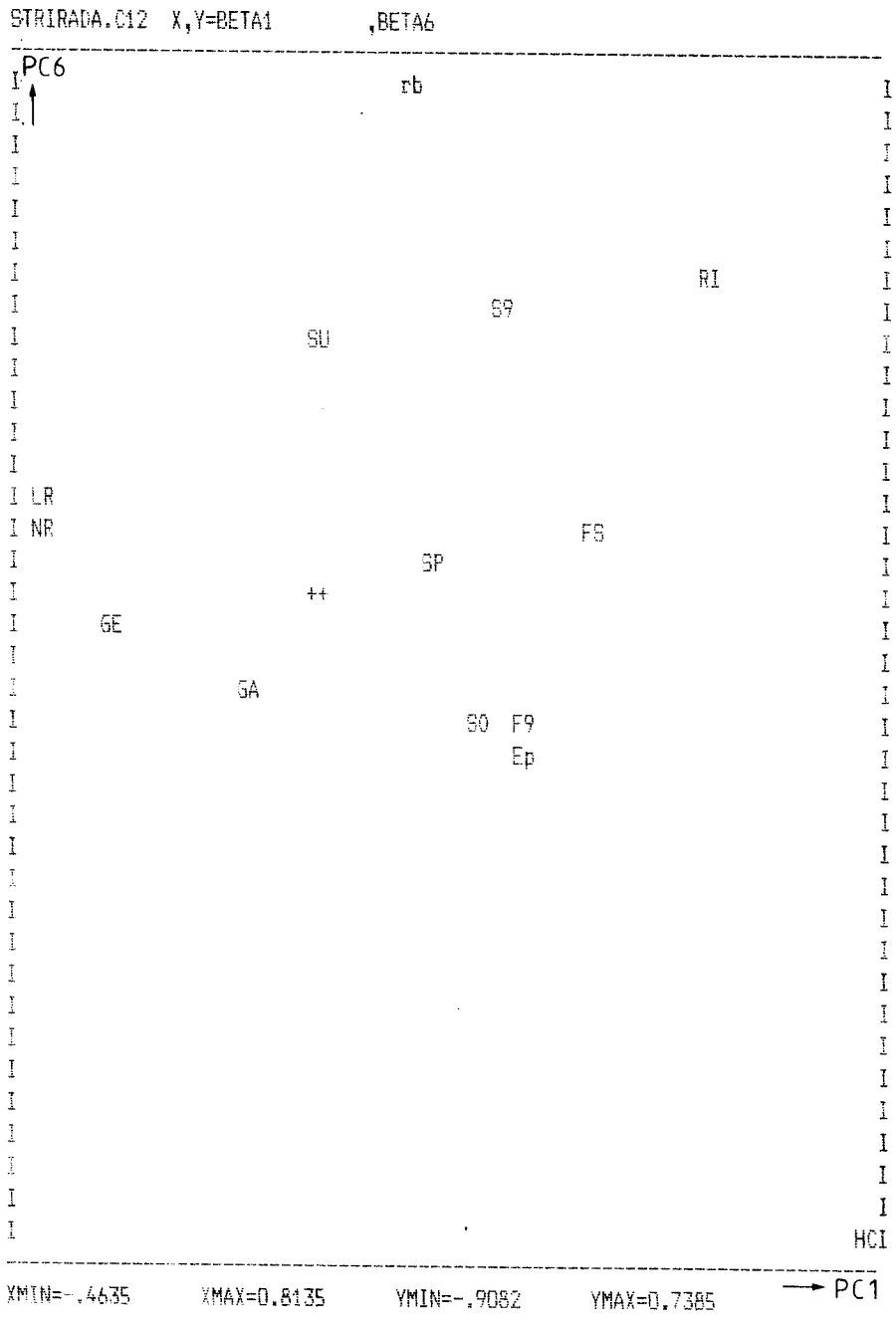

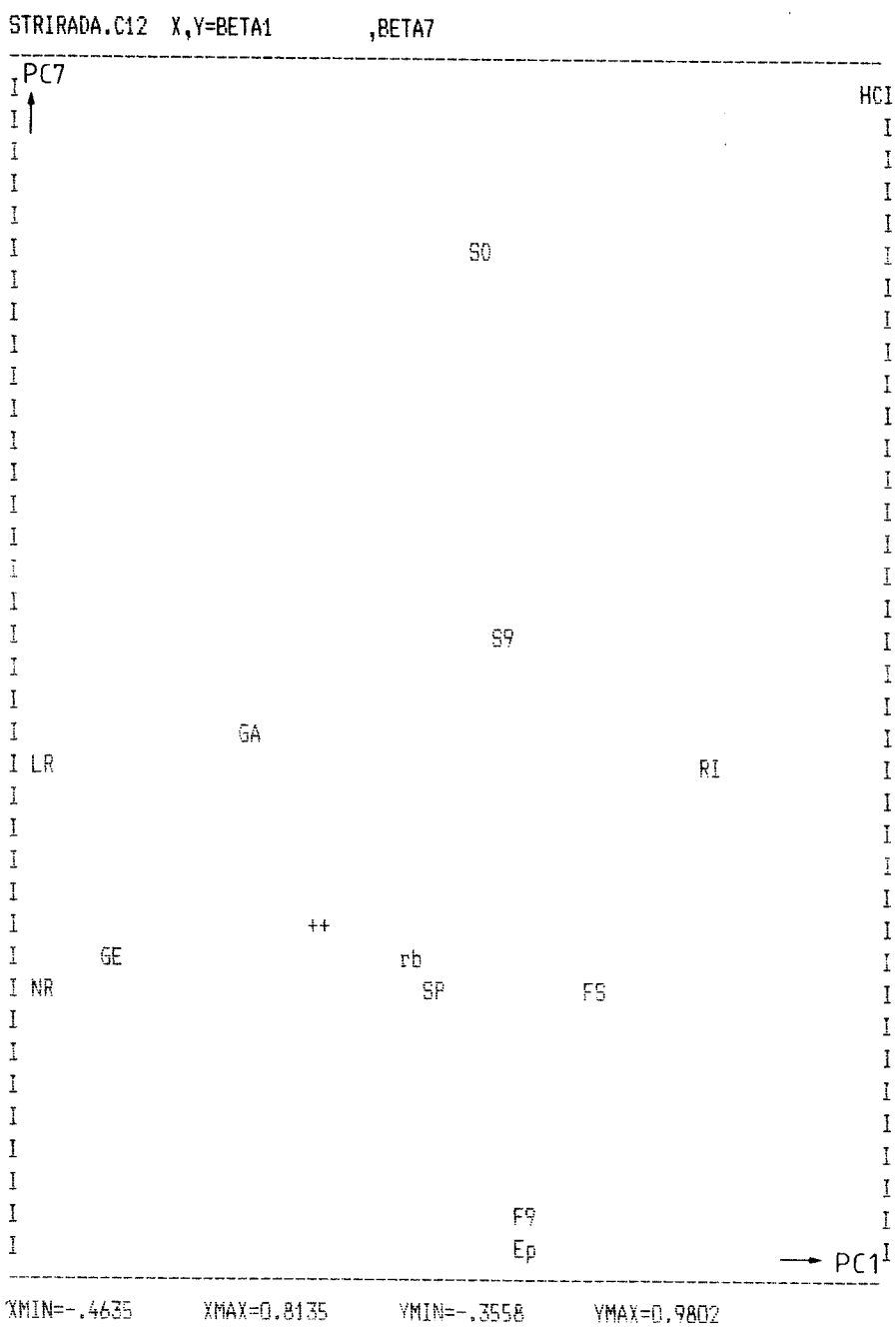

Fig C.59 Variable plot of the principal components from the PLS2 investigation of data from Stripa.

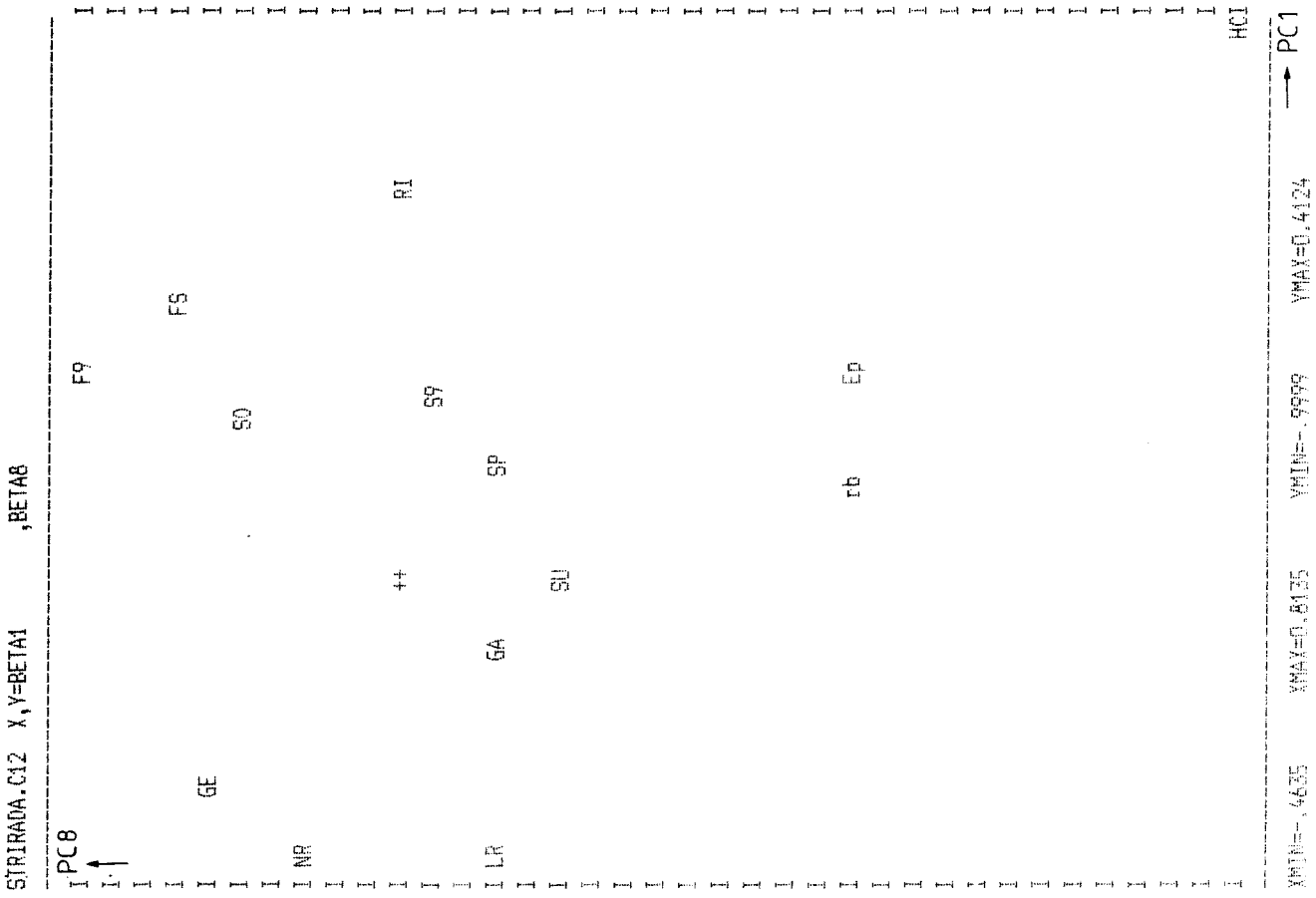

Fig C.60 Variable plot of the principal components from the PLS2 investigation of data from Stripa.

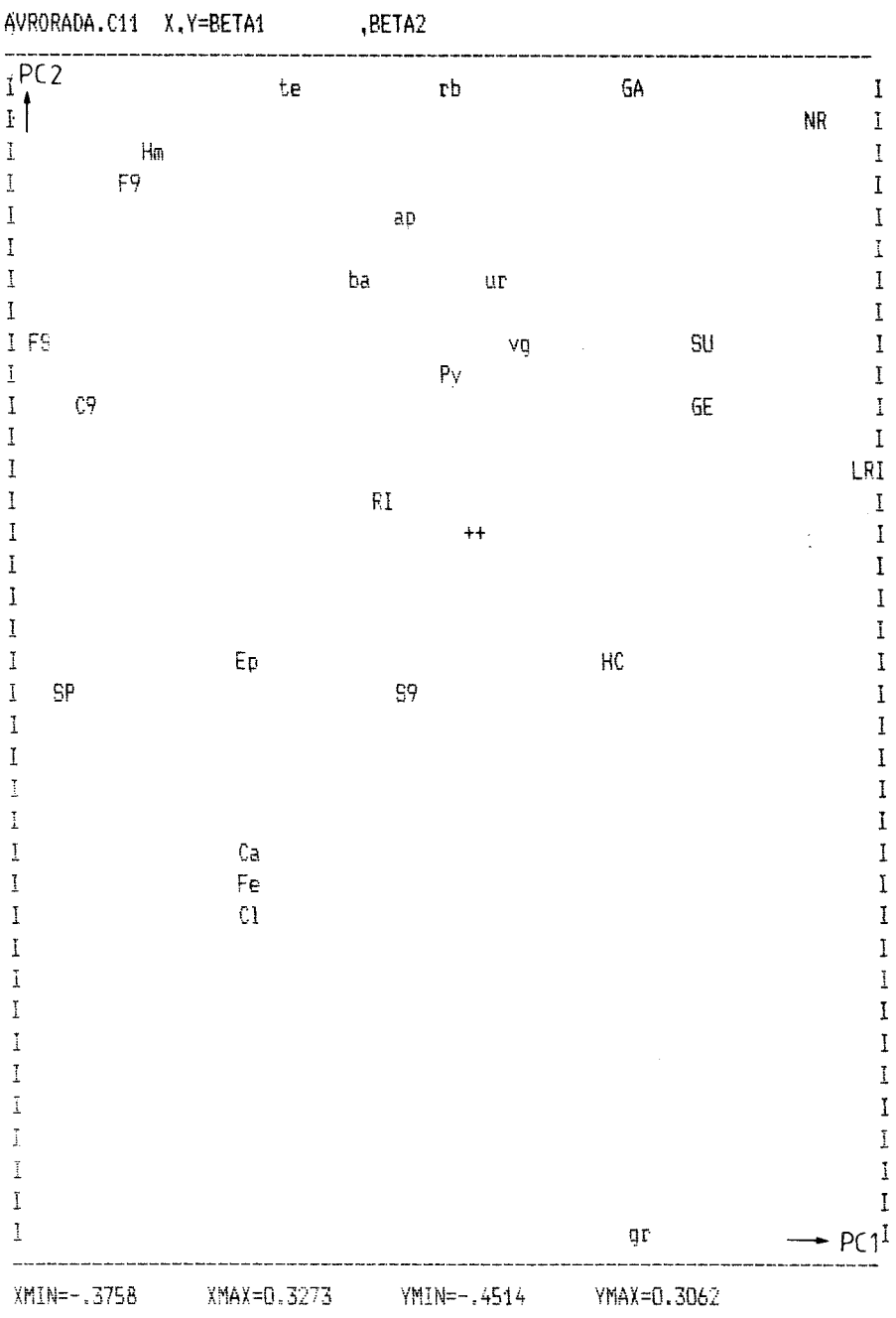

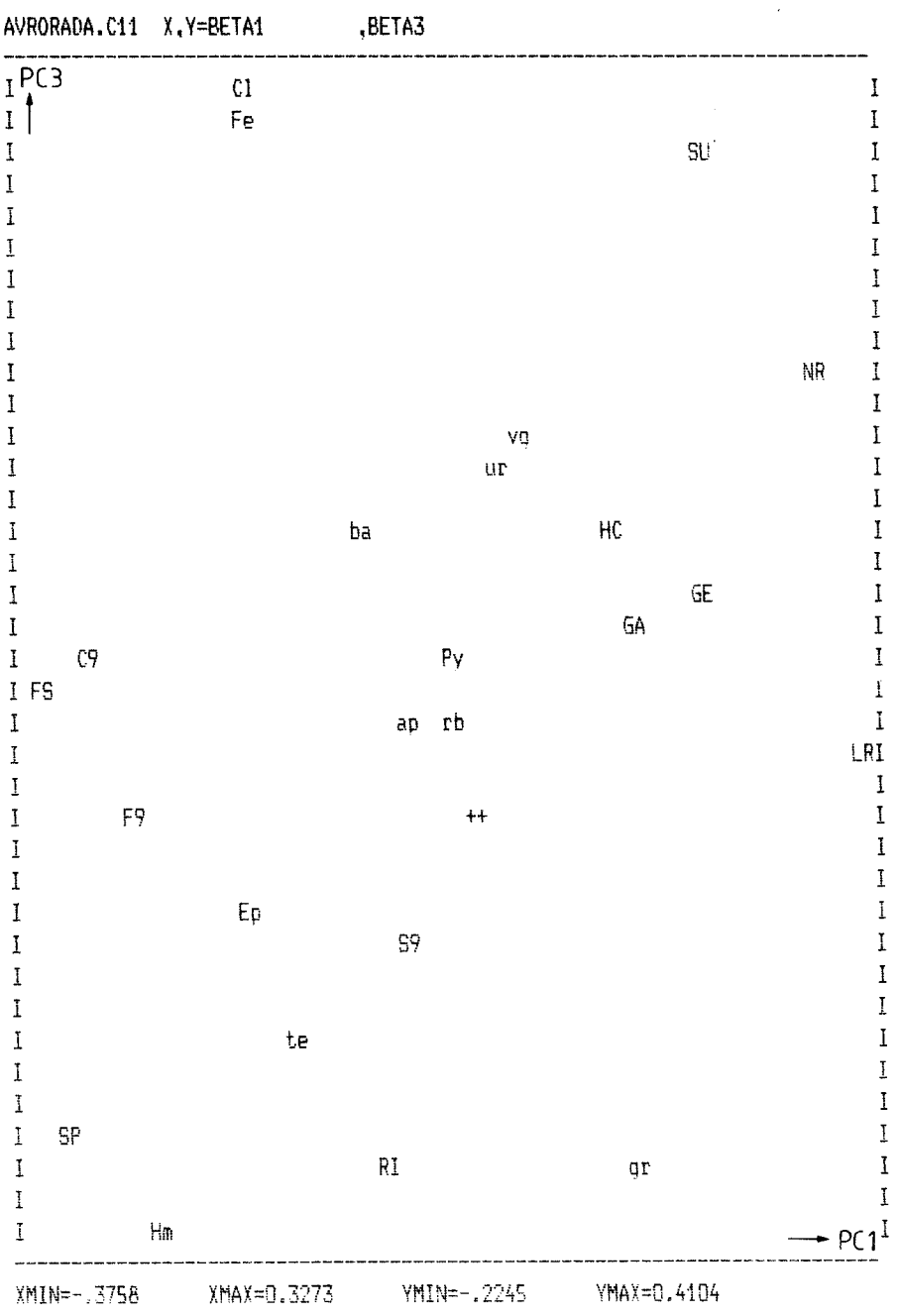

Fig C.61 Variable plots of principal components from PC-analysis of data from Ävrö.

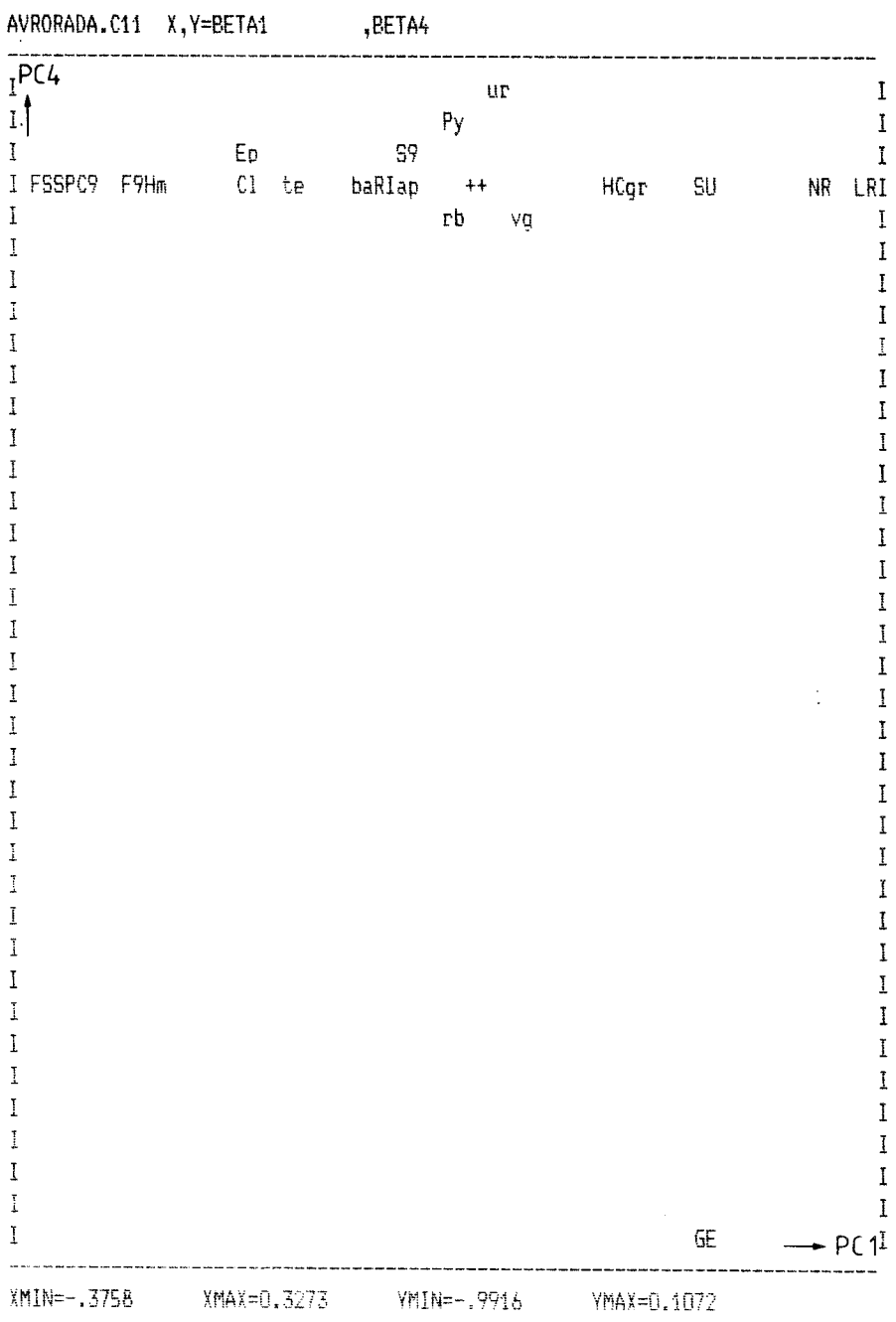

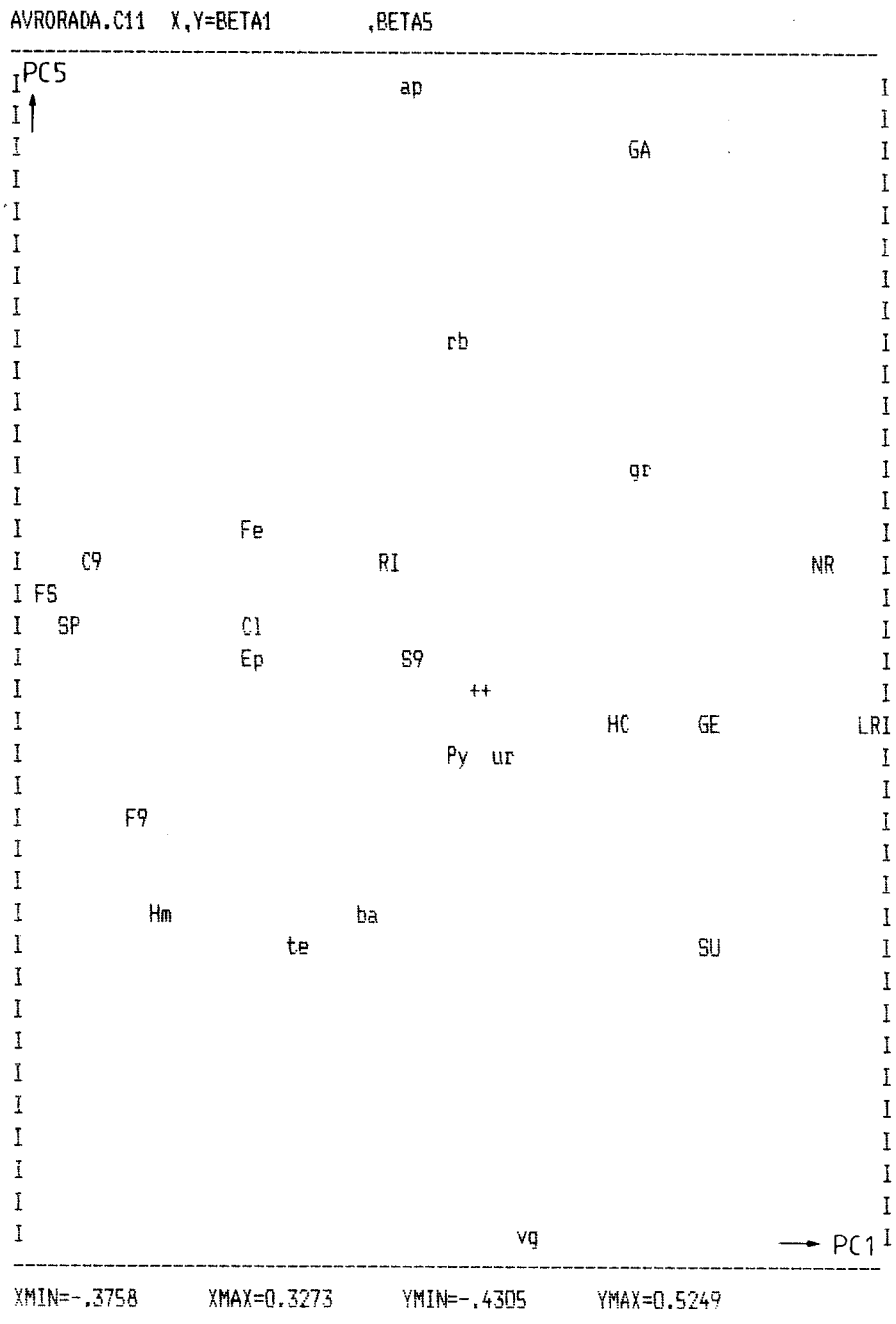

Fig C.62 Variable plots of principal components from PC-analysis of data from Ävrö.

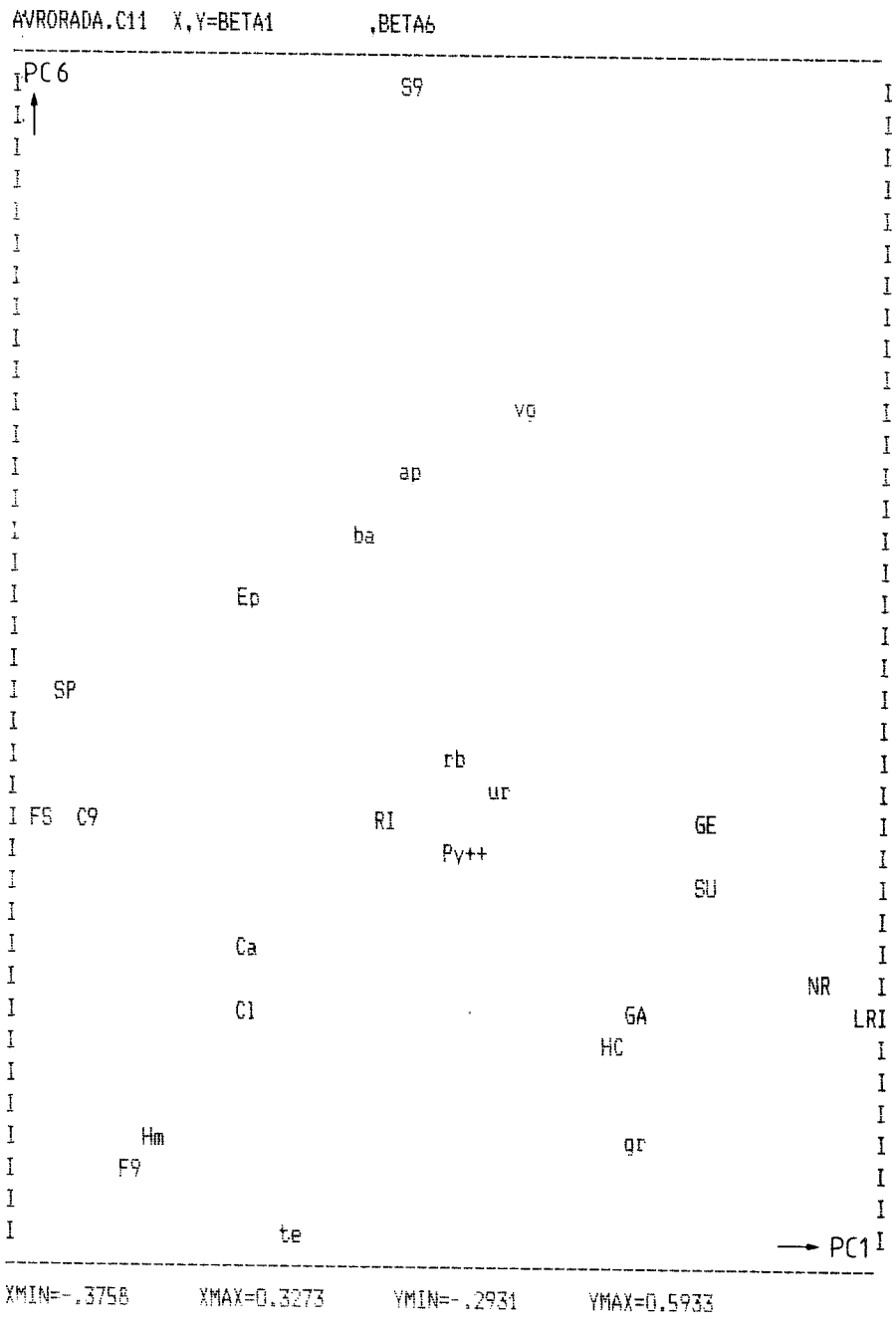

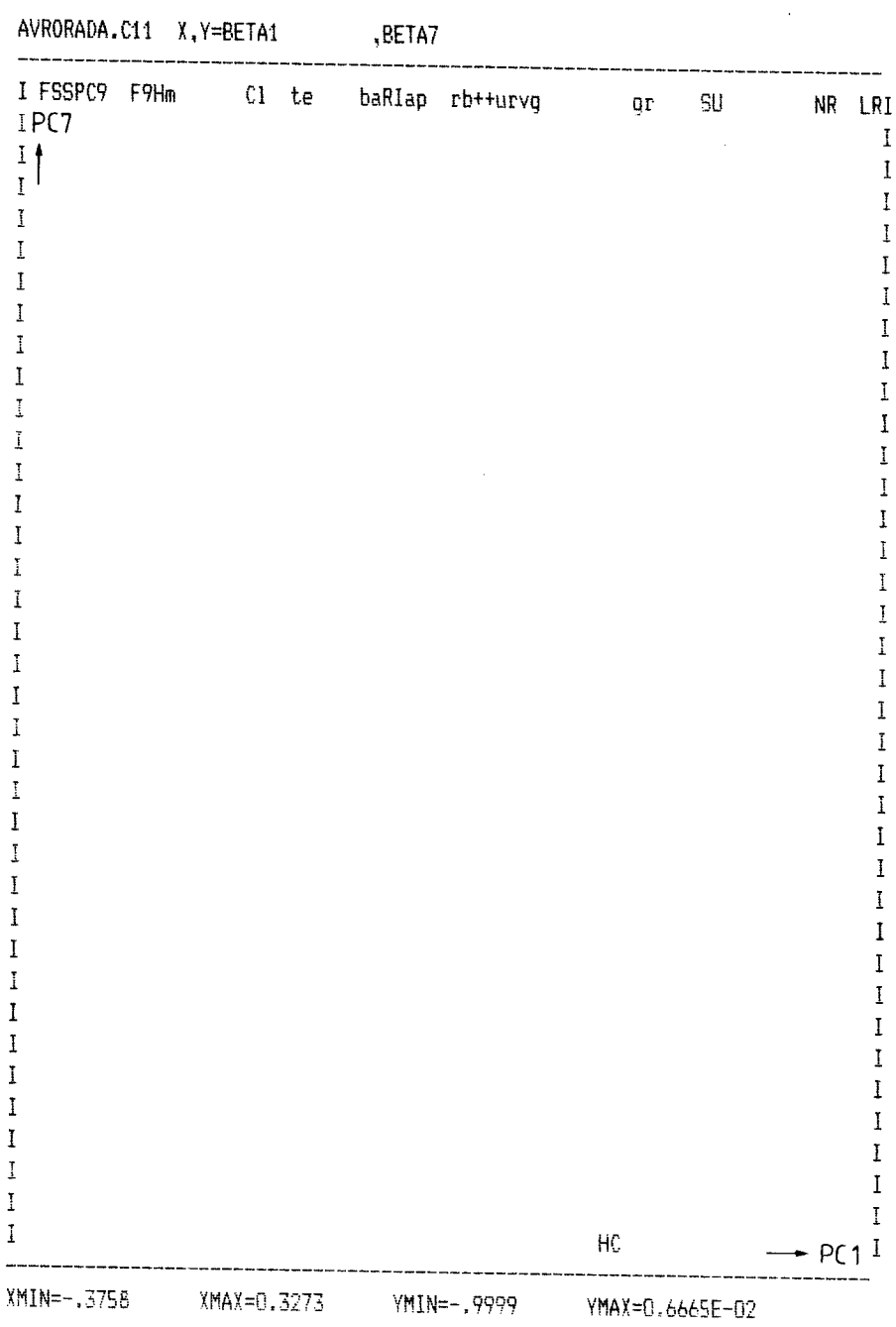

Fig C.63 Variable plots of principal components from PC-analysis of data from Ävrö.

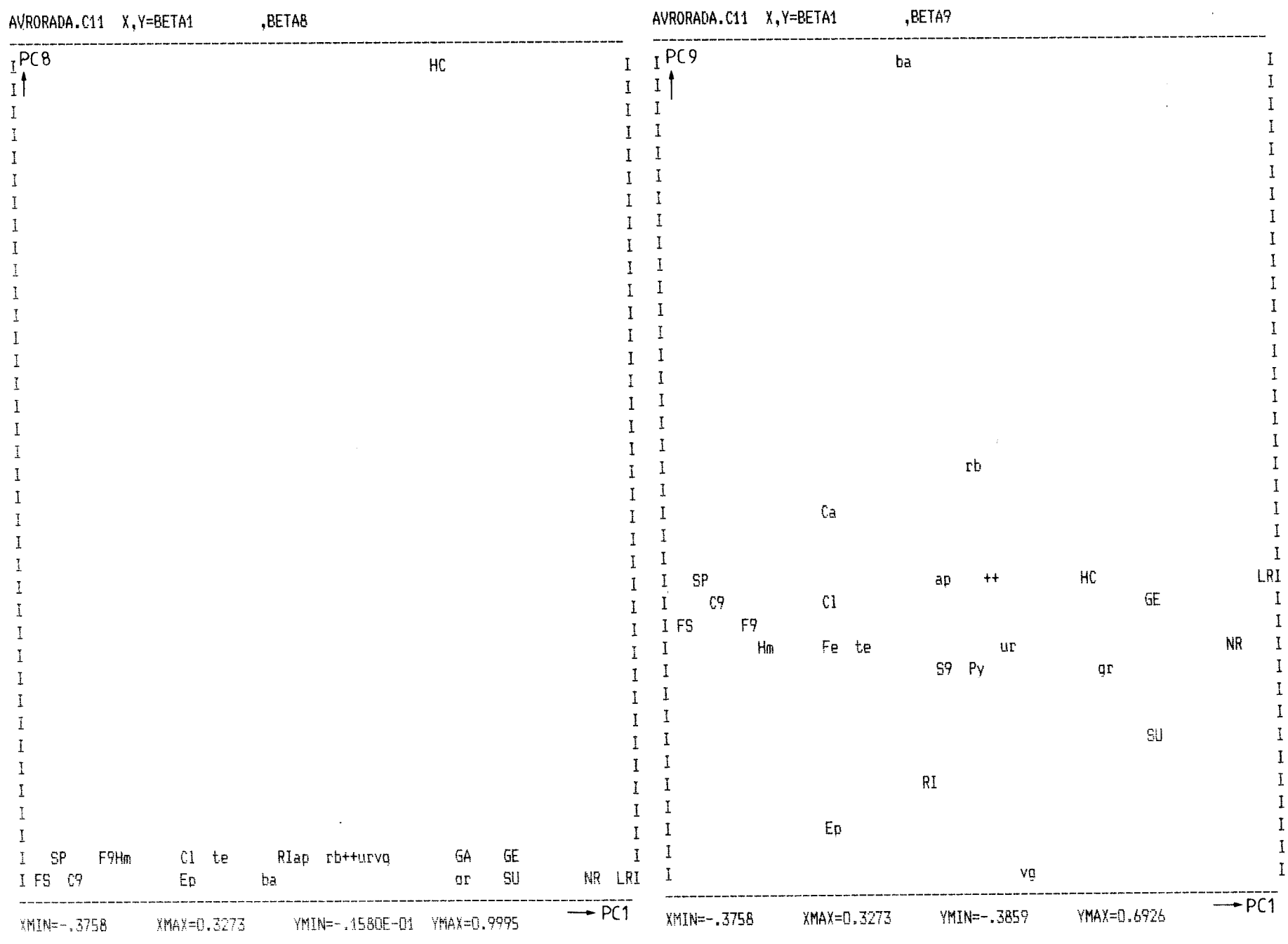

Fig C.64 Variable plots of principal components from PC-analysis of data from Ävrö.

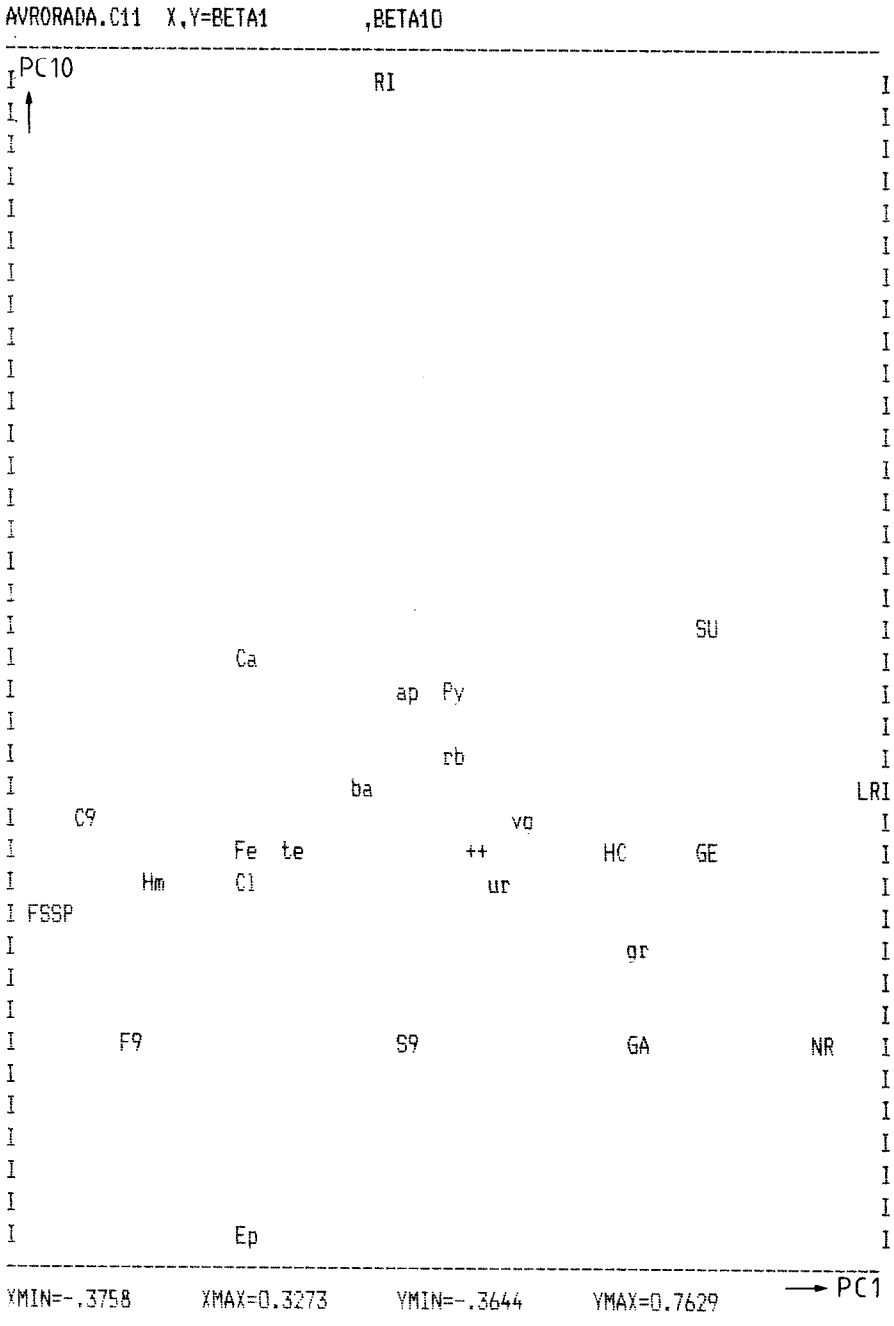

Fig C.65 Variable plots of principal components from PC-analysis of data from Ävrö.

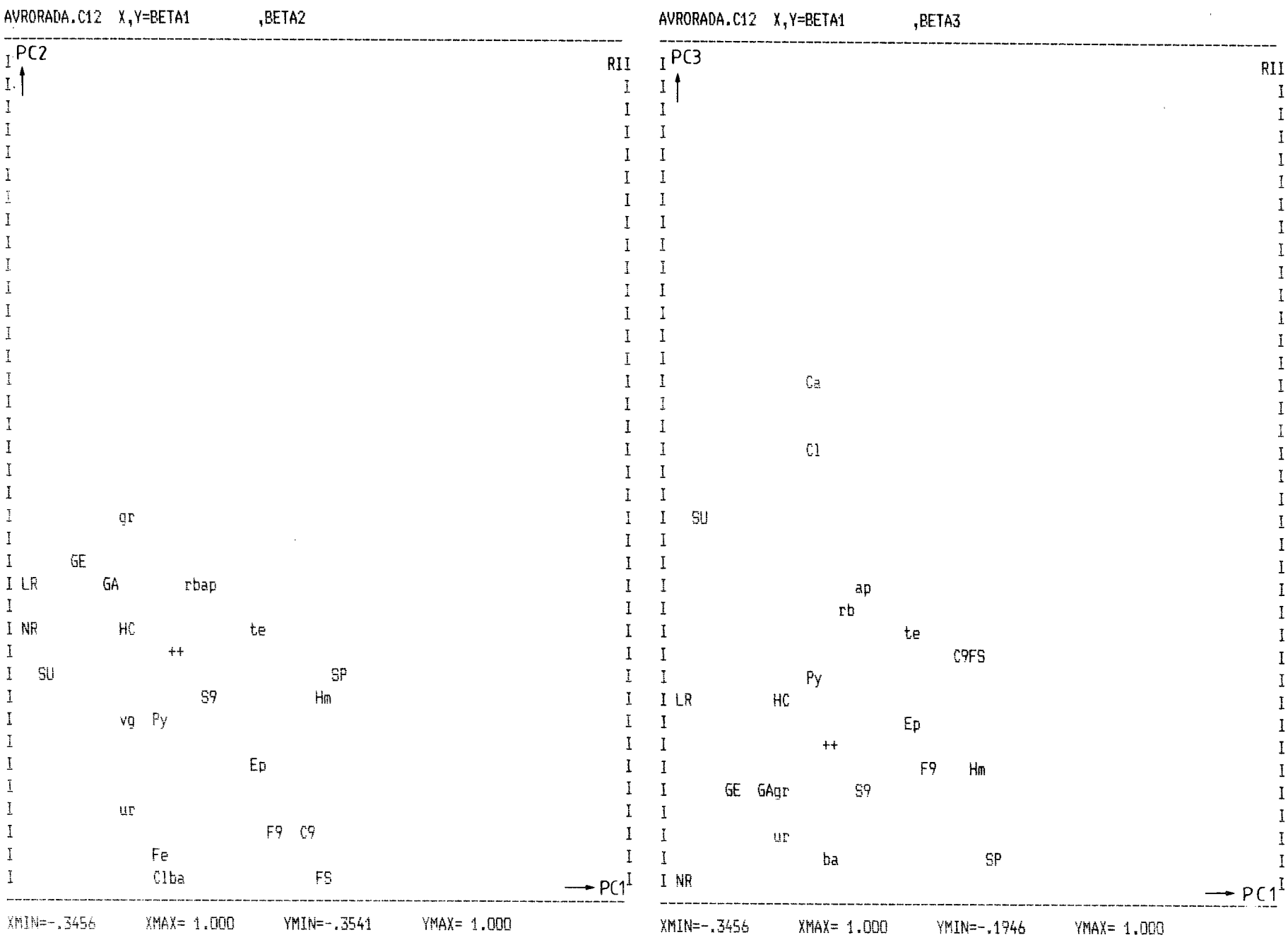

Fig C.66 Variable plots of the principal components from the PLS investigation of data from Ävrö.

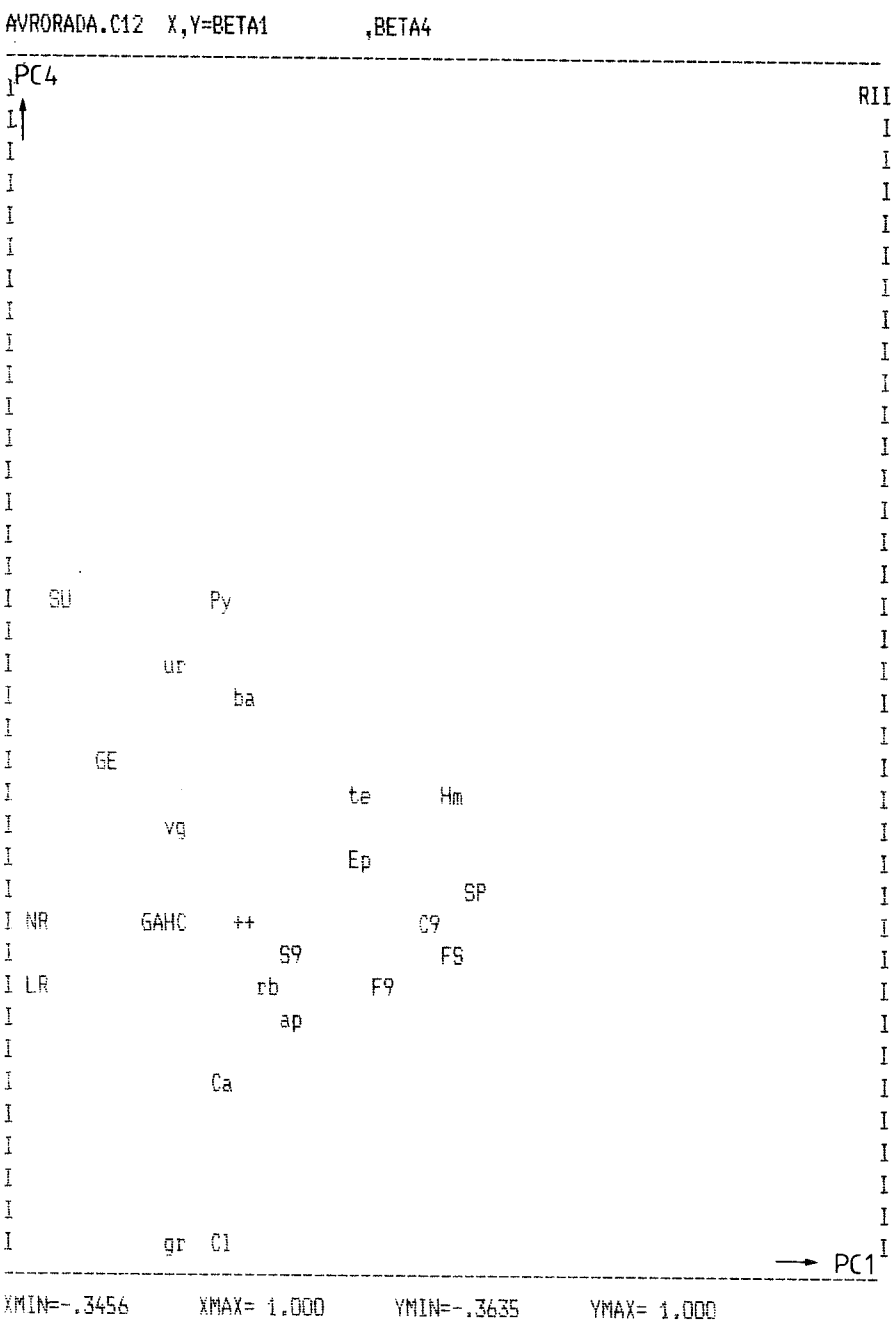

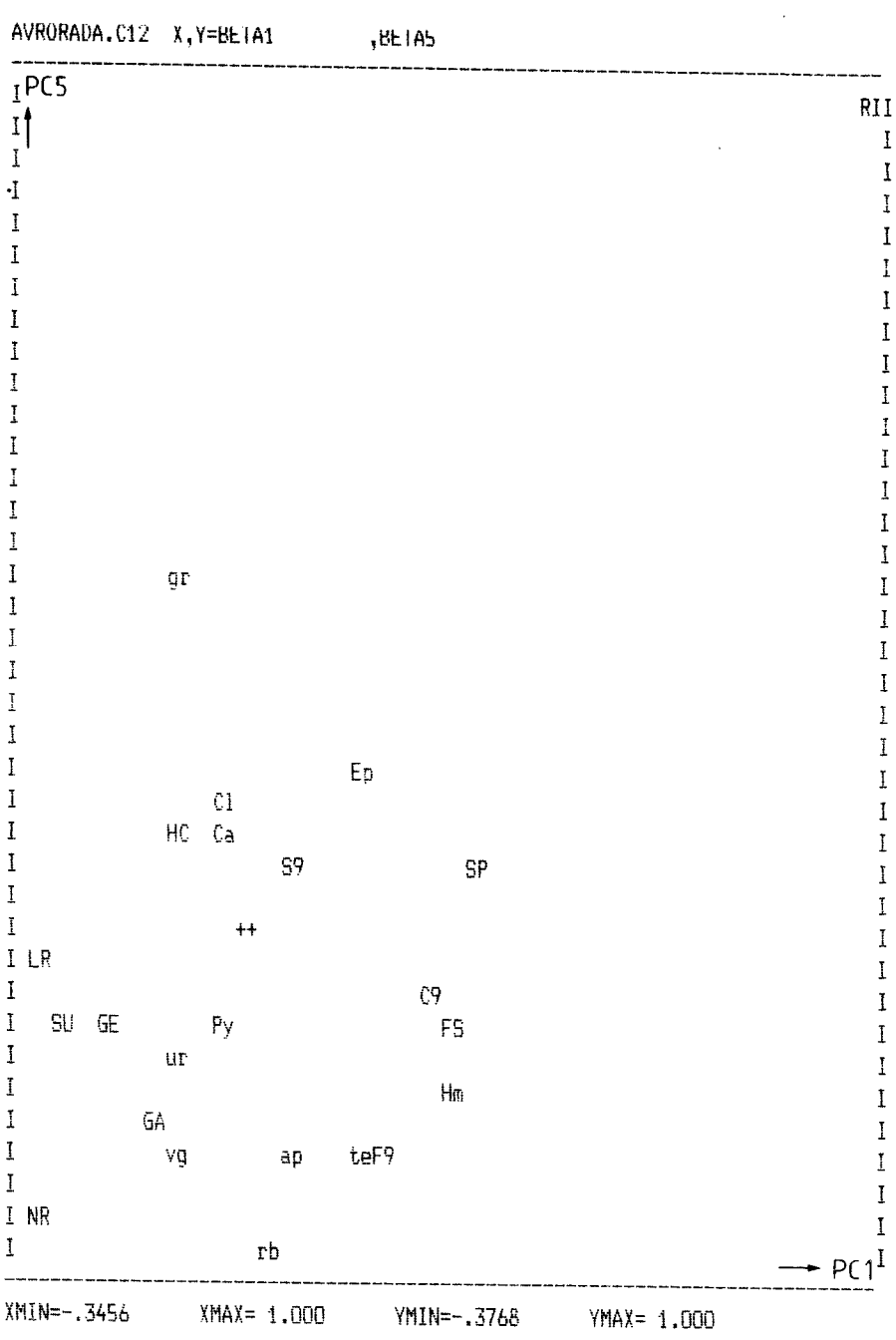

Fig C.67 Variable plots of the principal components from the PLS investigation of data from Ävrö.

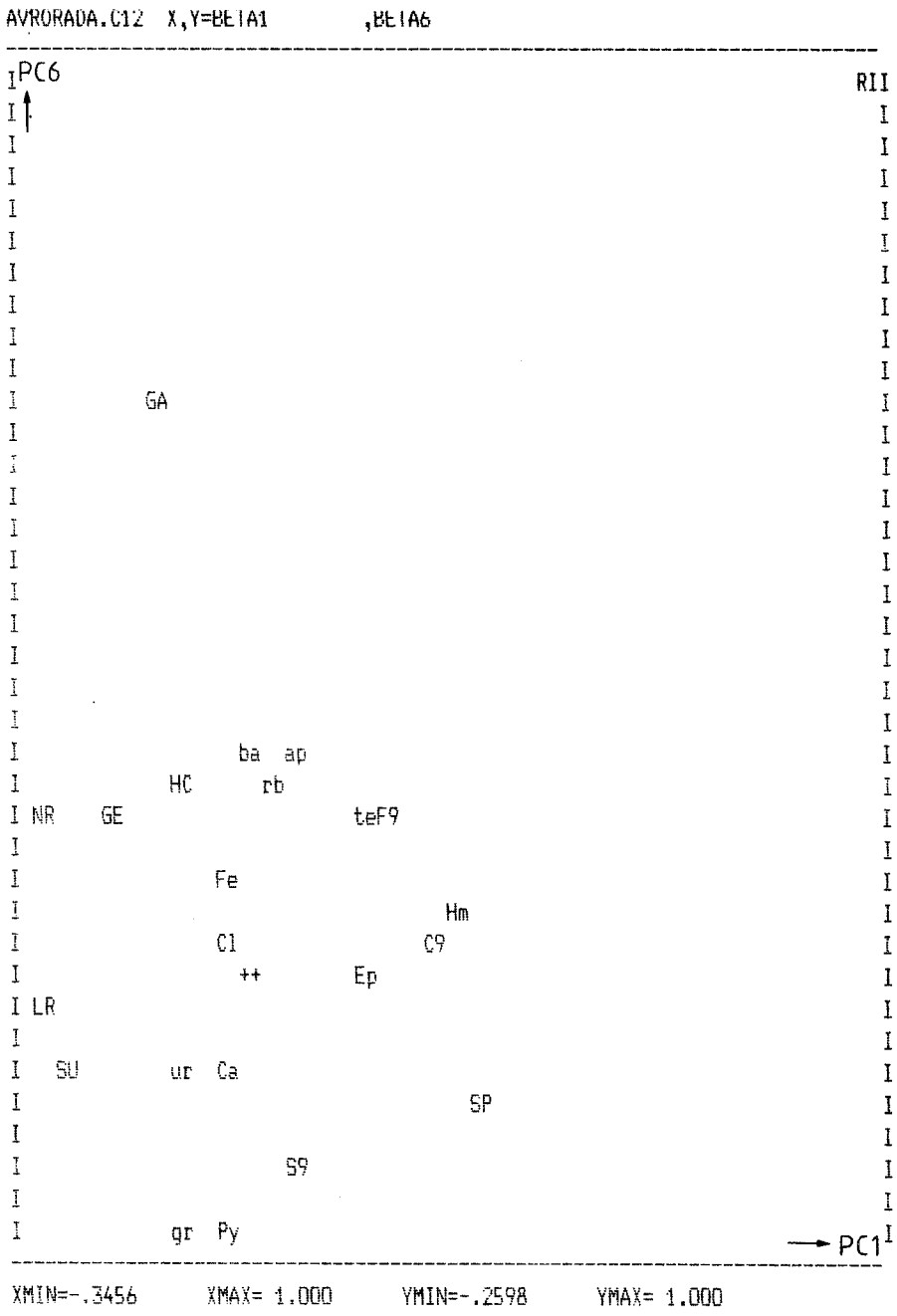

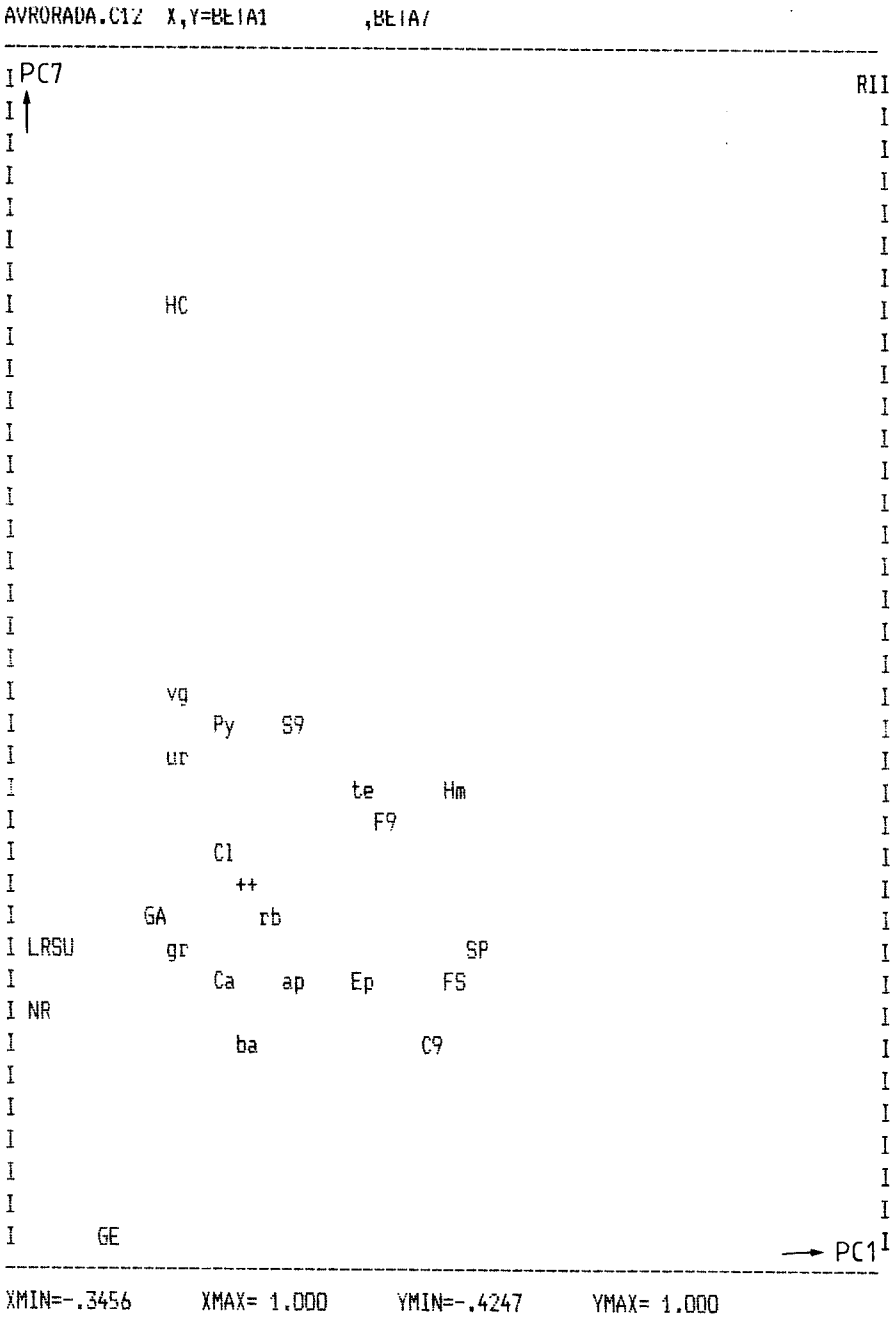

Fig C.68 Variable plots of the principal components from the PLS investigation of data from Ävrö.

Fig C.69 Variable plots of the principal components from the PLS investigation of data from Ävrö.

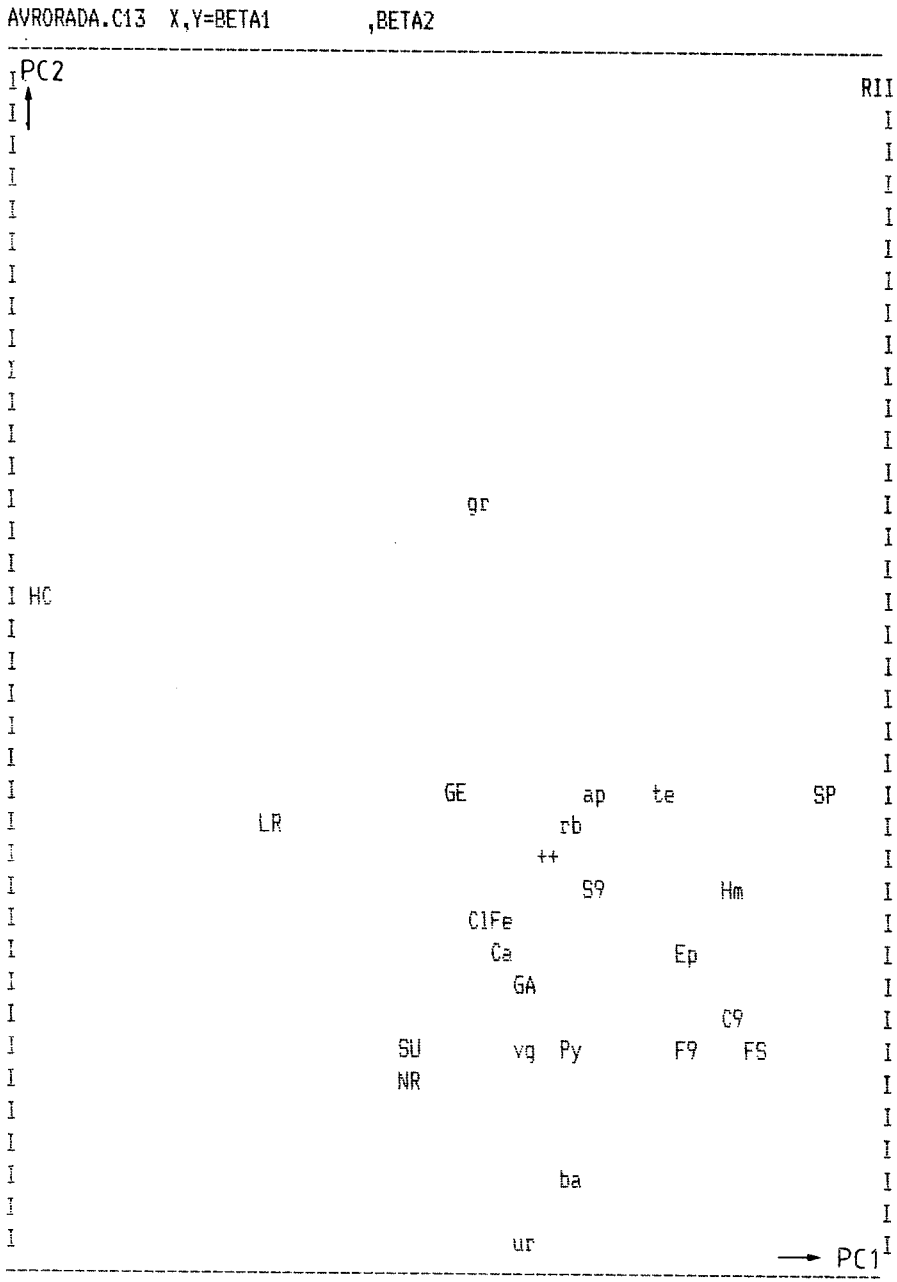

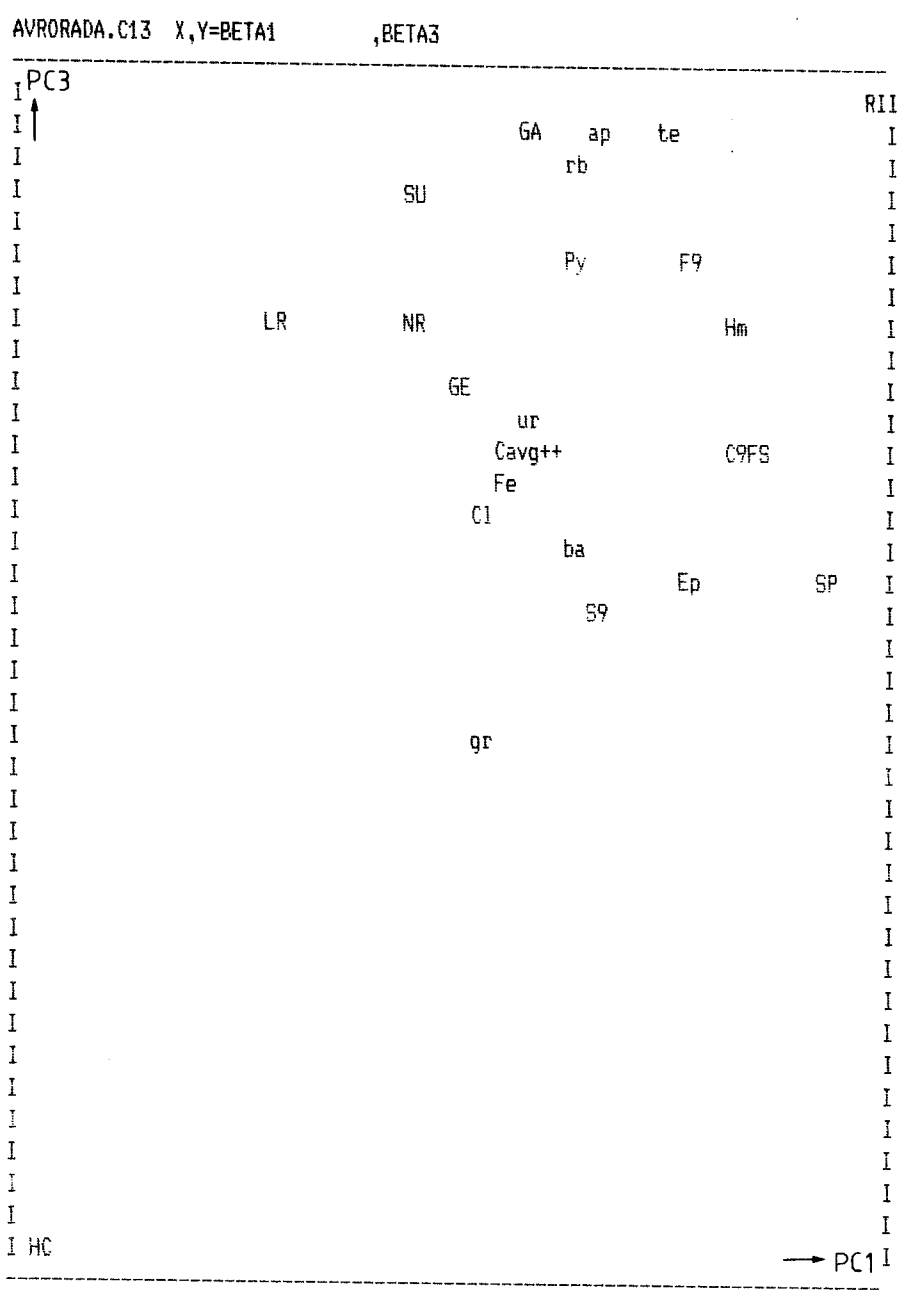

Fig C.70 Variable plot of the principal components from the PLS2 investigation of data from Ävrö.

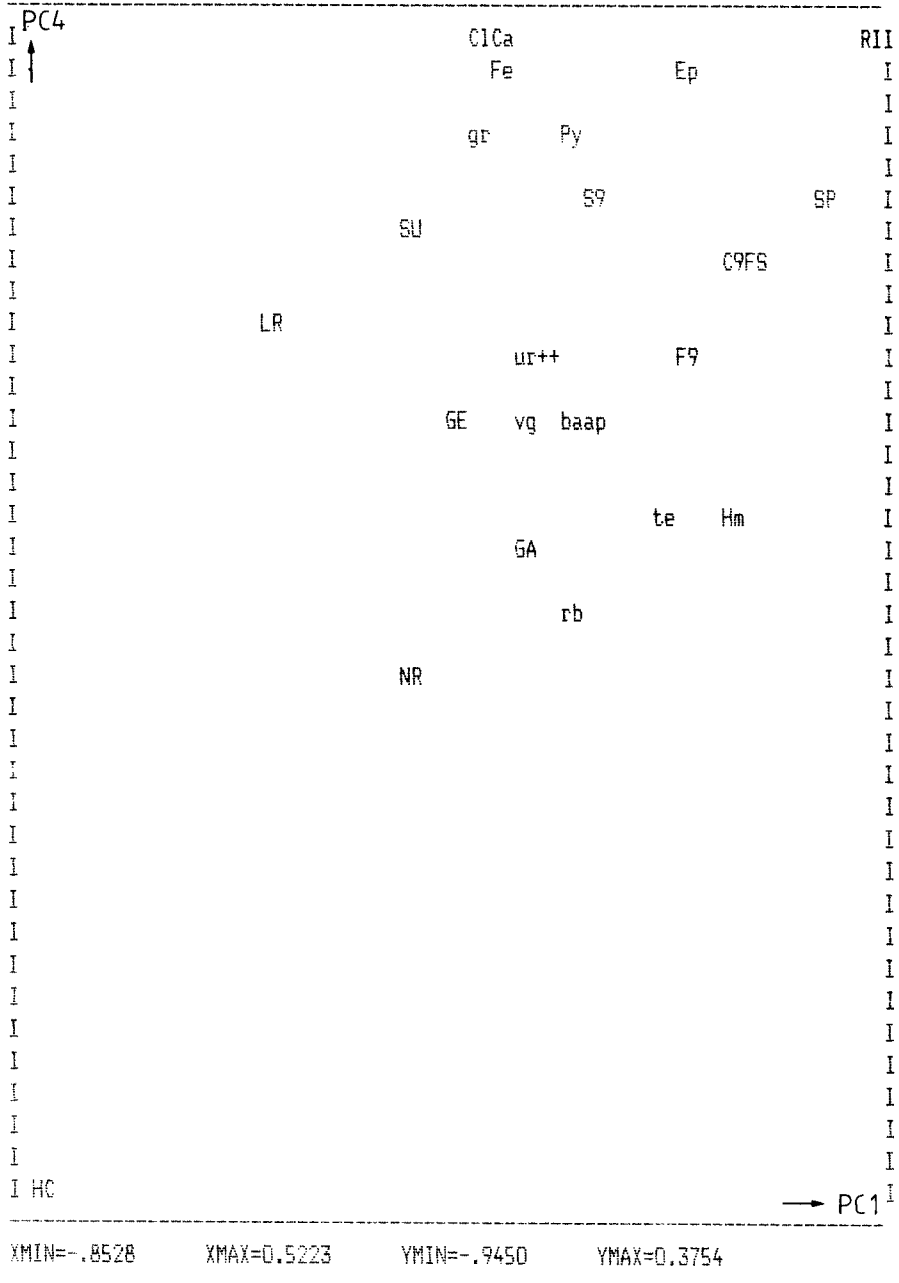

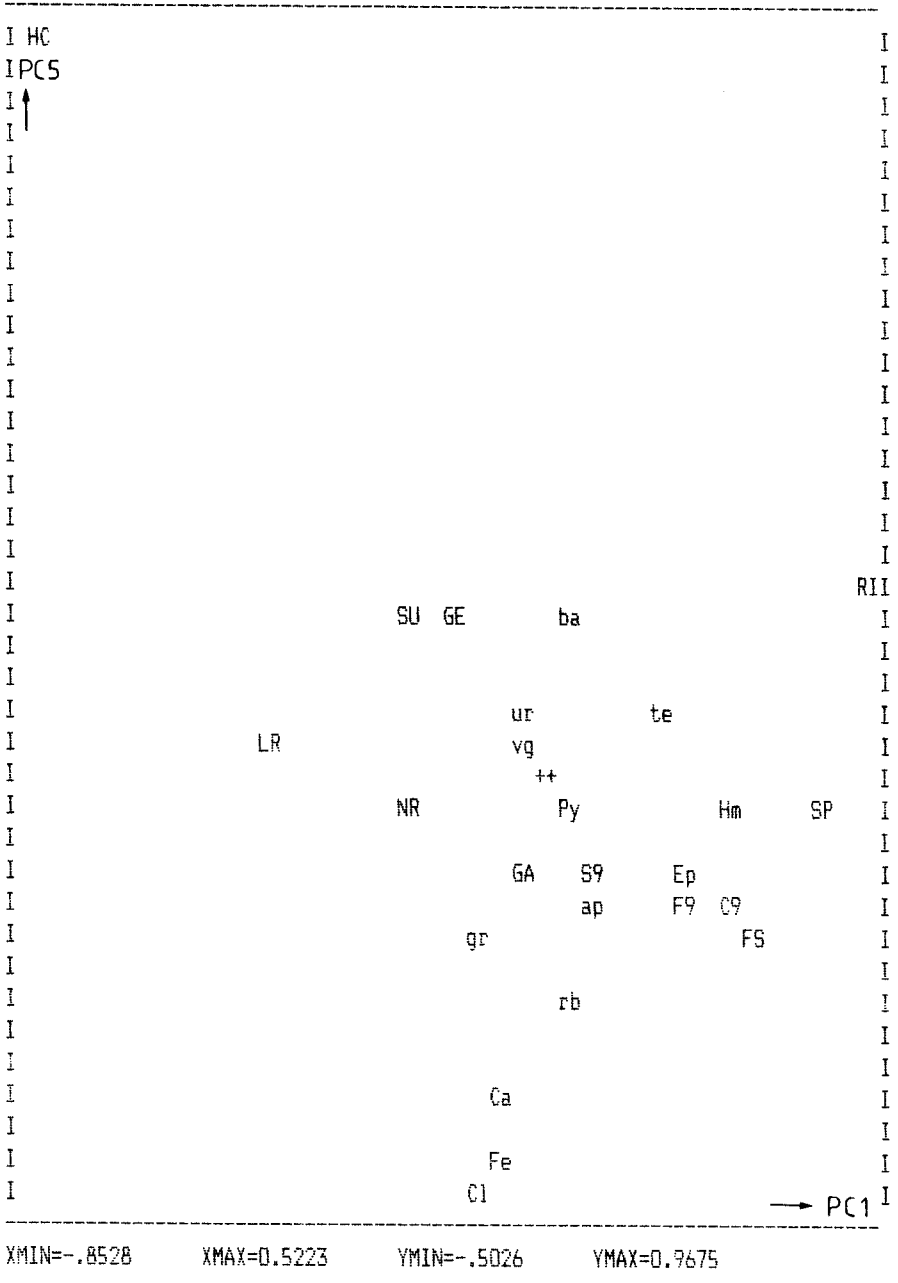

Fig C.71 Variable plot of the principal components from the PLS2 investigation of data from Ävrö.

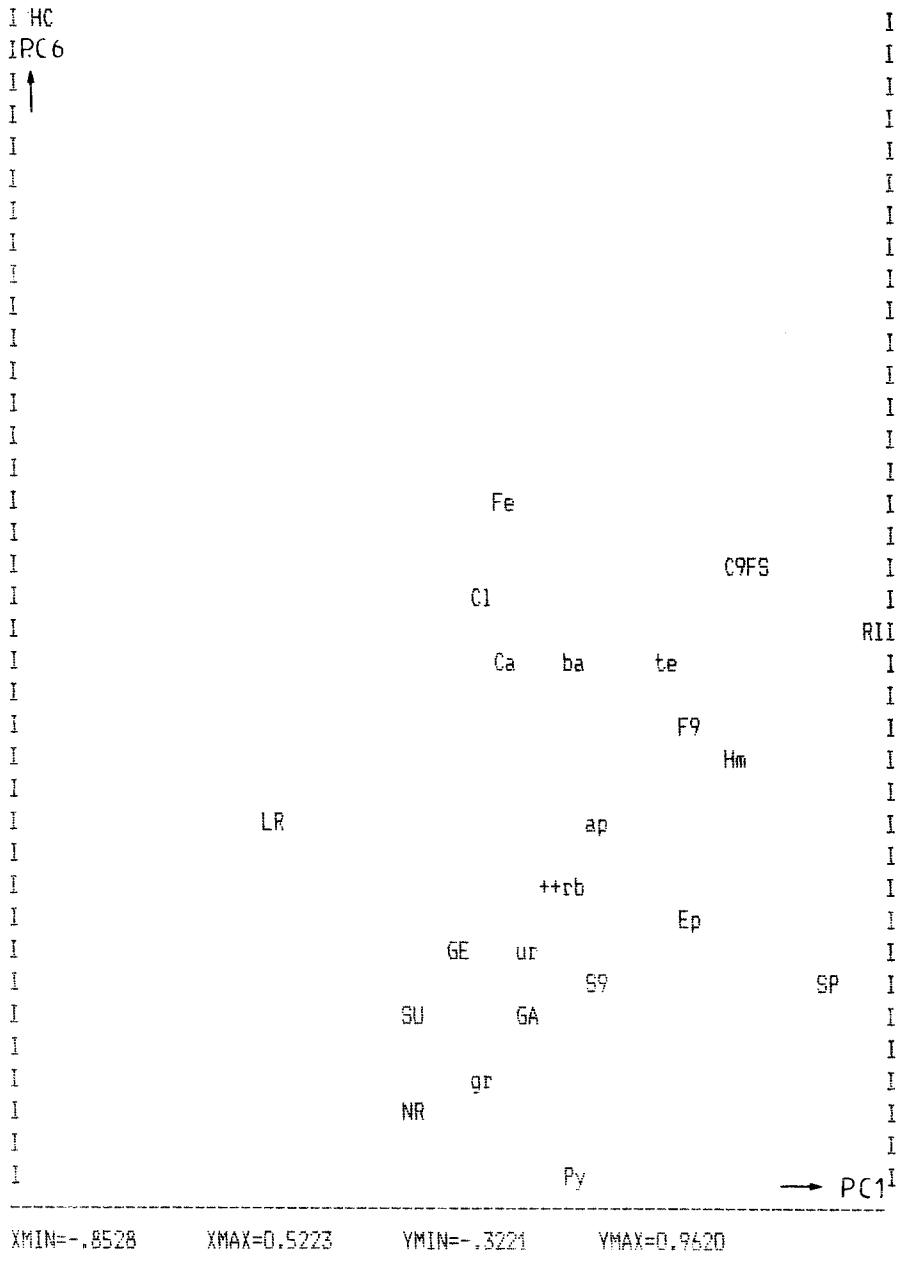

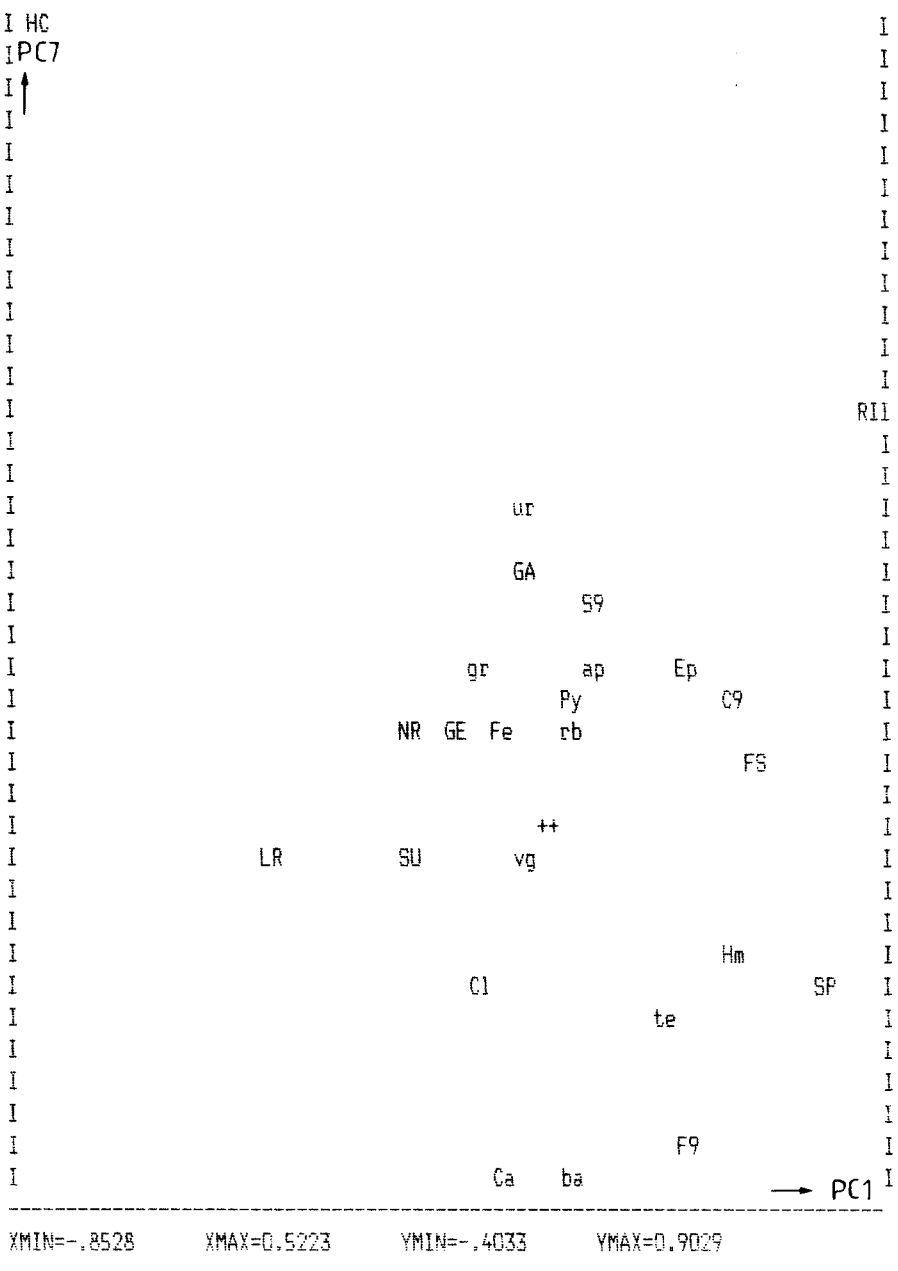

Fig C.72 Variable plot of the principal components from the PLS2 investigation of data from Ävrö.

Fig C.73 Variable plot of the principal components from the PLS2 investigation of data from Ävrö.

APPENDIX D

MEASUREMENTS ON CORE SAMPLES FROM THE BOREHOLES KFI09, KFI11, KKL02, and F2.

Table D.1 Dielectric constant, electrical conductivity, loss tangent and porosity on core samples from the boreholes KKL02, KFI11, KFI09 and F2.

Frequency MHz	Sample		ϵ(r)	σ (μS/m)	tgδ	Porosity %
0.025	KKL02	120.5	30.7	41.2	1.46	0.40
0.025	KKL02	125.5	23.1	12.6	0.56	0.23
0.025	KKL02	130.9	54.0	37.0	0.85	0.45
0.025	KKL02	134.0	23.0	28.7	1.29	0.71
0.025	KKL02	200.0	39.7	46.0	1.33	0.28
0.025	KKL02	390.1	52.3	54.8	1.27	0.29
0.025	KKL02	549.5	31.2	32.6	1.13	0.36
0.025	KKL02	586.2	20.7	29.7	1.46	0.21
0.025	KKL02	587.0	16.1	21.4	1.30	0.21
0.025	KKL02	588.0	47.5	27.0	0.67	0.30
0.025	KKL02	605.0	66.8	39.0	0.72	0.70
0.025	KKL02	609.0	56.6	32.1	0.70	0.35
0.025	KKL02	612.8	30.4	17.3	0.61	0.23
0.025	KKL02	721.9	44.6	38.2	1.01	0.43
0.025	KKL02	762.0	41.9	45.5	1.27	0.34
0.025	KKL02	763.1	31.2	38.2	1.33	0.29
0.025	KKL02	764.0	22.3	27.8	1.24	0.47
0.025	KKL02	804.5	26.2	35.5	1.40	0.62
0.025	KKL02	809.0	18.7	22.3	1.17	0.21
0.025	KKL02	838.0	29.2	36.4	1.32	0.21
0.025	KKL02	941.0	48.2	50.6	1.24	0.30
0.025	KKL02	941.9	42.8	40.5	1.08	0.34
0.025	KKL02	942.7	29.5	31.9	1.13	0.49
0.025	KKL02	944.0	32.2	4.8	0.16	0.06
0.025	KKL02	945.0	33.7	7.6	0.24	0.06
0.025	KKL02	952.0	34.8	7.4	0.23	0.08
0.025	KKL02	957.0	40.1	50.5	1.38	0.31
0.025	KFI11	56.4	26.5	23.1	0.94	0.21
0.025	KFI11	64.8	121.4	59.6	0.91	0.27
0.025	KFI11	65.9	49.8	47.0	1.20	0.28
0.025	KFI11	67.2	93.7	50.0	0.89	0.31
0.025	KFI11	109.3	46.2	51.7	1.33	0.27
0.025	KFI11	149.5	59.1	53.6	1.17	0.39
0.025	KFI11	201.1	142.8	63.7	0.78	0.51
0.025	KFI11	216.2	39.6	33.5	0.94	0.24
0.025	KFI11	218.1	47.9	49.5	1.21	0.30
0.025	KFI11	220.1	30.1	23.6	0.83	0.37
0.025	KFI11	251.7	82.6	53.7	0.90	0.79
0.025	KFI11	253.2	47.8	47.9	1.18	0.29
0.025	KFI11	254.1	43.7	48.1	1.25	0.28
0.025	KFI11	254.9	46.0	49.1	1.24	0.25
0.025	KFI11	262.5	38.3	29.7	0.87	0.29
0.025	KFI11	293.2	139.8	45.9	0.51	0.84
0.025	KFI11	296.0	113.7	62.8	0.91	0.66
0.025	KFI11	297.9	131.1	49.8	0.66	1.16
0.025	KFI11	329.1	75.3	47.5	0.85	0.87
0.025	KFI11	330.1	21.9	21.2	0.98	0.40

Table D.1 Dielectric constant, electrical conductivity, loss tangent and porosity on core samples from the boreholes KKL02, KFI11, KFI09 and F2. (Continued).

Frequency MHz	Sample	∈(r)	σ (μS/m)	tgδ	Porosity %
0.025	KFI11 331.1	33.1	33.1	1.08	0.63
0.025	KFI11 334.2	62.0	42.6	0.88	0.64
0.025	KFI11 337.0	29.5	32.4	1.16	0.41
0.025	KFI11 373.3	143.8	55.5	0.67	0.45
0.025	KFI11 384.1	43.5	39.6	1.04	0.27
0.025	KFI09 45.4	46.6	38.6	1.03	0.39
0.025	KFI09 93.1	66.7	37.6	0.79	0.97
0.025	KFI09 94.0	82.2	54.0	1.01	0.79
0.025	KFI09 95.0	81.3	44.5	0.84	0.75
0.025	KFI09 119.9	48.4	42.4	1.11	0.37
0.025	KFI09 127.9	54.6	45.7	1.10	0.56
0.025	KFI09 130.1	73.3	51.7	1.00	0.95
0.025	KFI09 132.4	57.8	45.0	1.00	0.78
0.025	KFI09 134.0	109.7	59.4	0.90	1.16
0.025	KFI09 136.0	71.4	51.6	0.95	1.26
0.025	KFI09 146.2	68.6	54.8	1.05	0.71
0.025	KFI09 147.2	79.4	54.4	0.95	0.62
0.025	KFI09 148.0	60.9	40.0	0.83	0.71
0.025	KFI09 158.9	61.9	41.4	0.86	1.16
0.025	KFI09 159.9	110.2	51.2	0.72	1.45
0.025	KFI09 162.0	45.5	36.5	0.95	0.88
0.025	KFI09 260.1	97.0	61.8	0.95	0.55
0.025	KFI09 262.1	54.3	44.7	1.00	0.36
0.025	KFI09 272.0	51.6	39.3	0.91	0.28
0.025	KFI09 309.4	56.4	57.7	1.26	0.46
0.025	KFI09 329.6	47.8	43.8	1.08	0.34
0.025	KFI09 331.5	22.4	32.4	1.47	0.44
0.025	KFI09 333.3	49.8	42.7	1.03	0.44
0.025	KFI09 359.9	42.4	31.4	0.85	0.50
0.025	F2 11.50	32.4	41.2		.28
0.025	F2 19.50	25.4	35.2		.24
0.025	F2 32.60	33.0	40.7		.29
0.025	F2 44.86	44.3	44.7		.72
0.025	F2 45.00	86.4	50.8		1.43
0.025	F2 45.17	39.8	31.2		.66
0.025	F2 45.53	26.4	25.1		.40
0.025	F2 46.15	24.7	29.9		.35
0.025	F2 49.35	23.4	28.5		.27
0.025	F2 57.20	28.0	39.7		.27
0.025	F2 72.10	22.6	32.8		.28
0.025	F2 91.20	45.9	56.5		.51
0.025	F2 105.10	7.1	26.4		.40
0.025	F2 110.10	28.9	31.4		.34
0.025	F2 110.42	30.6	34.6		.55
0.025	F2 110.95	33.1	40.4		.40
0.025	F2 111.36	75.6	53.0		4.78
0.025	F2 111.54	61.0	74.6		3.13

Table D.1 Dielectric constant, electrical conductivity, loss tangent and porosity on core samples from the boreholes KKL02, KFI11, KFI09 and F2. (Continued).

Frequency MHz	Sample		ϵ(r)	σ (μS/m)	tgδ	Porosity %
0.025	F2	111.79	74.3	71.0		2.73
0.025	F2	112.05	61.8	82.7		3.59
0.025	F2	112.29	111,	89.9		3.37
0.025	F2	112.48	107,	86.3		3.04
0.025	F2	112.80	55.2	55.9		.51
0.025	F2	113.80	27.0	36.0		.55
0.025	F2	115.68	17.0	22.9		.38
0.025	F2	116.86	16.8	21.2		.30
0.025	F2	117.13	12.7	8.4,		.49
0.025	F2	117.31	21.4	24.9		.45
0.025	F2	118.22	36.0	38.9		.85
0.025	F2	119.52	61.8	63.0		.68
0.025	F2	120.52	47.7	72.7		.56
0.025	F2	120.80	190.	82.7		1.33
0.025	F2	121.38	32.8	40.6		.53
0.025	F2	121.69	55.7	66.1		.64
0.025	F2	122.19	52.3	57.5		.51
0.025	F2	123.16	36.8	52.2		.40
0.025	F2	123.96	51.6	62.1		.43
0.025	F2	125.39	34.7	37.0		.42
0.025	F2	125.50	37.6	41.6		.37
0.025	F2	126.17	32.2	41.1		.33
0.025	F2	127.17	33.0	36.8		.49
0.025	F2	127.81	25.5	35.4		.38
0.025	F2	130.50	17.0	29.9		.35
0.025	F2	136.17	23.8	33.2		.36
0.025	F2	136.78	16.0	27.7		.45
0.025	F2	136.88	20.3	23.2		.40
0.025	F2	140.00	16.8	26.9		.35
0.025	F2	156.80	19.2	33.7		.48
0.025	F2	162.30	22.2	32.2		.42
0.025	F2	171.78	17.0	26.6		.35
0.025	F2	179.86	16.1	31.1		.37
0.025	F2	186.40	52.4	53.3		1.19
0.025	F2	188.94	69.4	60.8		.90
0.025	F2	190.18	18.6	23.9		.31
0.025	F2	194.25	16.4	29.1		.31
0.025	F2	200.70	21.1	34.0		.22
0.025	F2	204.06	22.8	33.7		.30
0.025	F2	205.64	77.0	72.9		.55
0.025	F2	207.43	24.6	39.1		.35
0.025	F2	211.20	24.9	53.1		.30
0.025	F2	211.30	40.0	37.0		.34
0.025	F2	214.07	12.2	11.9		.24
0.025	F2	222.40	22.6	29.3		.33
0.025	F2	231.28	24.8	35.1		.36
0.025	F2	231.97	31.9	33.9		.57

Table D.1 Dielectric constant, electrical conductivity, loss tangent and porosity on core samples from the boreholes KKL02, KFI11, KFI09 and F2. (Continued).

Frequency MHz	Sample		∈(r)	σ (μS/m)	tgδ	Porosity %
0.025	F2	232.61	19.9	25.4		.37
0.025	F2	239.52	19.2	24.2		.71
0.025	F2	240.47	20.3	28.6		.38
0.025	F2	249.00	27.8	39.9		.37
1	KKL02	120.5	7.6	152.0	0.46	0.40
1	KKL02	125.5	11.2	151.4	0.32	0.23
1	KKL02	130.9	15.1	356.5	0.58	0.45
1	KKL02	134.0	7.3	119.9	0.38	0.71
1	KKL02	200.0	7.3	160.2	0.51	0.28
1	KKL02	390.1	8.1	204.4	0.59	0.29
1	KKL02	549.5	7.6	145.9	0.44	0.36
1	KKL02	586.2	6.4	81.7	0.29	0.21
1	KKL02	587.0	6.5	71.8	0.25	0.21
1	KKL02	588.0	17.9	352.6	0.49	0.30
1	KKL02	605.0	21.7	643.7	0.76	0.70
1	KKL02	609.0	19.6	448.7	0.59	0.35
1	KKL02	612.8	14.7	287.3	0.48	0.23
1	KKL02	721.9	7.7	161.8	0.49	0.43
1	KKL02	762.0	7.2	108.5	0.35	0.34
1	KKL02	763.1	6.8	127.0	0.43	0.29
1	KKL02	764.0	7.0	88.3	0.29	0.47
1	KKL02	804.5	7.3	105.0	0.33	0.62
1	KKL02	809.0	6.8	87.6	0.30	0.21
1	KKL02	838.0	7.0	120.4	0.40	0.21
1	KKL02	941.0	8.0	140.3	0.41	0.30
1	KKL02	941.9	8.3	171.1	0.48	0.34
1	KKL02	942.7	8.1	130.3	0.37	0.49
1	KKL02	944.0	23.4	174.9	0.19	0.06
1	KKL02	945.0	23.6	173.1	0.19	0.06
1	KKL02	952.0	24.1	175.3	0.19	0.08
1	KKL02	957.0	7.8	137.7	0.41	0.31
1	KFI11	56.4	8.0	128.9	0.37	0.21
1	KFI11	64.8	13.5	403.8	0.72	0.27
1	KFI11	65.9	9.1	215.1	0.55	0.28
1	KFI11	67.2	11.7	364.9	0.74	0.31
1	KFI11	109.3	8.3	206.4	0.57	0.27
1	KFI11	149.5	10.1	260.5	0.60	0.39
1	KFI11	201.1	13.7	503.3	0.88	0.51
1	KFI11	216.2	10.1	217.7	0.50	0.24
1	KFI11	218.1	9.3	218.4	0.55	0.30
1	KFI11	220.1	12.0	168.6	0.33	0.37
1	KFI11	251.7	10.8	379.6	0.82	0.79
1	KFI11	253.2	9.4	224.6	0.55	0.29
1	KFI11	254.1	8.5	204.6	0.55	0.28
1	KFI11	254.9	8.9	212.8	0.56	0.25
1	KFI11	262.5	10.4	206.3	0.47	0.29
1	KFI11	293.2	20.0	696.6	0.83	0.84

Table D.1 Dielectric constant, electrical conductivity, loss tangent and porosity on core samples from the boreholes KKL02, KFI11, KFI09 and F2. (Continued).

Frequency MHz	Sample	ϵ(r)	σ (μS/m)	tgδ	Porosity %
1	KFI11 296.0	11.1	400.0	0.86	0.66
1	KFI11 297.9	13.7	462.1	0.81	1.16
1	KFI11 329.1	14.8	374.8	0.61	0.87
1	KFI11 330.1	7.3	107.2	0.34	0.40
1	KFI11 331.1	8.6	173.3	0.47	0.63
1	KFI11 334.2	13.4	324.3	0.58	0.64
1	KFI11 337.0	7.7	146.4	0.44	0.41
1	KFI11 373.3	20.1	644.8	0.80	0.45
1	KFI11 384.1	8.9	217.4	0.57	0.27
1	KFI09 45.4	10.4	230.9	0.53	0.39
1	KFI09 93.1	13.5	367.1	0.66	0.97
1	KFI09 94.0	12.8	378.1	0.71	0.79
1	KFI09 95.0	13.2	369.8	0.67	0.75
1	KFI09 119.9	7.9	199.5	0.59	0.37
1	KFI09 127.9	13.1	348.5	0.63	0.56
1	KFI09 130.1	12.4	334.1	0.64	0.95
1	KFI09 132.4	11.6	272.9	0.56	0.78
1	KFI09 134.0	12.6	419.7	0.79	1.16
1	KFI09 136.0	13.1	353.8	0.64	1.26
1	KFI09 146.2	13.3	356.8	0.64	0.71
1	KFI09 147.2	14.0	414.8	0.71	0.62
1	KFI09 148.0	13.1	341.4	0.62	0.71
1	KFI09 158.9	13.4	328.8	0.59	1.16
1	KFI09 159.9	15.2	555.9	0.88	1.45
1	KFI09 162.0	11.0	253.0	0.54	0.88
1	KFI09 260.1	12.6	404.0	0.76	0.55
1	KFI09 262.1	10.8	282.0	0.61	0.36
1	KFI09 272.0	11.5	290.8	0.60	0.28
1	KFI09 309.4	9.2	231.6	0.59	0.46
1	KFI09 329.6	9.3	223.3	0.56	0.34
1	KFI09 331.5	6.5	100.4	0.35	0.44
1	KFI09 333.3	10.5	257.8	0.58	0.44
1	KFI09 359.9	11.2	237.1	0.50	0.50
1	F2 11.5	7.1	140		.28
1	F2 19.5	6.6	116		.24
1	F2 32.6	6.6	124		.29
1	F2 44.9	7.4	162		.72
1	F2 45.0	12.5	299		1.43
1	F2 45.2	8.0	168		.66
1	F2 45.5	7.9	150		.40
1	F2 46.1	7.1	111		.35
1	F2 49.3	6.6	105		.27
1	F2 57.2	6.4	111		.27
1	F2 72.1	6.7	120		.28
1	F2 91.2	7.1	166		.51
1	F2 105.1	7.0	99		.40
1	F2 110.1	7.4	138		.34

Table D.1 Dielectric constant, electrical conductivity, loss tangent and porosity on core samples from the boreholes KKL02, KFI11, KFI09 and F2. (Continued).

Frequency MHz	Sample		∈(r)	σ (μS/m)	tgδ	Porosity %
1	F2	110.4	7.4	132		.55
1	F2	110.9	7.5	153		.40
1	F2	111.4	9.7	264		4.78
1	F2	111.5	9.0	233		3.13
1	F2	111.8	8.8	245		2.73
1	F2	112.0	9.0	237		3.59
1	F2	112.3	9.0	241		3.37
1	F2	112.5	9.0	241		3.04
1	F2	112.8	7.6	170		.51
1	F2	113.8	7.2	131		.55
1	F2	115.7	6.6	99		.38
1	F2	116.9	6.4	91		.30
1	F2	117.1	7.9	110		.49
1	F2	117.3	7.4	130		.45
1	F2	118.2	7.2	146		.85
1	F2	119.5	8.1	222		.68
1	F2	120.5	7.6	182		.56
1	F2	120.8	11.3	531		1.33
1	F2	121.4	7.5	154		.53
1	F2	121.7	7.8	192		.64
1	F2	122.2	8.6	231		.51
1	F2	123.2	7.3	165		.40
1	F2	124.0	7.9	202		.43
1	F2	125.4	7.2	159		.42
1	F2	125.5	7.6	167		.37
1	F2	126.2	7.2	143		.33
1	F2	127.2	6.7	143		.49
1	F2	127.8	6.0	101		.38
1	F2	130.5	6.2	104		.35
1	F2	136.2	7.0	92		.36
1	F2	136.8	6.4	93		.45
1	F2	136.9	6.9	87		.40
1	F2	140.0	5.8	93		.35
1	F2	156.8	6.0	113		.48
1	F2	162.3	6.5	84		.42
1	F2	171.8	5.9	96		.35
1	F2	179.9	5.4	93		.37
1	F2	186.4	7.4	253		1.19
1	F2	188.9	8.0	242		.90
1	F2	190.2	6.1	106		.31
1	F2	194.2	5.9	97		.31
1	F2	200.7	6.1	82		.22
1	F2	204.1	6.4	131		.30
1	F2	205.6	7.3	198		.55
1	F2	207.4	6.2	75		.35
1	F2	211.2	6.1	99		.30
1	F2	211.3	6.5	144		.34

Table D.1 Dielectric constant, electrical conductivity, loss tangent and porosity on core samples from the boreholes KKL02, KFI11, KFI09 and F2. (Continued).

Frequency MHz	Sample		ϵ(r)	σ (μS/m)	tgδ	Porosity %
1	F2	214.1	5.9	67		.24
1	F2	222.4	5.9	130		.33
1	F2	231.3	6.2	107		.36
1	F2	232.0	8.9	198		.57
1	F2	232.6	6.6	110		.37
1	F2	239.5	6.3	113		.71
1	F2	240.5	6.3	113		.38
1	F2	249.0	6.2	117		.37
5	KKL02	120.5	6.2	327.8	0.24	0.40
5	KKL02	125.5	9.1	575.5	0.30	0.23
5	KKL02	130.9	10.7	1141.0	0.51	0.45
5	KKL02	134.0	6.1	232.3	0.17	0.71
5	KKL02	200.0	5.9	209.4	0.16	0.28
5	KKL02	390.1	6.1	295.3	0.22	0.29
5	KKL02	549.5	6.1	237.4	0.18	0.36
5	KKL02	586.2	5.8	108.7	0.09	0.21
5	KKL02	587.0	5.8	108.2	0.08	0.21
5	KKL02	588.0	12.8	1243.6	0.46	0.30
5	KKL02	605.0	12.9	1578.5	0.58	0.70
5	KKL02	609.0	12.6	1247.6	0.47	0.35
5	KKL02	612.8	10.5	756.5	0.34	0.23
5	KKL02	721.9	6.3	313.3	0.23	0.43
5	KKL02	762.0	6.2	231.2	0.17	0.34
5	KKL02	763.1	4.5	208.3	0.21	0.29
5	KKL02	764.0	6.2	200.9	0.15	0.47
5	KKL02	804.5	6.4	230.9	0.17	0.62
5	KKL02	809.0	5.9	178.1	0.14	0.21
5	KKL02	838.0	5.9	232.5	0.18	0.21
5	KKL02	941.0	6.6	297.0	0.21	0.30
5	KKL02	941.9	6.6	355.5	0.25	0.34
5	KKL02	942.7	6.7	304.3	0.21	0.49
5	KFI11	56.4	6.6	279.5	0.19	0.21
5	KFI11	64.8	9.0	836.9	0.43	0.27
5	KFI11	65.9	6.8	457.8	0.31	0.28
5	KFI11	67.2	7.7	775.4	0.47	0.31
5	KFI11	109.3	6.4	385.6	0.27	0.27
5	KFI11	149.5	7.4	568.8	0.35	0.39
5	KFI11	201.1	8.2	992.8	0.56	0.51
5	KFI11	216.2	7.3	527.2	0.33	0.24
5	KFI11	218.1	7.2	474.5	0.30	0.30
5	KFI11	220.1	9.8	510.0	0.24	0.37
5	KFI11	251.7	6.7	740.3	0.50	0.79
5	KFI11	253.2	7.0	494.1	0.32	0.29
5	KFI11	254.1	6.6	402.3	0.28	0.28
5	KFI11	254.9	6.7	449.3	0.30	0.25
5	KFI11	262.5	7.8	509.7	0.30	0.29
5	KFI11	293.2	11.7	1627.4	0.63	0.84

Table D.1 Dielectric constant, electrical conductivity, loss tangent and porosity on core samples from the boreholes KKL02, KFI11, KFI09 and F2. (Continued).

Frequency MHz	Sample	∈(r)	σ (μS/m)	tgδ	Porosity %
5	KFI11 296.0	7.4	771.9	0.48	0.66
5	KFI11 297.9	9.1	918.6	0.47	1.16
5	KFI11 329.1	9.9	957.6	0.45	0.87
5	KFI11 330.1	6.2	244.2	0.18	0.40
5	KFI11 331.1	6.7	384.6	0.26	0.63
5	KFI11 334.2	9.3	800.9	0.40	0.64
5	KFI11 337.0	6.1	303.5	0.23	0.41
5	KFI11 373.3	11.2	1377.5	0.57	0.45
5	KFI11 384.1	6.7	437.9	0.30	0.27
5	KFI09 45.4	7.6	549.3	0.33	0.39
5	KFI09 93.1	8.7	849.7	0.45	0.97
5	KFI09 94.0	8.5	853.0	0.46	0.79
5	KFI09 95.0	9.1	840.9	0.43	0.75
5	KFI09 119.9	6.3	349.1	0.25	0.37
5	KFI09 127.9	8.8	852.2	0.45	0.56
5	KFI09 130.1	8.5	786.7	0.43	0.95
5	KFI09 132.4	7.9	659.2	0.38	0.78
5	KFI09 134.0	8.6	816.1	0.44	1.16
5	KFI09 136.0	9.0	833.8	0.43	1.26
5	KFI09 146.2	9.1	863.5	0.44	0.71
5	KFI09 147.2	9.0	993.6	0.52	0.62
5	KFI09 148.0	8.8	847.7	0.45	0.71
5	KFI09 158.9	9.3	840.0	0.42	1.16
5	KFI09 159.9	9.1	1119.5	0.57	1.45
5	KFI09 162.0	7.9	597.7	0.35	0.88
5	KFI09 260.1	8.5	891.2	0.49	0.55
5	KFI09 262.1	7.6	644.9	0.39	0.36
5	KFI09 272.0	7.7	662.8	0.39	0.28
5	KFI09 309.4	6.8	457.8	0.31	0.46
5	KFI09 329.6	7.0	454.7	0.30	0.34
5	KFI09 331.5	5.6	191.4	0.16	0.44
5	KFI09 333.3	7.4	571.1	0.35	0.44
5	F2 11.5	5.8	218		.28
5	F2 19.5	5.6	167		.24
5	F2 32.6	5.6	165		.29
5	F2 44.9	6.0	237		.72
5	F2 45.0	9.0	491		1.43
5	F2 45.2	6.3	259		.66
5	F2 45.5	6.2	270		.40
5	F2 46.1	6.0	184		.35
5	F2 49.3	5.6	158		.27
5	F2 57.2	5.5	161		.27
5	F2 72.1	5.6	191		.28
5	F2 91.2	5.7	227		.51
5	F2 105.1	6.0	203		.40
5	F2 110.1	6.1	274		.34
5	F2 110.4	6.1	273		.55

Table D.1 Dielectric constant, electrical conductivity, loss tangent and porosity on core samples from the boreholes KKL02, KFI11, KFI09 and F2. (Continued).

Frequency MHz	Sample		∈(r)	σ (μS/m)	tgδ	Porosity %
5	F2	110.9	6.1	276		.40
5	F2	111.4	7.3	436		4.78
5	F2	111.5	7.0	402		3.13
5	F2	111.8	6.8	378		2.73
5	F2	112.0	6.9	364		3.59
5	F2	112.3	7.2	432		3.37
5	F2	112.5	7.1	454		3.04
5	F2	112.8	6.1	331		.51
5	F2	113.8	6.0	275		.55
5	F2	115.7	5.7	224		.38
5	F2	116.9	5.6	202		.30
5	F2	117.1	6.7	263		.49
5	F2	117.3	6.1	283		.45
5	F2	118.2	6.0	284		.85
5	F2	119.5	6.4	389		.68
5	F2	120.5	6.2	357		.56
5	F2	120.8	7.7	917		1.33
5	F2	121.4	6.2	316		.53
5	F2	121.7	6.2	367		.64
5	F2	122.2	6.7	428		.51
5	F2	123.2	5.9	321		.40
5	F2	124.0	6.2	410		.43
5	F2	125.4	5.9	319		.42
5	F2	125.5	6.2	341		.37
5	F2	126.2	6.0	297		.33
5	F2	127.2	5.5	295		.49
5	F2	127.8	5.2	214		.38
5	F2	130.5	5.3	207		.35
5	F2	136.2	6.0	191		.36
5	F2	136.8	5.7	196		.45
5	F2	136.9	5.8	195		.40
5	F2	140.0	5.1	198		.35
5	F2	156.8	5.2	216		.48
5	F2	162.3	5.7	182		.42
5	F2	171.8	5.2	193		.35
5	F2	179.9	4.7	190		.37
5	F2	186.4	5.6	426		1.19
5	F2	188.9	5.9	438		.90
5	F2	190.2	5.2	202		.31
5	F2	194.2	5.1	195		.31
5	F2	200.7	5.4	160		.22
5	F2	204.1	5.5	264		.30
5	F2	205.6	5.9	358		.55
5	F2	207.4	5.5	157		.35
5	F2	211.2	5.3	210		.30
5	F2	211.3	5.6	225		.34
5	F2	214.1	5.2	148		.24

Table D.1 Dielectric constant, electrical conductivity, loss tangent and porosity on core samples from the boreholes KKL02, KFI11, KFI09 and F2. (Continued).

Frequency MHz	Sample		∈(r)	σ (μS/m)	tgδ	Porosity %
5	F2	222.4	5.2	187		.33
5	F2	231.3	5.3	225		.36
5	F2	232.0	6.9	476		.57
5	F2	232.6	5.7	249		.37
5	F2	239.5	5.4	202		.71
5	F2	240.5	5.3	225		.38
5	F2	249.0	5.3	233		.37
20	KKL02	120.5	5.7	639.0	0.13	0.40
20	KKL02	125.5	8.0	1147.1	0.17	0.23
20	KKL02	130.9	8.5	2211.6	0.30	0.45
20	KKL02	134.0	5.6	455.5	0.09	0.71
20	KKL02	200.0	5.4	369.0	0.08	0.28
20	KKL02	390.1	5.6	542.6	0.11	0.29
20	KKL02	549.5	5.7	459.4	0.09	0.36
20	KKL02	586.2	5.6	229.0	0.05	0.21
20	KKL02	587.0	5.4	239.2	0.05	0.21
20	KKL02	588.0	9.7	2620.7	0.32	0.30
20	KKL02	605.0	9.7	2878.9	0.35	0.70
20	KKL02	609.0	9.6	2364.3	0.29	0.35
20	KKL02	612.8	8.7	1372.5	0.18	0.23
20	KKL02	721.9	5.8	521.1	0.10	0.43
20	KKL02	762.0	5.5	451.8	0.09	0.34
20	KKL02	763.1	5.7	377.7	0.08	0.29
20	KKL02	764.0	5.8	418.9	0.08	0.47
20	KKL02	804.5	5.9	451.0	0.09	0.62
20	KKL02	809.0	5.5	311.8	0.06	0.21
20	KKL02	838.0	5.5	361.5	0.07	0.21
20	KKL02	941.0	6.0	543.7	0.10	0.30
20	KKL02	941.9	6.1	579.4	0.11	0.34
20	KKL02	942.7	6.0	575.9	0.11	0.49
20	KKL02	957.0	5.9	483.8	0.09	0.31
20	KFI11	56.4	6.1	513.0	0.10	0.21
20	KFI11	64.8	7.5	1087.2	0.17	0.27
20	KFI11	65.9	5.9	668.0	0.13	0.28
20	KFI11	67.2	6.1	918.5	0.17	0.31
20	KFI11	109.3	5.8	478.9	0.09	0.27
20	KFI11	149.5	6.1	935.8	0.17	0.39
20	KFI11	201.1	6.3	973.6	0.18	0.51
20	KFI11	216.2	6.1	962.7	0.18	0.24
20	KFI11	218.1	6.1	734.8	0.14	0.30
20	KFI11	220.1	8.2	1122.0	0.16	0.37
20	KFI11	251.7	5.6	676.0	0.14	0.79
20	KFI11	253.2	6.2	785.6	0.14	0.29
20	KFI11	254.1	5.9	566.8	0.11	0.28
20	KFI11	254.9	6.0	620.0	0.12	0.25
20	KFI11	262.5	6.7	1017.9	0.17	0.29
20	KFI11	293.2	8.3	2586.7	0.35	0.84

Table D.1 Dielectric constant, electrical conductivity, loss tangent and porosity on core samples from the boreholes KKL02, KFI11, KFI09 and F2. (Continued).

Frequency MHz	Sample	ϵ(r)	σ (μS/m)	tgδ	Porosity %
20	KFI11 296.0	6.1	1045.6	0.20	0.66
20	KFI11 297.9	7.2	1669.6	0.27	1.16
20	KFI11 329.1	7.6	2244.1	0.34	0.87
20	KFI11 330.1	5.7	509.8	0.10	0.40
20	KFI11 331.1	5.9	727.3	0.14	0.63
20	KFI11 334.2	7.3	1751.4	0.28	0.64
20	KFI11 337.0	5.6	536.0	0.11	0.41
20	KFI11 373.3	8.4	2108.5	0.29	0.45
20	KFI11 384.1	5.9	608.7	0.12	0.27
20	KFI09 45.4	6.3	1025.8	0.19	0.39
20	KFI09 93.1	6.9	1491.0	0.25	0.97
20	KFI09 94.0	6.7	1507.7	0.26	0.79
20	KFI09 95.0	7.3	1517.5	0.24	0.75
20	KFI09 119.9	5.8	510.7	0.10	0.37
20	KFI09 127.9	6.9	1640.9	0.28	0.56
20	KFI09 130.1	6.8	1572.3	0.27	0.95
20	KFI09 132.4	6.6	1304.0	0.23	0.78
20	KFI09 134.0	7.0	1458.8	0.24	1.16
20	KFI09 136.0	7.2	1749.3	0.28	1.26
20	KFI09 146.2	7.2	1794.8	0.29	0.71
20	KFI09 147.2	6.7	1813.4	0.31	0.62
20	KFI09 148.0	6.9	1664.2	0.28	0.71
20	KFI09 158.9	7.3	1852.8	0.29	1.16
20	KFI09 159.9	7.1	2003.5	0.33	1.45
20	KFI09 162.0	6.6	1254.1	0.22	0.88
20	KFI09 260.1	6.5	1468.1	0.26	0.55
20	KFI09 262.1	6.3	1128.2	0.20	0.36
20	KFI09 272.0	6.4	1185.8	0.21	0.28
20	KFI09 309.4	6.2	732.6	0.14	0.46
20	KFI09 329.6	6.0	733.1	0.14	0.34
20	KFI09 331.5	5.3	362.2	0.08	0.44
20	KFI09 333.3	6.4	1005.9	0.18	0.44
20	F2 11.5	5.3	472		.28
20	F2 19.5	5.2	359		.24
20	F2 32.6	5.3	340		.29
20	F2 44.9	5.2	527		.72
20	F2 45.0	7.5	1126		1.43
20	F2 45.2	5.7	608		.66
20	F2 45.5	5.4	722		.40
20	F2 46.1	5.5	491		.35
20	F2 49.3	5.2	356		.27
20	F2 57.2	5.2	313		.27
20	F2 72.1	5.3	372		.28
20	F2 91.2	5.4	446		.51
20	F2 105.1	5.6	462		.40
20	F2 110.1	5.5	569		.34
20	F2 110.4	5.6	554		.55

Table D.1 Dielectric constant, electrical conductivity, loss tangent and porosity on core samples from the boreholes KKL02, KFI11, KFI09 and F2. (Continued).

Frequency MHz	Sample		∈(r)	σ (μS/m)	tgδ	Porosity %
20	F2	110.9	5.5	560		.40
20	F2	111.4	6.7	721		4.78
20	F2	111.5	6.4	706		3.13
20	F2	111.8	6.2	659		2.73
20	F2	112.0	6.3	605		3.59
20	F2	112.3	6.4	712		3.37
20	F2	112.5	6.3	729		3.04
20	F2	112.8	5.5	633		.51
20	F2	113.8	5.5	507		.55
20	F2	115.7	5.2	449		.38
20	F2	116.9	5.2	390		.30
20	F2	117.1	6.2	551		.49
20	F2	117.3	5.5	599		.45
20	F2	118.2	5.4	533		.85
20	F2	119.5	5.8	709		.68
20	F2	120.5	5.6	735		.56
20	F2	120.8	6.4	1667		1.33
20	F2	121.4	5.6	678		.53
20	F2	121.7	5.6	745		.64
20	F2	122.2	6.2	822		.51
20	F2	123.2	5.5	617		.40
20	F2	124.0	5.5	779		.43
20	F2	125.4	5.4	625		.42
20	F2	125.5	5.6	693		.37
20	F2	126.2	5.4	588		.33
20	F2	127.2	5.2	547		.49
20	F2	127.8	4.9	359		.38
20	F2	130.5	5.1	413		.35
20	F2	136.2	5.7	457		.36
20	F2	136.8	5.2	479		.45
20	F2	136.9	5.5	422		.40
20	F2	140.0	4.8	364		.35
20	F2	156.8	4.9	348		.48
20	F2	162.3	5.3	410		.42
20	F2	171.8	4.9	343		.35
20	F2	179.9	4.5	328		.37
20	F2	186.4	4.1	731		1.19
20	F2	188.9	5.1	907		.90
20	F2	190.2	4.9	344		.31
20	F2	194.2	4.8	337		.31
20	F2	200.7	5.1	310		.22
20	F2	204.1	5.0	491		.30
20	F2	205.6	4.9	629		.55
20	F2	207.4	5.8	313		.35
20	F2	211.2	4.9	366		.30
20	F2	211.3	5.2	370		.34
20	F2	214.1	4.9	292		.24

Table D.1 Dielectric constant, electrical conductivity, loss tangent and porosity on core samples from the boreholes KKL02, KFI11, KFI09 and F2. (Continued).

Frequency MHz	Sample		ϵ(r)	σ (μS/m)	tgδ	Porosity %
20	F2	222.4	4.9	327		.33
20	F2	231.3	4.9	391		.36
20	F2	232.0	5.9	940		.57
20	F2	232.6	6.9	479		.37
20	F2	239.5	5.1	349		.71
20	F2	240.5	4.9	395		.38
20	F2	249.0	4.9	349		.37
70	KKL02	120.5	5.3	1357.7	0.08	0.40
70	KKL02	125.5	7.4	2507.1	0.11	0.23
70	KKL02	130.9	7.6	4204.4	0.18	0.45
70	KKL02	134.0	5.4	1080.2	0.06	0.71
70	KKL02	200.0	5.3	745.4	0.05	0.28
70	KKL02	390.1	5.4	1241.3	0.07	0.29
70	KKL02	549.5	5.4	1087.3	0.06	0.36
70	KKL02	586.2	5.5	554.4	0.03	0.21
70	KKL02	587.0	5.4	675.1	0.04	0.21
70	KKL02	588.0	8.3	6722.4	0.27	0.30
70	KKL02	605.0	8.2	6539.1	0.26	0.70
70	KKL02	609.0	8.6	5585.8	0.22	0.35
70	KKL02	612.8	8.2	3522.7	0.14	0.23
70	KKL02	721.9	5.5	1357.0	0.08	0.43
70	KKL02	762.0	5.6	1090.8	0.06	0.34
70	KKL02	763.1	5.4	952.2	0.06	0.29
70	KKL02	764.0	5.5	1097.8	0.06	0.47
70	KKL02	804.5	5.6	968.1	0.06	0.62
70	KKL02	809.0	5.4	662.7	0.04	0.21
70	KKL02	838.0	5.4	582.6	0.04	0.21
70	KKL02	941.0	5.6	1072.4	0.06	0.30
70	KKL02	941.9	5.7	1033.8	0.06	0.34
70	KKL02	942.7	5.7	1187.8	0.07	0.49
70	KKL02	957.0	5.7	908.8	0.05	0.31
70	KFI11	56.4	5.8	1222.4	0.07	0.21
70	KFI11	64.8	7.0	2401.7	0.11	0.27
70	KFI11	65.9	5.6	1590.3	0.09	0.28
70	KFI11	67.2	5.6	2014.5	0.12	0.31
70	KFI11	109.3	5.5	957.9	0.06	0.27
70	KFI11	149.5	5.6	2081.6	0.12	0.39
70	KFI11	201.1	5.9	2125.4	0.12	0.51
70	KFI11	216.2	5.7	2273.5	0.13	0.24
70	KFI11	218.1	5.8	1718.7	0.10	0.30
70	KFI11	220.1	7.6	2958.3	0.13	0.37
70	KFI11	251.7	5.1	1545.9	0.10	0.79
70	KFI11	253.2	5.6	1742.5	0.10	0.29
70	KFI11	254.1	5.6	1187.8	0.07	0.28
70	KFI11	254.9	5.6	1431.3	0.08	0.25
70	KFI11	262.5	6.1	2564.0	0.14	0.29
70	KFI11	293.2	6.9	5596.1	0.25	0.84

Table D.1 Dielectric constant, electrical conductivity, loss tangent and porosity on core samples from the boreholes KKL02, KFI11, KFI09 and F2. (Continued).

Frequency MHz	Sample	∈(r)	σ (μS/m)	tgδ	Porosity %
70	KFI11 296.0	5.6	2219.7	0.13	0.66
70	KFI11 297.9	6.3	3880.2	0.20	1.16
70	KFI11 329.1	6.4	5422.2	0.27	0.87
70	KFI11 330.1	5.4	1473.8	0.09	0.40
70	KFI11 331.1	5.5	1961.1	0.12	0.63
70	KFI11 334.2	6.4	4347.6	0.22	0.64
70	KFI11 337.0	5.2	1500.8	0.09	0.41
70	KFI11 373.3	7.5	4335.6	0.19	0.45
70	KFI11 384.1	5.6	1357.2	0.08	0.27
70	KFI09 45.4	5.7	2374.5	0.14	0.39
70	KFI09 93.1	6.1	3339.0	0.18	0.97
70	KFI09 94.0	5.7	3344.9	0.19	0.79
70	KFI09 95.0	6.4	3651.5	0.19	0.75
70	KFI09 119.9	5.5	1004.5	0.06	0.37
70	KFI09 127.9	6.0	3855.0	0.21	0.56
70	KFI09 130.1	6.0	3442.2	0.19	0.95
70	KFI09 132.4	5.9	3095.0	0.17	0.78
70	KFI09 134.0	6.2	3395.0	0.18	1.16
70	KFI09 136.0	6.2	3859.2	0.20	1.26
70	KFI09 146.2	6.3	4361.1	0.23	0.71
70	KFI09 147.2	5.9	3722.9	0.20	0.62
70	KFI09 148.0	6.0	3698.4	0.20	0.71
70	KFI09 158.9	6.2	4496.4	0.24	1.16
70	KFI09 159.9	6.1	4241.6	0.22	1.45
70	KFI09 162.0	6.0	2895.7	0.16	0.88
70	KFI09 260.1	5.9	3010.2	0.16	0.55
70	KFI09 262.1	5.8	2508.5	0.14	0.36
70	KFI09 272.0	5.8	2482.5	0.14	0.28
70	KFI09 309.4	5.8	1613.4	0.09	0.46
70	KFI09 329.6	5.7	1707.0	0.10	0.34
70	KFI09 331.5	5.1	888.0	0.06	0.44
70	KFI09 333.3	5.9	2203.8	0.12	0.44
70	KFI09 359.9	6.0	3004.8	0.16	0.50
70	F2 11.5	5.0	1001		.28
70	F2 19.5	5.1	693		.24
70	F2 32.6	5.1	702		.29
70	F2 44.9	5.2	638		.72
70	F2 45.0	6.9	2654		1.43
70	F2 45.2	5.3	1249		.66
70	F2 45.5	5.1	1657		.40
70	F2 46.1	5.2	1173		.35
70	F2 49.3	5.1	788		.27
70	F2 57.2	5.2	668		.27
70	F2 72.1	5.1	708		.28
70	F2 91.2	5.2	865		.51
70	F2 105.1	5.3	1140		.40
70	F2 110.1	5.2	1277		.34

Table D.1 Dielectric constant, electrical conductivity, loss tangent and porosity on core samples from the boreholes KKL02, KFI11, KFI09 and F2. (Continued).

Frequency MHz	Sample		ϵ(r)	σ (μS/m)	tgδ	Porosity %
70	F2	110.4	5.3	1152		.55
70	F2	110.9	5.2	1161		.40
70	F2	111.4	6.5	1599		4.78
70	F2	111.5	6.1	1348		3.13
70	F2	111.8	6.0	1300		2.73
70	F2	112.0	6.1	1173		3.59
70	F2	112.3	6.0	1266		3.37
70	F2	112.5	6.0	1355		3.04
70	F2	112.8	5.1	1351		.51
70	F2	113.8	5.2	898		.55
70	F2	115.7	5.0	898		.38
70	F2	116.9	5.0	839		.30
70	F2	117.1	5.9	1361		.49
70	F2	117.3	5.2	1353		.45
70	F2	118.2	5.2	1144		.85
70	F2	119.5	5.4	1545		.68
70	F2	120.5	5.2	1678		.56
70	F2	120.8	5.7	5030		1.33
70	F2	121.4	5.2	1600		.53
70	F2	121.7	5.3	1556		.64
70	F2	122.2	5.7	1689		.51
70	F2	123.2	5.2	1185		.40
70	F2	124.0	5.2	1720		.43
70	F2	125.4	5.1	3082		.42
70	F2	125.5	5.2	1601		.37
70	F2	126.2	5.2	1418		.33
70	F2	127.2	4.9	1141		.49
70	F2	127.8	4.7	761		.38
70	F2	130.5	4.9	844		.35
70	F2	136.2	5.4	1118		.36
70	F2	136.8	5.0	1149		.45
70	F2	136.9	5.2	1018		.40
70	F2	140.0	4.7	733		.35
70	F2	156.8	4.7	654		.48
70	F2	162.3	5.1	946		.42
70	F2	171.8	4.7	711		.35
70	F2	179.9	4.5	643		.37
70	F2	186.4	4.8	1300		1.19
70	F2	188.9	4.7	2092		.90
70	F2	190.2	4.7	679		.31
70	F2	194.2	4.7	685		.31
70	F2	200.7	5.0	641		.22
70	F2	204.1	4.7	924		.30
70	F2	205.6	5.1	1415		.55
70	F2	207.4	5.1	591		.35
70	F2	211.2	4.7	754		.30
70	F2	211.3	5.1	745		.34

Table D.1 Dielectric constant, electrical conductivity, loss tangent and porosity on core samples from the boreholes KKL02, KFI11, KFI09 and F2. (Continued).

Frequency MHz	Sample		∈(r)	σ (μS/m)	tgδ	Porosity %
70	F2	214.1	4.8	555		.24
70	F2	222.4	4.7	668		.33
70	F2	231.3	4.8	810		.36
70	F2	232.0	5.4	1839		.57
70	F2	232.6	4.9	960		.37
70	F2	239.5	4.9	682		.71
70	F2	240.5	4.8	837		.38
70	F2	249.0	4.8	716		.37

List of SKB reports

Annual Reports

1977–78
TR 121
KBS Technical Reports 1 – 120.
Summaries. Stockholm, May 1979.

1979
TR 79–28
The KBS Annual Report 1979.
KBS Technical Reports 79-01 – 79-27.
Summaries. Stockholm, March 1980.

1980
TR 80–26
The KBS Annual Report 1980.
KBS Technical Reports 80-01 – 80-25.
Summaries. Stockholm, March 1981.

1981
TR 81–17
The KBS Annual Report 1981.
KBS Technical Reports 81-01 – 81-16.
Summaries. Stockholm, April 1982.

1982
TR 82–28
The KBS Annual Report 1982.
KBS Technical Reports 82-01 – 82-27.
Summaries. Stockholm, July 1983.

1983
TR 83–77
The KBS Annual Report 1983.
KBS Technical Reports 83-01 – 83-76
Summaries. Stockholm, June 1984.

1984
TR 85–01
Annual Research and Development Report 1984
Including Summaries of Technical Reports Issued during 1984. (Technical Reports 84-01– 84-19)
Stockholm June 1985.

1985
TR 85-20
Annual Research and Development Report 1985
Including Summaries of Technical Reports Issued during 1985. (Technical Reports 85-01-85-19)
Stockholm May 1986.

1986
TR 86-31
SKB Annual Report 1986
Including Summaries of Technical Reports Issued during 1986
Stockholm, May 1987

1987
TR 87-33
SKB Annual Report 1987
Including Summaries of Technical Reports Issued during 1987
Stockholm, May 1988

1988
TR 88-32
SKB Annual Report 1988
Including Summaries of Technical Reports Issued during 1988
Stockholm, May 1989

Technical Reports

1989
TR 89-01
Near-distance seismological monitoring of the Lansjärv neotectonic fault region Part II: 1988
Rutger Wahlström, Sven-Olof Linder, Conny Holmqvist, Hans-Edy Mårtensson
Seismological Department, Uppsala University, Uppsala
January 1989

TR 89-02
Description of background data in SKB database GEOTAB
Ebbe Eriksson, Stefan Sehlstedt
SGAB, Luleå
February 1989

TR 89-03
Characterization of the morphology, basement rock and tectonics in Sweden
Kennert Röshoff
August 1988

TR 89-04
SKB WP-Cave Project
Radionuclide release from the near-field in a WP-Cave repository
Maria Lindgren, Kristina Skagius
Kemakta Consultants Co, Stockholm
April 1989

TR 89-05
SKB WP-Cave Project
Transport of escaping radionuclides from the WP-Cave repository to the biosphere
Luis Moreno, Sue Arve, Ivars Neretnieks
Royal Institute of Technology, Stockholm
April 1989

TR 89-06
SKB WP-Cave Project
Individual radiation doses from nuclides contained in a WP-Cave repository for spend fuel
Sture Nordlinder, Ulla Bergström
Studsvik Nuclear, Studsvik
April 1989

TR 89-07
SKB WP-Cave Project
Some Notes on Technical Issues

TR 89-08
SKB WP-Cave Project
Thermally incuded convective motion in groundwater in the near field of the WP-Cave after filling and closure
Polydynamics Limited, Zürich
April 1989

TR 89-09
An evaluation of tracer tests performed at Studsvik
Luis Moreno[1], Ivars Neretnieks[1], Ove Landström[2]
[1] The Royal Institute of Technology, Department of Chemical Engineering, Stockholm
[2] Studsvik Nuclear, Nyköping
March 1989

TR 89-10
Copper produced from powder by HIP to encapsulate nuclear fuel elements
Lars B Ekbom, Sven Bogegård
Swedish National Defence Research Establishment
Materials department, Stockholm
February 1989

TR 89-11
Prediction of hydraulic conductivity and conductive fracture frequency by multivariate analysis of data from the Klipperås study site
Jan-Erik Andersson[1], Lennart Lindqvist[2]
[1] Swedish Geological Co, Uppsala
[2] EMX-system AB, Luleå
February 1988

TR 89-12
Hydraulic interference tests and tracer tests within the Brändan area, Finnsjön study site The Fracture Zone Project – Phase 3
Jan-Erik Andersson, Lennart Ekman, Erik Gustafsson, Rune Nordqvist, Sven Tirén
Swedish Geological Co, Division of Engineering Geology
June 1988

TR 89-13
Spent fuel
Dissolution and oxidation
An evaluation of literature data
Bernd Grambow
Hanh-Meitner-Institut, Berlin
March 1989

TR 89-14
The SKB spent fuel corrosion program
Status report 1988
Lars O Werme[1], Roy S Forsyth[2]
[1] SKB, Stockholm
[2] Studsvik AB, Nyköping
May 1989